Deciphering the Functional Roles of Centrosomal Protein 55 (CEP55) in Development and Cancer

Behnam Rashidieh
MSc., Microbiology

School of Environment and Science,
Griffith University

Submitted in the fulfillment of the requirements of the degree of Doctor of Philosophy

October 2019

Abstract

Centrosomal protein CEP55 is a critical regulator of cytokinesis, and its deregulation has been linked to tumorigenesis. Loss of function mutations in Cep55 have also been shown to perturb embryogenesis, particularly affecting neural development. Cep55 expression in cells must be tightly regulated, as both overexpression and reduced levels of expression can cause cytokinetic abscission defects leading to genomic instability. *CEP55* also promotes PI3K/AKT signaling which confers a survival advantage to cancer cells. However, despite more than a decade of research into characterizing this protein, the molecular function of *CEP55* during tumorigenesis and embryonic development in mammals is not well defined.

In this thesis, we have generated a *Cep55* knockout (*Cep55*$^{-/-}$) mouse model, which is the first *in vivo* knockout model for this gene to our knowledge. *Cep55*$^{-/-}$ mice exhibited late embryonic lethality associated with a wide range of neural defects. We showed that *Cep55*$^{-/-}$ embryos at E14.5 exhibit depleted neural stem cells in the ventricular zone. This was caused by a significant decrease in proliferation with a concomitant increase in apoptosis of radial glial (RGCs : PAX6^{+}), intermediate progenitor cells (IPC: TBR2^{+}) and postmitotic neurons (PMN: TBR1^{+}). As a consequence, we observed reduced numbers of neurons in the cortical plate at later stages of embryonic development. Mechanistically, using Mouse Embryonic Fibroblasts (MEFs), we demonstrated that *Cep55* loss downregulates the pGsk3β/β-Catenin/Myc axis in an Akt-dependent manner, indicating the importance of these pathways in early development. Additionally, we showed that loss of *Cep55* leads to a significant reduction of both ciliated cells and cilia length, highlighting a definitive role of *Cep55* in regulating ciliogenesis. Overall, our study has identified a critical role of *Cep55* during brain development and suggests that defective

PI3K-Akt pathway activation during embryogenesis may cause the microencephaly seen in genetic syndromes associated with *Cep55* loss.

In addition to characterization of its role during embryogenesis, we also utilized a conditional knockout mouse model of *Cep55* to further understand its role in tumor development. To determine if *Cep55* loss would perturb transformation ability, we transformed $Cep55^{+/+}$ and $Cep55^{-/-}$ MEFs with *E1A*/*Ras* oncogenes. Strikingly, we found that anchorage-independent colony formation was reduced in E1A/Ras-$Cep55^{-/-}$ MEFs in colony formation and 3D culture assays compared to E1A/Ras-$Cep55^{+/+}$ counterparts. Similarly, loss of *Cep55* delayed tumor formation in NOD/SCID mice injected intraperitoneally with E1A/Ras-transformed $Cep55^{-/-}$ MEFs suggesting that *Cep55* regulates tumor formation. To validate these effects in a preclinical model, we utilized the tumor-prone model systems $Pten^{fl/fl}$;*Rosa26* Cre ERT(2) (hyperactive-AKT signaling) and *Kras* LSL G12D (hyperactive /MAPK/ERK signaling) to establish a hybrid line with $Cep55^{-/-}$ to investigate the consequences of *Cep55* loss in tumor formation in these mice. Our data confirm that loss of *Cep55* delayed *Pten*-deficient malignancies and increased overall survival in *Pten*-deficient mice. Moreover, in a lung-specific *Kras LSL G12D* mouse model, loss of *Cep55* decreased tumor burden. These data highlight a broader role of *Cep55* in contributing to tumorigenesis in these mouse models. Altogether, our data suggest that *Cep55* may be a valuable molecular target to prevent the initiation and progression of cancer.

Statement of Originality

This work has not previously been submitted for a degree or diploma in any university. To the best of my knowledge and belief, the thesis contains no material previously published or written by another person except where due reference is made in the thesis itself.

(Signed)

[redacted]

Behnam Rashidieh, 24th October 2019

Acknowledgments

First, I would like to extend my heartfelt gratitude to my supervisory team. Prof. Kum Kum Khanna, lab head of the Signal transduction laboratory and my principal supervisor, has given me the opportunity to learn under her guidance and has served as an amazing mentor for my career. Her trust in me and the intellectual freedom she has given me have been invaluable to enhance my critical thinking and decision-making. Her intellectual support, critical guidance, and patience have allowed me to build a better version of myself in scientific research. It was a great privilege to work at her world-class laboratory, where her enthusiasm for, and insistence on producing high-quality results motivated me to strive harder and more methodically to make the best use of my time. Moreover, her active engagement and attendance in all my presentations, despite having to work to a tight schedule, was extremely encouraging. This amount of dedication and commitment imbued a strong sense of responsibility in me and motivated me to focus on the timely and effective completion of my experiments.

Without my co-supervisor, Prof. Alejandro Lopez, I could not have accomplished my PhD. He helped me enormously to develop my skills, as well as gave valuable feedback and all-embracing support. His follow up and dedication to assist me in all aspects of my life has made me eternally grateful to him. Thank you to Dr. Amanda Bain, my associate supervisor for taking the reins at a critical point in my project. Thank you for helping me to keep my head and for always being so optimistic. Her insight and efforts - especially in the critical editing of my essays (even this one!) and support are hugely appreciated. Throughout my project, she has provided me with an immense amount of advice, guidance, and encouragement. Her inspiring and positive attitude coupled with patience has enabled me to develop my skills as a scientist and grow as an individual. I have gained an extensive amount of knowledge from Amanda and for this, I will be forever thankful. I was extremely fortunate to have her as a supervisor, but I am also privileged to be able to call her my friend too.

To all of the generous and caring Signal transduction laboratory members and peers, thank you for sharing your knowledge and helping me to progress and find my way where I faced a dead-end in the project. You have always provided me with excellent feedback regarding my experimental design, writing and presentation skills. I owe them so much, especially Stephen Miles our laboratory manager. He was always willing to provide his

assistance throughout this project, and his fantastic sense of humor and inclusiveness always made me feel comfortable and accepted in the group. I would also like to acknowledge the help of Dr. Debottam Sinha and Dr. Purba Nag the lovely couple and former PhD students in the lab who have given me a lot of support, training, and feedback for improvement and development. It was a blessing to have them around.

To everyone at the QIMR, which has been my second home for the last 3.5 years, I would like to express my greatest appreciation. I would like to thank the Flow Cytometry and Imaging Facility particularly, Dr. Nigel Waterhouse and Dr. Tam Hong Nguyen, who helped me to learn to work with a variety of microscopes and how to analyse data. Thank you to Dr. Andrew Masel and his histopathology team, for their effort, expertise, and generous guidance. I would also like to extend my thanks to the Animal facility, especially Dr. Jonathan Mauclair, Michael Damjancuk and Ben Fewster who helped me to organize and keep track of enormous number of mice in breeding and experimental procedures. If given a second chance, I would still choose to undertake my PhD at QIMR and I would like to wish all of my colleagues a successful and rewarding research career that will one day reward their massive efforts. I would also like to thank Griffith University for providing funds, financial assistance and facilitating the necessary education, training, and services that have enabled me to undertake my PhD.

It would be remiss not to also give credit to colleagues from Universities of Queensland, Melbourne and Adelaide who contributed a lot towards progressing this project. Prof. John Finnie, Dr. Dominic Ng, Dr. Michael Piper, and Belal Shohayeb, thank you for being wonderful collaborators and contributing to my PhD journey. I would also like to thank all my friends, who have had such a positive influence in my life and brought constant love, courage and hope to my life. It is crystal clear that living on the other side of the world does not impact our friendship; so, they are stuck with me for a lifetime! Also, I am thankful to all my new international and national friends who are amazing; thank you for the extensive support, aid, love, and encouragement in making this journey less lonely and less difficult.

Finally, I dedicate this dissertation to my family: my beloved wife, Nazgol, and my lovely parents, Gity and Hossein as well as my kind-hearted sister, Behnaz for giving me such love, hope, and support throughout my life. It is difficult to express in words how appreciative I am to these people. Nazgol, thank you for always being there for me, for your phenomenal support and love all along the way. You will always be my only one and everyone and you fill my soul with so much love! On top of that, you are, and will always be my best friend and companion; therefore, I will fearlessly chase my wildest dreams, I will never give up and I will never back down from what I believe in. I am indebted to my parents, sister, my parents-in-law and my sister-in-law for their support and kindness. Thank you to my Dad for your wishes, sacrifices and your care for me- your love is forever in my heart. I am who I am today thanks to my Mum- without you and your love, none of this would have been possible. To my Mum, you are my first, best and greatest mentor, my motivation and my deepest roots, and my perpetual belief in my limitless potential, which empowers me every single day. I am everlastingly grateful for your knowledge, love and life shared life lessons that I live by. To my parents, I am honored to be your son. Doing my PhD so far away from you has been the hardest thing I have ever done, but I hope I have made you proud.

DEDICATION

This thesis is dedicated to my beloved family: Mum, Dad, Sister, and my darling Wife, Nazgol. It is also dedicated to my grandmothers who are my cherished; my grandfathers, who sadly succumbed to cancer and to my aunt, Esmat, who always called me Doctor but passed away before she could see me officially, granted the title.

Table of Contents

Chapter 1. Literature Review 1

1.1 Centrosomal Protein 55 kDa 1

1.2 CEP55 during the Cell Cycle and Mitosis 2

1.2.1 The Cell Cycle 2

1.2.2 Mitosis 4

1.2.3 Cytokinesis 4

1.2.4 CEP55 regulates cytokinesis 5

1.3 CEP55 in Cancer 6

1.3.1 Definition of Cancer 6

1.3.2 Hallmarks of Cancer 10

1.3.3 PI3K/AKT signaling and Cancer 13

1.3.4 CEP55 and the PI3K/AKT pathway 15

1.3.5 CEP55 and FOXM1 16

1.3.6 CEP55 connection to p53 and other cell cycle regulators 17

1.3.7 CEP55 as a prognostic marker 18

1.3.8 CEP55 Regulates Stemness 20

1.3.9 CEP55 and the mitotic stress connection 21

1.3.10 Targeting CEP55 in cancer 22

1.4 CEP55 in Genetic Diseases and Disorders 25

1.5 Cep55 in Embryogenesis, Development and Neural Function 27

1.6 Significance, Aims and Hypotheses 28

1.6.1 Aim 1: To determine the functional role of CEP55 in early embryonic development 29

1.6.1.1 To generate and establish Cep55 constitutive and conditional KO models 29

1.6.1.2 To characterize the physiological role of Cep55 loss during embryonic development 29

1.6.1.3 To identify cellular and molecular role of CEP55 in regulation of the cell cycle, cell signaling and ciliopathy........ 29

1.6.2 Aim 2: To determine the functional role of CEP55 in tumorigenesis and cancer........ 29

1.6.2.1 Determine if Cep55 loss regulates E1A/Ras-mediated tumorigenesis... 29

1.6.2.2 Determine the contribution of Cep55 genetic depletion on Pten and Kras LSL G12D tumor prone mouse models........ 29

Chapter 2. Materials and methods........ 30

2.1 Animal work and Histopathology 30

2.1.1 Animal husbandry and ethics statement 30

2.1.2 Generation of constitutive Cep55 knockout mice 30

2.1.3 Generation of conditional Cep55 knockout mice 30

2.1.4 Genotype analysis........ 31

2.1.5 Timed mating........ 32

2.1.6 Organ/embryo isolation 33

2.1.7 Mouse xenografts 33

2.1.8 Tamoxifen induction 33

2.1.9 Intranasal delivery of Ad-Cre 34
2.1.10 Immunohistochemistry staining 34
2.1.11 β-Galactosidase staining 36
2.1.12 Whole-Mount Skeletal Staining 37
2.1.13 Hematology 37
2.2 Cell biology 37
2.2.1 Cell culture 37
2.2.2 MEF establishment 38
2.2.3 Doubling time assay 38
2.2.4 Cell proliferation assay 39
2.2.5 Cell cycle analysis 39
2.2.6 Cell viability assay (MTS) 39
2.2.7 Clonogenic assays 40
2.2.8 Soft agar Colony formation assay 40
2.2.9 3D cell culture 40
2.2.10 Gene transduction and transfection 41
2.2.11 Retrovirus and lentivirus packaging and transduction 42
2.2.12 Live-cell imaging 43
2.2.13 Immunofluorescence 43
2.2.14 Luciferase assays 44
2.3 Molecular biology 46
2.3.1 Immunoblotting 46

2.3.1.1 Cell and tissue lysate preparation 46

2.3.1.2 SDS-PAGE and western blot.. 47

2.3.2 DNA extraction 49

2.3.3 Polymerase chain reaction 49

2.3.4 RNA extraction.. 50

2.3.5 Quantitative RT PCR.. 50

2.4 Statistical analysis 52

Chapter 3. Generation of *Cep55* KO mouse model 53

3.1 Introduction 53

3.1.1 Mouse Models of Disease 53

3.1.2 Knockout transgenic mice 54

3.1.3 Knockout mouse models of Centrosomal Proteins 54

3.2 Results 56

3.2.1 Loss of Cep55 leads to embryonic lethality in mice 56

3.2.2 Cep55$^{+/-}$ heterozygotes are phenotypically normal 60

3.2.3 Expression pattern of CEP55 in human and mouse cells 62

3.2.4 Cep55 conditional KO mice are viable.. 65

3.3 Discussion... 67

Chapter 4. Phenotypic characterization of Cep55 loss during development 69

4.1 Introduction 69

4.2 Results 71

4.2.1 Cep55 loss causes gross morphological defects in mouse embryos............. 71

4.2.2 Cep55 loss causes microencephaly due to a reduction of neurons and neuroglia ... 74

4.2.3 Cep55 regulates cell fate of radial glial and intermediate progenitor cells ... 77

4.2.4 Cep55 regulates proliferation and apoptosis in neural progenitor cells ... 80

4.3 Discussion ... 82

Chapter 5. Characterization of the role of Cep55 in ciliogenesis and cellular homeostasis ... 85

5.1 Introduction ... 85

5.1.1 The primary cilia ... 85

5.1.2 Cilia and Hedgehog Signaling ... 86

5.1.3 PI3K/AKT signaling and ciliogenesis ... 87

5.1.4 Cep55 and Ciliopathy-like phenotypes ... 88

5.2 Results ... 89

5.2.1 $Cep55^{-/-}$ mice exhibit cilia abnormalities ... 89

5.2.2 Cep55 directly regulates cilial growth and is localized at the base of cilia ... 90

5.2.3 $Cep55^{-/-}$ MEFs exhibit proliferation defects and multinucleation ... 95

5.2.4 Cep55 regulates GSK3β, βCatenin, and Myc downstream of the Akt pathway ... 100

5.2.5 Rescue of Cep55 mutant phenotype by downstream effectors of the PI3K/AKT signaling pathway ... 104

5.3 Discussion ... 108

Chapter 6. *Cep55* loss impedes tumorigenesis *in vivo* ... 113

6.1 Introduction ... 113

6.1.1 CEP55 overexpression... 113

6.1.2 The PTEN tumor suppressor 115

6.1.3 Activating mutations in Kras and Tumor development 116

6.2 Results 118

6.2.1 A novel mouse model for inducible Cep55 KO 118

6.2.2 Cep55 KO impairs proliferation and transformation in vitro. 118

6.2.3 Delayed tumor progression in Cep55$^{-/-}$ cell-derived xenograft mouse model 121

6.2.4 Loss of Cep55 delays tumorigenesis in a Pten-deficient tumor-prone mouse model 124

6.2.5 Loss of Cep55 hinders tumorigenesis in a Kras-mutant tumor prone mouse model 130

6.3 Discussion... 136

Chapter 7. General discussion and future direction 143

7.1 General Discussion... 143

7.2 Conclusions and Future Directions.. 147

References.. 150

List of Figures

Figure 1.1 CEP55 structure and mechanism in regulating AKT signaling. 2

Figure 1.2 The cell cycle stages and phases. 3

Figure 1.3 The percent of oncogene mutations across human tumor types. 8

Figure 1.5 Pathways in human cancer. 13

Figure 1.6 Targeting hallmarks of cancer for therapy 23

Figure 3.1 Transgenic mouse models which show centrosomal dysfunction. 56

Figure 3.2 Schematic allele of Cep55 KO mouse model of and validation of its targeting. 58

Figure 3.3 Comparison of Cep55 $^{+/+}$ *and Cep55* $^{-/-}$ *embryos at E14.5 and E18.5.* 59

Figure 3.4 Phenotypic analysis of heterozygous mice. 61

Figure 3.5 Cep55 expression in embryonic and adult tissues. 63

Figure 3.6 Human and mouse Cep55 expression during embryonic brain development. 64

Figure 3.7 Breeding strategy for generation of Cep55 cKO mice. 66

Figure 4.1 Schematic of brain cortical layers in rodents. 71

Figure 4.2 Characterizing gross morphological defects in mouse embryonic brain. 73

Figure 4.3 KO brain size is smaller due to a reduction in neurons and astrocytes. 76

Figure 4.4 Characterization of Cep55 in the regulation of neural progenitor cells. 79

Figure 4.5 Characterizing mitotic, proliferation and apoptotic indices in NPCs. 81

Figure 5.1 Hedgehog (Hh) signaling in mammalian cells. 87

Figure 5.2 Cilia abnormalities in Cep55 $^{-/-}$ *mouse neocortex.* 90

Figure 5.3 Cilia abnormalities in Cep55 $^{-/-}$ *MEFs.* 91

Figure 5.4 Cep55 is localized to the basal body protein complex of cilia in MEFs. 92

Figure 5.5 CEP55 is localized to the base of cilia in RPE-1 cells. 94

Figure 5.6 Cep55 $^{-/-}$ *MEFs exhibit proliferation defects.* 96

Figure 5.7 Cep55 $^{-/-}$ *MEFs exhibit multinucleation.* 97

Figure 5.8 Cep55 $^{-/-}$ *MEFs exhibit cell cycle arrest in G2.* 98

Figure 5.9 Cep55$^{-/-}$ MEFs exhibit cytokinesis defects. 99

Figure 5.10 Cep55 regulates Akt/Gsk3β/ β-Catenin/ Myc axis. 101

Figure 5.11 Cep55 regulates Ctnnb1 and Myc in MEFs and brain. 103

Figure 5.12 Effect of Cep55 loss on β-catenin and Myc in brain tissue by IHC. 104

Figure 5.13 Downstream effectors can rescue Cep55 loss. 106

Figure 5.14 Proposed model of Cep55 signaling in neural development. 107

Figure 6.1 CEP55 is overexpressed across different tumors, and its overexpression is linked to poor survival. 114

Figure 6.2 Frequent genetic mutations in lung cancer 118

Figure 6.3 Proliferation defects in Cep55-/- MEFs 119

Figure 6.4 2D and 3D colony-forming potential of E1A/Ras-transformed Cep55$^{+/+}$ and Cep55$^{-/-}$ MEFs 120

Figure 6.5 Tumors of E1A/Ras-transformed MEFs in NOD/SCID mouse. 122

Figure 6.6 IHC analysis of E1A/Ras-transformed Cep55$^{+/+}$, and Cep55$^{-/-}$ tumors in mice. 123

Figure 6.7 OncoPrint of PTEN and CEP55 analyzed from Cancer Genomics cBio-Portal 124

Figure 6.8 Analysis of tumor spectrum in Pten and Cep55/Pten mice. 127

Figure 6.9 Survival of Cep55/Pten and Pten mice 129

Figure 6.10 OncoPrint of co-occurrence of KRAS and CEP55 alternations analyzed from Cancer Genomics cBio-Portal 130

Figure 6.11. Tumor spectrum in Kras G12D-driven lung cancer 132

Figure 6.12 Tumor quantification and tumor burden in Kras-driven lung cancer 133

Figure 6.13 Tumor quantification and tumor burden in Kras-driven lung cancer..... 135

Figure 6.14 Schematic model of Cep55 modulation of tumorigenesis....................... 136

List of Tables

Table 1.1 Frequency (%) of tumor suppressors loss.. 10

Table 2.1 List of PCR primers used in this thesis... 32

Table 2.2 The standard dewaxing protocol... 35

Table 2.3 List of siRNA and shRNA used in this thesis. 42

Table 2.4 List of antibodies used for Immunofluorescence.... 45

Table 2.5 List of antibodies used for WB 48

Table 2.6 PCR cycles protocol.. 50

Table 2.7 qRT PCR primers 51

Table 3.1 Number, percent and genotype of obtained offspring and embryos at different gestational stages 59

Table 6.1 Tumor burden in cKO Cep55/Pten and cKO Pten mice............................. 128

List of Abbreviations

AKT	Protein kinase B
ALIX	Asparagine-linked glycosylation 2–interacting X
ANOVA	Analysis of Variance
ATCC	American Type Culture Collection
AURKA	Aurora A
AURKA	Aurora B
BAD	Bcl-2-Associated Death Promoter
BC	Breast Cancer
BCL2	B-cell lymphoma 2
BLCA	Bladder Urothelial Carcinoma
BRCA	Breast Cancer susceptibility gene
BSA	Bovine Serum Albumin
bTRCP	Beta-transducin repeat-containing protein
BUB	Budding Uninhibited by Benzimidazoles
BUBR1	Budding Uninhibited by Benzimidazoles Receptor 1
CAK	CDK Activating Kinase
CAL	Chromosome Arm-Level
CCNB1	Cyclin B1
CCP	Cell-Cycle Progression
CD	Cluster of Differentiation
CDC	Cell Division Cycle
CDKs	Cyclin-Dependent Kinases
cDNA	Complementary DNA
CENPF	Centrosomal Protein F
CEP	Centrosomal Protein
CEP55	Centrosomal protein 55 kDa
CHFR	Checkpoint With Forkhead and Ring finger domains
CHK1/2	Checkpoint Kinase
CHMP	Charged multivesicular body protein
CIN	Chromosomal Instability
CK	CytoKeratin
cKO	Conditional KO (inducible)
CLs	Cancer Lines
CML	Chronic Myeloid Leukaemia
CNA	Copy Number Alterations
COAD	Colon adenocarcinoma
COADREAD	Colorectal Adenocarcinoma
CP	Cortical plate
CSCs	Cancer Stem Cells
CTA	Cancer Testes Antigen

DCIS	Ductal Carcinoma In Situ
DISC1	Disrupted In Schizophrenia 1 protein
DMEM	Dulbecco’s Modified Eagle’s Medium
DNA	DeoxyriboNucliec Acid
DUSP4	Dual-Specific Phosphatase-4
E14.5	Embryonic day of 14.5 (dpc)
EABR	ESCRT and ALIX-Binding Region
ECM	Extracellular matrix
EGF	Epidermal growth factor
EGFR	Epidermal growth factor receptor
EGL	External granule layer
Egr4	Early growth response-4
EMT	Epithelial-mesenchymal transition
ER	Estrogen Receptor
ERK	Extracellular signal-Regulated kinase
ESC	Embryonic stem cell
ESCRT	Endosomal Sorting Complex Required for Transport
ESCs	Embryonic Stem Cells
EV	Empty vector
FBS	Fetal Bovine Serum
FGFR	Fibroblast Growth Factor Receptor
FOXM1	Forkhead box M1
FOXO	Forkhead box protein O
Foxo1	Forkhead box protein O1
FRET	Florescence Resonance Energy Transfer
Gapdh	Glyceraldehyde 3-phosphate dehydrogenase
GBM	Glioblastoma multiforme
GE	Germinative external-granular
Gfra1	Glial-derived neurotrophic factor family receptor α-1
GIN	Genomic Instability
GLUT4	Glucose Transporter 4
GSI	Gonado-somatic index
GSK-3β	Glycogen Synthase Kinase-3 Beta
H&E	Hematoxylin and eosin
HCC	Hepatocellular Carcinoma
HDAC	Histone DeAcetylase
HER2	Human Epidermal Growth Factor Receptor-2
Het	Heterozygous

HGFR	Hepatocyte Growth Factor Receptor
HMECs	Human Mammary Epithelial Cells
Hom	Homozygous
HR	Homologous Repair
HSP90	Heat shock protein 90
IGF	Insulin-like growth factor
IGF-1R	Insulin-like Growth Factor-1 Receptor
INPP4B	Inositol Polyphosphate-4 Phosphatase Beta
IPC	Intermediate progenitor cells
IZ	Intermediate zone
JAK	Janus Activated Kinase
KD	Knock-down
k-MT	Kinetochore-Microtubule
KO	Knockout (constitutive)
LAMB1	Laminin subunit Beta-1
LAR	Luminal Androgen Receptor Expression
LATS1	Large Tumour Suppressor Kinase 1
Lhx	LIM homeobox
LIHC	Liver Hepatocellular Carcinoma
LOH	Loss Of Heterozygosity
LUAD	lung adenocarcinoma
LUSC	lung squamous cell carcinoma
MAD	Mitotic Arrest Deficient
MAPK	Mitogen-Activated Protein Kinase
MARCH	multinucleated neurons, anhydramnios, renal dysplasia, cerebellar hypoplasia, and hydranencephaly
MBds	midbody derivatives
MCL-1	Myeloid leukamia Cell differentiation protein-1
MDM2	Mouse double minute 2 homolog
MEFs	Mouse Embryonic Fibroblasts
MEK	MAPK or ERK kinase
METABRIC	Molecular Taxonomy of Breast Cancer International Consortium
MKLP1	Mitotic Kinesin-Like Protein
MKS	Meckel-like syndrome
MMP-2	Matrix MetalloProteinase-2
MNC	Multi-nucleated cells
MPS1	Mono Polar Spindle 1
mRNA	messenger RNA
MSL	Mesenchymal Stem-Like

MTMR	Myotubularin-related protein
mTORC	Mammalian Target of Rapamycin Complex
MYT1	Myelin Transcription factor 1

NAC	Neoadjuvant Chemotherapy
Ncx	Neocortex
NEKs	NIMA Related Kinase 1
NEO	neomycin
NF1	NeuroFibromin
NFKB1	NF-κB gene
NHEJ	Non-Homologous End Joining
NPM1	Nucleophosmin 1
NPs	Neural progenitor cells
NSCLC	Non-small cell lung cancer
NSCs	Neural stem cells
NUMA1	Nuclear Mitotic Apparatus Protein 1

OCSCC	Oral Cavity Squamous Cell Carcinoma
OE	Overexpression
OS	Overall Survival
OV	Ovarian serous cystadenocarcinoma

PAAD	Pancreatic adenocarcinoma
PARP	Poly (ADP-Ribose) Polymerase
PAS	Periodic Acid-Schiff
Pax-6	Paired box protein 6
PB1	Polar Body 1
PBDs	Polo Box Domains
PBS	Phosphate Buffered Saline
PBSX	Triton X-100 in PBS
PCL	Purkinje cell layer
PCM	PeriCentriolar Matrix
PCM1	PeriCentriolar Material 1
Pcna	Proliferating cell nuclear antigen
pCR	Pathological Complete Response
PCR	Polymerase Chain Reaction
PDGF	Platelet-derived growth factor
PDGFR	Platelet-Derived Growth Factor Receptor
PDK1	Phosphoinositide-dependent kinase-1
PFA	Paraformaldehyde
PGC	Primordial germ cell
PI3K	Phosphoinositide-3-kinase
PI3K-CA	Phosphatidylinositol-4,5-bisphosphate 3-kinase–catalytic subunit α

PIN1	Peptidyl-prolyl cis-trans Isomerase NIMA-interacting 1
PIP2	Phosphatidylinositol 4,5-bisphosphate
PIP3	Phosphatidylinositol 3,4,5 trisphosphate
PLK	Polo Like Kinases
Plzf	Promyelocytic leukemia zinc finger
PMN	Postmitotic neurons
PR	Progesterone Receptor
PRC1	Protein Regulator of cytokinesis 1
PTEN	Phosphatase and tensin homolog
PTTG	Pituitary tumor transforming gene
qRT-PCR	Quantitative Real-time PCR
RAF	Rapidly Accelerated Fibrosarcoma
RAS	Rat Associated Sarcoma
RB1	Retinoblastoma 1
RGCs	Radial glial cells
RNA	Ribonucleic acid
RNAi	RNA interference
ROR	Risk Of Relapse
RPM	Revolutions Per Minute
RTKs	Receptor Tyrosine Kinases
SAC	Spindle Assembly Checkpoint
SAG	Smoothened agonist
Sall	Sal-like
SD	Standard Deviation
SEM	Standard Error of the Mean
shRNA	Short Hairpin RNA
siRNA	Small Interfering RNA
Sohlh1	Spermatogenesis and oogenesis specific basic helix–loop–helix-1
Sox	Sex-determining region Y-box
STAT3	Signal Transducer and Activator of Transcription 3
STR	Short Tandem Repeats
SVZ	Subventricular zone (the basal surface)
TAA	Tumor-Associated Antigen
TBR1	T-domain transcription factor 1
TBR2	T-domain transcription factor 2
TCGA	The Cancer Genome Atlas
TEX14	Testes Expressed 14
Tg	Transgenic
TGFβ	Transforming growth factor β

TNBC	Triple Negative Breast Cancer
TPX2	Targeting protein for Xklp2
TSC	Tuberous sclerosis protein
TSG101	Tumour Susceptibility Gene 101
UBC	Ubiquitin C
VEGF	Vascular endothelial growth factor
VEGF-A	Vascular endothelial growth factor-A
VZ	Ventricular zone (the apical surface)
WB	Western blot
WES	Whole-Exome Sequencing
Wnt	wingless homolog
Wt	Wid-type

Units

°C	degrees Celsius
g	grams
h	hour(s)
IU	International Units
μg	microgram
μL	microlitre
μm	micrometre
μM	micromolar
kB	kilobases
kDa	kilodaltons
kg	kilograms
L	litre(s)
M	molar
mg	milligram
min	minutes
mL	millilitre
mM	millimolar
mm	millimetre
n	number (sample size)
nM	nanometres
rpm	revolutions per minute
sec	second(s)
U	unit(s)
w/v	weight per volume
v/v	volume per volume

Statement of contribution by others in the thesis

Cep55 floxed ES cells were purchased from the International Knockout Mouse Consortium (IKMC), and heterozygous Cep55 targeted (Cep55) mice were generated by the Australian Phenomics Network (APN) facility. All pathological analyses were performed in collaboration with APN and Professor John Finnie.

Neurohistology and ciliopathy analysis performed under the supervision of A/Professor Dominic Ng and A/Professor Michael Piper in collaboration with Mr. Belal Shohayeb and the QIMR histology facility. The phenotypic analysis of mitotic defects was performed in collaboration with A/Professor Andrew Burgess.

Publications and presentations

Manuscripts prepared for submission compromising a part of the thesis

Behnam Rashidieh, Amanda Louise Bain, Belal Shohayeb, Patrick Fortuna, Debottam Sinha, Andrew Burgess, J. Alejandro Lopez, Peter Blumbergs, John Finnie, Michael Piper, James Edward Hudson, Dominic Ng, Kum Kum Khanna **“Cep55 regulation of PI3K/Akt signaling is required for neocortical development and ciliogenesis“** (Submitted to Progress in Neurobiology (IF= 10.658): Developmental research chapters form this manuscript).

Behnam Rashidieh, Amanda Louise Bain, Debottam Sinha, Pascal Duijf, Rebecca Lane, Keshava Datta, J. Alejandro Lopez, Harsha Gowda, Michelle Hill, Pirjo Apaja, John Finnie, Kum Kum Khanna **“The loss of *Cep55* impedes *Pten* and *Kras*-dependent tumorigenesis in mouse”** (Preparation for finalizing the manuscript: Cancer research chapter form this manuscript).

Publications not relevant to the subject of the thesis but arising at the time of the thesis

Vahideh Assadollahi & Behnam Rashidieh*, Masoud Alasvand, Alina Abdolahi, J. Aljandro Lopez* **“Interaction and molecular dynamics simulation study of Osimertinib (AstraZeneca 9291) anti-cancer drug with Kinase domain of EGFR in native protein and mutated L844V and C797S”**: Journal of Cellular Biochemistry, March, 2019

Conference presentations

- Behnam Rashidieh*, Amanda Bain, Alejandro Lopez, Kum Kum Khanna “*CEP55* depletion can delay tumorigenesis through GSK3β/ β-Catenin/ Myc axis downstream of Akt signaling pathway, Lorne Cancer Conference, 2019.
- B. Rashidieh* ,A. Bain, B. Shohayeb, A. Lopez, D. Ng, K. Khanna, ”Cep55 regulates ciliogenesis and neocortex development in the embryonic mouse” The 38th Annual Scientific Meeting of the Australasian Neuroscience Society, 3- 6 December 2018, Brisbane.
- Oral Presentation, “Characterization of a knockout mouse model of cep55”: QIMRB student symposium, July 2018.
- Oral Presentation, “*In vivo* and *In vitro* investigations of the Centrosomal protein 55”: QIMRB Early career research seminar, Sep. 2017.
- Oral presentation, “Centrosomal protein 55 depletion can lead to embryonic lethality in a knock-out mouse model”: QIMRB student symposium, July 2017 .
- B Rashidieh*, Amanda Bain, A Lopez, K Khanna, “Investigating the *in vivo* role of Centrosomal protein 55”: QIMR Berghofer 9th biennial student retreat 14-15 September 2017, Binna Burra mountain lodge, lamington national park.
- B Rashidieh*, A Lopez, K Khanna “Centrosomal protein 55 depletion can lead to embryonic lethality in a breast cancer mouse model” : 12th international Breast Cancer Congress, SB Medical Uni, Tehran, Iran Feb 2017.

A note on nomenclature

The symbol of genes and proteins used in this thesis are based on standard nomenclature. Human gene symbols are fully in uppercase and italicized (*CEP55*), and protein symbols are all in uppercase, without italicization (CEP55). Mouse gene symbols are all italicized with only the first letter in uppercase (*Cep55*) while the mouse protein symbols are not italicized, with only the first letter in uppercase (Cep55).

Chapter 1. Literature Review

1.1 Centrosomal Protein 55 kDa

Centrosomal protein 55kDa (*CEP55, also known as FLJ10540*) was first discovered in our laboratory as a pivotal player of cytokinesis, the last stage of cell division (Fabbro, *et al.*, 2005). CEP55 is a cancer-testis antigen that is predominantly expressed in the testes but not in somatic tissues. Interestingly, the expression of *CEP55* is highly upregulated in a broad spectrum of tumors (Shiraishi *et al.*, 2011). Over the past decade, *CEP55* has been reported to play a critical role in multiple processes, including regulation of the PI3K/AKT pathway (Chen *et al.*, 2007), stemness (Kuo *et al.*, 2014), aneuploidy (Fabbro, *et al.*, 2005), maintaining genomic stability (Kalimutho *et al.*, 2018), and cell cycle progression (Kumar *et al.*, 2013). This literature review will provide an overview of *CEP55*, the topic of this thesis, in these processes (Fig. 1.1).

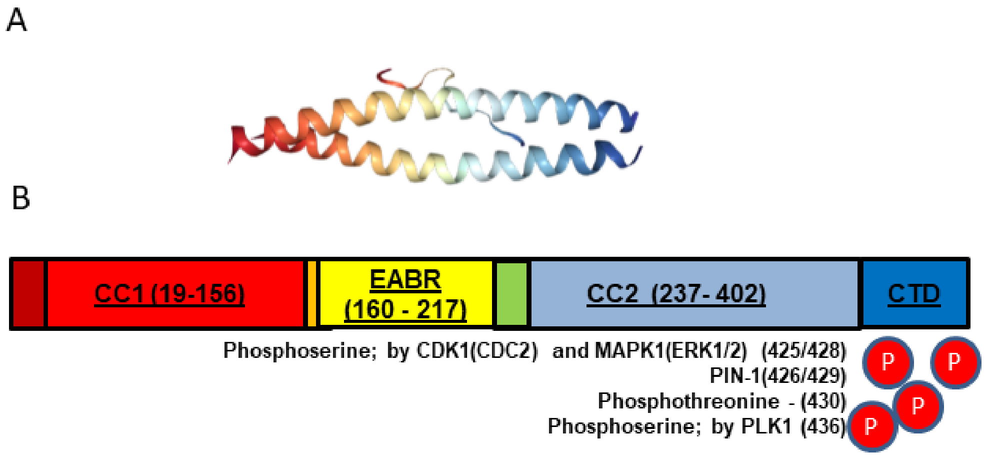
A
B
CC1 (19-156)
EABR
(160 - 217)
CC2 (237- 402)
CTD
Phosphoserine; by CDK1(CDC2) and MAPK1(ERK1/2) (425/428)
PIN-1(426/429)
Phosphothreonine - (430)
Phosphoserine; by PLK1 (436)
P
P
P
P

C

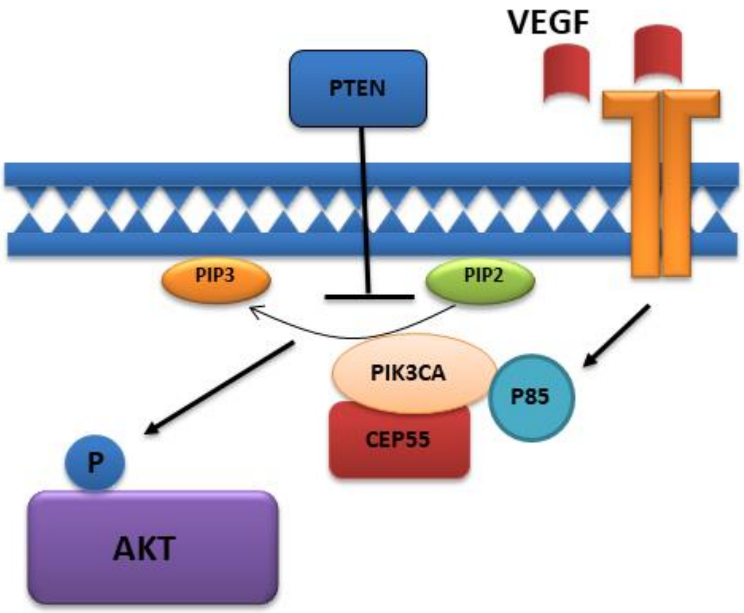

Figure 1.1 CEP55 structure and mechanism in regulating AKT signaling.

(A) The 3D structure of coiled-coil homodimer of CEP55, PDB ID= 3E1R, adopted (Lee et al., 2008); (B) Schematic presentation of CEP55 domains and phosphorylation sites. (C) CEP55 is a regulator of the AKT pathway. CEP55 after VEGF translocation into the cytoplasm binds to p110 (PIK3CA) and forms a complex to convert PIP2 into PIP3 and activate AKT by the phosphorylation. Diagram illustrated based on information from (J Jeffery *et al.*, 2016).

1.2 CEP55 during the Cell Cycle and Mitosis

1.2.1 The Cell Cycle

The cell cycle is comprised of 3 states and 4 phases, starting with the interphase state [Growth-1 (G_1), Synthesis (S), Growth-2 (G_2)], and followed by cell division (Mitosis (M). Additionally, some cell types, such as stem cells, experience a quiescent stage, referred to as the G_0 phase (Baserga, 1968; Boward, Wu and Dalton, 2016). Cell cycle homeostasis is mainly controlled by cyclin-dependent kinases (CDKs) and their reciprocal cyclin partners (Nasmyth, 1995; Sanchez-Martinez *et al.*, 2015; Orzáez, Medina and Pérez-Payá, 2016; Wingren and Nyesiga, 2018; Sánchez-Martínez *et al.*, 2019).

The first stage of the cell cycle, G_1, occurs with the cell synthesizing the requisite mRNA and proteins to undergo DNA replication. Following this, cells move to S phase, in which DNA replication occurs, and during G_2 the cell continues to grow and prepare for separation, ensuring proper mitosis (Boulikas, 1995; Zopf *et al.*, 2013), (Fig. 1.2). *Cep55* is involved in regulation of the final stage of mitosis called cytokinesis, a process that divides the cytoplasm equally between two daughter cells after karyokinesis i.e. segregation of daughter cell nuclei (Sontag *et al.*, 1995; Chemudupati, Johns and Osmani, 2019; Holder, Poser and Barr, 2019).

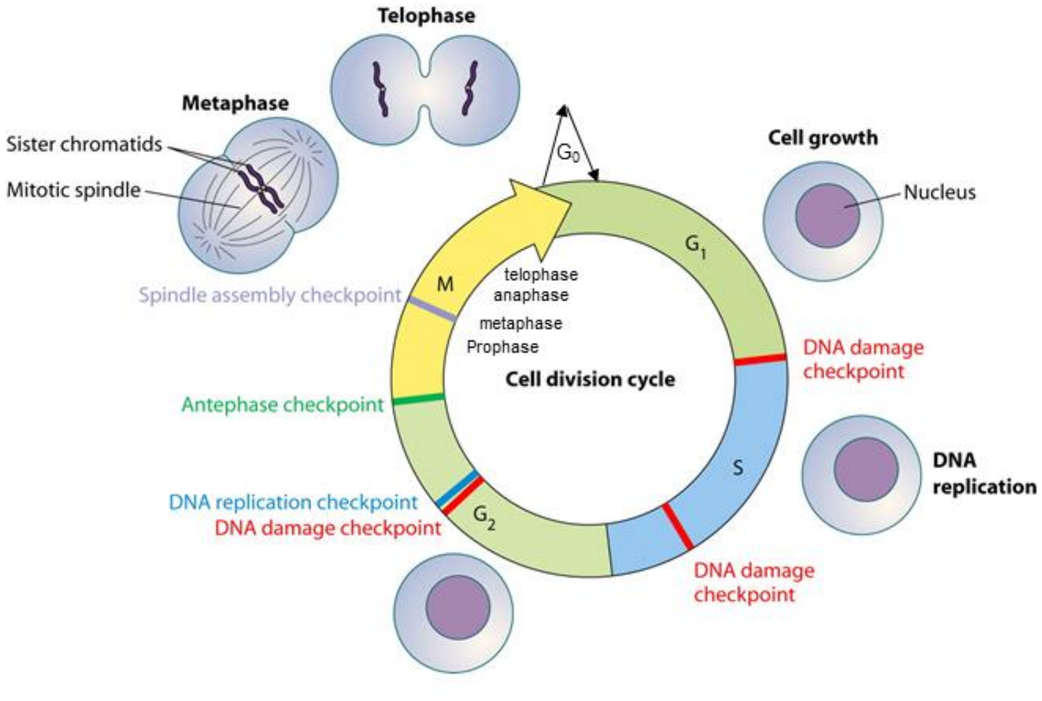
Telophase
Metaphase
Sister chromatids
Mitotic spindle
G_0
Cell growth
Nucleus
G_1
M
telophase
anaphase
metaphase
Prophase
Cell division cycle
Spindle assembly checkpoint
DNA damage checkpoint
Antephase checkpoint
S
DNA replication
DNA replication checkpoint
DNA damage checkpoint
G_2
DNA damage checkpoint

Figure 1.2 The cell cycle stages and phases.

The cell cycle in eukaryotes classified into two main stages: interphase (including $G_{0,}$ G_1, S, and G_2) and the mitosis (M) phase (including mitosis and cytokinesis). The cell cycle and checkpoint pathways such as DNA replication, DNA damage, and the spindle assembly checkpoint (SAC) prevent cells from undergoing mitosis in the presence of stress **(**Adopted from (Chin and Yeong, 2010), Copyright License # 3001471964).

1.2.2 Mitosis

There are four major mitotic phases: prophase, metaphase, anaphase, and telophase. During prophase, the nuclear membrane dissolves, and the condensed chromatin forms chromosomes. Following this, sister chromosomes are aligned after being attached by spindle fibers at the kinetochore (metaphase). The sister chromosomes are then pulled to opposite poles by centrioles (anaphase). Due to overlapping spindle microtubules during separation, the spindle mid-zone is formed, and this structure is able to stimulate the cortex of the cell to ensure proper ingression and cleavage furrow formation during cytokinesis. Finally, in telophase, the division of nuclear membrane takes place by the formation of two daughter nuclei prior to initiating cytokinesis (Eggert, Mitchison and Field, 2006; Hengeveld *et al.*, 2017; Ballew and Lacefield, 2019).

1.2.3 Cytokinesis

Cytokinesis begins with a cleavage furrow mediated by an actomyosin ring contraction (Steigemann and Gerlich, 2009; D'Avino, Giansanti and Petronczki, 2015). Following this, the transformation of the spindle mid-zone into the midbody occurs as an intercellular bridge that forms the last connection between the two daughter cells (Mullins and Biesele, 1977; Juanes and Piatti, 2016). This structure, also known as a Flemming body, consists of microtubules and provides an anchor to the intervening cleavage furrow. The midbody remains until cell abscission, the last stage of cytokinesis (Barr and Gruneberg, 2007; Ruchaud, Carmena and Earnshaw, 2007).

During cytokinesis, the midbody tightens the cytokinetic bridge at the cleavage furrow by recruiting the abscission machinery, and the rupturing of this bridge leads to final abscission (Mierzwa and Gerlich, 2014). The endosomal sorting complexes required for transport (ESCRT) machinery, consisting of cytosolic protein complexes, plays a central role in this abscission process (Raiborg and Stenmark, 2009; Addi, Bai and Echard, 2018).

1.2.4 CEP55 regulates cytokinesis

CEP55 is a coiled-coil protein, and similar to other coiled-coil proteins, including Pericentrin-B and CG-NAP, localizes to the centrosome, specifically the pericentriolar matrix during interphase (Fabbro *et al.*, 2005). During mitosis, CEP55 localizes to the spindle pole at late prophase, which becomes the mitotic spindle at prometaphase and metaphase. When the cell enters anaphase, CEP55 remains on the mitotic spindle until cytokinesis, when CEP55 localizes to the spindle midzone and then at the midbody (Zhao, Seki and Fang, 2006; Hu *et al.*, 2012; Xu *et al.*, 2015)

CEP55 protein contains a central functional domain known as the ESCRT and ALIX-binding region (EABR), which can bind to TSG101 or ALIX, respectively. The EABR region of CEP55 plays a vital functional role in cytokinesis (Jeffery *et al.*, 2016). At the C-terminal, CEP55 is phosphorylated at multiple residues during mitosis (S425, S428, S436) and these phosphorylation events are known to regulate stability and localization of CEP55 during mitosis (Fig. 1.1) (Fabbro, *et al.*, 2005; Martinez-Garay *et al.*, 2006; Bastos and Barr, 2010). The localization of CEP55 to the midbody is possibly dependent on other interactions, such as MKLP1 of the centralspindlin complex (Zhao, Seki and Fang, 2006) and breast and ovarian cancer susceptibility gene (BRCA2) (Mondal et al 2012). Additionally, Syntaxin16, a master regulator of cytokinesis and a membrane fusion protein, regulates cytokinesis by recruiting CEP55, endosomes, and recycling endosome-associated exocysts to the midbody and forming soluble N-ethylmalei-mide–sensitive factor attachment protein receptor (SNARE) complexes (Neto *et al.*, 2013). During mitosis, CDK1 and ERK2 phosphorylate CEP55 on serine 425 and 428 (Fabbro *et al.*, 2005) and facilitate its interaction with PIN1. This association with PIN1 stabilizes CEP55 and leads to further phosphorylation by Polo-like kinase 1 (PLK1) on serine 436 (van der Horst and Khanna, 2009). Phosphorylation also dictates how CEP55 plays its functional role in cellular events of cytokinesis because expression of a Cep55 mutant protein which was unable to be phosphorylated on these residues caused cytokinesis failure due to multinucleation and midbody arrest (Fabbro *et al.*, 2005). PLK1 mediated phosphorylation of CEP55 prevents its premature recruitment to the anaphase spindle (Bastos and Barr, 2010).

1.3 CEP55 in Cancer

1.3.1 Definition of Cancer

Cancer is the definition given to a group of genetic diseases in which transformed normal cells turn malignant and is one of the leading cause of death worldwide (Bray *et al.*, 2018). Based on their cellular origin, cancers can be broadly categorized into three groups. Most cancers stem from epithelial cells and are classified as carcinoma. However, mesoderm cells such as bone or muscle can lead to sarcoma, while adenocarcinoma can be driven from glandular tissues like the breast (Travis *et al.*, 2015).

During cancer formation, abnormal cells undergo rapid and uncontrolled division and can eventually invade other parts of the body leading to the spread of the disease (Lambert, Pattabiraman and Weinberg, 2017). This invasion, referred to as metastasis, can result in settlement of cancerous cells in a distant location from the primary tumor (Steeg, 2016). Metastasis is a significant cause of cancer-related mortality (Stewart and Wild, 2014).

Cancer is a multistage disease which stems from an interaction between individuals' internal genetic factors and external agents, (carcinogens), which can be physical (e.g. Ultraviolet or Ionizing Radiation), chemical (e.g Tobacco or Aflatoxin) or biological (particularly infection) (Minamoto, Mai and Ronai, 1999; Parsa, 2012). Most carcinogens can cause mutations, and are therefore also known as mutagens. Two classes of mutated genes are linked to cancer development, namely oncogenes and tumor suppressors (Weinberg, 1991; Pierotti *et al.*, 2016). A gene that has the potential to cause cancer by a gain of function, often through a mutation, is called an oncogene. A proto-oncogene is a normal gene with oncogenic potential that could become an oncogene due to mutation or increased expression. Oncogenes commonly encode proteins that regulate cell growth and differentiation, and some of the most well-characterized oncogenes such as *RAS*, *WNT*, *MYC*, *ERK*, and receptor tyrosine kinase (RTK) are involved in these processes (Lamballe, Klein and Barbacid, 1991; Sever and Brugge, 2015; Ghosh, Ghartimagar and Thapa, 2016; Wala and Beroukhim, 2016). Commonly, oncogenes can be categorized as growth factors or mitogens, receptors, and cytoplasmic tyrosine kinases or serine/threonine kinases, regulatory GTPases, or transcription factors (Fig. 1.3) (Yang and Huang, 2015).

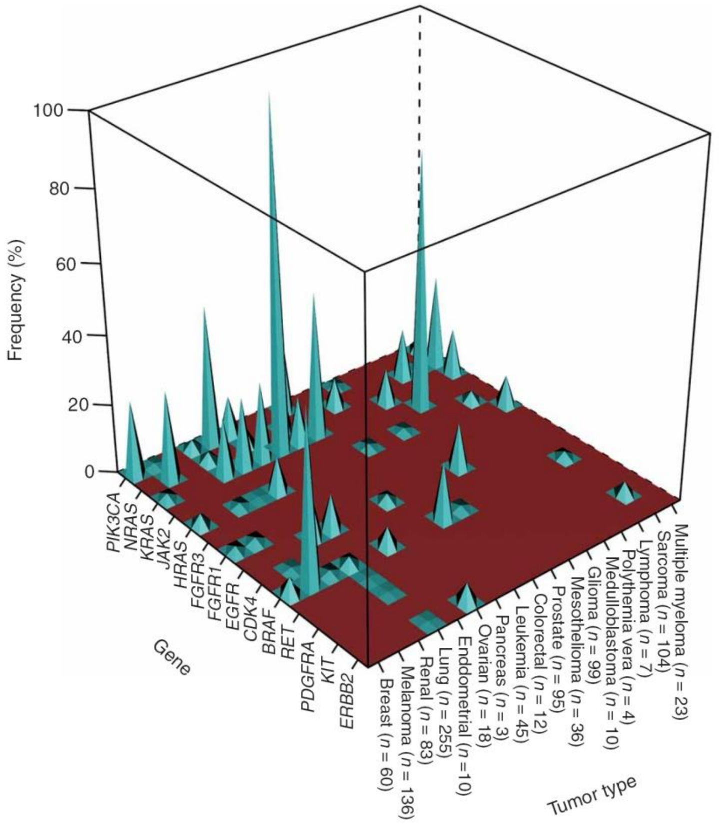

Figure 1.3 The percent of oncogene mutations across human tumor types.

The frequency of mutation in percent (Y-axis) of different oncogenes (Gene on X-axis) across various tumor types (Z-axis) and the corresponding number of patients in the study. (Adopted from Chial, H., 2008 Proto-oncogenes to oncogenes to cancer. Nature Education 1(1):33, under licensed CC BY-SA 3.0).

In contrast, tumor suppressors are genes in which reduction or loss of function (often by mutation) can lead to cancer. Tumor-suppressor genes often encode for proteins with a repressive effect on the regulation of the cell cycle or promote apoptosis. The most well-characterized tumor-suppressor gene, TP53, is mutated in more than 50% of cancers (Wang *et al.*, 2018). Retinoblastoma (Rb), *PTEN*, *ARF* and *INK4* are other common tumor-suppressors frequently observed to be mutated in cancers (Tab. 1.1) (Sherr, 1996; Cantley and Neel, 1999; Sherr and McCormick, 2002; White, 2005; Kim and Sharpless, 2006; Ozenne *et al.*, 2010; Flavahan, Gaskell and Bernstein, 2017).

Tp53 is mutated in about half of all tumors and it plays a key role in the carcinogenesis of various malignancies. The incidence of p53 mutations is high in solid tumors and lower in hematological malignancies. P53 mainly controls cell cycle arrest (through the regulation of genes including the cyclin-dependent kinase inhibitor p21Waf1/Cip1 and the protein GADD45) or apoptosis (via genes such as Bax and Bcl-2). Inactivation of p53, predominantly through point mutations, predisposes cells to the acquisition of oncogenic mutations and gives rise to genomic instability (Kirsch et al 1998, Xu et al 2011). Generally, the tumor suppressor function of p53 is lost after a mutation; however, some missense changes in Tp53 lead to gain-of- new functions (GOF) enabling them to act as oncogenes and subcellular localization of p53 mutants regulate different components of cell physiology and epigenetic signal transduction (Monique et al 2000, Bargonetti and Prives J Mol Cell Biol 2019). This GOF promotes tumor progression, invasion, metastasis, and drug resistance (Moshe Oren ET AL 2010). Particularly, GOF p53 mutants undergo stabilization in tumors. This stabilization generates an oncogenic addiction which may be useful to target mutant p53 as a therapeutic vulnerability (Schulz-Heddergott et al 2018).

	TSG	**LOH/HD (%)**	**Mutation (%)**
1	**TP53**	Leukemia (50), Brain(24-53), Head & Neck(47-66), Lung(90), Esophageal(67.5), Gastric(0-83), Colorectal(66), Hepatocellular (16), Bladder(73), Renal(20-48), Prostate(32-39), Breast(49), Ovarian(44-63), Cervical(20), Endometrial(19-32).	Leukemia (17.3), Brain (34), Head & Neck(47), Lung(88), Esophageal(50-60), Gastric(0-77), Colorectal(66), Pancratic(43), Hepatocellular (51), Bladder(23-61), Renal(0-33), Prostate(6-13), Breast(8-39), Ovarian(20.7-23), Endometrial(14-22).
2	**RB1**	Leukemia (33-55), Brain (0-25), Head & Neck(42-68), Lung(62.5), Esophageal(34), Gastric(29), Colorectal(50), Pancratic(6), Hepatocellular (33-50), Bladder(12.5-29), Renal(60), Prostate(5-60), Breast(26-47), Ovarian(61), Cervical(62.8),Endometrial(33).	Brain (0-30), Lung (20), Esophageal(9), Hepatocellular (15), Bladder(27), Prostate(16), Ovarian(67).
3	**p16** **INK4a**	Leukemia (4-76), Brain (31), Head & Neck(2-55), Lung(29), Esophageal(17-22), Gastric(0-9), Colorectal(81), Pancratic(30), Hepatocellular (7), Bladder(32), Renal(2-16), Prostate(4), Breast(0-10), Ovarian(0-14), Cervical(17), Endometrial(8-13).	Leukemia (0-7), Brain (1-45), Head & Neck (1-45), Lung(0-70), Esophageal(0-52), Gastric(0-2), Pancratic(17-38), Bladder(0-7), Prostate(0-6), Breast(3-5), Ovarian(0-11), Endometrial(13).
4	**p14** **ARF**	Leukemia (5), Brain (50: HD), Head & Neck (27-33), Lung (23-79), Esophageal(33), Gastric(71.4), Hepatocellular (69), Bladder(22), Renal(23.5-83), Prostate(4), Breast(21).	Leukemia (34), Brain (12), Head & Neck (12: HD), Lung (23), Hepatocellular (4).
5	**PTEN**	Leukemia (0-20), Brain (53), Head & Neck(41-71), Esophageal(9), Gastric(4.4), Colorectal(9), Pancratic(35), Bladder(24), Renal(27), Prostate(33), Breast(31-63.3), Ovarian(39), Cervical(36), Endometrial(50).	Brain (20-40), Head & Neck(9-23), Lung(1.6-9.8), Esophageal(3), Gastric(18.7), Colorectal(2-8), Hepatocellular (3), Bladder(2), Renal(5-7), Prostate(15), Breast(2-5), Ovarian(8), Cervical(4),Endometrial(45).
6	**BRCA1**	Gastric (40), Colorectal (39.8), Hepatocellular (12), Breast (21-42), Ovarian (66), Cervical (5-9), Endometrial (24).	Head & Neck (5.72), Breast (3.9), Ovarian (15), Endometrial (3).
7	**CHK** **1/2**	Colorectal (Frequent), Bladder (6), Breast (44), Ovarian (54).	Leukemia (0-2), Gastric (2), Bladder (3), Prostate (1.2), Ovarian (2.3).

Table 1.1 Frequency (%) of tumor suppressors loss of heterozygosity (LOH), heterozygous deficiency (HD), and mutations across different human tumor types. (extracted from available data of a review on tumor-suppressors (Wang et al., 2018)).

1.3.2 Hallmarks of Cancer

Studies have shown cancers to exhibit several common characteristics, collectively referred to as hallmarks of cancer (Hanahan and Weinberg, 2000, 2011)

1- Uncontrolled growth and proliferation (independence in growth signals)

2- Evading inhibitory growth signals (cell signaling and cell cycle deregulation)

3- Evading programmed cell death (apoptosis)

4- Limitless replicative potential leading to immortality through the bypass of senescence

5- Sustained angiogenesis

6- Tissue invasion and metastasis

In the updated hallmarks, Hanahan and Weinberg, 2011, proposed two new hallmarks: evading the immune surveillance and genomic instability as enabling characteristics of the last six main hallmarks.

These biological features are acquired during the multistage process of tumorigenesis. As mentioned above, underlying these hallmarks is genome instability that can drive tumor progression through the additional stress overload on the tumor, such as metabolic, proteotoxic, mitotic, oxidative, and DNA damage stress (Fig. 1.4) (Luo, Solimini and Elledge, 2009).

Multiple cellular pathways can lead to limitless replication potential of cancer cells. One example is through the maintenance of telomeres at a length above a critical threshold

(Harley, 2008). Telomeres consist of repetitive sequences of DNA (TTAGGG) connected to protein complexes, which prevent them from being recognized by the DNA-damage machinery (Greenberg *et al.*, 1999; Chiodi and Mondello, 2016). According to the inability of the DNA replication machinery to reach the ends of DNA, telomeres progressively shorten with multiple rounds of replication and activate growth arrest and senescence. However, in many cancers, aberrant activation of telomerase expression (Wright, Pereira-Smith and Shay, 1989; Shay, 2016) or the alternative mechanism (ALT) of recombination-based interchromosomal exchange DNA replication (Matsuoka *et al.*, 2007) can occur, maintaining telomere length and effectively immortalizing cancer cells.

Another mechanism that can promote tumor out-growth is the formation of new blood vessels (angiogenesis), which supply oxygen and nutrients to the cancer cell. Proliferating cells have an intrinsic ability to promote blood vessel growth, which enables their capability for expansion (Bouck, Stellmach and Hsu, 1996) through the regulation of angiogenic signals such vascular endothelial growth factor (VEGF) and acidic and basic fibroblast growth factors (FGF1/2) (Goel and Mercurio, 2013).

Mitogens or growth signals can transform inactive normal cells into an active proliferative state. This induction of mitosis activates signal transduction pathways, including mitogen-activated protein kinase (MAPK). Oncogenes can mimic this process to cause proliferation and stimulate cellular signals. Many cancer cells acquire the ability of synthesizing of growth factors (GFs) (Stoscheck and King, 1986; Thorpe, Yuzugullu and Zhao, 2015).

Another common pathway of cancer pathogenesis includes deregulation of cell surface receptors, which transduce growth-stimulatory signals and overexpression of GF receptors, often carrying tyrosine kinase activity in their cytoplasmic domains (Slamon, 1987; Regad, 2015) The constitutive activation of signaling pathways downstream of these abnormal receptors can provide growth factor independence and usually reduces or eliminates the sensitivity to growth-inhibitory signals. Insensitivity to antigrowth signals is a trait that enables cancer cells to evade from the cellular proliferation block (Ohtani and Hara, 2013; Zhao and Adjei, 2015; Hallinan *et al.*, 2016). Furthermore, the capacity of cancer cells for unrestricted growth relies not only on their ability to increase cell proliferation but also to escape cell death and develop resistance mechanisms to apoptosis. The apoptotic machinery components are continually monitoring cellular conditions to determine whether the cell undergoes death or remains alive. Any abnormalities such as signaling deregulation, DNA damage, survival factor insufficiency and hypoxia detected by sensors and effectors can activate apoptosis (Ashkenazi and Dixit, 1999; Roos and Kaina, 2006; Karimian, Ahmadi and Yousefi, 2016). Cancer cells can develop apoptotic resistance through a variety of mechanisms, including the loss of proapoptotic regulators such as the p53 tumor suppressor gene through mutation. In addition, activation of *PI3K/AKT* signaling, which transduces anti-apoptotic signals, is involved in apoptotic deregulation in multiple tumor types (Kuwahara *et al.*, 2000). This survival signaling can be triggered by extracellular factors such as IGF-1/2 or IL-3 (Evan and Littlewood, 1998), by intracellular signals from Ras (White, 2005), or by the loss of the phosphatase and tensin homolog deleted on chromosome ten (*PTEN*) tumor suppressor, a phospholipid phosphatase that typically attenuates the AKT survival signal (Cantley and Neel, 1999). Deregulation of cellular signaling (listed in Fig. 1.5) can lead to malignancy. *CEP55* is a well-known regulator of AKT signaling in which its deregulation from this signaling can result in cancer (Jeffery *et al.*, 2016). The binding of CEP55 to the *PI3K* catalytic subunit, PIK3CA (p110), promotes activation of downstream AKT pathway signaling (Chen *et al.*, 2012).

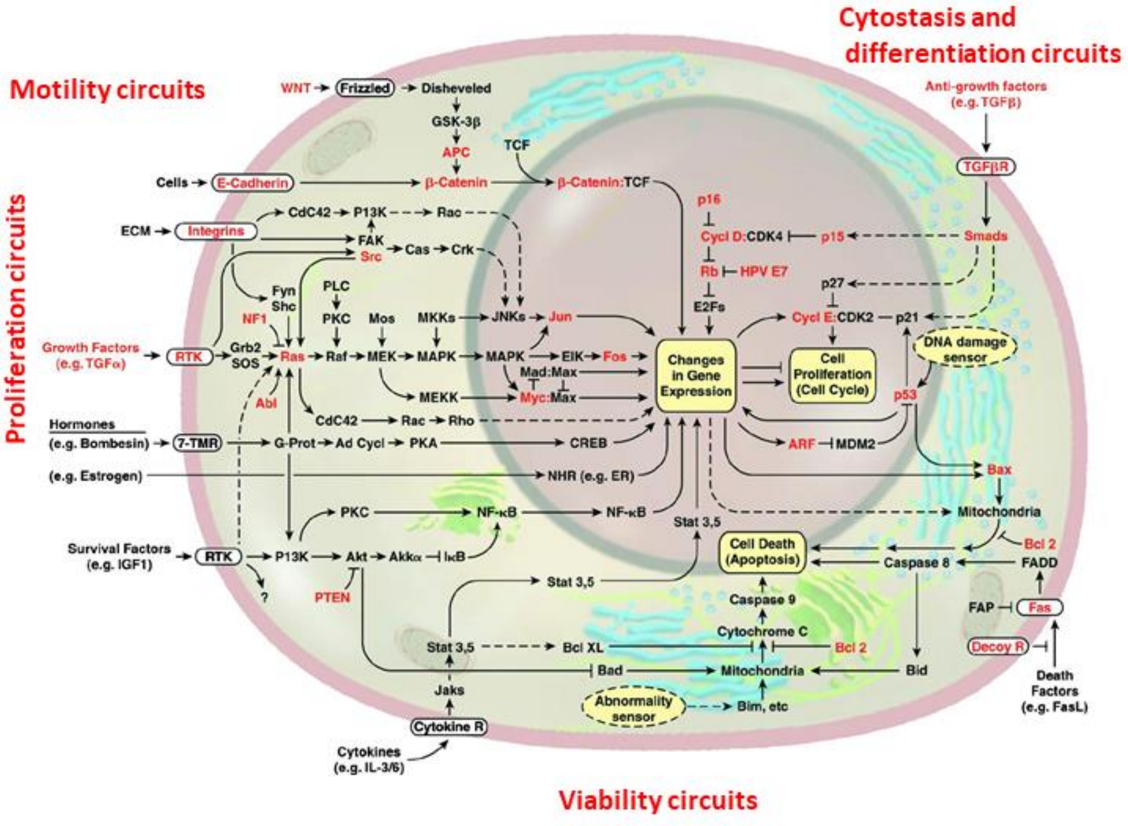
Motility circuits
Cytostasis and differentiation circuits
Proliferation circuits
Viability circuits
WNT
Frizzled
Disheveled
GSK-3β
APC
TCF
Cells
E-Cadherin
β-Catenin
β-Catenin:TCF
ECM
Integrins
CdC42
P13K
Rac
FAK
Src
Cas
Crk
Fyn
Shc
PLC
PKC
Mos
MKKs
JNKs
Jun
NF1
Growth Factors
(e.g. TGFα)
RTK
Grb2
SOS
Ras
Raf
MEK
MAPK
MAPK
ElK
Fos
Mad:Max
MEKK
Myc:Max
Abl
CdC42
Rac
Rho
Hormones
(e.g. Bombesin)
7-TMR
G-Prot
Ad Cycl
PKA
CREB
(e.g. Estrogen)
NHR (e.g. ER)
PKC
NF-κB
NF-κB
Survival Factors
(e.g. IGF1)
RTK
P13K
Akt
Akkα
IκB
?
PTEN
Stat 3,5
Stat 3,5
Stat 3,5
Bcl XL
Bad
Jaks
Cytokine R
Cytokines
(e.g. IL-3/6)
Anti-growth factors
(e.g. TGFβ)
TGFβR
Smads
p16
Cycl D:CDK4
p15
Rb
HPV E7
E2Fs
p27
Cycl E:CDK2
p21
Changes
in Gene
Expression
Cell
Proliferation
(Cell Cycle)
DNA damage
sensor
p53
ARF
MDM2
Bax
Mitochondria
Bcl 2
Cell Death
(Apoptosis)
Caspase 8
FADD
Caspase 9
Cytochrome C
Bcl 2
Mitochondria
Bid
FAP
Fas
Decoy R
Abnormality
sensor
Bim, etc
Death
Factors
(e.g. FasL)

Figure 1.5 Pathways in human cancer.

Diagram of a cell showing the interaction and connection of different signaling molecules and pathways to promote various cellular functions. Point arrows are activators of molecules or reactions, and in contrast, bar-ended arrows are inhibitors. Schematic view of active and inactive signaling molecules contributing to promote the specific function, i.e., Akt pathway categorized as viability (survival) signaling interacts the with Ras proliferative pathway. The growth and proliferation signaling circuit centered around Ras and the other components transmits antigrowth, differentiation, or apoptotic mediated signals. The highlighted genes in red are known to be functionally altered in cancer. (Adopted by permission (Hanahan and Weinberg, 2011) Licence No. #4613340163096)

1.3.3 PI3K/AKT signaling and Cancer

The phosphatidylinositol-3-kinase (PI3K)/AKT is one of the most crucial pathways for cell proliferation, growth, and survival, and its dysregulation has been observed in many cancer types (Faes and Dormond, 2015; Stark *et al.*, 2015; Mayer and Arteaga, 2016). The AKT pathway also modulates many additional signaling pathways through phosphorylation of various targets such as the mammalian target of rapamycin (mTOR)

(Bodine *et al.*, 2001), Glycogen synthase kinase 3 beta (GSK-3β) (Léger *et al.*, 2006), Mouse double minute 2 homolog (MDM2) (Mayo and Donner, 2001), nuclear factor kappa-light-chain-enhancer of activated B cells (NF-κB) (Grandage *et al.*, 2005), Forkhead Box O1 (FOXO1- aka FKHR) (Tang *et al.*, 1999) and BCL2-Associated agonist of cell death (BAD) (Datta *et al.*, 1997; Manning and Cantley, 2007).

Many tumors exhibit a dependency on AKT signaling to survive, and dysregulation of this pathway is frequently observed in neoplasms (Luo, Manning and Cantley, 2003). Mutations in *PIK3CA*, the catalytic and regulatory subunit of PI3K, are the most frequent genetic alteration of this pathway where these mutations increase the activity of AKT. This hyperactivity induces cellular transformation, increases growth factors, anchorage-independent growth, resistance to anoikis (a type of apoptosis), and as a consequence, induces tumorigenesis and accelerates cancer progression (Mayer and Arteaga, 2016). This pathway exhibits gain-of-function in many cancers and has therefore been a topic of intensive investigation for targeting in cancer therapy (Luo, Manning and Cantley, 2003). Akt, a serine/threonine kinase (also called protein kinase B or PKB) has three isoforms homologous in their catalytic domains but varying in their regulatory and other protein domains. Akt1 and Akt2 are ubiquitously expressed, while Akt3 is found predominantly in the brain, heart, and kidneys (Martelli *et al.*, 2012). While Akt2 plays a functional role in the insulin signaling pathway, Akt1 activation occurs downstream of PI3K as the first effector of PI3K pathway (Hyman *et al.*, 2017; McRee *et al.*, 2018).

The PI3K heterodimer consists of two subunits: the regulatory subunit (p85) and the catalytic subunit (PI3KCA, p110). The regulatory subunit (p85) that binds and inhibits p110alpha in a hetero-dimer. Upon release of this inhibitory effect after growth factor stimulation, p85 allows p110 activation which generates the second messenger PIP3 that in turn activates AKT on T308 (Cantley, 2002). These PI3K subunits phosphorylate phosphatidylinositol 4,5 bisphosphate (PIP2) to phosphatidylinositol 3,4,4-triphosphate (PIP3), leading to subsequent phosphorylation of Akt and activation of its downstream signaling to impact cell survival, cell cycle, and proliferation (Zhao and Vogt, 2008).

Conversely, PTEN, a major tumor suppressor, can dephosphorylate PIP3 into PIP2 (Maehama and Dixon, 1998). The loss of PTEN and activating mutations in PIK3CA are among the most common aberrations seen in human malignancies, including breast cancer (BC) (Zardavas, Phillips and Loi, 2014). Although PI3K/AKT has drawn considerable attention in the cancer biology setting for targeting as an anticancer treatment, accumulating studies have revealed high toxicity and adverse effects of treatment with pan-PI3K/AKT inhibitors (Wang, Chen and Hay, 2017). Resistance to these drugs further limits the use of PI3K/AKT inhibitors for cancer treatments, especially in breast cancer (Berns *et al.*, 2007; Gil, 2014; Bahrami *et al.*, 2018).

1.3.4 CEP55 and the PI3K/AKT pathway

CEP55 overexpression is associated with progression of multiple cancer types, including breast (Inoda *et al.*, 2009), lung (C. H. Chen *et al.*, 2009), colon (Sakai *et al.*, 2006), prostate (Shiraishi *et al.*, 2011), ovary (Zhang *et al.*, 2016), head and neck (Waseem *et al.*, 2010), naso/oropharyngeal (Janus *et al.*, 2011; Shiraishi *et al.*, 2011), glioma (F. Li *et al.*, 2018) and liver (M. Li *et al.*, 2018). In tumors, *CEP55* upregulation often correlates with activation of the PI3K/AKT pathway, and this correlation has been shown to alter the tumor microenvironment across multiple cancers (Lien, Dibble and Toker, 2017).

CEP55 overexpression has been reported to promote the progression of hepatocellular carcinoma (HCC) and lung adenocarcinoma through stimulating invasion and cell migration in a PI3K/AKT dependent manner (Chen et al., 2007, Chen et al., 2009b). Similarly, elevated levels of *CEP55* stimulated upregulation of PI3K/AKT in gastric carcinoma, which consequently inhibited p21^{Cip1} expression to dysregulate the cell cycle (Tao *et al.*, 2014). As described above, stimulation of the AKT pathway results from Phosphoinositide 3-kinase (PI3K)-driven conversion of phosphatidylinositol 4,5-bisphosphate (PIP2) to phosphatidylinositol 3,4,5 trisphosphate (PIP3) by phosphorylation which results in phosphorylation and activation of AKT (Manning and Cantley, 2007; Hemmings and Restuccia, 2012). CEP55 has been shown to bind to PI3KCA (Catalytic subunit of PI3K, p110) and modulate this process where the interaction between CEP55 and p110 stabilizes this catalytic subunit and enhances S473 phosphorylation and subsequently increases AKT activation (Chen *et al.*, 2007). VEGF-A can also facilitate this process, stimulating the translocation of CEP55 from the cytoplasm to the plasma membrane, where the interaction between CEP55 and p110 occurs (C. H. Chen *et al.*, 2009). This localization is promoted by the interplay between VEGF-A and the extracellular matrix protein, Fibulin-5 (Hwang *et al.*, 2013). Both amplification of VEGF-A expression (promotes angiogenesis) (Goel and Mercurio, 2013) and Fibulin-5 dysregulation (antagonizes angiogenesis) is correlated with tumorigenesis (Yanagisawa, Schluterman and Brekken, 2009).

1.3.5 CEP55 and FOXM1

CEP55 is known to be a direct transcriptional target of Forkhead Box M1 (FOXM1) (Gemenetzidis *et al.*, 2009; Waseem *et al.*, 2010). FOXM1 overexpression has also been reported in several cancers (Laoukili, Stahl and Medema, 2007; Myatt and Lam, 2008). During the G2/M phase, the activation of FOXM1 transcription stimulates mitotic progression (Laoukili *et al.*, 2005) mainly via the induction of other cell cycle-associated genes such as *Aurora Kinase B* (*AURKB*), Cyclin B1 (*CCNB1*), Centromere Protein F (*CENP-F*), *PLK1*, and *CEP55*. *PLK1* is an important cytokinesis regulator which initiates cleavage furrow formation and negatively regulates *CEP55* (Bastos and Barr, 2010). In head and neck squamous cell carcinoma, overexpression of FOXM1 correlates with overexpression of *CEP55* in lymph node metastasis (Waseem *et al.*, 2010). Consistently, *FOXM1* is associated with *CEP55* expression in a feedback loop in oral cavity squamous cell carcinoma (OCSCC) lines, which leads to enhanced transcription of matrix metalloproteinase-2 (MMP-2), enabling cell migration and invasion (C.-H. Chen *et al.*, 2009). Recently, elevated expression of *FOXM1*, *CEP55*, and *PLK1*, which hypothetically might form a mutual feedback loop, has been reported in bladder cancer patients (Seyedabadi *et al.*, 2018). However, the exact molecular mechanism of this regulation requires further exploring.

1.3.6 CEP55 connection to p53 and other cell cycle regulators

The guardian of the genome, p53, has been shown to negatively regulate CEP55, although this regulation is likely to be an indirect effect (Chang *et al.*, 2012). This is due to p53 also negatively regulating transcription factors that target *CEP55* such as *FOXM1* and *MYC* as well as multiple cell cycle regulatory genes such as *PLK1* and Cyclin B1 (*CCNB1*) (Zambetti *et al.*, 1992; Innocente *et al.*, 1999; Heikaus, Pandit and Klevit, 2009; Sachdeva *et al.*, 2009; Dupuy, Mackenzie and Haseloff, 2010). *PLK1* negatively regulates CEP55 localization to the anaphase spindle through phosphorylation and endogenous CEP55 functions similarly following treatment of cells with PLK1 inhibitors BI2536 or GW842862 (Bastos and Barr, 2010). Therefore, it is possible that this p53-PLK1-CEP55 axis regulates *CEP55* expression and localization for the completion of cytokinesis (Chang *et al.*, 2012). Additionally, the p53–p21–DREAM–E2F/CHR pathway has also been shown to downregulate *CEP55* as well as many other cell cycle genes (Engeland, 2018). p53 is known to be repressed by MDM2, a downstream target of AKT which is indirectly regulated by *CEP55* and forms a feedback loop (Shi and Gu, 2012).

Furthermore, *CEP55* has been shown to regulate NF-κB/IκBα signaling in pancreatic cancer (PANC), wherein elevated expression of *CEP55* is correlated with the progression of the disease (Peng *et al.*, 2017). Mechanistically, NF-κB/IκBα signaling regulates proliferation, migration, and invasion in PANC cells via *CEP55*-dependent upregulation of MMP2, MMP9, and Cyclin D1 *in vivo* in PANC xenografts (Peng *et al.*, 2017). In another report, the upregulation of *CEP55* was associated with enhanced cell motility through a JAK2/STAT3/MMPs axis in hepatocellular carcinoma (M. Li *et al.*, 2018). The authors concluded that migration and invasion in hepatocellular carcinoma are due to an interaction between *CEP55* and *JAK2*, leading to phosphorylation of *STAT3*, and *MMP2/9* expression (M. Li *et al.*, 2018).

1.3.7 CEP55 as a prognostic marker

CEP55 has been identified as a prognostic marker across multiple gene signatures for a variety of tumor types. *CEP55* is among a 70-genes signature for CIN analyzed across 12 cancers and representing six cancer types (breast, lung, lymphoma, mesothelioma, medulloblastoma, glioma). The overexpression of these genes (CIN70) was predictive of poor clinical outcome and increased metastasis (Carter *et al.*, 2006). *CEP55* has further been classified as part of a 10-gene functional subset of CIN70, responsible for myeloma drug resistance, rapid relapse, and hyperactive cell proliferation (Zhou *et al.*, 2013). Elevated expression of CEP55 has been linked to poor survival in breast cancer (BC) across multiple studies (Montero-Conde *et al*., 2008, Cheng *et al.*, 2013, Ma *et al.*, 2003, Naderi *et al*., 2007, Hu *et al*., 2012, Coutant *et al*., 2011). Moreover, *CEP55* is one of the top 30 genes extracted based on gene ontology and pathway analysis of 2239 genes analyzed across 33 breast cancer gene signatures (Huang, Murphy and Xu, 2018).

CEP55 is consistently identified across multiple gene signatures for a variety of cancers such as: 206 genes triggering CIN and aggressiveness in triple-negative breast cancer

(TNBC) (Al-Ejeh *et al.*, 2014a), 100 genes responsible for CIN in breast, ovarian, and colon cancers (Cheng *et al*., 2013), 23 genes linked to poor prognosis in thyroid cancer (Montero-Conde *et al.*, 2008), a 39 gene signature associated with metastasis in renal cancer (Jones *et al.*, 2005), 85 genes in invasive ductal carcinoma (IDC) (Ma *et al.*, 2003), 16 gene in IDC (Colak *et al.*, 2013), and 109 overexpressed genes responsible for cancer invasion risk and progression in IDC (Chen, 2010). *CEP55* was also identified in a 31 cell-cycle progression-associated gene signature of prostate adenocarcinoma as a predictor of cancer death outcomes (Cuzick *et al.*, 2012). This gene signature is also related to disease aggressiveness, tumor stage, and prostate-specific antigen (PSA) levels and predicts ten-year fatality risk (Cuzick, 2014). Altogether, *CEP55* is a significant cancer marker, primarily for prognosis, survival, and clinical outcome.

Recently, two distinct studies demonstrated essential roles of *CEP55* in the prognosis of lung adenocarcinoma and myeloproliferative neoplasms. Wu *et al.* revealed the correlation between *CEP55* and the enhancer of zeste homologue 2 (EZH2) in the prognosis of lung adenocarcinoma. They hypothesized that *CEP55* is a downstream target of EZH2, and EZH2 overexpressing tumors show low methylation of *CEP55*, providing a theoretical mechanism of epigenetic modifying factors regulating *CEP55* expression in lung adenocarcinoma (S. Wu *et al.*, 2019). Guo *et al.* identified *CEP55* among three fibrosis-associated gene-signatures of transcripts alterations in platelets from myeloproliferative neoplasms and has implicated *CEP55* as a useful prognosis tool for the early prediction of progression to marrow fibrosis (Guo *et al.*, 2019).

1.3.8 CEP55 Regulates Stemness

Several studies have suggested a role of *CEP55* in stemness to control stem cell quiescence, proliferation, differentiation, and self-renewal. The stemness ability of *CEP55* is linked to the regulation of midbody remnants (Ettinger *et al.*, 2011; Kuo *et al.*, 2011) and exosomes (Hong *et al.,* 2009). Exosomes or extracellular vesicles (EVs) are produced and released from endosomal membranes of cells, and these vesicles are essential for the secretion and transportation of cell signaling and regulatory molecules (Cruz *et al.*, 2018; Stahl and Raposo, 2019). Exosomes play a more critical role within cells than was initially thought in cellular physiology, as exosomes carry proteins, as well as nucleic acids such as miRNA, and noncoding RNA (Schorey and Bhatnagar, 2008). Exosomes are also considered to be information carriers in cell communication between cancerous and non-cancerous cells via specific surface markers, including CD63, CD81, ALIX, TSG101 to promote self-renewal and stemness (Sun *et al.*, 2018). They also contribute to different features of cancers, such as angiogenesis, metastasis, tumor invasion, and resistance mechanisms (Zhang and Grizzle, 2011; Azmi, Bao and Sarkar, 2013). Proteomic analysis of exosomes from human colon cancer cell lines revealed a protein signature which included *CEP55* which along with cell cycle-regulating signaling molecules, protein trafficking, and cytoskeletal proteins. (Mathivanan *et al.*, 2010). However, further evidence of the specific circumstances under which CEP55 may contribute to exosome trafficking and stemness remains unexplored.

The other mechanism by which *CEP55* can affect stemness is by regulating midbody fate. After completion of cytokinesis, CEP55 interacts with the autophagy receptor, NBR1, to degrade midbody derivatives (MBds). Accumulation of MBds is associated with an increase in stemness (Kuo et al., 2011, Ettinger et al., 2011). *CEP55* overexpression or NBR1 depletion resulted in decreased MBd degradation enhancing stemness (Kuo et al., 2011). Similarly, knockdown of either *CEP55* or its interactors: ALIX and TSG101 can impair midbody fate, which resembles an abscission defect. Impaired midbody-release sensitizes cells to a differentiation stimulus, which stimulates cells to switch from proliferation to differentiation (Ettinger *et al.*, 2011).

1.3.9 CEP55 and the mitotic stress connection

Mitotic stress stems from the unequal distribution of daughter cell DNA and failure to maintain euploidy leading to aneuploidy. This missegregation is referred to as chromosome instability (CIN) and is a common occurrence in solid and hematological cancers (Cahill *et al.*, 1998). Consequently, the shifting of chromosome distribution enables tumor cells to proliferate. Any defects in a variety of mitotic pathways can lead to CIN including defects in mitotic proteins that accomplish chromosome separation and defects in the spindle assembly checkpoint, which coordinates anaphase entry with proper alignment of chromosomes on the mitotic spindle (Cahill *et al.*, 1998; Thompson, Bakhoum and Compton, 2010). Furthermore, perturbation of mitotic checkpoint proteins such as Aurora kinase A (AURKA) (Bischoff *et al.*, 1998; Katayama *et al.*, 1999; Li *et al.*, 2003) Aurora kinase B (AURKB) (Chieffi *et al.*, 2006; Shi *et al.*, 2013) Budding uninhibited by benzimidazoles 1 homolog (BUB1) (Imai *et al.*, 1999; Gemma *et al.*, 2000; Hempen *et al.*, 2003) MAD2 (Alizadeh, 2000; Han *et al.*, 2000), and Polo-like kinase 1 (PLK1) (Deeraksa *et al*, 2013) have been shown to be sufficient to initiate tumorigenesis in mouse models.

A CIN phenotype can also result from the presence of extra centrosomes in tumor cells or from stresses placed on the mitotic machinery due to the need to segregate supernumerary chromosomes (Ganem, Storchova and Pellman, 2007). CIN and mitotic stress can also arise indirectly as a result of genomic instability following oncogene activation (Halazonetis, Gorgoulis and Bartek, 2008). Mutations in certain oncogenes (*i.e.*, Ras) and tumor suppressors (*i.e.*, p53) have been suggested to associate with CIN (Denko *et al.*, 1994). *CEP55* has also been shown to be a key player in promoting aneuploidy and genomic instability when present at high levels (Sinha *et al.*, 2019).

1.3.10 Targeting CEP55 in cancer

Deregulation of specific genes during different cellular processes such as proliferation, cell growth, apoptosis, and cell division can lead to tumorigenesis. The understanding of genome deregulation in neoplastic diseases has led to the discovery and improvement of cancer treatment in the form of targeted therapy (Lee *et al.*, 2015; Wang and Wang, 2017). Targeted therapy differs from conventional chemotherapy in that it selects for specific oncogenes, proteins, or tissue environments contributing to cancer growth and survival for treatment (Katsnelson, 2013). Hence, a better understanding of the hallmarks and mechanisms of cancer development can advance cancer therapeutic strategies. Amongst these hallmarks, various processes have been targeted for treatment and including genome instability, tumor-promoting inflammation, energy metabolism reprogramming, and avoidance of immune destruction (Hanahan and Weinberg, 2000) (Fig. 1.6). New drivers and players promoting cancer development and progression are being identified, providing opportunities for safer and more effective targeting opportunities to be identified (Gagan and Van Allen, 2015; Shruthi and Palani Vinodhkumar, 2016).

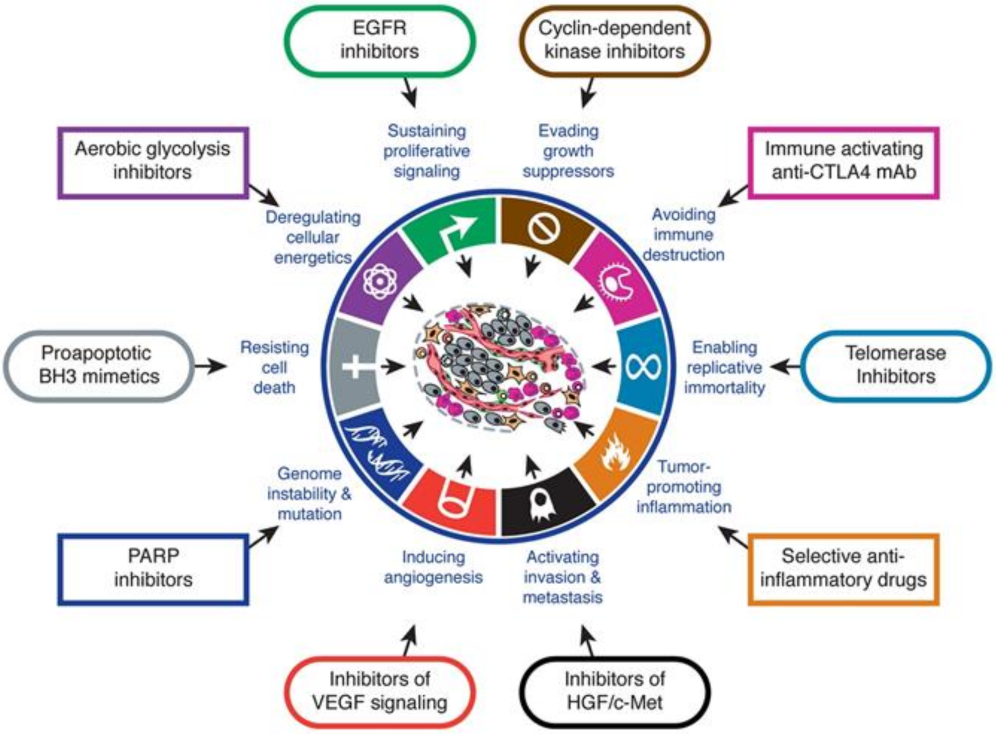
EGFR inhibitors
Cyclin-dependent kinase inhibitors
Aerobic glycolysis inhibitors
Sustaining proliferative signaling
Evading growth suppressors
Immune activating anti-CTLA4 mAb
Deregulating cellular energetics
Avoiding immune destruction
Proapoptotic BH3 mimetics
Resisting cell death
Enabling replicative immortality
Telomerase Inhibitors
Genome instability & mutation
Tumor-promoting inflammation
PARP inhibitors
Inducing angiogenesis
Activating invasion & metastasis
Selective anti-inflammatory drugs
Inhibitors of VEGF signaling
Inhibitors of HGF/c-Met

Figure 1.6 Targeting hallmarks of cancer for therapy

Targeting the essential acquired capabilities of tumor initiation, growth and progression by development of drugs that affect and inhibit the hallmarks of cancer. These drugs have already been approved or are in process of clinical trial approval in human cancer. (Adopted by permission (Hanahan and Weinberg, 2011) Licence No. #4612870509190).

The new wave of drug design for cancer targets multi-component cellular machinery that is not involved in direct growth and proliferation and is, therefore, less toxic (Bhat *et al.*, 2015). These drugs are referred to as “non-oncogenic addiction drugs” and interfere with molecular pathways that are essential for cancer cells to survive. DNA replication, DNA repair, and cell division are the central cellular machinery that has been highlighted as anti-cancer targets with a therapeutic perspective. Moreover, DNA damage pathways, chaperones, ribosome biogenesis, metabolic, oxidative, and mitotic stress are gaining more consideration (Dobbelstein and Moll, 2014). Genomic integrity is threatened constantly by DNA damage. The DNA Damage Response (DDR) is a system in place to ensure DNA sequence information remains original during the cell's life span, particularly following DNA replication and mitosis (Gavande *et al.*, 2016; Pedersen *et al.*, 2016). Failure of this system can cause genomic instability and supports malignant transformation (O'Connor, 2015). Genomic instability (GIN) is a common feature of almost all cancers and especially solid tumors which pass through various levels of GIN that result in the accumulation of mutations, insertion, deletions, chromosome rearrangements and aneuploidy (Hartwell and Kastan, 1994; Jeggo, Pearl and Carr, 2016). In response to DNA damage, the DDR can halt proliferation, induces cellular senescence or provokes apoptosis in normal cells (Bartkova *et al.*, 2005; Tian *et al.*, 2015). Cancer cells, on the other hand, have evolved to overcome the anti-proliferative effects of DNA damage, to continue replication in the presence of DNA damage and this can promote cancer development (Halazonetis, Gorgoulis and Bartek, 2008). Alteration in copy-number and aneuploidy which can result in corresponding changes in transcript levels can change the relative homeostasis of growth and survival signals, thus promoting tumorigenesis (Perou *et al.*, 2000; Tsafrir *et al.*, 2006; Nakad and Schumacher, 2016).

Our laboratory showed that *CEP55* is a new regulator of GIN and this role of *CEP55* can enhance its capacity for targeting in cancer therapy. Aneuploidy is the main linker of *CEP55* to GIN (Kalimutho *et al.*, 2018). GIN is a hallmark of cancer as previously discussed. Chromosomal instability (CIN) is a subclass of GIN which is the alteration of chromosomal number or structure due to defective mitosis or the failure in cytokinesis. Cep55 is linked to this hallmark of cancer. Wild-type TP53 can suppress CEP55 indirectly by regulation of PLK1 and consequently elevated CEP55 levels can often be seen in cancers with TP53 mutations. CEP55 is re-expressed in a wide range of human cancers and numerous studies have revealed a link between CEP55 overexpression and poor prognosis in human cancers (Jeffery et al. 2015). This increase in the level of CEP55 expression is associated with aneuploidy. CEP55 overexpression also leads to increased proliferation, cellular transformation, and epithelial to mesenchymal transition (EMT), invasion and cell migration mostly coincident with the upregulation of the PI3K/AKT signalling (Sinha et al. 2019).

CEP55 was initially identified as a Cancer/testis (CT) antigen and tumor-associated antigen (TAA) (Inoda *et al.*, 2009; Fratta *et al.*, 2011). CT antigens are a class of proteins where their expression is normally restricted to male germ cells but exhibit overexpression in cancer cells. As CT antigens can serve as a locus of immune activation and induce a tumor-directed immune response, they are highly attractive targets in cancer immunotherapy for cancer vaccines (Fratta *et al.*, 2011). Preliminary investigations have proposed the potential of CEP55-based immunotherapy vaccines for targeting chemotherapy-resistant colon cancer stem cells and tumor-initiating cells (Inoda *et al.*, 2009).

Our laboratory recently described a strategy to target overexpressed *CEP55* in Triple-Negative Breast Cancers. We showed that *CEP55* knockdown could induce premature *CDK1* activation and caspase-dependent mitotic cell death in breast cancer lines. Also, dual inhibition of *PLK1* and *MEK1/2* can mimic the effects of *CEP55* depletion to enforce mitotic cell death and decrease tumor growth in basal-like syngeneic and human breast tumor xenograft models (Kalimutho, Sinha, *et al.*, 2018). Collectively, given the critical role of *CEP55* in cancer, its targeting may be a promising therapeutic approach for personalized medicine.

1.4 CEP55 in Genetic Diseases and Disorders

The first case of genetic disruption of *CEP55* in humans was identified in a disorder with a chromosomal translocation Xp22/10q24 causing multiple clinical symptoms with a wide range of brain abnormalities (white matter reduction, enlarged ventricles, motor retardation and absence of the corpus callosum). In this patient, three copies of *CEP55* (located on Chromosome 10) were identified, in addition to disruption of additional genes (including the Family With Sequence Similarity 9 Member B (FAM9) protein family located on chromosome X) (Martínez-Garay *et al.*, 2007).

A decade later, a second report of *CEP55* perturbation in a genetic disorder was published. A homozygous nonsense mutation in *CEP55* was shown to cause a novel autosomal recessive lethal syndrome termed MARCH (Multinucleated neurons, Anhydramnios, Renal dysplasia, Cerebellar hypoplasia, and Hydranencephaly) affecting three siblings of Mennonite parents. A truncating mutation in the C-terminal region of *CEP55* (c.1274C>A transversion/ p.S425X) was identified, causing the loss of *CEP55* function. When expressed *in vitro* in COS-7 cells, the *Cep55* S425X mutant failed to localize to the midbody and caused multinucleation and intracellular bridges due to failure of cytokinetic abscission. Moreover, while the full-length protein was able to rescue the abnormal phenotypes of zebrafish harboring CRISPR/CAS9-mediated knockout of *cep55* (the zebrafish ortholog of Cep55), expression of the truncating mutation failed to rescue this phenotype (Frosk et al., 2017). The overall conclusion from the study was that cytokinesis failure or possible impaired PI3K/AKT signaling may contribute to MARCH pathogenesis.

A third report described a syndrome termed “Meckel-like” syndrome, due to its similarities with Meckel Syndrome. The authors described an autosomal recessive prenatal lethal ciliopathy linked to a homozygous nonsense mutation at the C-terminal end of CEP55 (c.256C>T/ p.R86X). The observed clinical disorder was identified in two fetuses of Swedish descent, characterized by brain malformation (occipital encephalocele), dysplastic kidneys (renal cystic dysplasia), cystic hygroma, and polydactyly (Bondeson et al., 2017). Consistent with these findings, a fourth report demonstrated the same MKS syndrome in two affected fetuses of Amish descent with hydranencephaly and Potter sequence (clubbed feet, pulmonary hypoplasia, cranial anomalies) secondary to cystic renal dysplasia and anhydramnios. The homozygous loss of function variants in CEP55 (c.514dup p. /Ile172Asnfs*17) caused Meckel-like lethal fetal disorder profoundly affecting brain and kidney development in these cases, and the authors suggested possible impaired neuronal migration regulated by *CEP55* may be a causative mechanism (Rawlins *et al.*, 2019).

Apart from these reports, there are other historical cases with overlapping phenotypes which have not been attributed to perturbation of CEP55 (Hamby, Krauss and Beswick, 1950; Strauss *et al.*, 1984; Bendon *et al.*, 1987; Gschwendtner *et al.*, 1997; Chu *et al.*, 1998; Rawlins *et al.*, 2019)

1.5 Cep55 in Embryogenesis, Development and Neural Function

The first *in-vivo* description demonstrating a role for Cep55 in embryogenesis came from a Zebrafish model system published by our laboratory. In this report, a critical role for cep55 in regulating the PI3K/AKT pathway in development was demonstrated using both morpholinos and genetic mutation of cep55 (Jeffery *et al.*, 2015). This zebrafish model harbored a C115T mutation causing a premature stop codon at residue 39, leading to a non-functional protein and ablating Cep55. No prominent defects were observed in heterozygote mutants (*cep55*$^{+/-}$) harboring one copy of the mutation when compared to the wild-type siblings. However, homozygous mutants (*cep55*$^{-/-}$) exhibited larval lethality predominantly due to abnormal development in the head concomitant with a significant increase in apoptosis through AKT destabilization (Jeffery et al., 2015). This investigation was the first phenotypic analysis showing a role of cep55 in embryonic development through mediating PI3K/Akt signaling.

Recently, the Khanna laboratory also described phenotypic characterisation of a mouse model overexpressing Cep55 from the *Rosa26* locus. This study demonstrated that mice with homozygous transgenic *Cep55* overexpression are infertile due to suppression of nuclear localization of hyperactivated Foxo1 in an Akt-dependent manner (Sinha *et al.*, 2018). This is consistent with a study demonstrating that CEP55 colocalizes and interacts with TEX14 in mouse testis intercellular bridges and its disruption in germ cells causes abscission defects during spermatogenesis leading to male sterility (Iwamori et al. 2010). Sinha *et al.* (2018) also demonstrated that Cep55 overexpression caused Ret upregulation (Sinha *et al.*, 2018). Ret is an RTK proto-oncogene regulating spermatogonial self-renewal as well as many other developmental functions such as kidney formation, regulation of dopaminergic neurons, motor neurons and neural crest progenitors (Schuchardt *et al.*, 1994; Enomoto *et al.*, 2001; Kramer *et al.*, 2006, 2007; Naughton *et al.*, 2006; Luo *et al.*, 2009).

1.6 Significance, Aims and Hypotheses

Over a decade of investigation on *CEP55* has led to significant discoveries of the function of this protein. However, there are limited models testing the *in vivo* role of this protein, and its role in development and tumorigenesis is not well defined. We hypothesized that loss of Cep55 would cause defects during embryogenesis, and that its abrogation would inhibit the tumorigenic process. This thesis utilizes a model of *Cep55* knockout to further understand the pathophysiological roles of this important protein in development and disease, with a particular focus on neurogenesis and cancer development. A knockout mouse model of Cep55 has not been previously described, and the outcomes of this project give important preclinical information as to how Cep55 contributes to tumorigenesis and how to target it more effectively for cancer therapy.

1.6.1 Aim 1: To determine the functional role of CEP55 in early embryonic development

1.6.1.1 To generate and establish Cep55 constitutive and conditional KO models

1.6.1.2 To characterize the physiological role of Cep55 loss during embryonic development

1.6.1.3 To identify cellular and molecular role of CEP55 in regulation of the cell cycle, cell signaling and ciliopathy

1.6.2 Aim 2: To determine the functional role of CEP55 in tumorigenesis and cancer

1.6.2.1 Determine if Cep55 loss regulates E1A/Ras-mediated tumorigenesis

1.6.2.2 Determine the contribution of Cep55 genetic depletion on Pten and Kras LSL G12D tumor prone mouse models

Chapter 2. Materials and methods

2.1 Animal work and Histopathology

2.1.1 Animal husbandry and ethics statement

All experimental animals used in this thesis were from a C57BL/6J strain except the NOD/SCID mouse used for Xenograft experiments. Mice were housed at the QIMR Berghofer Medical Research Animal Facility in OptiMICE® caging (Centennial, Colorado, USA) at 25°C with a 12h light/dark cycle. This research was carried out in strict accordance with the Australian code for the care and use of animals for scientific purposes. All protocols were approved by the QIMR Berghofer Medical Research Institute Animal Ethics Committee (number A0707-606M).

2.1.2 Generation of constitutive Cep55 knockout mice

Cep55 floxed ES cells were purchased from the International Knockout Mouse Consortium (IKMC) and heterozygous *Cep55*-targeted mice were generated by the Australian Phenomics Network (APN) facility, according to standard protocols. Cep55 transgenic (Tg) mice obtained contained a “knockout-first” allele which can act as a gene-trap for constitutive Cep55 loss, or be further crossed to form a conditional allele. *Cep55*$^{+/Tg}$ mice (hereafter referred to as *Cep55*$^{+/-}$ mice) were intercrossed to obtain *Cep55*$^{-/-}$ embryos at a 25% ratio according to mendelian genetics.

2.1.3 Generation of conditional Cep55 knockout mice

To obtain *Cep55 conditional knockout* (*cKO*) mice, several breeding steps were performed. Firstly, *Cep55*$^{Tg/+}$ heterozygous mice (obtained from the Australian Phenomics Facility) were crossed with FlpE mice to remove the neo cassette (resulting in *Flp*; *Cep55*$^{Fl/+}$ mice) and subsequently backcrossed to the wild-type C57BL/6 background to remove the *Flp* transgene. Following these crosses, heterozygous *Cep55*$^{Fl/+}$ mice were intercrossed to generate *Cep55*$^{Fl/Fl}$ offspring. These mice were then crossed to *RosaCre*^{ERT2} transgenic mice to obtain *RosaCre*^{ERT2}; *Cep55*$^{Fl/+}$ mice which were further crossed to *Cep55*$^{Fl/Fl}$ mice to generate *RosaCre*^{ERT2}; *Cep55*$^{Fl/Fl}$ offspring. The *RosaCre*^{ERT2}; *Cep55*$^{Fl/Fl}$ were administered tamoxifen to activate Cre, resulting in *Cep55 cKO* generation.

2.1.4 Genotype analysis

Genotyping was performed using genomic DNA extracted from mouse ear. DNA was extracted by QuickExtract™ DNA Extraction Solution (Lucigen, USA) according to the manufacturer's protocol. To genotype wild-type and Cep55 transgenic alleles, we designed a 3-primer PCR. This design has the advantage of a positive control in each reaction where each genotyping reaction should produce at least one PCR product. With this strategy, we designed a common forward primer (P1) and two different reverse primers (P2 and P3) which can differentiate between different allele forms. *Cep55*$^{+/+}$ (wild-type) mice generate a single band of 381 bp whereas genotyping of *Cep55*$^{+/-}$ (heterozygous) mice exhibit a band at 381 bp and 454 bp. Genotyping of *Cep55*$^{-/-}$ (homozygous) mice produces a single band of 454 bp. All primers were optimized for annealing temperature. Primer sequences to genotype for Cre, FLPe (Dymecki, 1996), Pten (Gu *et al.*, 2011) and Kras (Zou *et al.*, 2015) were described previously. Sequences for all primers used in this study are listed in table 1.

No.	Name	Sequence
1.	Cep55 P1	TGGGTCTTTAACTCATGGTC
2.	Cep55 P2	AGGAGTGAAAAGTCCTCACA
3.	Cep55 P3	GTACCGCGTCGAGAAGTT
4.	Cre recombined	AACTGATGGCGAGCTCAGA
5.	FLPe F	GTGGATCGATCCTACCCCTTGCG
6.	FLPe R	GGTCCAACTGCAGCCCAAGCTTCC
7.	Pten F	GCCCCGATGCAATAAATA
8.	Pten R	ACTCAAGGCAGGGATGAG
9.	Kras P1	GTCTTTCCCCAGCACAGTGC
10.	Kras P2	CTCTTGCCTACGCCACCAGCTC
11.	Kras P3	AGCTAGCCACCATGGCTTGAGTAAGTCTGCA
12.	rcm2_CreF	TGTGGACAGAGGAGCCATAAC
13.	rcm2_CreR	CATCACTCGTTGCATCGACC
14.	ROSA26 locus F	AGCACTGGAAATGTTACCAAGGAAC
15.	ROSA26 locus R	GGCTGGCTAAACTCTGGCCCTACA

Table 2.1 List of PCR primers used in this thesis.

2.1.5 Timed mating

Successful timed matings were assessed by the presence of a copulation vaginal plug present the morning following post timed mating set up (designated embryonic day 0.5, E0.5).

2.1.6 Organ/embryo isolation

Mice were anaesthetized with AttaneTM Isoflourene (Biomac Pty Ltd, Hornsby, NSW) and culled by cervical dislocation. Embryos were collected and organs dissected using a Nikon SMZ45stereo dissecting microscope (Nikon Inc, Tokyo, Japan). Isolated organs or embryos were washed in ice-cold Phosphate Buffered Saline (PBS). For protein or mRNA extraction, samples were snap frozen on dry ice. For histology staining, embryos were fixed in either Bouin's solution (Sigma-Aldrich) (pathology investigation) or 4% PFA (immunohistochemical staining) for 24-48 h.

2.1.7 Mouse xenografts

MEF xenografts were generated by injection of E1A/Ras-immortalized MEFs into non-obese diabetic/severe combined immunodeficiency (NOD/SCID) mice and allowed to grow. 1.0×10^6 or 4.0×10^6 cells were resuspended in 50% Matrigel (BD, Biosciences, Bedford, USA)/50% PBS (v/v) to be injected intraperitoneally into 6-10 week-old NOD/SCID mice at a final volume of 100 µL. Tumor growth was monitored and measured thrice weekly by calliper measurements and tumor size calculated by the following formula: $V = (W(2) \times L)/2$ where V = tumor volume, W = tumor width, and L = tumor length.

2.1.8 Tamoxifen induction

For induction of Cre activity, Tamoxifen (Sigma Aldrich®, T5648-1G) was prepared (100mg/kg/mouse) in 100 µl of warmed sunflower oil containing 100% ethanol (0.5µl/ 10ml of drug solution) following by 20 min of rapid vortexing to dissolve. Drug was prepared fresh for each injection session. MEF induction was performed by adding 5 mg of 4-hydroxy tamoxifen (4-OHT) (Sigma Aldrich®, H7904-5MG) in 1.29 ml 100%

ethanol (EtOH) for a stock of 10 mM. For gene deletion optimization, 1, 2 and 3 µM of 4-OHT was added to cells and at different time points and gene deletion was confirmed by western blot. 2 µM 4-OHT after 96 h incubation was determined to be the optimal dose for gene knock down.

2.1.9 Intranasal delivery of Ad-Cre

To generate sporadic lung-specific tumors, the inoculation of replication-deficient adenoviruses expressing Cre (Ad-Cre: University of Iowa, Gene Transfer Vector Core) was used to deliver transient Cre expression to infected cells of the lung in *Kras*$^{LSL\ G12D}$ $^{fl/+}$ mice. The inhalation solution contained a titer of 2.5×10^8 PFU (titered at University of Iowa) of Ad Cre per mouse diluted in 62.5 µl of Minimal Essential Media (MEM, Sigma, M4655) and 2 M $CaCl_2$ (Mallinckrodt, Catalog #4160). The solution was incubated for 20 min on ice. Ad-Cre was precipitated with calcium phosphate to improve the efficiency of delivery of viral infection in the lung epithelium. Mice were anaesthetized with isofluorane and virus was administered intranasally (IN) drop-wise with sterile tips using a P200 pipette.

2.1.10 Immunohistochemistry staining

For histopathologic investigation with hematoxylin and eosin (H&E), tissues were collected and fixed in Bouin’s solution (Sigma-Aldrich, USA) for 48 h and embedded in paraffin blocks. Sections (5 µm thick) were prepared for H&E staining with a Leica Autostainer XL. For periodic acid–Schiff (PAS) staining, whole brains were removed from male mice and fixed in 4% PFA for 24-48 h. Tissues were embedded in paraffin and Wax embedded tissues were sectioned at 5-10 µm using a microtome and stored at room temperature. Sections were then mounted onto Superfrost plus slides (Thermo Fisher

Scientific) using the Sakura Tissue-Tek® TEC™ (Sakura Finetek, Tokyo, Japan). Slides were then dewaxed and rehydrated according to standard protocols (Tab.2).

Chemical	**Duration**
Xylene	2 mins
Xylene	2 mins
Xylen	2 mins
100% EtOH	2 mins
100% EtOH	2 mins
90% EtOH	2 mins
70% EtOH	2 mins
Running water	2 mins

Table 2.2 The standard dewaxing protocol

Antigen retrieval was performed with 10 mM Sodium citrate buffer pH=6.0 (2.94 g Sodium tri-citrate in 1 litter of MilliQ water/ adjusted the pH to 6 with HCL 37%) using the Decloaking Chamber ™ NxGen (Biocare Medical,USA) for 15 min at 95°C. Sections were permeabilized and blocked in blocking buffer at RT for at least 1 h (20% FBS + 2% BSA + 0.2% TritonX in 50 mL PBS: 1g BSA + 10mL FCS + 40mL PBS, filtered, then add 100 µL TritonX). Then, primary antibody was diluted in blocking buffer and incubated at 4°C overnight in a humidified chamber. Immunostaining was performed with the following primary antibodies: Ki67 1:500 (rabbit, NCL-ki67p; Novacastra, Wetzlar, Germany); mouse anti γ-tubulin (1:400, T5326 Sigma), rabbit anti γ-tubulin (1:400, T5192 Sigma), rabbit anti Arl13b (1:300, 17711-1-AP Proteintech), mouse anti α-tubulin (1:300, T5168 Sigma), mouse anti Arl13b (1:300, 75287, Antibodies Inc.), rabbit anti TBR1 (1:200, ab31940 Abcam), Monoclonal Anti-Acetylated Tubulin antibody produced in mouse clone 6-11B-1(Sigma Aldrich®) , rat anti-TBR2 488 (1:200, 53-4875-80 eBioscience), rabbit anti-phospho-histone H3 (1:300, ab47297 Abcam), mouse anti-PAX6 (1:200, DSBH), DAPI was used for nuclear staining (D9564; MilliporeSigma). ApopTag staining was performed with the ApopTag peroxidase *in-situ* apoptosis detection kit (S7100; MilliporeSigma, Billerica, MA, USA).

Slides were washed three times with PBSX, and the diluted Alexa Fluor–conjugated secondary antibodies (Jackson Immuno-Research Laboratories, West Grove, PA, USA, and Thermo Fisher Scientific) added for incubation at RT for 3 h in a humidified chamber. The slides were mounted by Vectashield (Vector Laboratories, Burlingame, CA, USA) and cover-slipped using the Leica CV5030 (Leica Biosystems, Wetzlar, Germany) glass coverslipper and Shandon Consul-Mount mounting media (Life Technology^{TM}). Finally, slides were scanned with Aperio® Scanscope® FL/XT (Aperio®, Vista, USA) using 20X or 40X magnification and imaged with the Inverted LSM780 confocal microscope (Zeiss, Jena Germany) before analyzing with Image Scope software (Leica Biosystems, Buffalo Grove, IL, USA) "Nuclei count", version 9 algorithm to score immune-positive cells or using Imaris software (Bitplane Scientific Software, Belfast, United Kingdom).

2.1.11 β-Galactosidase staining

Detection of β-Galactosidase Activity using LacZ reporter and X-gal Staining was performed as described by (Burn, 2012). X-gal (5-Bromo-4-chloro-3-indoxyl-beta-D-galactopyranoside, Goldbio) was used to detect reporter gene expression marked by a dark blue stain. Briefly, whole embryos/organs were dissected and fixed (4% PFA for 30 minutes) following by washing (three times with wash buffer (0.02% NP-40, 0.01% deoxycholate in PBS) and chromogenic staining with staining solution (5 mM K3Fe(CN)6, 5 mM K4Fe(CN)6, 0.02% NP-40, 0.01% deoxycholate, 2 mM $MgCl_2$, 5 mM EGTA, 1 mg/mL X-gal in PBS) in the dark at 37°C overnight.

2.1.12 Whole-Mount Skeletal Staining

Embryo skeleton and cartilage staining was performed with a modification of Richard Behringer's protocol as described in (Rigueur and Lyons, 2014). First, embryos were skinned to remove soft tissues, and viscera were removed. Fixation was performed in 100% ethanol overnight at 4°C on a rocker. Cartilage was stained in 0.3mg/ml Alcian blue in 20% glacial acetic acid and 80% EtOH for 48 h and then rinsed briefly in 95% EtOH. Afterward, samples were incubated in 2% KOH for 24 h to dissolve residual soft tissue. Following this, the bone was stained in 75µg/ml of Alizarin red in 1% KOH for 24 h. Sample clearing was then performed in 1% KOH / 20% glycerol for a few weeks (2-3). Samples were stored 50% glycerol:50% EtOH at RT before imaging on a Nikon SMZ45 stereo dissecting microscope (Nikon Inc, Tokyo, Japan).

2.1.13 Hematology

Tail vein blood was collected in EDTA-coated tubes (Greiner Bio-One, Kremsmünster, Austria), and full blood counts were performed on a Hemavet 950 Analyzer (Drew Scientific, Waterbury, CT, USA).

2.2 Cell biology

2.2.1 Cell culture

Cell lines were purchased from the American Type Culture Collection (ATCC, Manassas, Virginia, USA). Cell lines were cultured and maintained as per ATCC guidelines. All cell lines were authenticated using short tandem repeat (STR) profiling and annually tested for Mycoplasma infection by scientific services at QIMR Berghofer Medical Research Institute.

2.2.2 MEF establishment

MEFs were isolated from E13.5 embryos from *Cep55*$^{+/-}$ inter-crosses for the constitutive MEFS and CreERT2;*Cep55*$^{FL/+}$ X *Cep55*$^{FL/FL}$ crosses to generate conditional MEFs. To generate MEFs, embryos were isolated from E13.5 pregnant dams into sterile Petri-dishes with ice-cold PBS. Embryos were separated into individual 30 mm dishes and washed twice in ice-cold sterile PBS. Embryo heads were separated for genotyping, and internal organs and liver were removed. Embryos were then placed in a sterile Petri dish with 1 mL of trypsin-EDTA (Sigma Aldrich®, St Louis, USA) and were minced by mechanical shearing using a sterile scalpel blade. The dispersed tissues were incubated for 20 min at 37 °C, further homogenized by repeated trituration, and then seeded into 25cm^2 flasks (Corning®) to adhere overnight. Primary MEFs were maintained in Dulbecco's Modified Eagle's Medium (DMEM) (Life Technologies TM, Carlsbad, CA, USA) containing 20% Fetal Bovine Serum (SAFC Biosciences^{TM}, Lenexa, USA) 1% penicillin-streptomycin (Life Technology TM) and 1% Amphotericin B. Primary MEFs prior to passage 5 were used for experiments. For immortalized MEFs, primary MEFs were immortalized by retroviral SV40T transduction.

2.2.3 Doubling time assay

MEFs were plated in a 10 cm petri dish, at a density of 10^5 cells per well, in triplicate, for each genotype in a total media volume of 2 mL for 6 days. Every other day, cells from each genotype were collected, and the overall cell density was determined using a Countess® automated cell counter (Life Technologies^{TM}).

2.2.4 Cell proliferation assay

Cells were plated in a 12-well plate at two densities of 5×10^5 and 10×10^5 cells per well in duplicate and cultured overnight. The following morning, plates were transferred to an incubator equipped with an IncuCyte® S3 Live-Cell Analysis system (Essen BioSciences Inc, USA) for 6 days. Cell confluency was analyzed using the in-built IncuCyte® S3 software. Drug treatment or tamoxifen induction was performed at the time of cell seeding where indicated.

2.2.5 Cell cycle analysis

Cells were plated in 6-well plates in duplicate at a density of 1×10^5 cells per well and were harvested using 1 mL of trypsin-EDTA (Sigma Aldrich®, St Louis, USA) at individual time-points. Then, cells were washed twice in ice-cold fresh FACS medium (1%FBS in PBS) and were fixed in 100% Ethanol for 24 h. After fixation, cells were further washed twice in ice-cold FACS medium (1 % FBS in PBS) and suspended in 360 µL staining solution 150 µL of 1 mg/mL of propidium iodide (Sigma Aldrich®) and 15 mg/mL RNAse; and subsequently incubated at 37ºC for 30 minutes in the dark. Cells were analyzed for DNA content using a FACScanto II flow cytometry (BD Biosciences, Mountain View, CA). The proportion of cells in G0/G1, S phase and G2/M were quantified using ModFit LT™ 4.0 software (Verity Software House, Topsham, ME, USA) to calculate the percentage of cells in each phase.

2.2.6 Cell viability assay (MTS)

Cell viability assay was performed using the CellTiter 96® AQueous one cell viability assay reagent (Promega, WI, USA) as previously described (Al-Ejeh *et al.*, 2014b). Briefly, 1000 cells were plated per well in an overall media volume of 500 µL in a 48-

well tissue-culture plate (BD FalconTM). The next morning, drug treatment was performed on individual wells and cells incubated at 37ºC, 20 % oxygen, 5 % CO2 for six days. On the sixth day after adding a drug, 100 µL media containing 10 % MTS reagent was added into each well. Then, the plate was incubated for 3 h, and the OD was read at 490 nm on a Biotek PowerwaveTM XS2 microplate spectrophotometer (Winooski, VT, USA).

2.2.7 Clonogenic assays

MEFs were plated on a 6 well plate at a density of 500 or 1000 cells per well and incubated for 14 days to determine colony viability. Colonies were fixed with 0.05 % crystal violet for 30 minutes, washed and quantified for crystal violet colony counting and measurement by imaging on a GE InCell 2000 microscope and analysis by GE InCell 2000 3-D Deconvolution Software (GE Health care, Life Sciences, USA).

2.2.8 Soft agar Colony formation assay

Colony formation in soft agar was performed as described previously (Borowicz et al., 2014). Briefly, MEFs were seeded at 500 or 1000 cells/well in an upper layer of filter-sterilized melted 0.6 % nobel agar (Sigma-Aldrich, USA) dissolved in the cell culture medium, plated on top of a bottom layer of 1 % nobel agar in the cell culture medium. Cells were left to grow for 14 days, followed. By imaging and analysis, as described in section 2.2.7.

2.2.9 3D cell culture

As previously described, (Ryan *et al,* 2019) 3D culture was performed using an advanced suspension medium (ASM) liquid matrix (Happy Cell® ASM 3D Medium, Vale Life Sciences, Australia). MEFs were seeded at a concentration of 500 cells/mL in 6 well plate mini-bioreactors (Corning). The 3D model formation was monitored over 14 days by regular sampling and visual observation using an inverted microscope. After two weeks, the inactivation liquid was added to the suspended cells as per the manufacturer's protocol. After 30 min incubation, the sedimented colonies were treated with Hoechst 33342 (1 mg/mL) (Sigma Aldrich) and incubated for a further 10 min. Cells were imaged at 4 X magnification using the Cytell Cell Imaging System (GE Healthcare, Life Sciences, USA), and the images analyzed using the GE InCell 2000 3-D Deconvolution Software (GE Health care, Life Sciences, USA).

2.2.10 Gene transduction and transfection

For the generation of stable and constitutive cell lines with overexpression or knockdown of Cep55, we used Flag-*Cep55* cloned into the pLenti PGK Hygro Dest vector (addgene#19066), or mouse small-hairpin RNAs (shRNAs) in the pLKO plasmid (Sigma Aldrich®, St Louis, USA) (sequences are available in Table 3). Cells were transduced by spinfection for 1 h in the presence of Hexadimethrine bromide (Polybrene) (Sigma Aldrich®, St Louis, USA) and media collected and filtered at 48 h and 72 h post-transfection For human cell lines, constitutive CEP55-knockdown was performed as previously described (Fabbro, B.-B. Zhou, *et al.*, 2005). The Selection of clones was performed using 400 µg/mL Hygromycin, 50 µg/mL Zeocin, 5 µg/mL Blastocydin (Life TechnologyTM) or 5 µg/mL of Puromycin (Life Technology^{TM}). Transient Cep55 silencing was performed by reverse transfection using 10-20 nM of individual small interfering RNAs (siRNAs manufactured by Shanghai Gene Pharma, China) and Lipofectamine RNAiMAX (Life TechnologiesTM) for 48 h (sequences are available in Table 2.3).

No.	Gene of interest	Sense (5’-3’)
1.	*Cep55*_Scr	CCGGCGCTGTTCTAATGACTAGCATCTCGAGATGCTAGTCATTAGAACAGCGTTTTTT
2.	*Cep55*_sh#2	CCGGCAGCGAGAGGCCTACGTTAAACTCGAGTTTAACGTAGGCCTCTCGCTGTTTTTG
3.	*Cep55*_sh#4	CCGGGAAGATTGAATCAGAAGGTTACTCGAGTAACCTTCTGATTCAATCTTCTTTTTT
4	SiRNA *Cep55*_Scr	Sense (5’-3’): CAAUGUUGAUUUGGUGUCUGCA Anti-sense (5’-3’) : UGAAUAGGAUUGUAAC
5	SiRNA *Cep55*_SEQ1	Sense (5’-3’): CCAUCACAGAGCAGCCAUUCCCA CT Anti-sense (5’-3’) : AGUGGGAAUGGCUGCUCUGUGAUGGUA
6	SiRNA *Cep55*_SEQ2	Sense (5’-3’): AGCUACUGAGCAGUAAGCAAACAUU Anti-sense (5’-3’) : AAUGUUUGCUUACUGCUCAGUAGCUUU

Table 2.3 List of siRNA and shRNA used in this thesis.

2.2.11 Retrovirus and lentivirus packaging and transduction

For the production of retrovirus or lentivirus, Phoenix Amphotropic (retrovirus) or Hek293T cells (lentivirus) were plated at 90 % confluency in a T75 flask and transfected with 5 µg of DNA and 15 µL Polyethylenimine or PEI (Polysciences, Inc., 23966-2, POL) (1:3 ratio) in Optimum media. At 5 h post-transfection, media was changed and the packaging cells incubated for 72 h. At 48 h and 72 h post-transfection, the media was filtered using a 0.45 µm filter onto target cells prior to spinfection (at 1000 X g for an 1 h at 25° C) in the presence of hexadimethrine bromide (polybrene; Sigma Aldrich®, H9268-5G). Media was removed after spinfection and cells were allowed to recover for the next 48 h before selection with the corresponding antibiotic was carried out to select for transduced cells. Antibiotic selection was sustained until an untransduced control plate of cells had all died.

2.2.12 Live-cell imaging

Live-cell imaging was performed on an EVOS Fl Auto or Spinning disk confocal microscopes (as indicated), and images were acquired with the MetaMorph® Microscopy Automation and Image Analysis Software. Images were analyzed using analySIS LS Research, version 2.2 (Applied Precision), as described previously (Jeffery, Neyt, Moore, Paterson, Neil I Bower, *et al.*, 2015).

2.2.13 Immunofluorescence

For immunofluorescence (IF) assay, cells were counted and seeded up to 50,000 cells on a sterile glass coverslip. For ciliogenesis experiments, MEFs were serum-starved for 48 h. Drug treatments were added 12-24 h before fixation, as indicated. Coverslips were fixed after washing twice with PBS in 4 % PFA/PBS (Sigma Aldrich®, St Louis, USA) for 20 minutes at RT followed by washing 3 times in 1X PBS. Cells were then permeabilized in 0.1 % TritonX-100 (Sigma Aldrich®) for 90 seconds (ciliogenesis experiments) or 10 minutes at RT. Coverslips were then blocked with filtered 1 % bovine serum albumin (BSA) (Sigma Aldrich®) (ciliogenesis experiments) or 3 % BSA in PBS for 1 h in a humidified chamber at RT. Next, primary antibodies were diluted in blocking buffer and added to the coverslips and incubated in a humidified chamber overnight at 4° C (Cep55 staining) or for 1 h in an incubator at 37°C. Following the incubation with primary antibodies (Table 4), cells were washed (3x PBS) and incubated in Alexa-conjugated secondary antibodies and counterstained with DAPI for DNA staining (Sigma Aldrich®). Secondary antibodies were diluted in 3 % BSA (1:1000) and incubated for 30 minutes at 37° C in a humidified chamber in the dark. Following incubation with the secondary antibody, coverslips were washed (3 x PBS) and mounted using Prolong® gold anti-fade mounting medium (Life Technology^{TM}). Images were acquired with a DeltaVision personal DV deconvolution microscope (Applied Precision, GE Healthcare, Issaquah, WA). Image analysis was performed by GE DeltaVision software package, and automated counting was performed using script modules of Fiji ImageJ software (Java3D, Minnesota, USA).

2.2.14 Luciferase assays

Transcriptional activity assays were performed as previously described (Rabellino *et al.*, 2016) with the Dual-Glo® Luciferase Assay System (Promega, USA) according to the manufacturer’s protocol. Briefly, the Luciferase Reporter Assay was used to investigate promoter activity by measuring light output from the firefly luciferase enzyme expressed under the control of a Myc-responsive promoter (E-box). HEK293T cells were co-transfected by PEI with 2 µg of either *CEP55* empty vector or *CEP55* shRNA and reporter plasmid (E-box) or mutant E-box promoter. Luciferase activity was measured 48 h after transfection, according to the manufacturer's protocol. The Firefly/Renilla activity ratio was generated by dividing the control reporter by that of the Knockdown sample.

Antibody Specificity	**Company**	**Cat. No**	**Dilution**
Cep55	Santa Cruz biotechnology	sc-374051	1:500
γ-Tubulin	Sigma Aldrich	T5192	1:400
α-Tubulin	Sigma Aldrich	T9026	1:300
β-Actin	BD Pharmingen	612656	1:2000
Ki67	Novacastra	NCL-ki67p	1:500
Rabbit α Pericentrin,	Covance	PRB-432C	1:1000
Mouse α acetylated tubulin	Sigma	T7451	1:1000
Phospho-Histone H3$^{(S10)}$	Cell Signaling Technology	4499	1:200
Rabbit anti β-Catenin	Cell Signaling Technology	9582	1:1000
Rabbit anti Cleaved Caspase-3	Cell Signaling Technology	9664	1:500
Rabbit anti pAKT^{S473}	Cell Signaling Technology	4060	1:1000
Rabbit anti AKT	Cell Signaling Technology	9271	1:1000
Rabbit anti MYC (Y69)	Abcam	ab32072	1:1000
Mouse anti γ-tubulin	Sigma	T5326	1:400
Rabbit anti γ-tubulin	Sigma	T5192	1:400
Rabbit anti Arl13b	Proteintech	17711-1-AP	1:300
Mouse anti Arl13b	Antibodies Inc	75287	1:300
Rabbit anti TBR1	Abcam	ab31940	1:200
Rat anti TBR2-488	eBioscience	53-4875-80	1:200
Mouse anti PAX6	DSBH	AB_528427	1:200
Rabbit Secondary (peroxidase)	Sigma Aldrich	A0545	1:4000
Mouse Secondary (peroxidase)	Sigma Aldrich	A9044	1:4000

Table 2.4 List of antibodies used for Immunofluorescence.

2.3 Molecular biology

2.3.1 Immunoblotting

2.3.1.1 Cell and tissue lysate preparation

For preparation of the tissue lysate, organs were diced using a sterile scalpel blade followed by lysis in RIPA (25 mM Tris-HCl (pH 7.6), 150 mM NaCl, 1 % NP40, 1 % Sodium deoxycholate and 0.1 % SDS) or Urea lysis buffer (8 M urea, 1 % SDS, 100 mM NaCl, 10 mM Tris) and samples were sonicated for 10 seconds on a Branson Sonifier 450 (Branson Ultrasonic Corporation, Danbury, CT, USA). The cell debris was removed by 13,000 RPM centrifugation at 4º C for 30 minutes following by supernatant collection in a fresh tube. For the phosphoprotein blotting preparation of the cell lysate, adherent cells were harvested by scraping into PBS, Ortho-Vanadate buffer (PBS containing Sodium Fluoride (100 mM; Sigma Aldrich®) and Sodium Ortho-Vanadate (Sigma Aldrich®). The harvested cells were centrifuged at 2000 RPM for 5 minutes and were then resuspended in RIPA or Urea lysis buffer prior to 15 pulses of sonication (Sonicator Branson S250 Ultrasonics Corporation, Danbury, Connecticut, U.S.A.). Cell debris was removed by 13,000 RPM centrifugation at 4º C for 30 minutes, followed by supernatant collection in a fresh tube.

Protein concentration was quantified using the Pierce BCA Protein Assay Kit with Bio-Rad Protein Assay Dye Reagent (Thermo-Scientific). After quantification, Laemmli buffer (1 mL Glycerol, 10% SDS, 0.5 M Tris HCl (pH =6.8), 2.5 mL β-mercaptoethanol, and 0.25 g Bromophenol blue) was added to pre-aliquoted 30 µg or 60 µg of protein followed by heating of the samples at 95º C for 5 minutes prior to electrophoresis.

2.3.1.2 SDS-PAGE and western blot

Polyacrylamide gels were cast as previously described by (Mahmood and Yang, 2012). Prepared protein samples were subjected to electrophoresed at 120 V using the Bio-Rad Mini-PROTEAN® Tetra system in SDS running buffer (25 mM Tris-HCl, 192 mM glycine, 0.1 % SDS (v/v)). Gel transfer was performed using the Invitrogen X-cell SureLock™ transfer system at 80 V for 90 minutes in 1X transfer buffer (50 mM Tris, 40 mM Glycine, 20 % methanol) onto Amersham Hybond nitrocellulose membrane (GE Healthcare, Waukesha, WI, USA), and transfer efficiency assessed by Ponceau S staining (0.1 % (w/v) Ponceau S in 5 % acetic acid). Membranes were blocked in blocking buffer (5 % Skim milk powder (Diploma Brand) in PBS containing 0.5 % Tween-20- PBS-T) for 1 h on a shaker at RT following overnight incubation with primary antibodies (listed in Table) at 4º C. The following day, the membranes were washed (3x PBS-T) and incubated in secondary antibodies (listed in Table) for 1 h.

Antibody Specificity	**Company**	**Cat. No**	**Dilution**
Cep55	In House developed (aminoacids 55-250)	-	1:1000
Cep55	Santa Cruz biotechnology	sc-374051	1:500
Vinculin	Cell Signaling Technology	13901	1:2000
β-Actin	BD Pharmingen	612656	1:2000
PCNA (PC10)	Cell Signaling Technology	2586	1:500
β-Catenin	Cell Signaling Technology	9582	1:1000
pERK1/2(T202/Y204)	Cell Signaling Technology	4370	1:2000
ERK1/2	Cell Signaling Technology	4695	1:2000
GSK 3β	Cell Signaling Technology	9369	1:1000
pGSK 3β(Ser9)	Cell Signaling Technology	9322	1:1000
Cleaved Caspase-3	Cell Signaling Technology	9664	1:500
pAKT^{S473}	Cell Signaling Technology	4060	1:1000
AKT	Cell Signaling Technology	9271	1:1000
MYC (Y69)	Abcam	ab32072	1:1000
p Myc (T58)	Abcam	ab28842	1:1000
Rabbit Secondary (peroxidase)	Sigma Aldrich	A0545	1:4000
Mouse Secondary (peroxidase)	Sigma Aldrich	A9044	1:4000

Table 2.5 List of antibodies used for WB

2.3.2 DNA extraction

Genomic DNA from animal tissue or cell pellet was extracted using QuickExtract DNA solution (Gene target solutions, QE09050). For quick extraction, 50 µL of the extraction solution was added to a small tissue section or cell pellet followed by 15-second vortex and 6 minutes incubation at 65° C. To deactivate the proteinase K within the extraction buffer, an additional 2 minutes of incubation at 98° C was performed. DNA was stored at -20° C until PCR analysis.

2.3.3 Polymerase chain reaction

PCR was performed using GoTaq® Master Mix (Promega, M7123) in a total volume of 20 µl consisting of 10 µl of 2X master mix, 10 picomoles of each primer, 1 µL of extracted DNA and 10 µl of sterile water. Primers were designed using the Primer 3 online tool. Each genotyping reaction was performed with positive and negative no-template control (NTC) in order to exclude DNA contamination. All PCR reactions were performed using a GeneAmp® PCR system 9700 (Applied Biosystems™, Waltham, Massachusetts, USA) thermocycler. The genotyping protocol for PCR cycling was modified based on primers and reactions, as shown in Table 6. PCR products were electrophoresed at 80 V in 2 % agarose gel made in Tris-Acetate EDTA (TAE) buffer with SYBR Safe, DNA Gel Stain added according to manufacturer's recommendations (Thermo Fisher Scientific). Visualization of bands was performed using a Bio-Rad Molecular Imager® Gel Doc™ XR transilluminator system (Bio-rad Laboratories Inc.).

Cycles /Reaction	**Initial Denaturation**	**Denaturation**	**Annealing**	**Extension**	**Cycles**	**Final Extension**
Cep55	94°C	95°C	52°C	72°C	x34	72°C
	2:00 min	0:30 sec	0:30 sec	0:45 sec		5:00 min
Cre	94°C	94°C	55°C	72°C	x34	72°C
	2:00 min	0:30 sec	0:30 sec	0:30 sec		4:00 min
Flpe	94°C	94°C	60°C	72°C	x35	72°C
	3:00 min	0:30 sec	0:30 sec	1:00 min		0:10 sec
Kras	94°C	95°C	54°C	72°C	x35	72°C
	1:30 min	1:00 min	2:00 min	1:00 min		2:00 min
Pten	94°C	95°C	55°C	72°C	x35	72°C
	0:15 sec	1:00 min	2:00 min	1:00 min		2:00 min

Table 2.6 PCR cycles protocol

2.3.4 RNA extraction

RNA extraction was performed using QIAgen RNeasy® Plus Mini kit (Qiagen, 74106, Valencia, CA, USA). Tissue or cells were dissolved in 350 µL of RLT buffer and stored in -80° C for RNA extraction. The extraction was performed as per the user's manual. After RNA elution in 30 µL of nuclease-free water, the quality and quantity of extracted RNA were measured using the Nanodrop ND-1000 spectrophotometer (Thermo-Scientific).

2.3.5 Quantitative RT PCR

Reverse Transcription was performed using the SuperScript First-Strand Synthesis System for RT-PCR. This cDNA was then used as the template for real-time PCR with gene-specific primers as outlined in Table 7. A control reaction was performed without reverse transcriptase to ensure no genomic DNA had contaminated the samples, as well as a no-template control. The qRT-PCR was performed in 96-well plate format using a master-mix of Light Cycler 480 Sybr green (Roche Applied Science, Basel, Switzerland) with a CFX96 Touch Real-Time PCR Detection System (Bio-Rad Laboratories, US). The total volume of each reaction was 8 µL including 4 µL of Sybr green, 1 µL of each primer

(1 picomole of each), 1µL of cDNA (10ng) and 2 µL of sterile water. The following qRT PCR protocol was used:

1. 50° C 2 min, 1 cycle
2. 95° C 10 min, 1 cycle
3. 95° C 15 s → 60 °C 30 s → 72 °C 30 s, 40 cycles
4. 72° C 10 min, 1 cycle

The specificity of qRT PCR amplification was examined by checking the melting curves and running each sample on a 2 % agarose gel. The results were analyzed by the ΔΔCt method. Actin was used as a housekeeping gene.

No	**Gene**	**Sequence**
1.	mActb F	GGCTGTATTCCCCTCCATCG
2	mActb R	CCAGTTGGTAACAATGCCATGT
3	m cMyc F	CGGACACACAACGTCTTGGAA
4	m cMyc R	AGGATGTAGGCGGTGGCTTTT
5	m Mycn F	CCTCCGGAGAGGATACCTTG
6	m Mycn R	TCTCTACGGTGACCACATCG
7	m Ctnnb F	TGGACCCTATGATGGAGCATG
8	m Ctnnb R	GGTCAGTATCAAACCAGGCCA
9	m Cep55 F	CCTAGTAGCTCCAAGTCAGAC
10	m Cep55 R	ACCTTAGGTGGTCTTTGAGTC

Table 2.7 qRT PCR primers

2.4 Statistical analysis

Two-tailed unpaired or paired Student’s t-test, one-way or two-way ANOVA with post hoc Bonferroni, log-rank testing were performed where appropriate using Prism v7.0 (Graph Pad Software, La Jolla, CA, USA) and the P-values were calculated as stated in the Figure legends. Statistical significance was noted to each Figure as follows: “no significance” (ns), $P > 0.05$; $*P \leq 0.05$; $**P \leq 0.01$, $***P \leq 0.001$, and $****P \leq 0.0001$.Mean ± SEM: Mean and standard error of the mean were used to describe the variability within the sample in our analysis.

Chapter 3. Generation of *Cep55* KO mouse model

3.1 Introduction

3.1.1 Mouse Models of Disease

Mouse models have contributed significantly to the investigation of human disease, including developmental disorders and cancer. These models are useful tools that not only determine the function of proteins in a physiological setting but also allow us to study new treatments and the efficacy and safety profile of new drugs. The relative similarities between humans and mice in genes, physiology, pathology, cellular, and molecular characteristics have given rise to the use of mouse models for preclinical testing (Lampreht, et al. 2018). These similarities are the main reason for adopting mouse models to replicate human pathogenesis.

The use of mouse models for research was revolutionized with the development of genetically engineered mouse models (GEMMS), also known as transgenic mouse models (Paez-Ribes *et al.*, 2016). Using approaches such as retroviral infection, DNA microinjection, and gene-targeted transgenes have enabled researchers to express different oncogenes or silence tumor suppressors constitutively or conditionally in the mouse (Kumar *et al.*, 2009). However, these mouse models have drawbacks such as difficulties with accurate embryonic stem cell-specific targeting and the long production time required for initial generation and development of the required genotypes. Recently, the more efficient strategy of CRISPR-based genome editing has developed and provided better solutions to address these issues, allowing the manipulation of, in some cases, several genes at once (Lampreht Tratar, Horvat and Cemazar, 2018).

3.1.2 Knockout transgenic mice

Loss of function of a gene by depleting or silencing in a transgenic mouse is called knockout (KO). KO models can provide important information regarding the functional and pathophysiological role of a gene in a living organism. KO mice can be broadly categorized into two types: constitutive and conditional KO. In constitutive or whole-body KO, the gene is permanently inactivated in every cell of the mouse. The use of constitutive mouse models can be limiting, especially if the targeted gene is embryonically lethal or pups die soon after birth, precluding detailed characterization of phenotypes (Li, Kwak and DeMayo, 2005). To circumvent this problem, conditional KO mouse models have been developed to allow control of gene loss, in terms of both timing and localization of the recombination events (i.e. Targeting to a particular cell or tissue type). Conditional knockout models usually utilize recombination of loxP or FRT consensus sites around one or more exons of the target gene. This model allows recombination upon activation of Cre or FLP recombinases, respectively, which can be activated in a time- or tissue-specific manner, causing recombination and excision of the flanked exon(s). One commonly utilized conditional Cre system is the RosaCre-ERT2 system. In this model, a Cre-ERT2 (Cre fused to mutated ligand binding domain of the Estrogen Receptor, rendering it tamoxifen-responsive) cassette has been inserted into the *Rosa26* locus, a ubiquitously expressed locus on mouse chromosome 6. The administration of tamoxifen allows translocation of Cre-ERT2 to the nucleus to initiate recombination (Metzger and Chambon, 2001).

3.1.3 Knockout mouse models of Centrosomal Proteins

The Centrosome is a cellular organelle composed of a pair of centrioles surrounded by an amorphous complex of proteins called the pericentriolar material (PCM), including γ-tubulin, pericentrin and ninein (Binarová *et al.*, 2006; Avidor-Reiss and Gopalakrishnan, 2013). The centrosome serves as a major microtubule-organizing centre (MTOC) in animal cells as well as integrates complex cytoskeleton and signal transduction events to influence important cellular processes including as cell cycle progression, cell migration, axonal growth and genomic stability (Badano et al., 2005; Brown et al., 2013). The older centriole, termed the mother centriole, plays a key role in the formation of cilia and flagella in the cells (Rieder et al., 2001).

Based on Gene Set Enrichment Analysis (Subramanian *et al.*, 2005), there are 851 genes that are related to centrosomes while the human protein atlas shows 520 proteins localize experimentally to the centrosome or centriolar satellites, and CEP55 is one of these proteins. The centrosome proteome functional enrichment analysis designates biological processes associated with centrosomes to include cellular organization and transportation, organization of microtubules, cell cycle progression and cell division (Human protein atlas). Dysfunction of centrosomal components are known to play both direct and indirect roles in the pathogenesis of a variety of kidney diseases, and ciliopathy-associated disorders including Joubert, Meckel, and Bardet-Biedl syndrome, asphyxiating thoracic dystrophy and microcephaly neurodegenerative disorders, mainly due to the role of centrosomes in neuronal migration (Badano, Teslovich and Katsanis, 2005b). Mutations in centrosome-associated genes such as *STIL*, *CPAP*, *Cep152*, *Cep63*, and *Cep135* can cause autosomal recessive primary microcephaly (Sir *et al.*, 2011). The connection between the centrosome, cilia, and the basal body are highlighted in many human syndromes in which malfunction or defects in these structures leads to a range of disorders (Simms *et al.*, 2011; Abdelhamed *et al.*, 2013; Forsythe and Beales, 2013). An overview of some of the phenotypes associated with abrogation of centrosomal proteins in mouse models based on data mining of the MGI database is shown in (Fig. 3.1) (Eppig *et al.*, 2015).

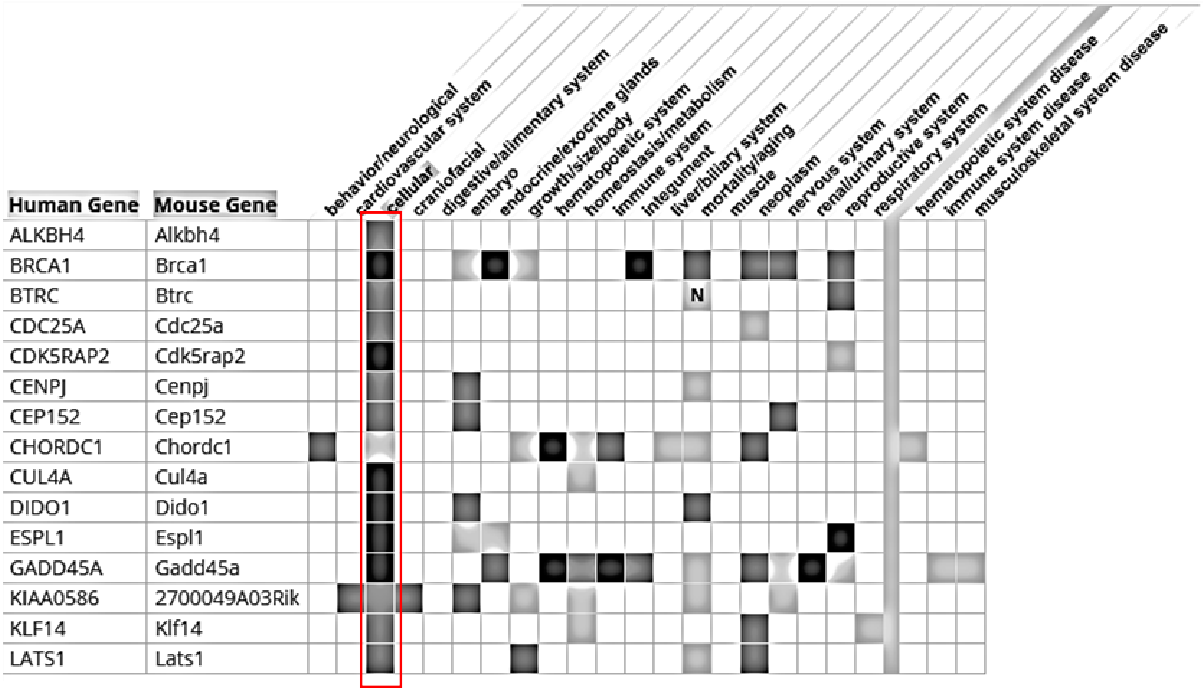

Figure 3.1 Transgenic mouse models which show centrosomal dysfunction.

Figure showing centrosomal-associated genes and their associated phenotypes in mouse knockout models.

3.2 Results

3.2.1 Loss of Cep55 leads to embryonic lethality in mice

To investigate the physiological role of *CEP55* in cancer and development, we obtained gene-targeted mice harboring a transgenic *Cep55* allele generated using the "knockout first" targeting approach, where the targeted allele acts as a gene-trap to form a non-functional (KO) allele (Fig.. 3.2A). Correct targeting was validated by genotyping PCR alongside *Cep55* transcript and protein expression using qRT-PCR and immunoblotting analysis, respectively (Fig. 3.2B-D). To obtain homozygous *Cep55* KO mice, we initially intercrossed *Cep55*$^{+/-}$ heterozygous mice, with the expectation that approximately 25 %

of offspring would be *Cep55*$^{-/-}$ (KO) according to Mendelian ratios. However, after genotyping more than 77 offspring from these breedings across 19 litters, we were unable to obtain any offspring of a *Cep55*$^{-/-}$ genotype, indicating that *Cep55* KO may be embryonically lethal (Table 3.1A). In support of this, we noted that the average litter size of *Cep55*$^{+/-}$ intercrosses were 4.0 pups, compared with an average litter size of 4.8 pups for *Cep55*$^{+/-}$ X *Cep55*$^{+/+}$ crosses (data not shown). To determine the cause of lethality, we set up intercrosses of *Cep55*$^{+/-}$ heterozygotes, dissected pregnant dams at different gestational stages, and collected embryos for both genotypic and phenotypic analysis. Interestingly, we were able to obtain *Cep55*$^{-/-}$ offspring until embryonic day 18.5 (E18.5), but not at the time of birth (Table 3.1B). These results suggest that *Cep55* knockout is lethal prenatally.

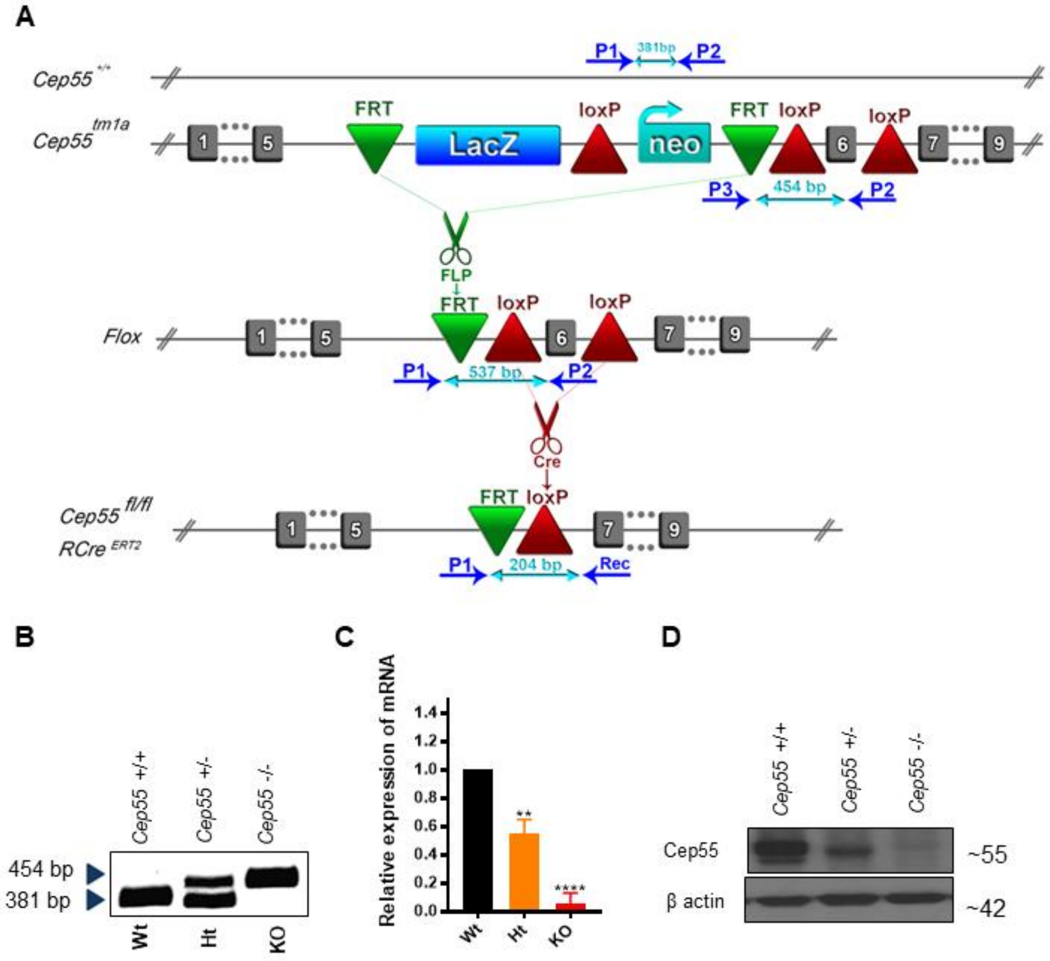
A
Cep55+/+
P1
381bp
P2
Cep55tm1a
1
5
FRT
LacZ
loxP
neo
FRT
loxP
6
loxP
7
9
P3
454 bp
P2
FLP
FRT
loxP
loxP
Flox
1
5
6
7
9
P1
537 bp
P2
Cre
FRT
loxP
Cep55 fl/fl
RCre ERT2
1
5
7
9
P1
204 bp
Rec
B
Cep55 +/+
Cep55 +/-
Cep55 -/-
454 bp
381 bp
Wt
Ht
KO
C
Relative expression of mRNA
1.4
1.2
1.0
0.8
0.6
0.4
0.2
0.0
**
****
Wt
Ht
KO
D
Cep55 +/+
Cep55 +/-
Cep55 -/-
Cep55
β actin
~55
~42

Figure 3.2 Schematic allele of *Cep55* KO mouse model of and validation of its targeting.

(A) Schematic representation showing *Cep55* wt (*Cep55*$^{+/+}$), transgenic (*Cep55*^{tm1a}; gene trapped), floxed (*Cep55*^{Flox}) and Cre-recombined alleles of murine *Cep55*. Blue arrows indicate genotyping primers; (B) PCR genotyping showing *Cep55*$^{+/+}$, *Cep55*$^{+/-}$ and *Cep55*$^{-/-}$ genotypes; (C) mRNA expression of *Cep55* in *Cep55*$^{+/+}$, *Cep55*$^{+/-}$ and *Ce55*$^{-/-}$ E14.5 mouse heads. *ACTB* was used as a housekeeping gene for normalization. Data represent the mean ± SEM, n = 2 mice per genotype, 3 independent experiments, Student's t-test *P < 0.05, **P < 0.01, ***P < 0.001, ****P < 0.0001); (D) Immunoblot analysis of Cep55 protein expression from *Cep55*$^{+/+}$, *Cep55*$^{+/-}$ and *Cep55*$^{-/-}$ E14.5 mouse heads. B-actin was used as a loading control.

A

P0	**Wt**	**Ht**	**KO**	**Total**
Observed	34	43	0	77
%	44.15%	55.85%	0	
Expected	19.25	38.5	19.25	77
%	25%	50%	25%	1

B

Embryonic day	**Attempts**	**Wt**	**Ht**	**KO**	**Total**
E11.5	1	6	1	3	10
%		60%	10%	30%	100%
E13.5	7	18	20	16	54
%		33.3%	37%	29.6%	100%
E14.5	4	5	17	6	28
%		17.9%	60.7%	21.4%	100%
E15.5	1	3	5	3	11
%		27.3%	45.5%	27.3%	100%
E16.5	3	7	14	4	25
%		28%	56%	16%	100%
E18.5	4	11	14	12	37
%		29.7%	37.8%	32.4%	100%
P0	2	3	5	0	8
%		37.5%	62.5%	0%	100%
Total	22	53	76	44	173
%		30.6%	43.9%	25.5%	100%

Table 3.1 Number, percent and genotype of obtained offspring and embryos at different gestational stages

(A) Number and percentage of observed and expected offspring of *Cep55*$^{+/+}$ (WT), *Cep55*$^{+/-}$ (HET), and *Cep55*$^{-/-}$ (KO) genotypes at time of birth (P=0) from *Cep55*$^{+/-}$ intercrosses. Expected percentages are based on Mendelian ratios; (B) Number and percentage of observed and expected embryos of indicated genotypes from *Cep55*$^{+/-}$ intercrosses at multiple gestational stages.

Although we were able to recover embryos of a *Cep55*$^{-/-}$ genotype until late gestational stages, we noted that these embryos exhibited dwarfism when compared to their control *Cep55*$^{+/+}$ and *Cep55*$^{+/-}$ counterparts, based on the crown-rump length measured at both E14.5 and E18.5 (Fig. 3.3A-C). We also observed that the neck of Cep55 embryos at E18.5 was thickened, and the head had a flattened morphology (Fig. 3.3A).

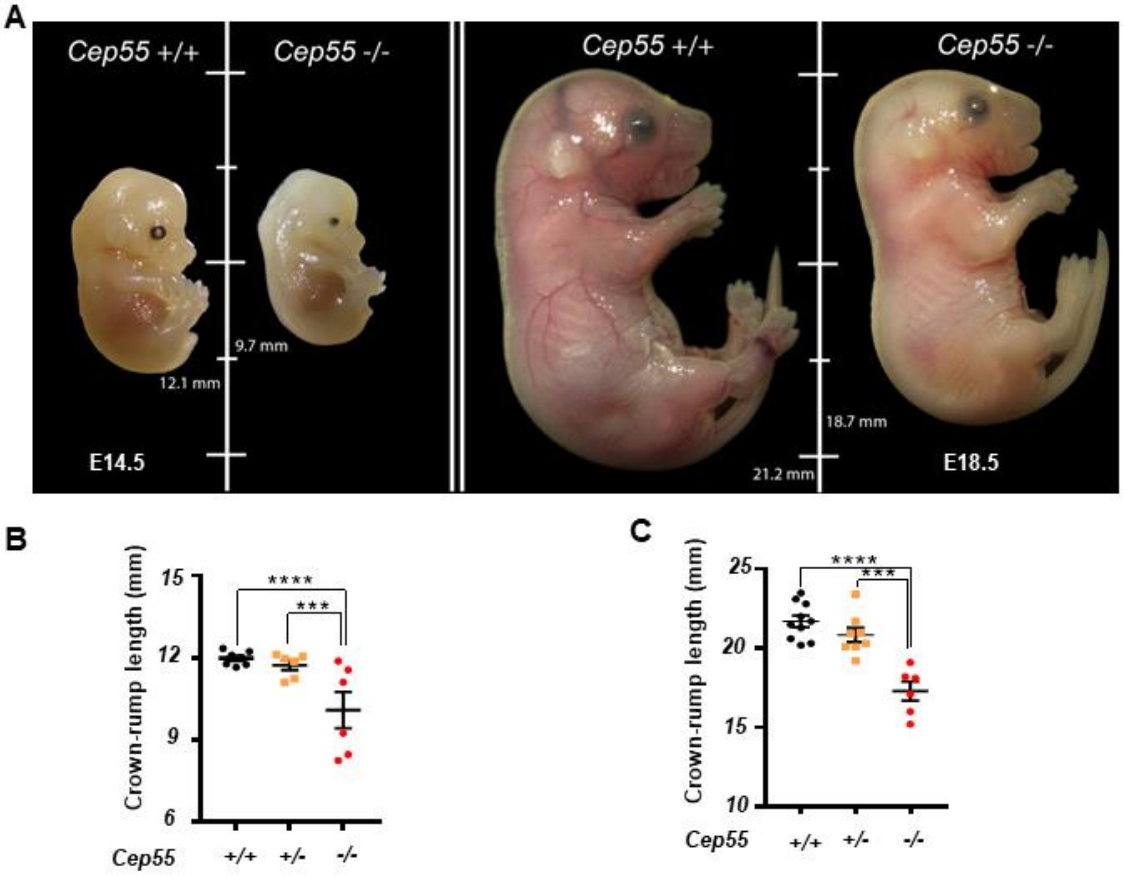
A
Cep55 +/+
Cep55 -/-
9.7 mm
12.1 mm
E14.5
Cep55 +/+
Cep55 -/-
18.7 mm
21.2 mm
E18.5
B
Crown-rump length (mm)
15
12
9
6
****
***
Cep55
+/+
+/-
-/-
C
Crown-rump length (mm)
25
20
15
10
****
***
Cep55
+/+
+/-
-/-

Figure 3.3 Comparison of *Cep55*$^{+/+}$ and *Cep55*$^{-/-}$ embryos at E14.5 and E18.5.

(A) Comparison of size and morphology of E14.5 (left) and E18.5 (right) *Cep55*$^{+/+}$ and *Cep55*$^{-/-}$ embryos. Length of the embryo is indicated in mm; (B) Comparison of the crown-rump length (mm) of E14.5 (left) and E18.5 (right) *Cep55*$^{+/+}$ and *Cep55*$^{-/-}$ embryos.

Data represent the mean ± SEM, n = 6–10 embryos per genotype from a minimum of 3 litters per timepoint. (Students' t-test $^*P < 0.05$, $^{**}P < 0.01$, $^{***}P < 0.001$, $^{****}P < 0.0001$).

3.2.2 *Cep55*$^{+/-}$ *heterozygotes are phenotypically normal*

We next wanted to determine whether the loss of a single allele of *Cep55* would result in any phenotype or whether the loss of both alleles is required. Therefore, we examined age-matched eight-week-old *Cep55*$^{+/+}$ and *Cep55*$^{+/-}$ adult mice for any histological abnormalities. Four age-matched eight-week-old *Cep55*$^{+/+}$ (n=2) and *Cep55*$^{+/-}$ (n=2) mice were sent to the Australian Phenomics Network (APN) for detailed analysis. All systemic organs including but not limited to spleen, kidneys, thymus, heart, pituitary gland, tail, bone marrow, testes, sperm numbers, and different parts of the brain (forebrain, midbrain, and hindbrain) underwent detailed phenotypic examination. These preliminary investigations revealed no significant differences between *Cep55*$^{+/-}$ and their *Cep55*$^{+/+}$ control counterparts when all organs and tissues were assessed (Fig. 3.4A). Moreover, the monitoring of a long-term survival cohort for 54 weeks showed no differences in overall survival (data not shown), and no differences in body weight between *Cep55*$^{+/+}$ and Cep55$^{+/-}$ mice over a 20-week period (Fig. 3.4B)**.** Coronal sections of the brains of *Cep55*$^{+/+}$ and *Cep55*$^{+/-}$ stained with Haematoxylin and Eosin (H&E) and Luxol fast blue stain (LFB; used to detect demyelination in the central nervous system [CNS]), showed no gross morphological or pathological defects (Fig. 3.4C). However, upon routine tail-tipping of these mice, we observed that some mice appeared to exhibit slower blood coagulation, a phenotype that seemed to be specific to *Cep55*$^{+/-}$ mice. To further investigate this phenomenon, we collected mouse tail blood on an age-matched cohort. Our analysis revealed that the platelet counts for *Cep55*$^{+/-}$ (heterozygous) mice were significantly lower than that of *Cep55*$^{+/+}$ ($P< 0.01$ Fig. 3.4D). Although no other variations in blood-related factors were observed (Fig. S1 f-g), the mean platelet volume of *Cep55*$^{+/-}$ mice was slightly higher (Fig. 3.4D).

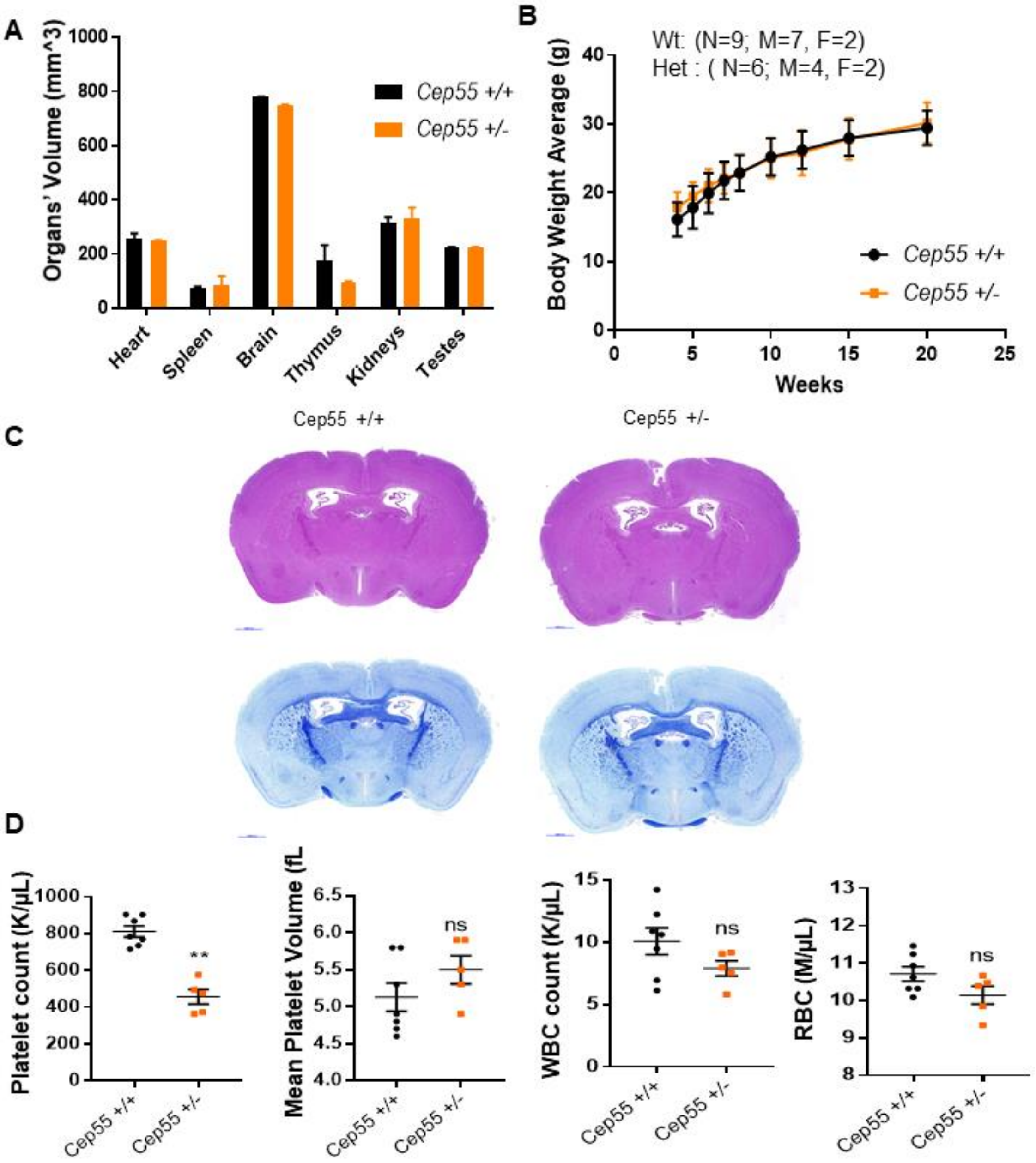

Figure 3.4 Phenotypic analysis of heterozygous mice.

(A) Comparison of organ volumes of 8 week-old *Cep55*$^{+/+}$ and *Cep55*$^{+/-}$ mice. Brain and Thymus size is slightly smaller in *Cep55*$^{+/-}$ (Het) mice. n=2 per group; (B) Mean body weights of *Cep55*$^{+/+}$ and *Cep55*$^{+/-}$ offspring measured at the indicated timepoints until 20 weeks. n=6-9 mice per group; (C) Coronal section of 8 week old mouse brain of *Cep55*$^{+/+}$ and *Cep55*$^{+/-}$ stained with H&E (upper panel) and Luxol fast blue (lower panel; LFB) show no gross morphological/pathological defects; (D) Blood analysis by Hemavet analyser from peripheral blood collected by tail vein bleeding in *Cep55*$^{+/+}$ and *Cep55*$^{+/-}$ showing platelet count, mean platelet volume (MPV), White blood cell (WBC) count and Red blood cell (RBC) count. (Mean ± SEM, n= 5-10, Student's t-test, **$P < 0.01$).

3.2.3 *Expression pattern of CEP55 in human and mouse cells*

Given the essential role of Cep55 during embryonic development, we sought to further examine its expression pattern by bioinformatic analysis. Analysis of the murine RNA-Seq Cap Analysis of Gene Expression (CAGE) datasets revealed that *Cep55* RNA expression levels are highest in major organs during embryonic development compared to juvenile or adult stages, where expression is predominantly restricted to the testes (Fig. 3.5A) (Ramos *et al.*, 2013). Apart from testes, CEP55 in adult tissues is expressed most highly in thymus and lymph nodes but to a lesser degree in the small intestine, colon, and ovary, and minimally in other tissues (Fagerberg *et al.*, 2014). We confirmed this expression profile at the protein level by immunoblot analysis in 8-week old mice, where the highest expression of Cep55 was seen in testis, at modest levels in the spleen and intestines, and there was the undetectable expression in the other tissues analyzed (Fig. 3.5B). In keeping with loss of a single allele of *Cep55*, *Cep55*$^{+/-}$ testes and spleens had lower protein expression levels compared to *Cep55*$^{+/+}$ control (Fig. 3.5C-D).

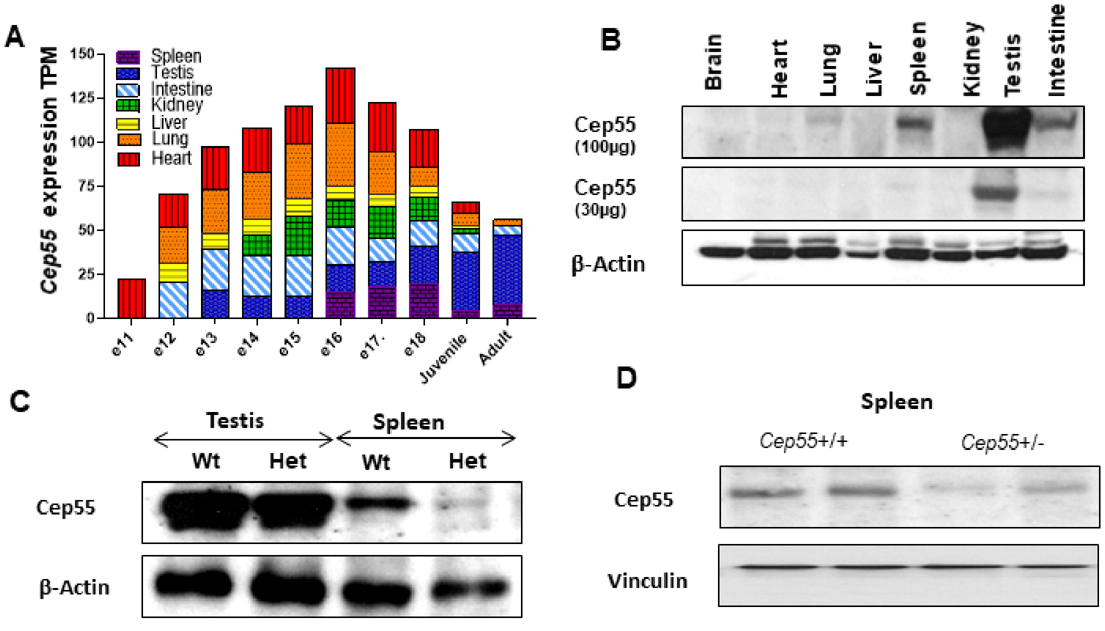

Figure 3.5 *Cep55* expression in embryonic and adult tissues.

(A) *Cep55* expression (Transcripts per Kilobase Million; TPM) comparison in different organs across the indicated ages based on RNA-Seq CAGE (Cap Analysis of Gene Expression) analysis of mouse tissues in the RIKEN FANTOM5 project available at EBI expression atlas; (B) Upper blot: Immunoblot analysis of Cep55 expression in 8 week old mice in the indicated organs; (C) Immunoblot analysis of *Cep55* expression in 8-week old *Cep55*$^{+/+}$ and *Cep55*$^{+/-}$ testes and spleens of a male mouse for the indicated genotypes; (D) Immunoblot analysis of *Cep55* expression in 8-week old *Cep55*$^{+/+}$ and *Cep55*$^{+/-}$ spleen of two female mice per genotype. β-actin and Vinculin served as a loading controls, respectively.

Several recent reports have shown that *Cep55* functional loss in humans leads to a range of congenital abnormalities, all featuring defective brain development (Bondeson *et al.*, 2017; Frosk *et al.*, 2017; Rawlins *et al.*, 2019). Therefore, we next sought to examine the expression pattern of *Cep55* by analysis of single-cell transcriptomic data of mouse neocortical development. This analysis revealed that *Cep55* expression levels are highest in the neuronal progenitor cells of E14 embryos (Loo *et al.*, 2019) (Fig. 3.6A). Moreover, data mining of human fetal brain revealed that expression of *CEP55* peaks from 8 to 12 weeks of gestation, followed by a reduction after 16 weeks. It is then minimally detected between 27-35 weeks and again detectable three weeks prior to the birth (Fig. 3.6B) (Shen, Overly and Jones, 2012). This expression pattern corresponds with the timing of human neurogenesis in the neocortex through neurogenic divisions and neuronal differentiation from the radial glial cells (Vied *et al.*, 2014). Importantly, data mining of RNA-seq data revealed that in the CNS a higher expression of *CEP55* is associated with structures such as the cerebral cortex, cerebellum, and astrocytes (Fig. 3.6C) (Lachmann *et al.*, 2018).

The knockout-first (Targeted) allele of *Cep55* contains a *LacZ* reporter, allowing spatio-temporal analysis of *Cep55* expression during development upon enzymatic reaction with the X-gal substrate. To examine the expression pattern of *Cep55* during development, we performed β-galactosidase staining in *Cep55*$^{+/-}$ mice, harboring one copy of the targeted allele. We observed ubiquitous expression of *Cep55* in whole-mount staining of E11.5 embryos, with staining intensity diminishing at later embryonic stages (Fig. 3.6D). In the isolated brain of mouse embryos, a gradient of expression of *Cep55* was detected at E12.5, and this expression level diminished at E14.5 to become undetectable at E16.5 in the neocortex (Fig. 3.6E). Collectively, these data demonstrate a specific pattern of *Cep55* expression during embryogenesis.

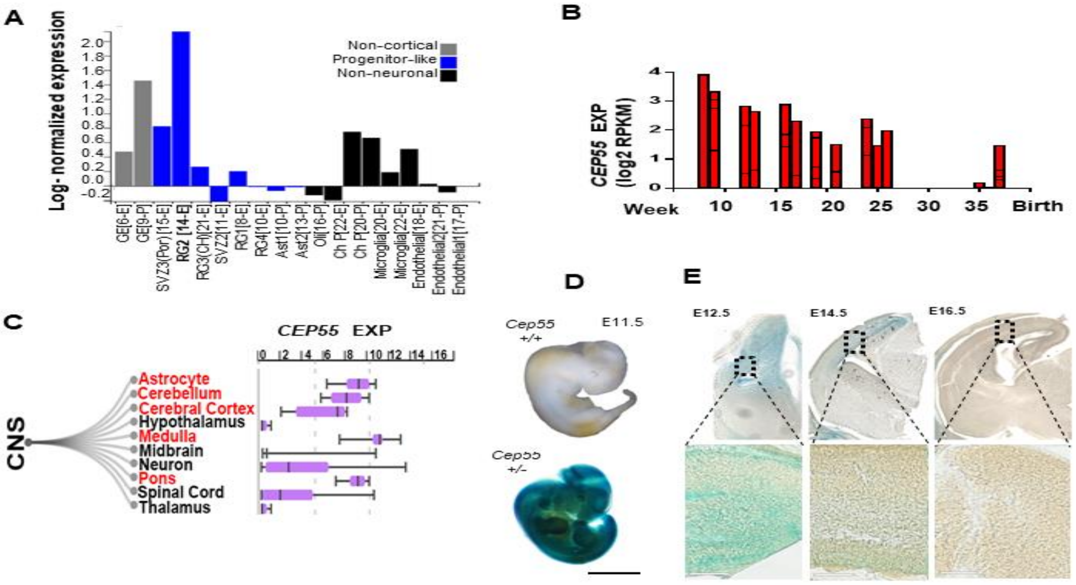

Figure 3.6 Human and mouse Cep55 expression during embryonic brain development.

(A) *Cep55* expression in the single-cell transcriptomic analysis of mouse neocortical development visualized based on the available data at Zylka lab dataset (Loo *et al.*, 2019); (B) *CEP55* expression (reads per kilobase million; RPKM) in human fetal brain at the indicated gestational stages of gestation until birth. Raw data were obtained from the Allen brain atlas (Shen, Overly and Jones, 2012); (C) Metadata annotation for *CEP55* expression of gene counts from HiSeq 2500 and NextSeq 500 platforms for human and mouse experiments from Gene Expression Omnibus (GEO) by ARCHS^4 data server. Clustering data shows *CEP55* expression associated with different CNS regions (Lachmann *et al.*, 2018). The structures shown in red have higher than median expression of *Cep55*; (D) Whole-mount β-galactosidase staining of *Cep55*$^{+/+}$ (control) and *Cep55*$^{+/-}$ (harboring a single copy of the transgenic allele containing a LacZ reporter) in E11.5 embryos, Scale=2 mm; (E) β-galactosidase staining of coronal sections of *Cep55*$^{+/-}$ mouse embryonic brain at the indicated timepoints. The dotted black box indicates the magnified area shown on the right, Scale=100 µm.

3.2.4 Cep55 conditional KO mice are viable

Given the difficulties in studying the effects of constitutive *Cep55* loss in adult mice due to the late embryonic lethality observed, we nexted wanted to generate conditional *Cep55 KO* (cKO) mice, allowing knockout in adult tissues. To achieve this, we utilized the Rosa-CreER^{T2} system, where the Cre-ER^{T2} transgene is inserted into the *Rosa26* locus (*RosaCreERT2*$^{+}$), allowing ubiquitous expression of Cre when activated by injection of tamoxifen (Fig. 3.7A). *Cep55*$^{Fl/Fl}$ mice were crossed against RosaCreERT2 transgenic mice to generate *RosaCreERT2*$^{+}$*; Cep55*$^{Fl/Fl}$ mice, allowing the loss of Cep55 upon tamoxifen administration. Eight-week-old *RosaCreERT2*$^{+}$*; Cep55*$^{Fl/Fl}$ mice were injected with tamoxifen (n=8) or vehicle control (n=6). The knockout of *Cep55* was validated by western blot in the spleen, a tissue that we previously showed to have detectable expression of Cep55 (Fig. 3.7B). We monitored control mice (*Cre*$^{+}$*; Cep55*$^{Fl/Fl}$ injected with vehicle and *Cre*$^{-}$*; Cep55*$^{Fl/Fl}$ injected with tamoxifen) and *Cep55* cKO (*Cre*$^{+}$*; Cep55*$^{Fl/Fl}$, tamoxifen-treated) mice for 25 weeks following treatment, and all mice were viable and healthy during this time. Dissection of these animals showed no gross morphological defects in all major organs, including heart, lung, liver, kidney, testes, and spleen between cKO and control counterparts, and their overall weight profiles did not exhibit any major differences (data not shown). Together, these results suggest that *Cep55* is dispensable for adult tissue homeostasis.

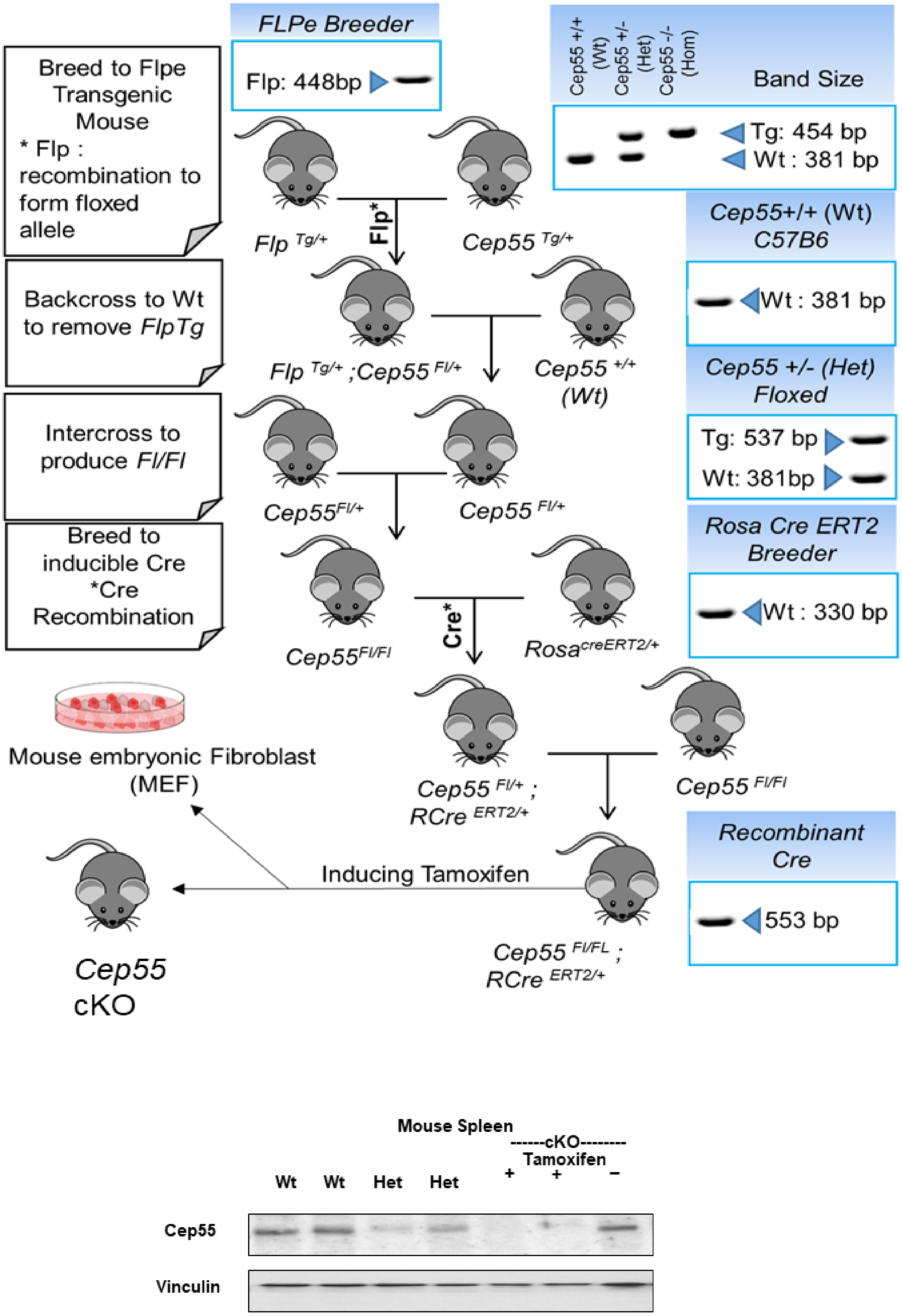
FLPe Breeder
Flp: 448bp
Cep55 +/+ (Wt)
Cep55 +/- (Het)
Cep55 -/- (Hom)
Band Size
Tg: 454 bp
Wt : 381 bp
Breed to Flpe Transgenic Mouse
* Flp : recombination to form floxed allele
Flp Tg/+
Flp*
Cep55 Tg/+
Cep55+/+ (Wt) C57B6
Wt : 381 bp
Backcross to Wt to remove FlpTg
Flp Tg/+ ;Cep55 Fl/+
Cep55 +/+ (Wt)
Cep55 +/- (Het) Floxed
Tg: 537 bp
Wt: 381bp
Intercross to produce Fl/Fl
Cep55Fl/+
Cep55 Fl/+
Rosa Cre ERT2 Breeder
Wt : 330 bp
Breed to inducible Cre
*Cre Recombination
Cep55Fl/Fl
Cre*
RosacreERT2/+
Mouse embryonic Fibroblast (MEF)
Cep55 Fl/+ ; RCre ERT2/+
Cep55 Fl/Fl
Recombinant Cre
553 bp
Inducing Tamoxifen
Cep55 cKO
Cep55 Fl/FL ; RCre ERT2/+
Mouse Spleen
------cKO--------
Tamoxifen
Wt
Wt
Het
Het
+
+
−
Cep55
Vinculin

Figure 3.7 Breeding strategy for generation of Cep55 cKO mice.

(A) Schematic of breeding strategy for generating *Cep55* conditional knockout (cKO) mice; (B) WB analysis of Cep55 expression level in *Cep55*$^{+/+}$ (Wt), *Cep55*$^{+/+}$(Het), *Cep55*$^{fl/fl}$ Cre- tamoxifen-treated (cKO -) and *Cep55*$^{fl/fl}$ *Cre*$^{+}$ tamoxifen-treated (cKO +) mice in spleens of 8-week old mice. Vinculin served as a loading control.

3.3 Discussion

In this chapter, we describe the generation of constitutive and conditional KO of *Cep55*. We found that loss of *Cep55* leads to late embryonic lethality in mice, emphasizing its essential role during embryogenesis. However, we demonstrate that Cep55 is dispensable for adult tissue homeostasis. The expression of Cep55 in the embryo and adult mouse was consistent with bioinformatic analysis of its expression profile.

We observed that knockout of *Cep55* is late embryonically lethal, as we were able to recover *Cep55*$^{-/-}$ embryos until late gestational stages but not following birth. The expression analysis using the *LacZ* transgene demonstrates that *Cep55* is expressed in the neocortex during embryogenesis, and the observed lethality may therefore arise from neurological changes in *Cep55*$^{-/-}$ embryos (this is discussed in further detail in the next chapter). Heterozygous loss of *Cep55* did not cause any phenotypic abnormalities, nor did we observe any gross morphological defects in induced *Cep55* cKO adult mice monitored over a period of 25 weeks. As Cep55 is expressed at low levels in most adult tissues, this is not entirely surprising. Of course, it is also important to note that conditional knockout of Cep55 will not occur in all tissues to the same degree. Moreover, as Cep55 is expressed at low levels in most adult tissues, it is difficult to assess the degree of loss that has occurred upon recombination.

The lack of phenotype in adult *Cep55* cKO mice could occur due to several reasons. One is that *Cep55* plays a predominant role in stem cell or developing cells, and thus, inducible KO of *Cep55* has no effect on developed organs. It is also important to note that recombination will not occur in all cells across tissues equally and mosaicism would occur. Low levels of recombination may not be sufficient for a phenotype to manifest in this case. Alternatively, it is possible, given the high expression of Cep55 in the embryonic brain, that *Cep55* plays a major role in this organ. Unfortunately, a major caveat of the RosaCre$^{\mathrm{ERT2}}$ system is that tamoxifen is unable to efficiently cross the blood-brain barrier, precluding analysis of the effects of *Cep55* loss in the brain. To further examine the role of *Cep55* in adult brain homeostasis, the *Nestin-CreER*^{T2}*/R26R* transgenic mouse model could be utilized, where CreER$^{\mathrm{T2}}$ induces recombination in multipotent neural stem cells (NSCs) upon tamoxifen administration. However, this system is not without its caveats, as a recent study demonstrated that short tamoxifen treatment in transgenic mouse models does not have a measurable impact on adult neurogenesis (Rotheneichner *et al.*, 2017).

Collectively, our data demonstrate an essential role of *Cep55* during embryogenesis, but that *Cep55* is dispensable for adult tissue homeostasis. The high levels of *Cep55* expression in the brain during embryogenesis warrant further investigation into the role that *Cep55* plays in neural development during embryogenesis, which is examined in greater detail in the next chapter.

Chapter 4. Phenotypic characterization of Cep55 loss during development

---

4.1 Introduction

Embryonic brain development is a complex process, requiring the spatio-temporal convergence of multiple signaling cascades including Sonic Hedgehog (Shh), PI3K/AKT and Wingless-related integration site (Wnt) in neural progenitor cells (NPs). These pathways are highly conserved, and tightly regulated in NP cells to ensure their sustained self-renewal and timely differentiation to generate neurons and glia that populate the central nervous system (CNS). Imbalances in any of these components can lead to severe neurodevelopmental consequences characterized by abnormal brain sizes, cortical malformations, and learning deficits (Hsieh *et al.*, 2014).

Corticogenesis is the process by which the cerebral cortex, the outer layer of the brain, forms. The cerebral cortex is the most evolutionarily conserved area of the mammalian brain and the centre for processing and regulating cognitive behaviours as well as somatosensory skills (Braga *et al.*, 2012; Kaas, Gharbawie and Stepniewska, 2013; Rockland, Kaas and Peters, 2013). The cerebral cortex is mainly comprised of neurons and glial cells, which are mostly generated from neural progenitors (NPs) during embryonic development (Ming and Song, 2005). Neurons, the functional and structural subunit of the brain, are generated and differentiated in the procedure of neurogenesis.

Neurogenesis in the developing neocortex occurs with the contribution of two types of progenitor cells: radial glial cells (RGCs) and intermediate progenitor cells (IPCs) (Englund, 2005; Taverna, Götz and Huttner, 2014). RGCs express the homeodomain transcription factor, PAX6, and divide at the ventricular zone (VZ; the apical surface) to ultimately produce neurons and glia. IPCs, which are derived from radial glial cells, produce only neurons, divide within the basally located subventricular zone (SVZ) and express TBR2, a T-domain transcription factor. The transition from IPCs to postmitotic projection neurons is marked by the onset of TBR1 expression (Englund, 2005). In addition to molecular markers, NPs are classified based on their cellular characteristics, such as mitotic location (apical or basal), polarity, and proliferation or differentiation potential (Taverna, Götz and Huttner, 2014).

In mice, corticogenesis begins at approximately E11.5 and continues until E18.5. The first wave of neurons is produced at the VZ by apical progenitors and forms the preplate (PP), which later divides into the marginal zone (MZ) and subplate (SP), delaminating the cortical plate (CP). Each layer of the six-layer neocortex in the mouse is comprised of a specific neuronal subtype with an explicit function. The neocortex develops from inside to outside, in which newly generated neuroblasts migrate through the intermediate zone (IZ) to their destination at the cortical layer (Molyneaux *et al.*, 2007).

In this chapter, we provide a detailed analysis of the phenotype of *Cep55* knockout mice, which exhibit a predominantly neural defect phenotypes such as the presence of microcephaly, cerebellar hypoplasia, and multinucleated neurons. Furthermore, I perform a detailed characterisation of the mechanism by which *Cep55* regulates neurogenesis during cortical development.

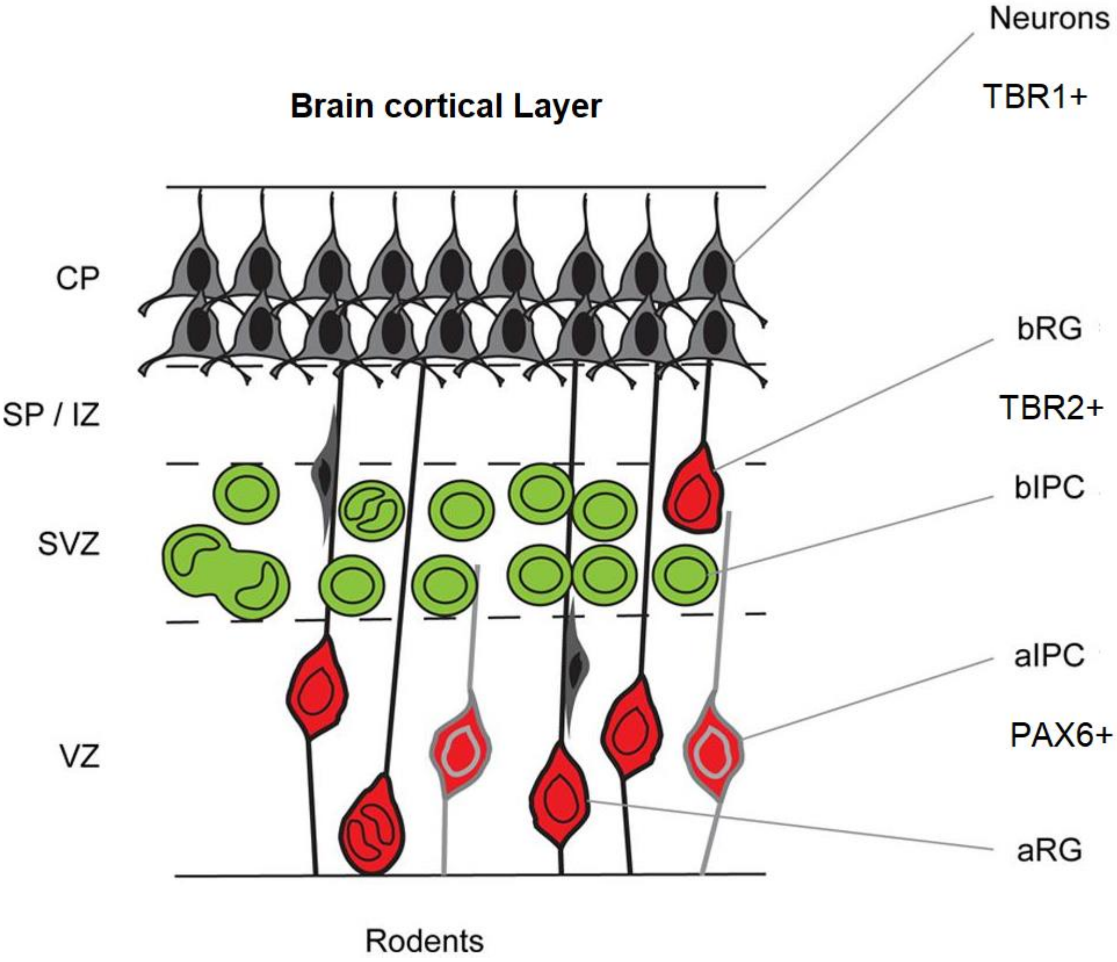

Figure 4.1 Schematic of brain cortical layers in rodents.

Coronal section view of the mouse developing cortex demonstrates progenitor cell types and their markers Pax6 (red), TBR2 (green), and TBR1 (gray). The layers (outside to inside) consist of CP, cortical plate; SP, subplate; IZ, intermediate zone; SVZ, subventricular zone; ISVZ, inner subventricular zone; OSVZ, outer subventricular zone; VZ, ventricular zone; aRG, apical radial glia; bRG, basal radial glia; aIPC, apical intermediate progenitor cell; bIPC, basal intermediate progenitor cell (Manuel *et al.*, 2015).

4.2 Results

4.2.1 Cep55 loss causes gross morphological defects in mouse embryos

We demonstrated in chapter 3 that constitutive Cep55 loss causes late embryonic lethality. To further understand the underlying cause of this phenotype, we first performed hematoxylin and eosin (H&E) staining of sagittal and coronal sections of E18.5 embryos of *Cep55*$^{+/+}$, *Cep55*$^{+/-}$ and *Cep55*$^{-/-}$ genotypes. In collaboration with the APN and A/Prof. John Finnie, we assessed these embryos to identify any gross morphological defects. We observed no notable phenotypic differences in the lung, intestine or liver among the respective genotypes. We also investigated whether the architecture of the skeleton was changed in E18.5 *Cep55*$^{-/-}$ mice by performing whole-mount staining with alcian blue and alizarin red to observe cartilage and mineralized bone, respectively, but did not observe any phenotypic differences (data not shown). Interestingly, we observed that the kidneys of *Cep55*$^{-/-}$ embryos appeared to exhibit tubular degeneration, suggesting that Cep55 may play a role in renal development.

We noted prominent abnormalities of the brain of E18.5 *Cep55*$^{-/-}$ embryos when compared to respective controls, with hypoplasia and dysplasia of the brain. Specifically, the cerebellum was hypoplastic, with marked thinning of the germinative external-granular layer (EGL) and a diminution and disorganization of cortical neurons. In addition, the neuronal population of the olfactory bulb was disorganized and depleted (Fig. 4.2A). Coronal sectioning of the brain revealed neocortical depletion of neurons and ventricular dilatation, as well as smaller germinal regions in both the dorsal and ventral telencephalon (Fig. 4.2B). The neocortices of *Cep55*$^{-/-}$ were hypoplastic and dysplastic, with diminished and disorganized neurons. In addition to apoptosis in the neocortex, there were also multifocal areas of cortical necrosis and parenchymal loss, with evidence of phagocytosis of affected neurons by macrophage-like cells (Fig. 1h, upper panel). Numerous bi-nucleated neurons were also found in the neocortex of *Cep55*$^{-/-}$ (Fig. 4.2B, lower panel). Moreover, the quantification of multinucleated neurons immunostained by NeuN showed an increase in numbers of multinucleated cells in the cortical region of *Cep55*$^{-/-}$ mice compared to that of *Cep55*$^{+/+}$ controls ($P<0.01$ Fig. 4.2D-E), a phenotype reminiscent of that described in human embryos with MARCH (Frosk *et al.*, 2017).

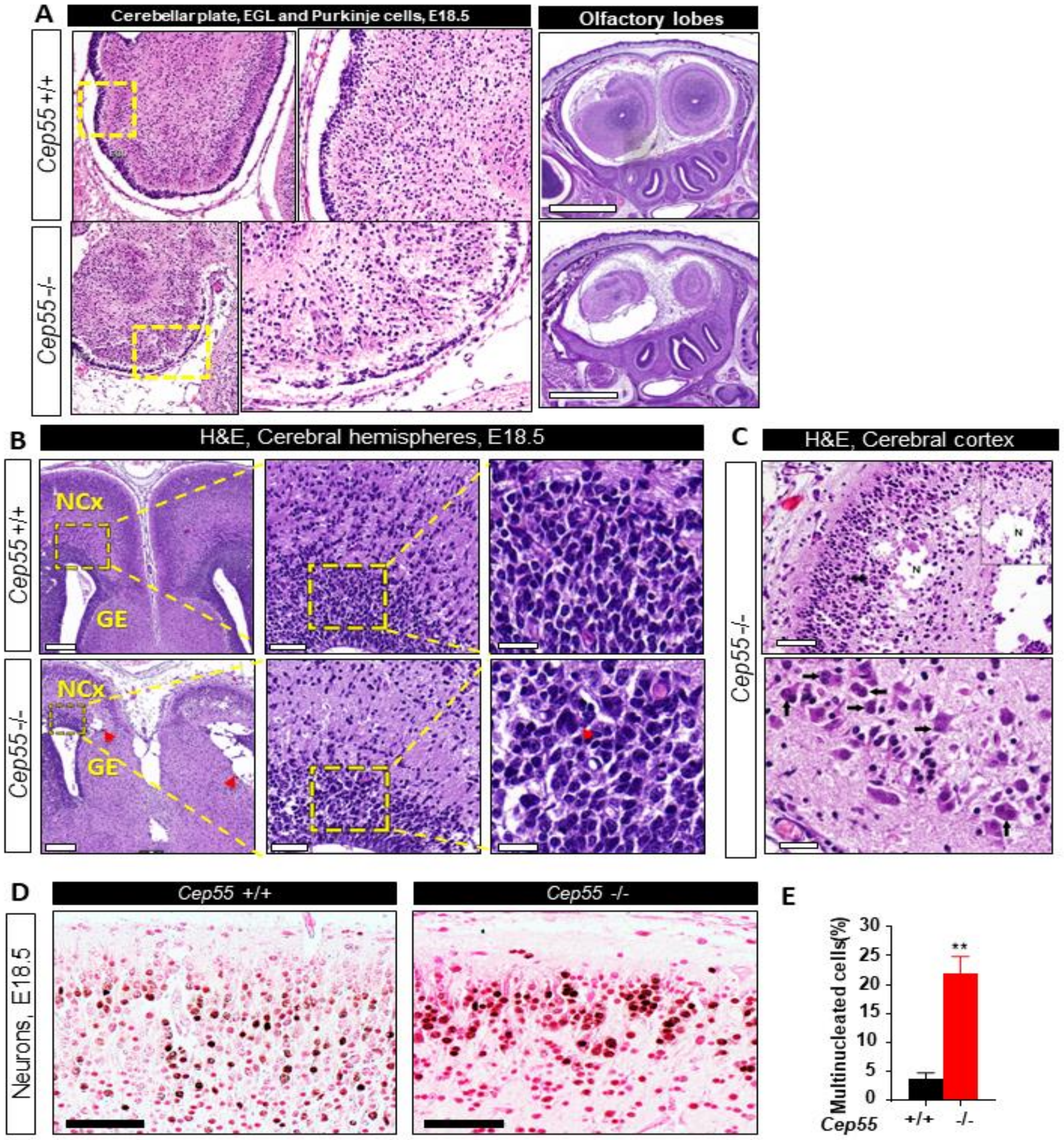
A
Cerebellar plate, EGL and Purkinje cells, E18.5
Olfactory lobes
Cep55 +/+
Cep55 -/-
B
H&E, Cerebral hemispheres, E18.5
NCx
GE
Cep55 +/+
Cep55 -/-
C
H&E, Cerebral cortex
N
Cep55 -/-
D
Cep55 +/+
Cep55 -/-
Neurons, E18.5
E
Multinucleated cells(%)
30
25
20
15
10
5
0
**
Cep55
+/+
-/-

Figure 4.2 Characterizing gross morphological defects in mouse embryonic brain.

(A) Cerebellar hypoplasia. Compared to the *Cep55*$^{+/+}$ (upper panel) to *Cep55*$^{-/-}$ mouse (lower panel) there is a marked reduction in thickness of the external granular layer (EGL) in a *Cep55*$^{-/-}$ mouse (left,bottom). The cerebellar cortical neuronal population in (bottom) is deficient and disorganized. Higher power views of both cerebellar cortices are also shown; The olfactory bulb is also neuron-deficient and disorganized in a *Cep55*$^{-/-}$ mouse compared to a *Cep55*$^{+/+}$ mouse (right). Scale = 60µm. (B) Comparison of E18.5 *Cep55*$^{+/+}$ cerebral hemisphere (neocortex and germinal centeral/lateral ventricles) from *Cep55*$^{+/+}$ (upper panel) and *Cep55*$^{-/-}$ (lower panel) E18.5 embryos. Left panels: ventricular dilatation in *Cep55*$^{-/-}$ (lower panel). Red arrows designate structural dilation, distortion and disorganization, and necrotic area with neural tissue loss. Scale= 200µm. Middle panels: magnification of boxed area, Depletion of subependymal germinal neuroblasts in *Cep55*$^{-/-}$ (lower panel) Scale= 50µm. Right panels: magnification of boxed area, neocortical neuronal depletion in cerebral hemispheres and reduction of cortical neuronal population in *Cep55*$^{-/-}$ (lower panel). Red arrow designates multinucleated neurons. Scale= 20µm. (C) Upper panel: neocortical hypoplasia/dysplasia. Diminished and disorganised neurons with an area of parenchymal necrosis (N) and neural tissue loss. Phagocytosed neuronal cellular debris is arrowed. Scale=120 µm. Lower panel: numerous bi-nucleated neurons (arrows) in the neocortex of a *Cep55*$^{-/-}$ E18.5 embryos. Scale=180 µm, (D) Representative image of NeuN (brown) and Eosin (pink) immunohistochemical staining of E18.5 sections from Cep55$^{+/+}$ (left) and Cep55$^{-/-}$ (right) sections showing multinucleation. Scale= 50µm; (E) Graphical representation of percentage of multinucleated cells. Data represent mean ± SEM of four embryos, N=4, average count of duplicate technical repeats, Student's t-test, *P < 0.05, **P < 0.01, ***P < 0.001, ****P < 0.0001).

4.2.2 Cep55 loss causes microencephaly due to a reduction of neurons and neuroglia

In order to further characterize the gross morphological defects observed by histopathology, we first measured the size of the brains of *Cep55*$^{+/+}$ and *Cep55*$^{-/-}$ embryos. Strikingly, brain sizes of *Cep55*$^{-/-}$ E18.5 embryos were found to be significantly smaller compared to that of *Cep55*$^{+/+}$ control counterparts (Fig. 4.3A). Interestingly, this reduction in size (*Cep55*$^{-/-}$ brain area, $P<0.001$) likely resulted from both decreases in total cell number ($P<0.001$) and neurons ($P<0.0001$), since the density of the cells (cells/area) after normalization to total brain area, was not significantly different between genotypes (Fig. 4.3B).

Our previous analysis of the expression pattern of Cep55 by lacZ staining revealed forebrain expression of *Cep55* at E12.5 and E14.5 in the neocortex. To investigate the impact of *Cep55* loss on distinct neural cell populations in the neocortex, we performed detailed immunohistological (IHC) staining for cell populations within the neocortex at E18.5. Initially, we stained for NeuN (RBFOX3) to mark mature neurons and glial fibrillary acidic protein (GFAP), a component of intermediate filaments expressed by CNS cells such as astrocytes and ependymal cells. The mature neurons (NeuN-positive cells) were reduced in numbers when assessed across the full brain section ($P<0.0001$) and when assessed across a 100µm area of the neocortex ($P<0.001$) in *Cep55*$^{-/-}$ compared to that of *Cep55*$^{+/+}$ embryos even after normalization to the total cell number to account for size differences between brains (Fig. 4.3C). Interestingly, GFAP-positive filaments in the neocortex were reduced in *Cep55*$^{-/-}$ embryos ($P<0.001$) when compared to *Cep55*$^{+/+}$, suggesting potential defects in the central nervous system development. In the cortical region, GFAP can be a marker of either astrocytes or radial-glial-like neuronal stem cells and represents mature radial glia, which can be seen in the medial region (glial wedge). In keeping with this, the population of mature astrocytes was also markedly reduced in *Cep55*$^{-/-}$ brain ($P<0.001$) comparing to that of *Cep55*$^{+/+}$ leading to defects in the corpus callosum (Fig. 4.3D), where development is reliant on medially-located astrocytic populations (Mori and Leblond, 1969). Notably, we observed dysgenesis of the corpus callosum in the brain of *Cep55*$^{-/-}$ embryos. This staining also revealed the disorganization of astrocytes within the *Cep55*$^{-/-}$ brain, which is consistent with the overall neurological defects observed in *Cep55*$^{-/-}$ embryos.

Taken together, these data show that loss of *Cep55* results in a range of neural defects in mice; specifically, we observed that a majority of areas analyzed for *Cep55*$^{-/-}$ embryos exhibited hypoplasia, including the neocortex, olfactory lobes, and cerebellum. Additionally, we observed the development of multifocal areas of parenchymal necrosis in the neocortex and binucleated neurons were commonly observed.

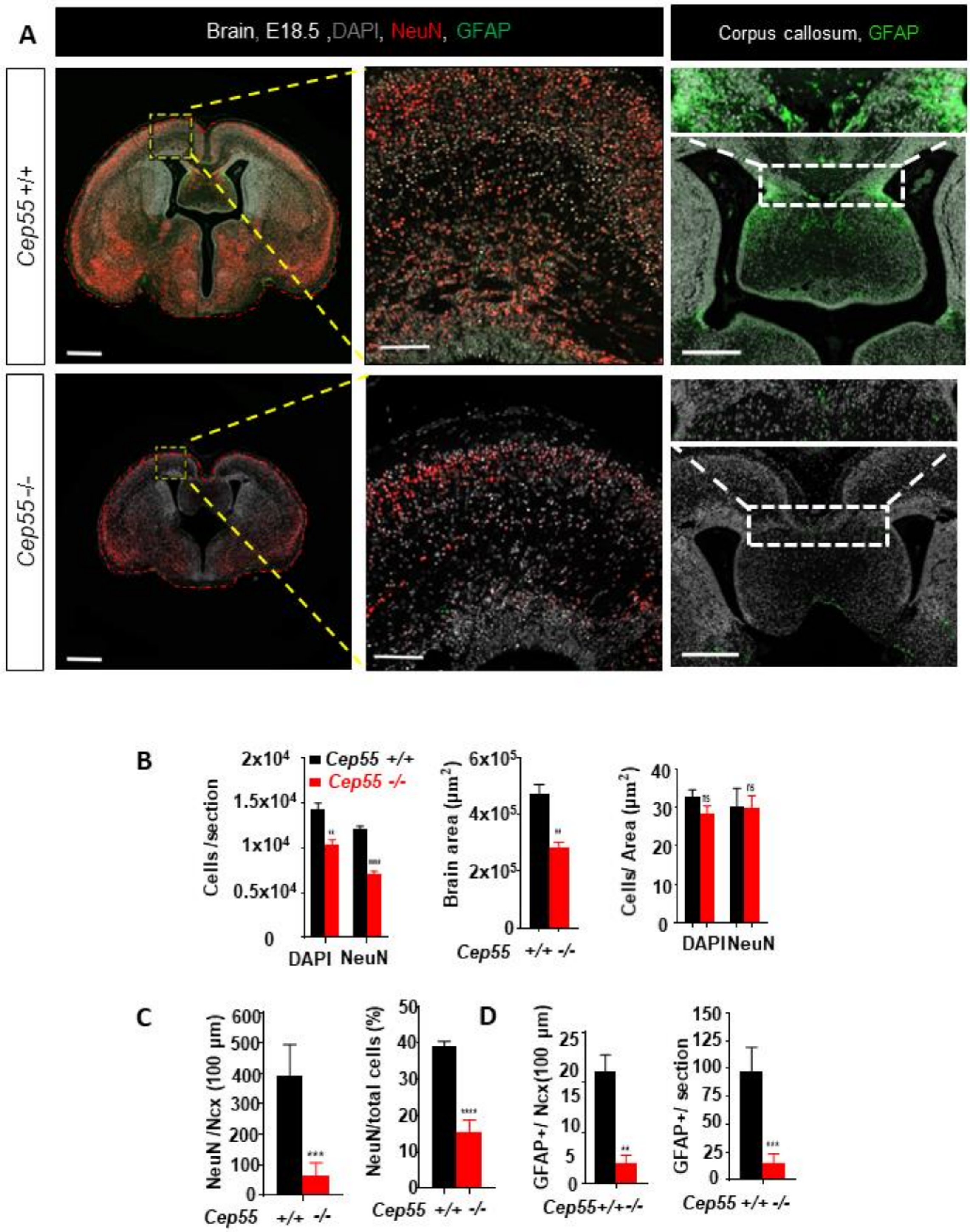
A
Brain, E18.5 ,DAPI, NeuN, GFAP
Corpus callosum, GFAP
Cep55 +/+
Cep55 -/-
B
Cells /section
2x10⁴
1.5x10⁴
1x10⁴
0.5x10⁴
0
Cep55 +/+
Cep55 -/-
DAPI
NeuN
Brain area (µm²)
6x10⁵
4x10⁵
2x10⁵
0
Cep55 +/+ -/-
Cells/ Area (µm²)
40
30
20
10
0
ns
DAPI
NeuN
C
NeuN /Ncx (100 µm)
600
500
400
300
200
100
0
Cep55 +/+ -/-
NeuN/total cells (%)
50
40
30
20
10
0
Cep55 +/+ -/-
D
GFAP+/ Ncx(100 µm)
25
20
15
10
5
0
Cep55+/+-/-
GFAP+/ section
150
125
100
75
50
25
0
Cep55 +/+ -/-

Figure 4.3 KO brain size is smaller due to a reduction in neurons and astrocytes.

(A) Representative image from immunohistochemical staining of whole coronal section (left), magnified region (middle) and medial region or glial wedge (right) of E18.5 *Cep55*$^{+/+}$ (upper panels) and *Cep55*$^{-/-}$ (lower panels) embryonic mouse brains. Sections have been stained for NeuN (neuronal nuclei, mature neurons) and GFAP (Glial fibrillary acidic protein, marks astrocytes, and ependymal cells during development). Right panels show the population of mature radial glia. Corpus callosum dysgenesis in *Cep55*$^{-/-}$ brain (lower right panel), the boxed area in this panel shows GFAP expression in a magnified zone of the glial wedge. Scale= 600 µm (left panel), Scale= 100 µm (middle panel), Scale= 400µm (right panel); (B) Comparison of *Cep55*$^{+/+}$ and *Cep55*$^{-/-}$ overall cell and neuron number (left), brain area (middle), and cell/neuron density (right). n=4, P< 0.0036, 0.0001; (C) Comparison of *Cep55*$^{+/+}$ and *Cep55*$^{-/-}$ neuron (NeuN-positive) numbers in 100 µm area of the neocortex (Ncx; left) and percent of NeuN-positive across whole brain section to the total neural cells (right panel). This graph shows the proportion of NeuN-positive cells divided by the number of DAPI-positive cells in the indicated areas. Data represent mean ± SEM across two regions from n=4 independent embryos per genotype. Student's t-test, *P < 0.05, **P < 0.01, ***P < 0.001, ****P < 0.0001); (D) Comparison of *Cep55*$^{+/+}$ and *Cep55*$^{-/-}$ GFAP-positive cell count per 100 µm-width box of cortical section (left) and the comparison of GFAP count in the whole section (right). Data represent mean ± SEM of four embryos per genotype, average of duplicate technical repeats, Student's t-test, *P < 0.05, **P < 0.01, ***P < 0.001, ****P < 0.0001).

4.2.3 Cep55 regulates cell fate of radial glial and intermediate progenitor cells

As we found a reduced number of both neurons and astrocytes, we next sought to determine how *Cep55* regulates neural stem cell (NSC) differentiation and development during neurogenesis and focused on the six neuroepithelial layers of the developing neocortex as our developmental model. As neurogenesis in neocortical layers peaks at around E14.5 (Caviness Jr, 1982; Finlay and Darlington, 1995; Clancy, Teague-Ross and Nagarajan, 2009), we chose this gestational age for characterization. Similar to what we observed at E18.5, we noted reduced brain size (P<0.001) and fewer neural cells (P<0.05) in the cortex of *Cep55* $^{-/-}$ when compared to *Cep55* $^{+/+}$ brains at E14.5 (Fig. 4.4A-B). The relative size of the ventricle to total brain area was larger in *Cep55*$^{-/-}$ (P<0.001) and was dilated, consistent with our previous histopathological observations (Fig. 4.4AB). We also observed that the thickness of the cortex was reduced in *Cep55*$^{-/-}$ (P<0.0001) brains, in line with the reduction of the cortical plate that is seen later in development (Fig. 4.4C).

We next sought to investigate the different populations of progenitor cells within the nascent cortex, to ascertain where deficits in cortical neuron number may arise. During developmental differentiation from radial glial cells (RGCs) to intermediate progenitor cells (IPCs) that subsequently generate postmitotic projection neurons, sequential expression of the transcription factors PAX6, TBR2, and TBR1 delineates these cell types, respectively (Englund, 2005). We categorized RGCs as the PAX6^{+} TBR2$^{–}$ population, as some nascent TBR2^{+} IPCs retain PAX6 expression transiently, as previously described (Harris *et al.*, 2016). This population of PAX6^{+} TBR2^{-} cells was diminished in *Cep55*$^{-/-}$ (P<0.001) cortices when compared to *Cep55*$^{+/+}$ mice, and this trend remained unchanged even after normalization to the total cell number of the region (P<0.01, Fig. 4.4D, E). Furthermore, in *Cep55*$^{-/-}$ embryos, we found decreased numbers of both IPCs (identified by TBR2^{+}) distributed in the basal ventricular zone (VZ) and lower intermediate zone (IZ) (Fig. 4E, P<0.01), and the postmitotic neurons (indicated by TBR1^{+}) scattered in the IZ, subplate, cortical plate, and marginal zone (Fig. F,G P<0.01). Moreover, the population of TBR1^{+} (P<0.001) and TBR2^{+} (P<0.05) cells were also reduced relative to total cell count. The deficiencies in the IPC population observed in *Cep55*$^{–/–}$ mice could potentially occur as a result of increased direct neurogenesis from RGCs; however, our findings suggest an overall decline in all contributing stem cells and, consequently, a drop in neuron number. Moreover, we observed that a proportion of neurons did not complete mitosis and exhibited cell separation defects (binucleated neurons).

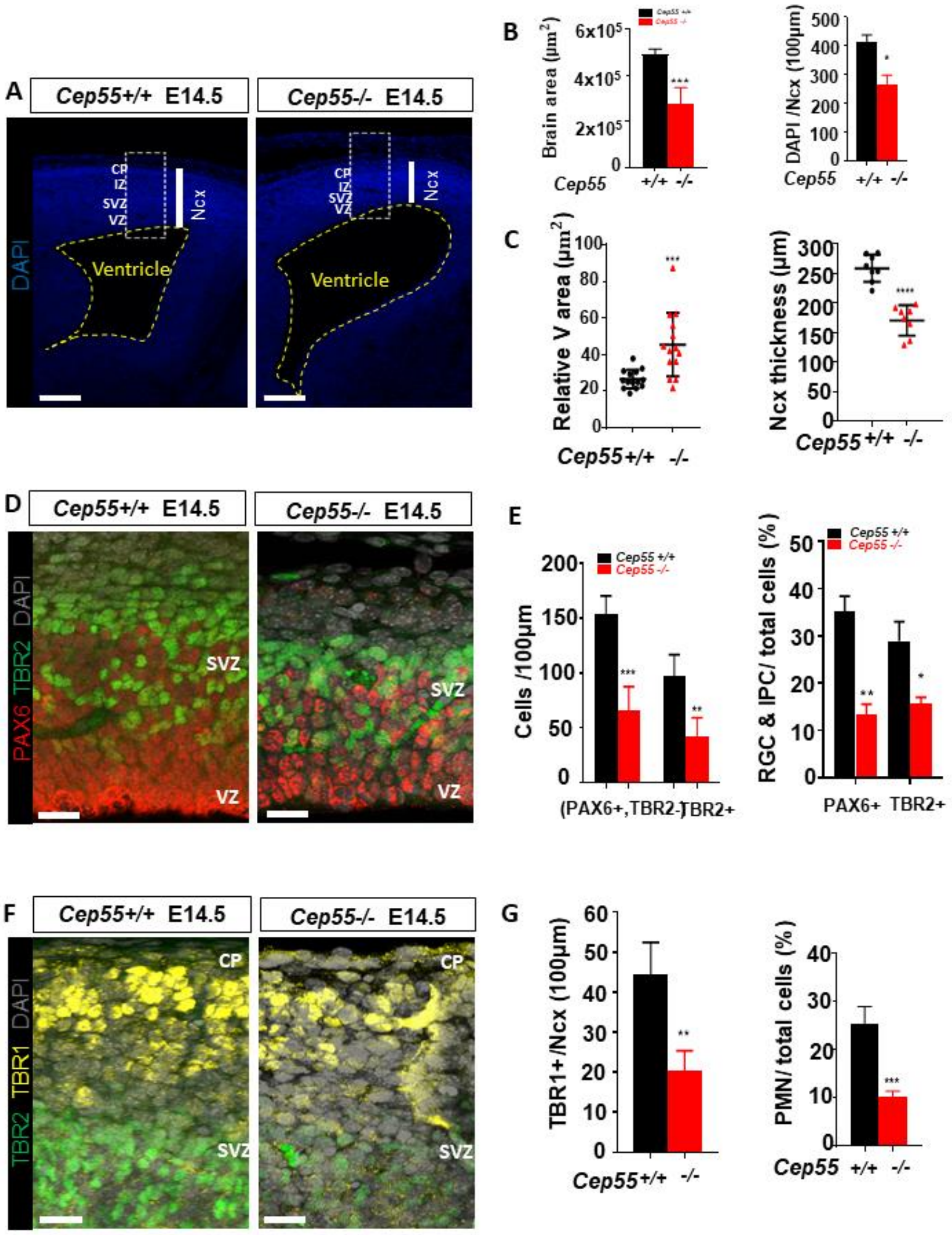
A
Cep55+/+ E14.5
Cep55-/- E14.5
DAPI
CP
IZ
SVZ
VZ
Ncx
Ventricle
B
Cep55 +/+
Cep55 -/-
Brain area (µm²)
6x10⁵
4x10⁵
2x10⁵
0
***
Cep55
+/+
-/-
DAPI /Ncx (100µm)
500
400
300
200
100
0
*
C
Relative V area (µm²)
100
80
60
40
20
0
***
Ncx thickness (µm)
300
250
200
150
100
50
0
****
D
PAX6
TBR2
DAPI
SVZ
VZ
E
Cells /100µm
200
150
100
50
0
***
**
(PAX6+,TBR2-)
TBR2+
RGC & IPC/ total cells (%)
50
40
30
20
10
0
**
*
PAX6+
TBR2+
F
TBR2
TBR1
DAPI
CP
SVZ
G
TBR1+/Ncx (100µm)
60
50
40
30
20
10
0
**
PMN/ total cells (%)
40
30
20
10
0
***

Figure 4.4 Characterization of Cep55 in the regulation of neural progenitor cells.

(A) Representative images of *Cep55*$^{+/+}$ and *Cep55*$^{-/-}$ neocortexes (Ncx) at E14.5 showing different sections of the Ncx: VZ, SVZ, IZ and CP. Vertical line represents the thickness of the Ncx, dashed line shows the ventricle area and box designates the analysis area. Scale= 50 µm; (B) Comparison of brain area of *Cep55*$^{+/+}$ and *Cep55*$^{-/-}$ E14.5 embryos (left) and brain cell density (DAPI count within 100 µm-width box of the neocortex). (Mean ± SEM of four embryos measured in duplicate, Student's t-test, $*P < 0.05$, $**P < 0.01$, $***P < 0.001$, $****P < 0.0001$); (C) Comparison of *Cep55*$^{+/+}$ and *Cep55*$^{-/-}$ for left: relative ventricle area (µm²; total area showed/total brain area) and right: Ncx thickness; Quantification was performed from two fields of 100 µm-width box which spanned the length of the neocortex. For analysis, sections were imaged through a depth of 10 µm (consecutive 1 µm z-steps) using a 60X objective of a confocal microscope. Then, the z-stack was flattened, and the analysis was performed manually and computationally. Comparison of *Cep55*$^{+/+}$ and *Cep55*$^{-/-}$ Ncx at E14.5 showing: (D) radial glial cells (RGC; PAX+, red) at VZ, intermediate progenitor cells (IPC; TBR2+,green) at SVZ and total cells (DAPI, gray); (E) Left: RGCs (PAX6+, TBR2-) and IPCs (TBR2+) numbers in 100µm box. Right: RGCs and IPCs normalised to total cell number (DAPI); (F) IPCs (TBR2+, green) at SVZ, post-mitotic neurons (TBR1+, yellow) at CP and total cells (DAPI, gray); (G) Left: post-mitotic neurons (TBR1+) count in the 100 µm-width box; Right: TBR1+ count normalised to total cell number (DAPI).

4.2.4 Cep55 regulates proliferation and apoptosis in neural progenitor cells

Next, we wanted to investigate how *Cep55* may regulate proliferation and apoptosis in the developing neocortex, and how this may impact on mitosis. Therefore, we concentrated on the analysis of proliferative, mitotic (Colman *et al.*, 2006) and apoptotic (de Torres *et al.*, 1997) indices defined by Ki67, phosphohistone H3-S10 (pH3), and TUNEL staining, respectively. Interestingly, the *Cep55*$^{+/+}$ neocortex exhibited a higher percentage of pH3-positive RGCs (P<0.01) and IPCs (P<0.05, Fig. 4.5A-B). Moreover, when the pH3-positive cell pool was normalized to the total number of cells, the proportion of pH3-positive cells remained elevated (P<0.05). The proliferation index for both the total number of Ki67+ (P<0.0001) and Ki67+ / total cell ratio (P<0.01) were significantly reduced in *Cep55*$^{-/-}$ animals (Fig. 4.5C-D). Furthermore, levels of apoptosis as marked by TUNEL staining in *Cep55* $^{-/-}$ brains compared to the controls was elevated when assessed as both total numbers (P<0.0001) and percentage (P<0.01) of cells (Fig. 4.5E-F). Interestingly, Western blot analysis of embryonic brain (E14.5) extract also showed upregulation of cleaved caspase-3 in *Cep55*$^{-/-}$ brains when compared to control samples, confirming the IHC results and histopathology observations (Fig. 4.5G).

Collectively, these data suggest that *Cep55*-deficient RGCs undergo decreased divisions, possibly due to defective cytokinesis, reduced numbers of each progenitor population, and exhibit more cell death, which subsequently leads to a reduced neuronal population during early neocortical development. Similar findings were observed at E16.5, indicating that defects identified persisted through to later stages of cortical development (data not shown). Cell homeostasis during development is dictated by the ability of stem cells to self-renew and expand versus differentiate. Our data suggest a role for *Cep55* in maintaining the viability of RGC and IPC populations in the developing neocortex.

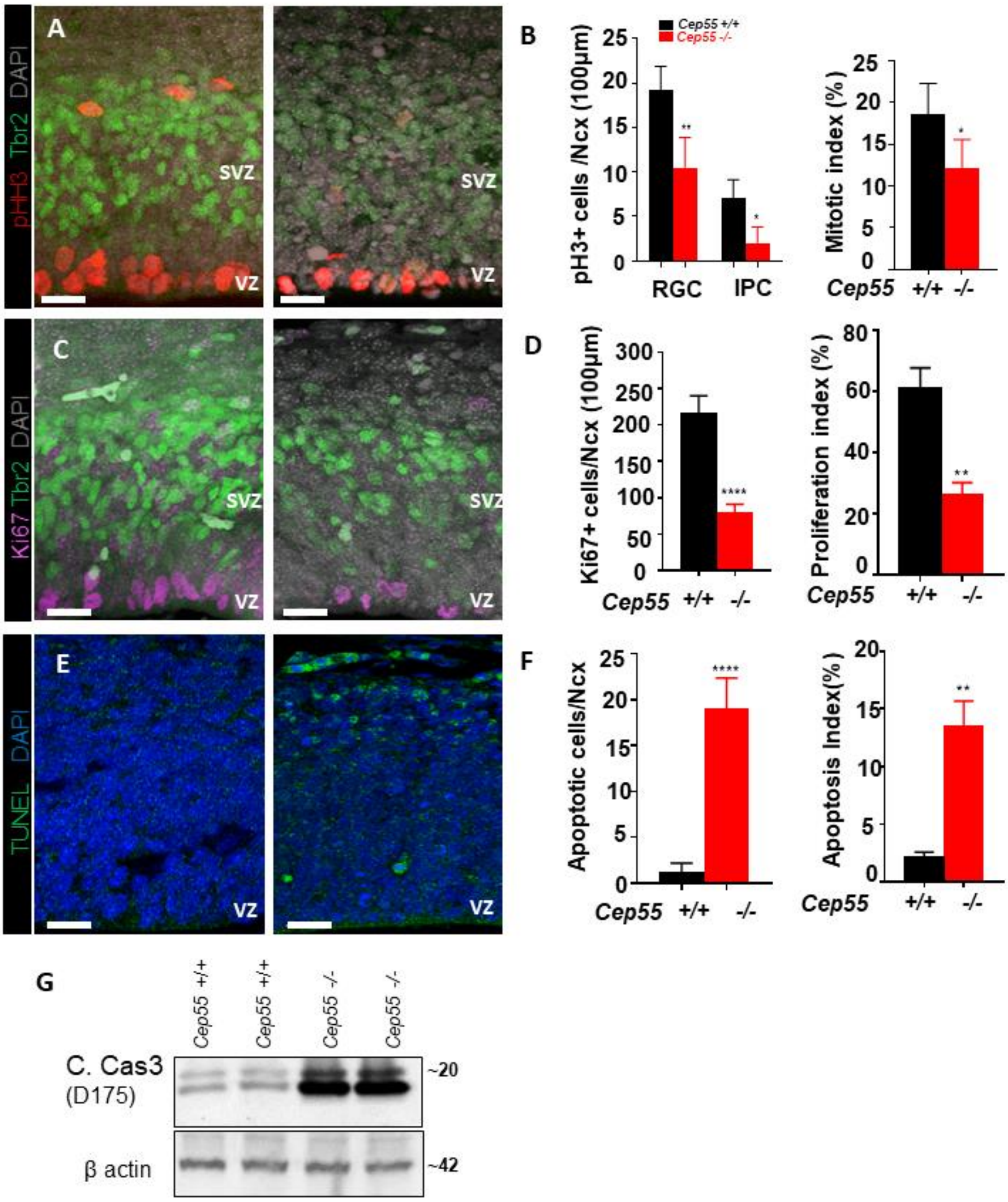
A
pHH3 Tbr2 DAPI
SVZ
VZ
B
Cep55 +/+
Cep55 -/-
pH3+ cells /Ncx (100µm)
25
20
15
10
5
0
**
*
RGC
IPC
Mitotic index (%)
*
Cep55 +/+ -/-
C
Ki67 Tbr2 DAPI
D
Ki67+ cells/Ncx (100µm)
300
250
200
150
100
50
****
Proliferation index (%)
80
60
40
20
**
E
TUNEL DAPI
F
Apoptotic cells/Ncx
****
Apoptosis Index(%)
G
Cep55 +/+
Cep55 +/+
Cep55 -/-
Cep55 -/-
C. Cas3
(D175)
β actin
~20
~42

Figure 4.5 Characterizing mitotic, proliferation and apoptotic indices in NPCs.

(A) Phosphohistone H3 (pH3, red; mitotic cells) at VZ and SVZ, IPCs (TBR2+,green; SVZ) and total cells (DAPI, gray); (B) Left: pH3 positive cells in the 100 µm-width box. Right: total pH3 count normalised to total cells number (DAPI) to show mitotic index;

(C) Proliferating cells (Ki67+, purple), IPCs (TBR2+, green) showing the SVZ, and total cells (DAPI, gray); (D) Left: Ki67 positive cells in the 100 µm-width box. Right: total Ki67 counts normalized to total cells (DAPI) to show proliferation index; (E) Apoptotic cells (TUNEL, green) and total cells (DAPI, blue) in the Ncx; (F) Left: Apoptotic cell (TUNEL) count in the 100 µm-width box. Right: Apoptotic cell count normalized to total cell (DAPI) number; (G) Immunoblot analysis performed on E14.5 mouse embryonic brain extract of *Cep55*$^{+/+}$ and *Cep55*$^{-/-}$ for cleaved caspase 3. β actin or Vinculin served as loading controls.

4.3 Discussion

In this chapter, we performed detailed phenotypic characterization of the consequences of Cep55 loss during development. As was discussed in the previous chapter, the loss of Cep55 results in prenatal lethality as a major phenotype. In this chapter, we aimed to characterize the cause of lethality. For this reason, we collected embryos through multiple stages of gestation and found that we could recover *Cep55*$^{-/-}$ embryos until late gestational stages (E18.5). We analyzed different embryonic organs and tissues for phenotypic characterization initially by H&E staining and demonstrated the major morphological defect was seen in the brain where cellular homeostasis was disrupted. Specifically, we demonstrated that the brain of *Cep55*$^{-/-}$ embryos was fully hypoplastic and dysplastic with disorganized cellular architecture and binucleation as a result of a defect in cell division. Furthermore, there was evidence of apoptotic and necrotic cells, which contributed to cellular dysplasia.

Previous studies of *Cep55* loss by mutation or morpholino treatment in zebrafish have demonstrated that *Cep55* loss leads to defective head morphology, characterized by the presence of apoptosis (Jeffery *et al.*, 2015). More recently, several reports described human syndromes in which *Cep55* expression is disrupted due to mutations that were incompatible with life (Bondeson *et al.*, 2017; Frosk *et al.*, 2017; Rawlins *et al.*, 2019). These reports showed a number of phenotypes, including multinucleated neurons, anhydramnios, renal dysplasia, cerebellar hypoplasia, and hydranencephaly. Notably, across these reports, the presence of hydranencephaly (fluid-filled cavities) was observed by ultrasound. In the case of *Cep55*$^{-/-}$ embryos, it is conceivable that the necrosis observed in our model could progress to a major loss of cerebral hemisphere parenchyma, resulting in marked cavitation, leaving only a small amount of residual cortical tissue, and compensatory expansion of the lateral ventricles (hydranencephaly) or porencephaly, if the cystic change and parenchymal loss was less severe. In addition to this, we observed that the brains of *Cep55*$^{-/-}$ mice exhibited multinucleated neurons and cerebellar hypoplasia. Collectively, we observed defects in the olfactory bulb, cerebellum and cerebrum of the brain of *Cep55*$^{-/-}$ embryos, likely leading to the microencephaly observed. In addition to the neural phenotypes, we also observed renal tubular degeneration of the kidneys, consistent with reports of Cep55 loss in humans. However, due to time constraints, this phenotype was not investigated in further detail.

The lethal phenotype of *Cep55* mutation in humans precluded a detailed analysis of the underlying cause of the phenotypes observed. We sought to use our mouse model to further understand the changes occurring in the brain upon *Cep55* loss and focused on the development of the neocortex as a model system. We observed that the smaller size of the brain in *Cep55*$^{-/-}$ embryos was likely due to a reduction in neuron populations, and also observed a decline in astrocyte numbers. Moreover, we demonstrated that Cep55 plays a vital role in the regulation of progenitor cells of the neocortex. We showed that apical radial glial cells (PAX6+), basal intermediate progenitor cells (TBR2+), and immature neurons (TBR1+) all exhibited a decline in population numbers concomitant with decreased proliferation and increasing apoptosis in *Cep55*$^{-/-}$ embryos.

Data mining of BIOGRID (Stark *et al.*, 2006) for potential *Cep55* interacting partners in mice revealed *Cep55* interactions with other centrosomal proteins such as *Cep131* and *Cep72,* which are both linked to ciliopathy (Stowe *et al.*, 2012; Hall *et al.*, 2013).

Moreover, data mining of BIOGRID for humans revealed that in addition to well known interacting partners TSG101 and ALIX, additional centrosomal proteins including *CEP162, CEP120* and *CEP128* which are related to ciliopathy as well as *CENPJ* , *CEP63* and *CEP135* which result in microcephaly were identified (Xie *et al.*, 2007; Hussain *et al.*, 2012; Wang *et al.*, 2013; Garcez *et al.*, 2015; Marjanović *et al.*, 2015; Roosing *et al.*, 2016).

In conclusion, our data show that Cep55 is an essential regulator of neurogenesis in the neocortex, a phenotype that we characterize in more detail at the molecular level in the next chapter.

Chapter 5. Characterization of the role of Cep55 in ciliogenesis and cellular homeostasis

5.1 Introduction

5.1.1 The primary cilia

The primary cilia is a signaling organelle, which project from the cell as an antenna-like structure (Powles-Glover, 2014). Primary cilia are predominantly composed of microtubules emanating to form the axoneme from the centriole which forms the basal body (Rieder, Faruki and Khodjakov, 2001b). The basal body is a protein complex (a modified centriole) located at the base of the cilia that functions as a nucleation site for the growth of the axoneme microtubules. These microtubules are involved in vesicle trafficking (Marshall, 2008; Schrøder *et al.*, 2011). The basal bodies organize primary cilia at the plasma membrane during G_0. On cell cycle entry, cilia resorb following the migration of the basal body near the nucleus where it functions to organize centrosomes (Jones *et al.*, 2008; Kim and Dynlacht, 2013).

Malfunction of the ciliary axoneme, basal body or cilia anchoring structures leads to defects in cilia organization and function, triggering ciliopathies (Adams et al., 2008). Aberrations in genes involved in the structure or function of the cilia or its associated components can lead to a class of disorders collectively called ciliopathies, and can manifest with a wide range of features including retinal degeneration, renal disease and cerebral anomalies (Fuchs and Schwark, 2004; Han *et al.*, 2008). To date, more than 35 ciliopathies have been described, associated with defects in 187 different genes (Reiter and Leroux, 2017).

Moreover, a growing body of evidence has linked cilia dysfunction to neurogenetic disorders such as Meckel-Gruber, Joubert, Bardet-Biedl, and COACH syndrome (Hartill et al., 2017). Cilia are mostly formed after neuroblast migration; however, cilia elongation may not be required for migration nor neural polarity, and their precise role in the development of the neocortex remains somewhat unclear (Arellano et al., 2012; Lee, Park, & Jang, 2019). However, deficiency in a number of human and mouse genes required for cilia formation or function can lead to cortical defects (Fuchs and Schwark, 2004; Han *et al.*, 2008).

5.1.2 Cilia and Hedgehog Signaling

Cilia as sensors play a crucial role in modulating several signaling pathways, including Sonic Hedgehog (Shh), and are integral to the normal functioning of this signaling pathway (Fig. 5.1). The Hedgehog (Hh) signaling pathway is a crucial regulator of cell differentiation and migration in embryonic development (Li *et al.*, 2012). There are three homologs of Hh: Desert (Dhh), Indian (Ihh), and Sonic (Shh), and the latter is the most well characterized. Shh signaling starts with the binding of the glycoprotein Shh to the protein Patched (Ptch1), which inactivates the inhibitor of Smoothened G protein-coupled receptor (Smo). Consequently, Smo activates Gli, which initiates the Shh downstream signaling cascade (Riobo, Lu and Emerson, 2006). Mediation of Shh signaling through cilia plays an important role in the signaling of neurogenesis, and neuron-specific knockout of a number of hedgehog components using Nestin-Cre has been shown to lead to ciliopathy-associated neural phenotypes including disruption of neuronal migration and differentiation as well as neural progenitor development (Guo *et al.*, 2015). In this report knockdown of 17 ciliary genes in the developing neocortex led to delayed neuronal and glial radial migration (Guo *et al.*, 2015). Two independent studies also showed that knockdown of cilia-associated genes *Kif3a* or *Ift88 in the* developing cortex resulted in similar developmental defects due to cell cycle catastrophe in NPCs and defects in interkinetic nuclear migration (Foerster *et al.*, 2017; Chen, Chang and Tsai, 2018).

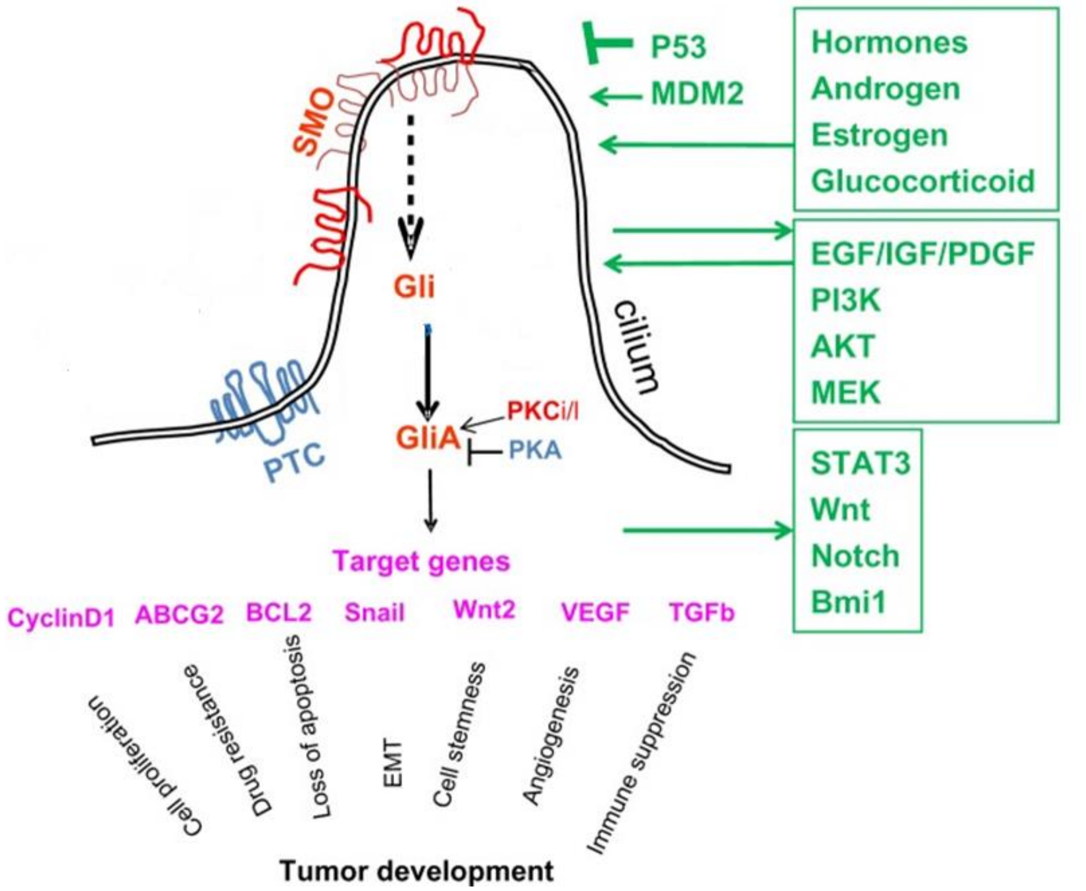
SMO
P53
MDM2
Hormones
Androgen
Estrogen
Glucocorticoid
EGF/IGF/PDGF
PI3K
AKT
MEK
Gli
cilium
GliA
PKCi/l
PKA
PTC
STAT3
Wnt
Notch
Bmi1
Target genes
CyclinD1
ABCG2
BCL2
Snail
Wnt2
VEGF
TGFb
Cell proliferation
Drug resistance
Loss of apoptosis
EMT
Cell stemness
Angiogenesis
Immune suppression
Tumor development

Figure 5.1 Hedgehog (Hh) signaling in mammalian cells.

Smoothened (SMO) is the key signal transducer of the Hh pathway. In the absence of the Hh ligands, Hh receptor patched (PTC) is localized in the cilium to inhibit SMO signaling. Positive regulators of the Hh pathway are in red, negative regulators in blue, and target genes are in pink. Interacting pathways are in green. (Adopted from (Xie *et al.*, 2013)).

5.1.3 PI3K/AKT signaling and ciliogenesis

A number of studies have demonstrated direct or indirect modulation of PI3-kinase/Akt activation in mediating the target effects of Shh (Kanda *et al.*, 2003; FU *et al.*, 2006; Riobó *et al.*, 2006)'. Akt has been shown to mediate Gli inactivation downstream of Shh, positively regulating Shh signaling through PKA- and GSK3β-mediated phosphorylation of Gli2 to reduce its transcriptional activity (Riobó *et al.*, 2006). GSK3β inhibition can also be regulated by Shh in a posttranscriptional manner to reduce the accumulation of N-myc and regulate cell cycle progression (Mill *et al.*, 2005).

Akt and Shh signaling have also been shown to converge on N-Myc to control neural progenitor proliferation and cell cycle progression (Kenney, Widlund and Rowitch, 2004). The uncontrolled synergistic correlation between Akt and Shh signaling can also contribute to tumor formation (Rao *et al.*, 2004). Dysregulation of Shh has also been reported to have a neuroprotective effect on astrocytes by activating Akt through antiapoptotic survival protein, BCl-2, via interaction with the proapoptotic proteins Bax and Bak, thereby protecting neurons against oxidative stress (Xia *et al.*, 2012). Although AKT has been shown to regulate Shh signaling, the effect of AKT signaling in cilia formation remains poorly understood. While one study suggested that inhibition of AKT1/2 inhibits cilia formation and length, another found that PI3K/AKT signaling causes cilia loss (Suizu *et al.*, 2016; Conduit *et al.*, 2017).

5.1.4 Cep55 and Ciliopathy-like phenotypes

Recently, *Cep55* mutation has been associated with a lethal ciliopathy-like phenotype (Bondeson *et al.*, 2017; Rawlins *et al.*, 2019) in humans, but the exact mechanism by which Cep55 regulates cilia function remains elusive. To further understand the role that *Cep55* plays in this process, in this chapter, we perform a detailed characterization of the effect of *Cep55* loss on ciliogenesis and the signal transduction pathway changes associated with this phenotype.

5.2 Results

5.2.1 Cep55$^{-/-}$ mice exhibit cilia abnormalities

We demonstrated in the previous chapter that the loss of *Cep55* in the embryo leads to defective neocortical development. Many centrosomal proteins have been shown to play an essential role in the functioning of cilia. Cilia are requisite in guiding the process of development and during neurodevelopment, where they are mostly localized to the lateral ventricle and extend from RGCs but can be found amongst different NPs and neuron populations (Fuchs and Schwark, 2004).

We hypothesized that *Cep55* might play an important role in the formation or functioning of cilia in the developing neocortex. To examine whether this was the case, we chose to investigate the neocortices of *Cep55*$^{-/-}$ and matched *Cep55*$^{+/+}$ control mice at E14.5, a time-point where ciliogenesis peaks. Initially, we performed immunostaining on E14.5 brain sections from *Cep55*$^{+/+}$ and *Cep55*$^{-/-}$ mice using Arl13b (marker of ciliary membranes; Green), γ-tubulin (marker of basal body protein complex component; Red), DAPI (marker of DNA; Blue) and *Cep55* (Yellow) to evaluate and compare their expression and localization. We observed fewer cilia in the vicinity of the VZ of *Cep55*$^{-/-}$ brains at E14.5 compared to *Cep55*$^{+/+}$ brain (Fig. 5.2A). Moreover, our analysis revealed increased numbers ($P<0.01$) and percentage ($P<0.001$) of ciliated cells throughout the cortical layers, particularly in apical progenitors localized in the ventricle membrane of *Cep55*$^{+/+}$ compared to *Cep55*$^{-/-}$ brains (Fig. 5.2B). Furthermore, in *Cep55*$^{+/+}$ mouse brain, *Cep55* staining was evident in the VZ layer and was closely associated with the distribution of cilia near the VZ. Our data revealed that ciliated cells in the VZ layer were significantly reduced in the Cep55$^{-/-}$ neocortex compared to *Cep55*$^{+/+}$ controls. Together, these data indicate that *Cep55* may be required for regulation of cilia in the developing brain especially in the neocortex.

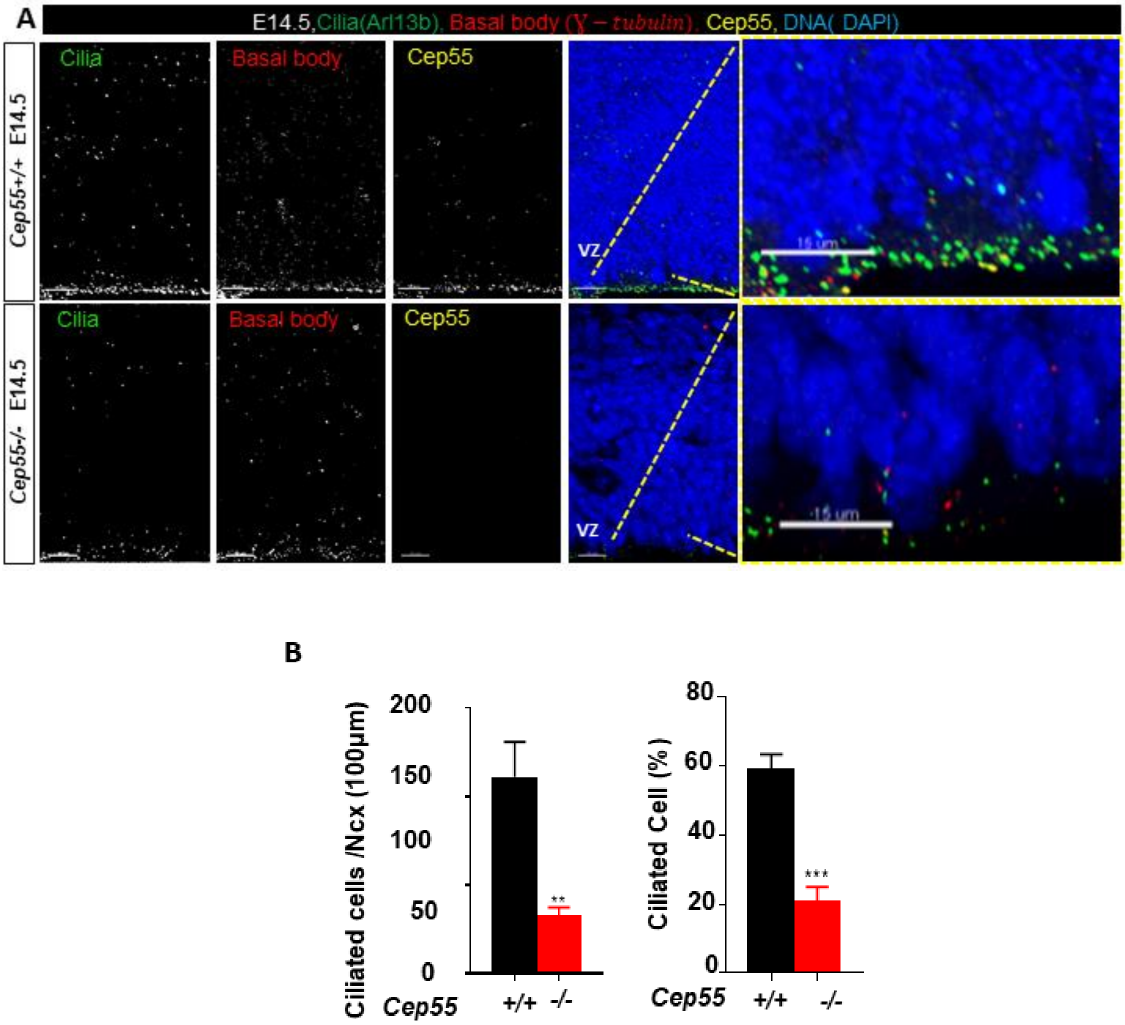
A
E14.5,Cilia(Arl13b), Basal body (Ɣ − tubulin), Cep55, DNA(DAPI)
Cep55+/+ E14.5
Cep55-/- E14.5
Cilia
Basal body
Cep55
VZ
15 um
Cilia
Basal body
Cep55
VZ
15 um
B
Ciliated cells /Ncx (100µm)
200
150
100
50
0
Cep55
+/+
-/-
**
Ciliated Cell (%)
80
60
40
20
0
Cep55
+/+
-/-
***

Figure 5.2 Cilia abnormalities in *Cep55*$^{-/-}$ mouse neocortex.

(A) E14.5 mouse neocortex immunostained for cilia (Arl13b +; green), basal body protein complex component (Ɣ-tubulin; red), Cep55 (yellow), and DAPI from Figure 2m, showing individual channels; (B) Left: Cilia-positive cells in a 100 µm-width box. Right: The precent of ciliated cells: cilia counts normalized to total cell (DAPI) number.

5.2.2 Cep55 directly regulates cilial growth and is localized at the base of cilia

To validate the broader of Cep55 in the regulation of ciliogenesis, we initially examined the impact of *Cep55* loss on cilia formation by immunofluorescence in established Mouse Embryonic Fibroblast (MEF) of each genotype. Ciliogenesis usually occurs in G_0 and G_1, and serum starvation is widely used to arrest cells in G_1 to stimulate cilia formation. We stained *Cep55*$^{-/-}$ and matched *Cep55*$^{+/+}$ control MEFs using antibodies against acetylated tubulin and Arl13b to detect cilia. Strikingly, we observed that *Cep55*$^{-/-}$ cells had a significant reduced number of ciliated cells when compared to control MEFs. Moreover, cilia that were apparent in *Cep55*$^{-/-}$ cells were often shorter, doubled, or remnant in appearance compared to *Cep55*$^{+/+}$ (Fig. 5.3A-B). In contrast, we observed that the number of basal bodies protein complex components (Mühlhans, Brandstätter and Gießl, 2011) (marked with pericentrin (Miyoshi *et al.*, 2006)) per cell was not significantly different in *Cep55*$^{-/-}$ compared to *Cep55*$^{+/+}$ MEFs. These results were validated using hTERT-immortalized Retinal Pigment Epithelium (RPE-1) cells, a widely used model in the literature to study ciliogenesis (Spalluto, Wilson and Hearn, 2013). Transient knock-down of *CEP55* in RPE-1 cells using specific siRNAs led to a reduction in the percentage of ciliated cells (P<0.01) when compared to si-Scramble control (Fig. 5.3C).

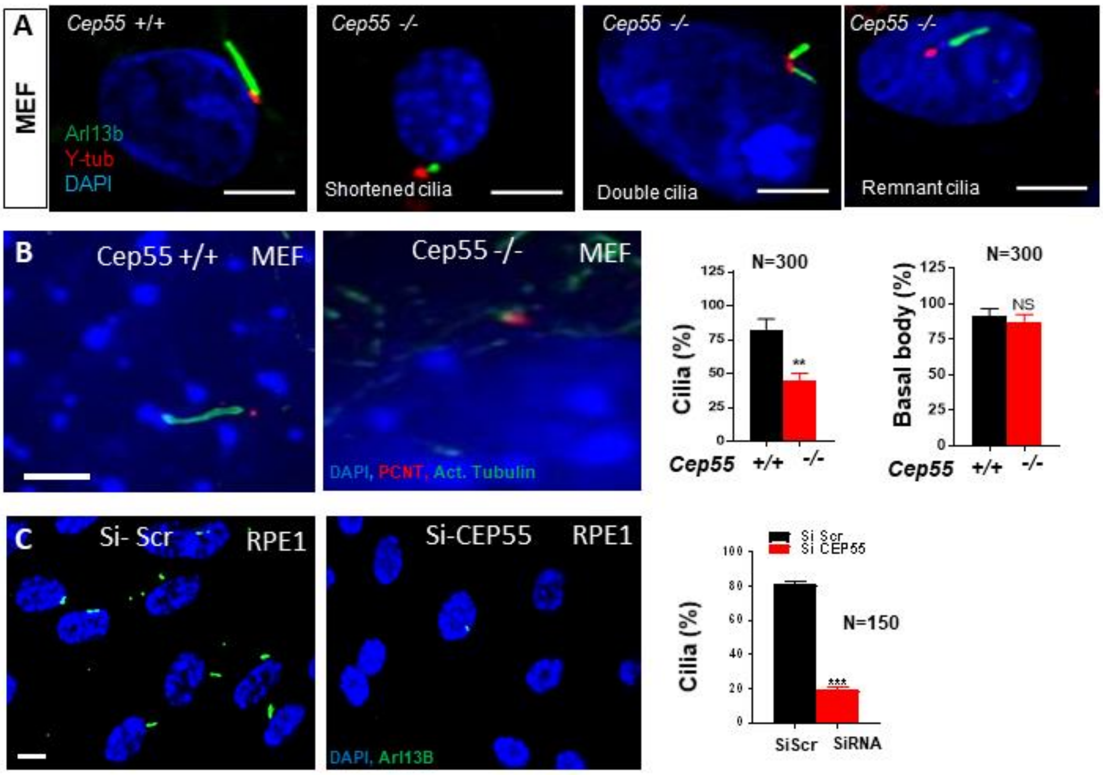
A
MEF
Cep55 +/+
Arl13b
Y-tub
DAPI
Cep55 -/-
Shortened cilia
Cep55 -/-
Double cilia
Cep55 -/-
Remnant cilia
B
Cep55 +/+ MEF
Cep55 -/- MEF
DAPI, PCNT, Act. Tubulin
N=300
Cilia (%)
125
100
75
50
25
0
**
Cep55 +/+ -/-
N=300
Basal body (%)
125
100
75
50
25
0
NS
Cep55 +/+ -/-
C
Si- Scr RPE1
Si-CEP55 RPE1
DAPI, Arl13B
Si Scr
Si CEP55
100
80
60
40
20
0
Cilia (%)
N=150
***
SiScr SiRNA

Figure 5.3 Cilia abnormalities in *Cep55*$^{-/-}$ MEFs.

(A) Representative images of different phenotypes of cilia in *Cep55*$^{+/+}$ and *Cep55*$^{-/-}$ MEFs (shortened cilia, double cilia and remnant cilia); (B) Representative images of *Cep55*$^{+/+}$ (left) and *Cep55*$^{-/-}$ (right) MEFs showing cilia (acetylated tubulin +, green), basal body (PCNT +, red), and DNA (DAPI, blue). The left bar chart shows a comparison of the percentage of ciliated cells for *Cep55*$^{+/+}$ and *Cep55*$^{-/-}$ MEFs. The right bar chart shows a comparison of the basal body protein complex (pericentrin positive cells) for *Cep55*$^{+/+}$ and *Cep55*$^{-/-}$ MEFs. (Mean ± SEM, n=300 cells per each group: 2 biological repeats and 3 independent experiments, Student's t-test, $^{**}P < 0.01$); (C) Representative images of RPE-1 cells treated with si-Scramble (left) or with siRNA against *CEP55* for 48 h (right) showing cilia (Arl13b +, green), and nuclei (DAPI, blue). The bar chart shows a comparison of the percentage of ciliated cells. (Mean ± SEM, n=150 cells and 2 independent experiments, Student's paired t-test, $^{***}P < 0.001$).

To further evaluate whether defective ciliogenesis is a direct consequence of *Cep55* loss, we attempted to rescue cilia formation by ectopic overexpression of *Cep55* in *Cep55*$^{-/-}$ MEFs. As expected, ectopic *Cep55* expression was able to restore cilia formation to levels comparable with *Cep55*$^{+/+}$ MEFs ($P<0.05$, Fig. 5.4).

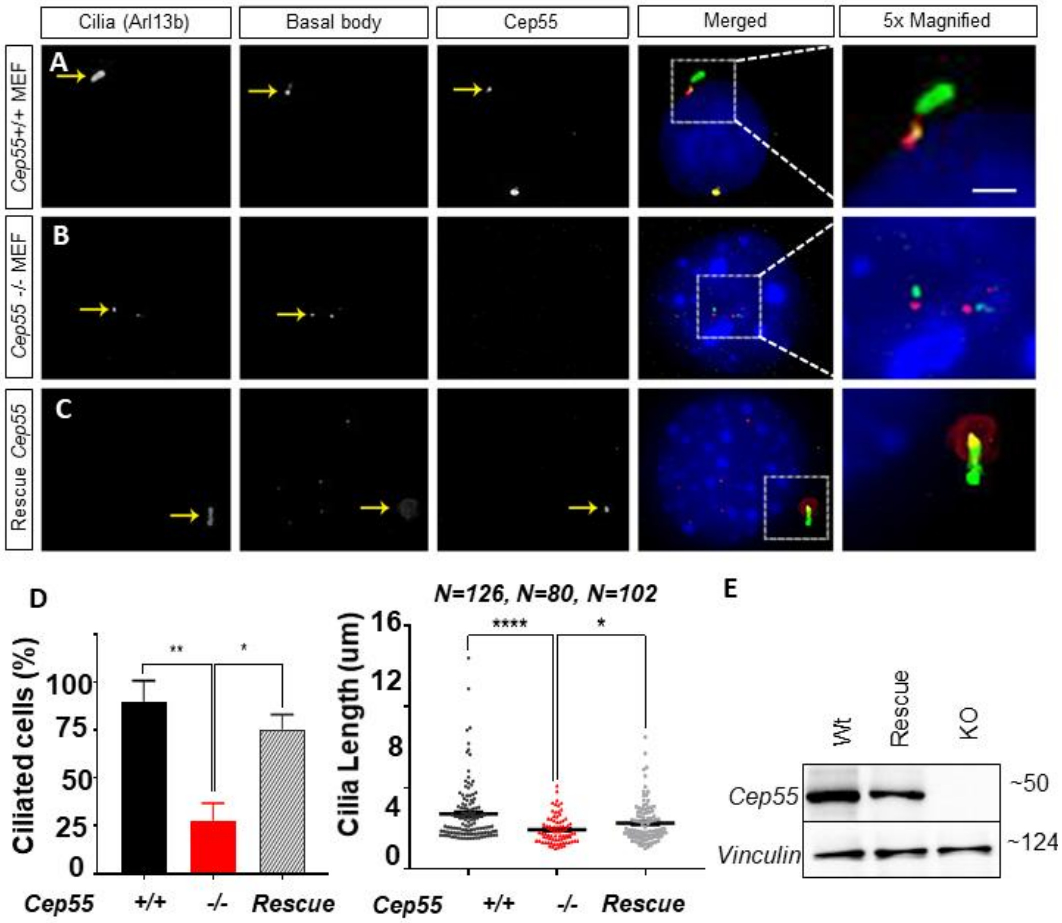
Cilia (Arl13b)
Basal body
Cep55
Merged
5x Magnified
Cep55+/+ MEF
Cep55 -/- MEF
Rescue Cep55
A
B
C
D
Ciliated cells (%)
100
75
50
25
0
**
*
Cep55
+/+
-/-
Rescue
N=126, N=80, N=102
Cilia Length (um)
16
12
8
4
0
****
*
Cep55
+/+
-/-
Rescue
E
Wt
Rescue
KO
Cep55
~50
Vinculin
~124

Figure 5.4 Cep55 is localized to the basal body protein complex of cilia in MEFs.

Cilia (Arl13b), basal body protein complex component (Ɣ-tubulin) and Cep55 staining in serum-starved (A) *Cep55*$^{+/+}$ (Wt) MEFs; (B) *Cep55*$^{-/-}$ (KO) MEFs; (C) *Cep55*$^{-/-}$ MEFs with ectopic expression of Flag-Cep55 (Rescue); (D) (Left) Percentage of ciliated cells in *Cep55*$^{+/+}$, *Cep55*$^{-/-}$ and *Cep55*$^{-/-}$ cells reconstituted with a Cep55 construct. Data represent mean ± SEM of 300 cells per genotype, measured in duplicate across two independent experiments. Student's t-test, $*P < 0.05$, $**P < 0.01$, $***P < 0.001$, $****P < 0.0001$); (Right) Scatter plot showing cilia length (µm) in *Cep55*$^{+/+}$, *Cep55*$^{-/-}$ and Cep55-reconstituted MEFs. Data were measured across two independent experiments. Student's t-test, $*P < 0.05$, $**P < 0.01$, $***P < 0.001$, $****P < 0.0001$); (E) Immunoblotting showing *Cep55* expression in *Cep55*$^{+/+}$, *Cep55*$^{-/-}$ reconstituted with Cep55 (rescue) and *Cep55*$^{-/-}$ MEFs. Vinculin was used as a loading control.

This phenotype was also rescued upon overexpression of Cep55 in *Cep55*-KO RPE cells, where we observed an increase in both the number ($P<0.01$) and length ($P<0.001$) of cilia (Fig. 5.5A-E). As *Cep55* appears to be necessary for cilia formation, we also examined *Cep55* localization in cilia by co-localizing Cep55 (Yellow) with markers of the cilia axoneme (Arl13b; green) or with a protein that localizes in the vicinity of the basal body (γ-tubulin; red). We observed co-localization of Cep55 with γ-tubulin in vicinity of the basal body, with levels of co-localization reduced in RPE-1 cells with Cep55 knock-down (Fig. 5.5F). Together, these findings illustrate that Cep55 localizes at the base of cilia as a component of the basal body protein complex (basal body associated PCM or centriolar satellite), and is required for normal cilia formation.

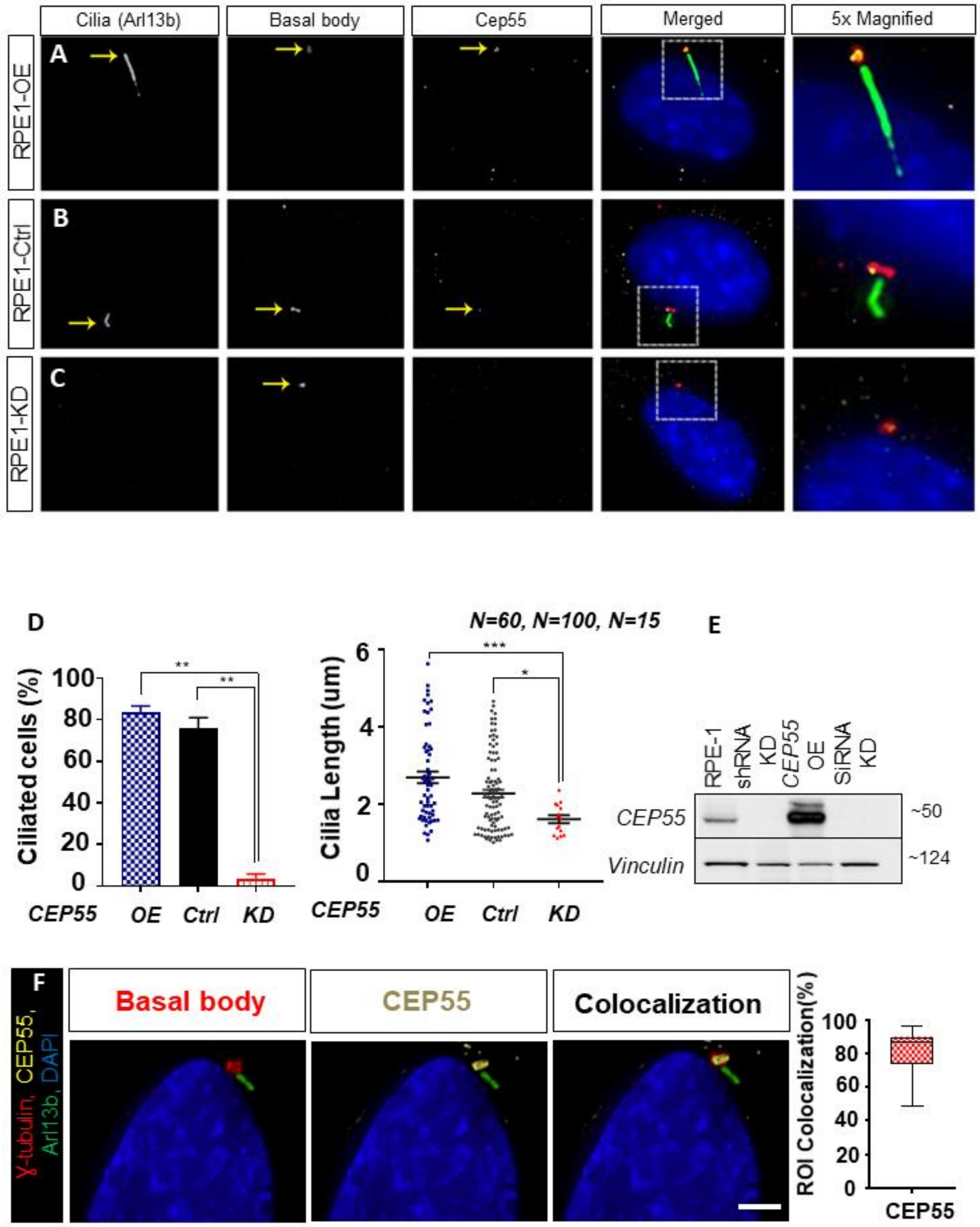
Cilia (Arl13b)
Basal body
Cep55
Merged
5x Magnified
A
RPE1-OE
B
RPE1-Ctrl
C
RPE1-KD
D
Ciliated cells (%)
100
80
60
40
20
0
**
**
CEP55
OE
Ctrl
KD
N=60, N=100, N=15
Cilia Length (um)
6
4
2
0
***
*
CEP55
OE
Ctrl
KD
E
RPE-1
shRNA KD
CEP55 OE
SiRNA KD
CEP55
Vinculin
~50
~124
F
Ɣ-tubulin, CEP55, Arl13b, DAPI
Basal body
CEP55
Colocalization
ROI Colocalization(%)
100
80
60
40
20
0
CEP55

Figure 5.5 CEP55 is localized to the base of cilia in RPE-1 cells.

Cilia (ARL13b), basal body protein complex component (Ɣ-Tubulin) and CEP55 staining in serum starved: (A) RPE-1 cells with lentiviral overexpression of Flag-CEP55; (B) RPE-1 cells transfected with a control lentiviral vector (Ctrl); (C) RPE-1 cells with lentiviral knockdown of CEP55; (D) (Left) Percentage of ciliated cells in RPE-1 cells with ectopic *CEP55* overexpression or knockdown. Data represent mean ± SEM of 300 cells per genotype, measured in duplicate across two independent experiments. Student's t-test, $^{*}P < 0.05$, $^{**}P < 0.01$, $^{***}P < 0.001$, $^{****}P < 0.0001$) ; (Right) Scatter plot showing Cilia length in RPE-1 cells with ectopic CEP55 overexpression or knockdown. Data were measured across two independent experiments. Student's t-test, $^{*}P < 0.05$, $^{**}P < 0.01$,

***$P < 0.001$, ****$P < 0.0001$); (E) Immunoblot of *CEP55* expression in RPE-1 Ctrl, RPE1 with shCep55, Cep55 overexpressing (OE) and or siCep55-treated (siRNA KD) RPE-1 cells. Vinculin was used as a loading control; (F) (Left) Representative images of individual channels showing cilia axoneme (Arl13b; green), basal body (Ɣ-tubulin; red), and *Cep55* (yellow) and DAPI, showing the colocalization of Cep55 and Ɣ-tubulin at the basal body position of cilia. Scale=5 µm; (Right) Chart showing the percent of localization between *Cep55* and Ɣ-tubulin in the region of interest at the basal body. Data were measured across two independent experiments. Student's t-test, *$P < 0.05$, **$P < 0.01$, ***$P < 0.001$, ****$P < 0.0001$).

5.2.3 Cep55$^{-/-}$ MEFs exhibit proliferation defects and multinucleation

Analysis of the brain phenotype of *Cep55*$^{-/-}$ in the previous chapter suggested that *Cep55* plays a crucial role in the regulation of cellular proliferation and survival. As *Cep55*$^{-/-}$ primary MEFs underwent limited passages in culture, we immortalized *Cep55*$^{+/+}$, *Cep55*$^{+/-}$ and *Cep55*$^{-/-}$ using the SV40 T-antigen. To investigate a potential proliferation defect, we calculated the doubling time of *Cep55*$^{+/+}$ and *Cep55*$^{-/-}$ lines and found a significantly decreased rate of growth in *Cep55*$^{-/-}$ lines ($P<0.0001$ Fig. 5.6A) compared to *Cep55*$^{+/+}$ control cells. To measure this difference more accurately, we examined proliferation by IncuCyte™ analysis over a period of seven days. Interestingly, we observed a dose-dependent reduction in proliferation rate with *Cep55*$^{-/-}$ MEFs having a significantly slower growth rate than their *Cep55*$^{+/+}$ and *Cep55*$^{+/-}$ counterparts ($P<0.0001$, Fig. 5.6B). This deficiency was also seen in cKO MEFs when treated with tamoxifen (Cre-activation-induced KO) compared to vehicle control (EtOH) treated cells ($P<0.0001$; Fig. 5.6C). Moreover, we were able to rescue this proliferation defect by ectopically expressing *Cep55* in *Cep55*$^{-/-}$ MEFs (Fig. 5.4D). Overall, the in *vitro* proliferation deficiency in *Cep55*$^{-/-}$ MEFs was consistent with the observed phenotype in neuronal progenitors.

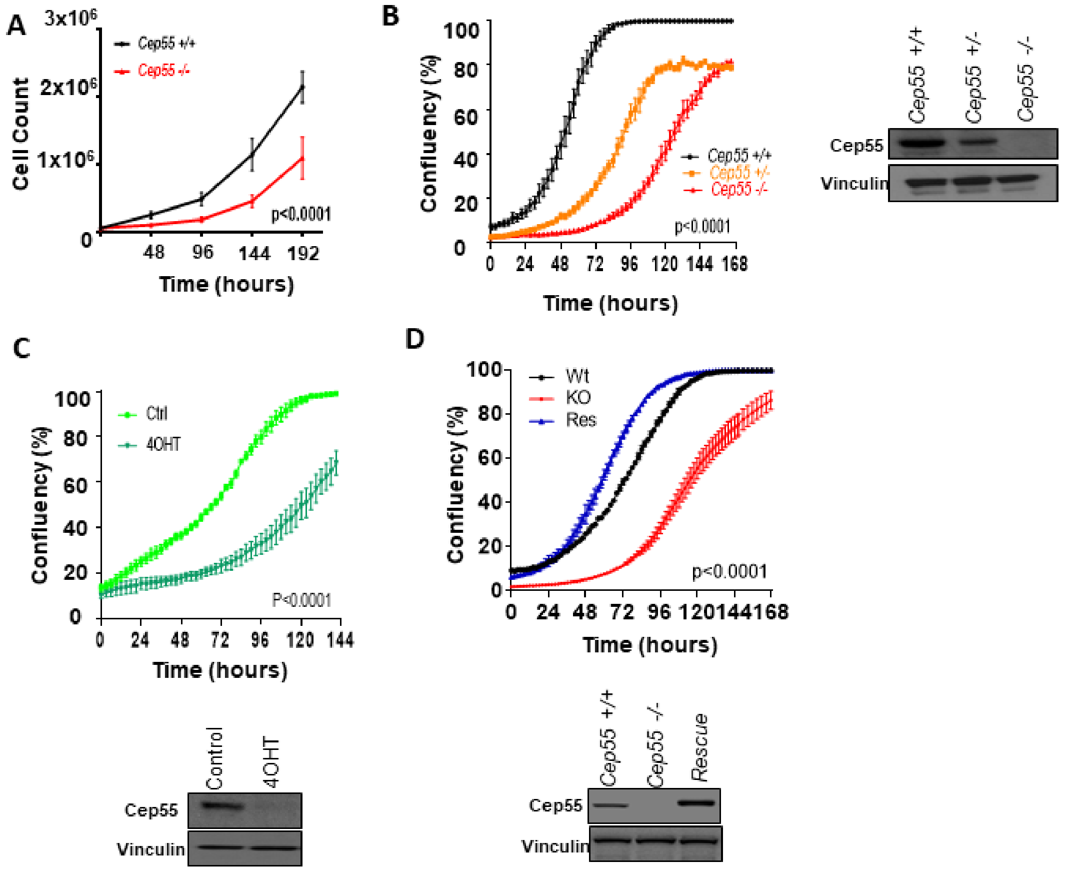

Figure 5.6 *Cep55$^{-/-}$* MEFs exhibit proliferation defects.

(A) Doubling time of *Cep55$^{+/+}$* and *Cep55$^{-/-}$* MEFs (Mean ± SEM, n=2 biological repeats and 3 independent experiments Student's t-test, ****P < 0.0001); (B-D) Proliferation of : (B) *Cep55$^{+/+}$*, *Cep55$^{+/-}$* and *Cep55$^{-/-}$* MEFs, (C) conditional *Cre+;Cep55$^{fl/fl}$* MEF treated with vehicle (Ctrl) or 2 µg tamoxifen (4OHT) and (D) *Cep55$^{+/+}$* (Wt), *Cep55$^{-/-}$* (KO) and Cep55-reconstituted (Rescue) MEFs (Mean ± SEM, average of 2 biological repeats and 2 independent experiments. Student's t-test, ****P < 0.0001). Corresponding immunoblotting for *Cep55* expression is shown below each graph. Vinculin was used as a loading control.

Loss or overexpression of Cep55 has previously been shown to result in multinucleation, a phenotype we also observed in *Cep55$^{-/-}$* neurons. Consistent with this, we observed that *Cep55$^{-/-}$* MEFs also demonstrated a higher proportion of multinucleated cells (P<0.05) when compared to control counterparts (Fig. 5.7A). This defect was also observed in our cKO MEF system following tamoxifen induction (P<0.01, Fig. 5.7B). We also measured the average number of nuclei per multinucleated cell in these lines and observed that the number of nuclei also significantly increased in *Cep55$^{-/-}$* MEFs when compared to

Cep55$^{+/+}$. Although this trend was not observed in the cKO system, this may be a secondary effect of the amount of time that Cep55 knockout has occurred for (Fig. 5.7C).

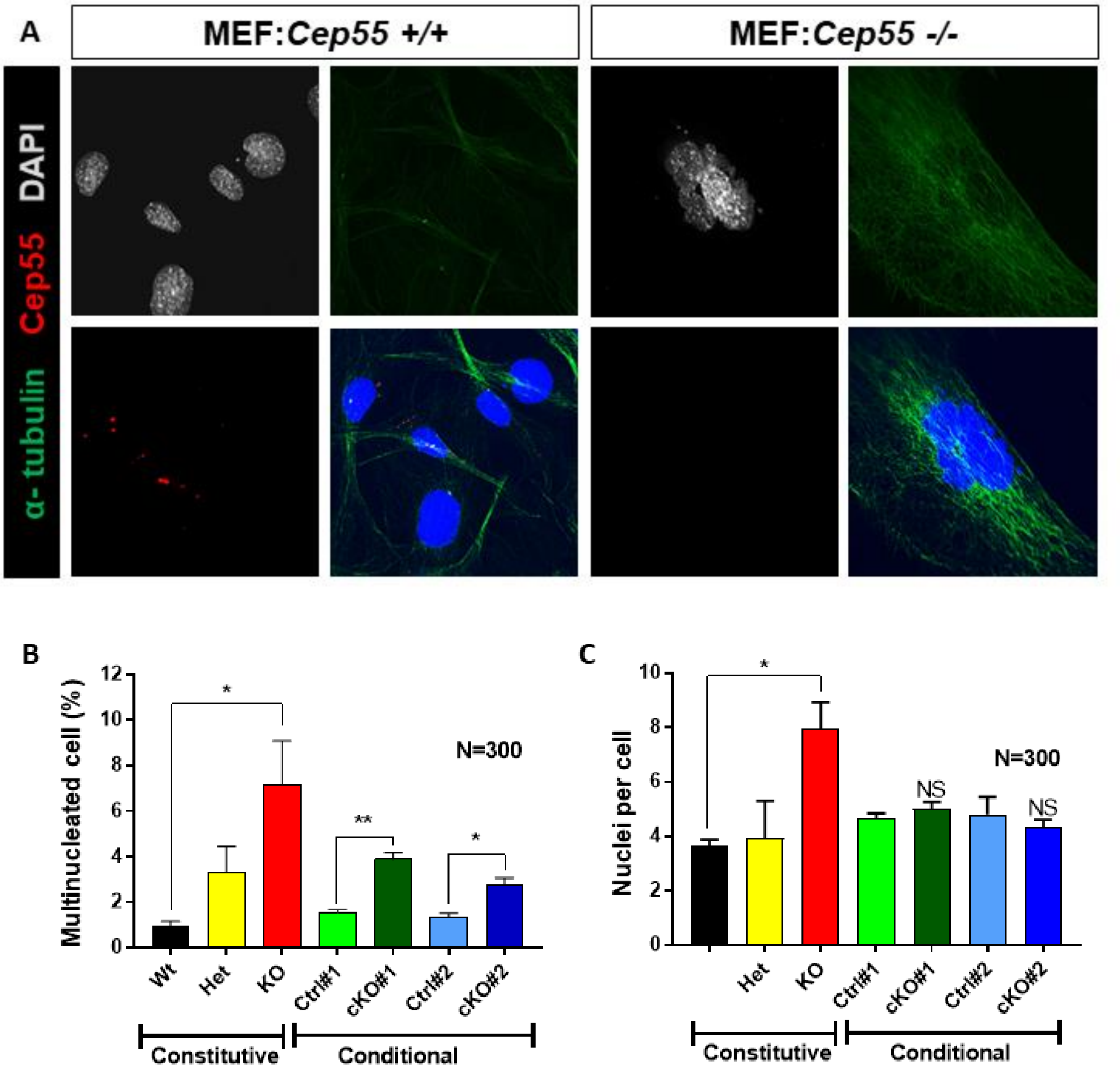

Figure 5.7 *Cep55*$^{-/-}$ MEFs exhibit multinucleation.

(A) Representative images of individual channels showing α-tubulin (cytoskeleton, green), Cep55 (red) and nuclei (DAPI, blue) in *Cep55*$^{+/+}$ (left) and *Cep55*$^{-/-}$ (right) MEFs; Bar chart showing (B) percent of multinucleated cells; (C) The average number of nuclei counted per cell in constitutive MEF (*Cep55*$^{+/+}$ (wt), *Cep55*$^{+/-}$ (Het) and *Cep55*$^{-/-}$(KO)) and across two sets of conditional MEF (treated by vehicle (Ctrl) or tamoxifen (cKO)) (Mean ± SEM, n=300 cells counted from 2 biological repeats and 3 independent experiments. Student's t-test, $*P < 0.05$, $**P < 0.01$, $***P < 0.001$).

We next performed cell cycle analysis to determine if the observed proliferation defect was related to arrest at a particular cell cycle stage. We therefore, performed flow cytometry using propidium iodide (PI)-stained cells. FACS analysis revealed significant differences in the cell cycle profile of *Cep55*$^{+/+}$ and *Cep55*$^{-/-}$ primary MEFs in G_1 and G_2 ($P<0.01$) where the *Cep55*$^{-/-}$ cells showed a modest enrichment of cells in G_2 and a concomitant reduction in the G_1 population (Fig. 5.8).

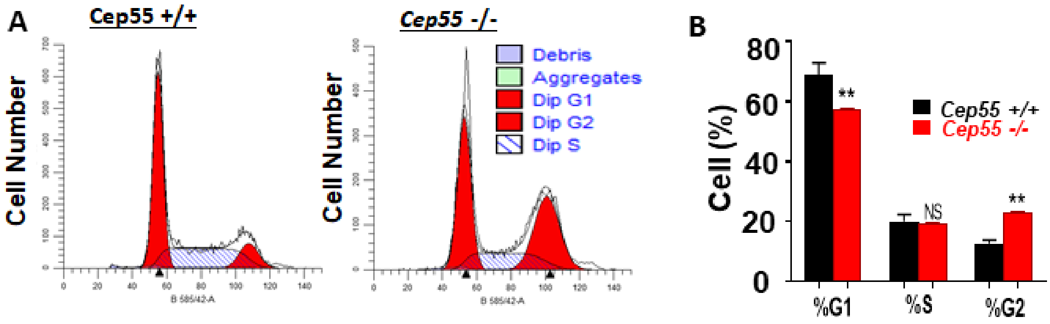

Figure 5.8 ***Cep55***$^{-/-}$ **MEFs exhibit cell cycle arrest in G2.**

(A) Modfit histogram of cell cycle analysis by FACS showing cell cycle distribution of *Cep55*$^{+/+}$ and *Cep55*$^{-/-}$ MEFs; (B) Graph showing the percent of cells in G1, S and G2 for each genotype. Data represent mean ± SEM of two lines per genotype, measured in duplicate across three independent experiments.

Next, we performed live-cell imaging by time-lapse microscopy to examine the cellular division of *Cep55*$^{+/+}$ and *Cep55*$^{-/-}$ cells transduced with mCherry-histone H2B. We found that the time to undergo cell division (mitotic length) was significantly increased in Cep55$^{-/-}$ cells when compared to *Cep55*$^{+/+}$ control lines (Fig. 5.9A-B). In line with what has previously been shown in the literature, *Cep55*$^{-/-}$ cells showed defective cytokinesis, taking a longer time to divide effectively, and 17% of the population were multinucleated ($P<0.05$) (Fig. 5.9C). For further characterization of this phenotype, we also performed analysis using the Spinning Disk Confocal microscopy to asses these changes at a higher resolution. We observed a small but not significant increase in the number of anaphase bridges in *Cep55*$^{-/-}$ MEFs when compared to control counterparts, and no significant increase in lagging chromosomes and mitotic slippage (Fig. 5.9D, E).

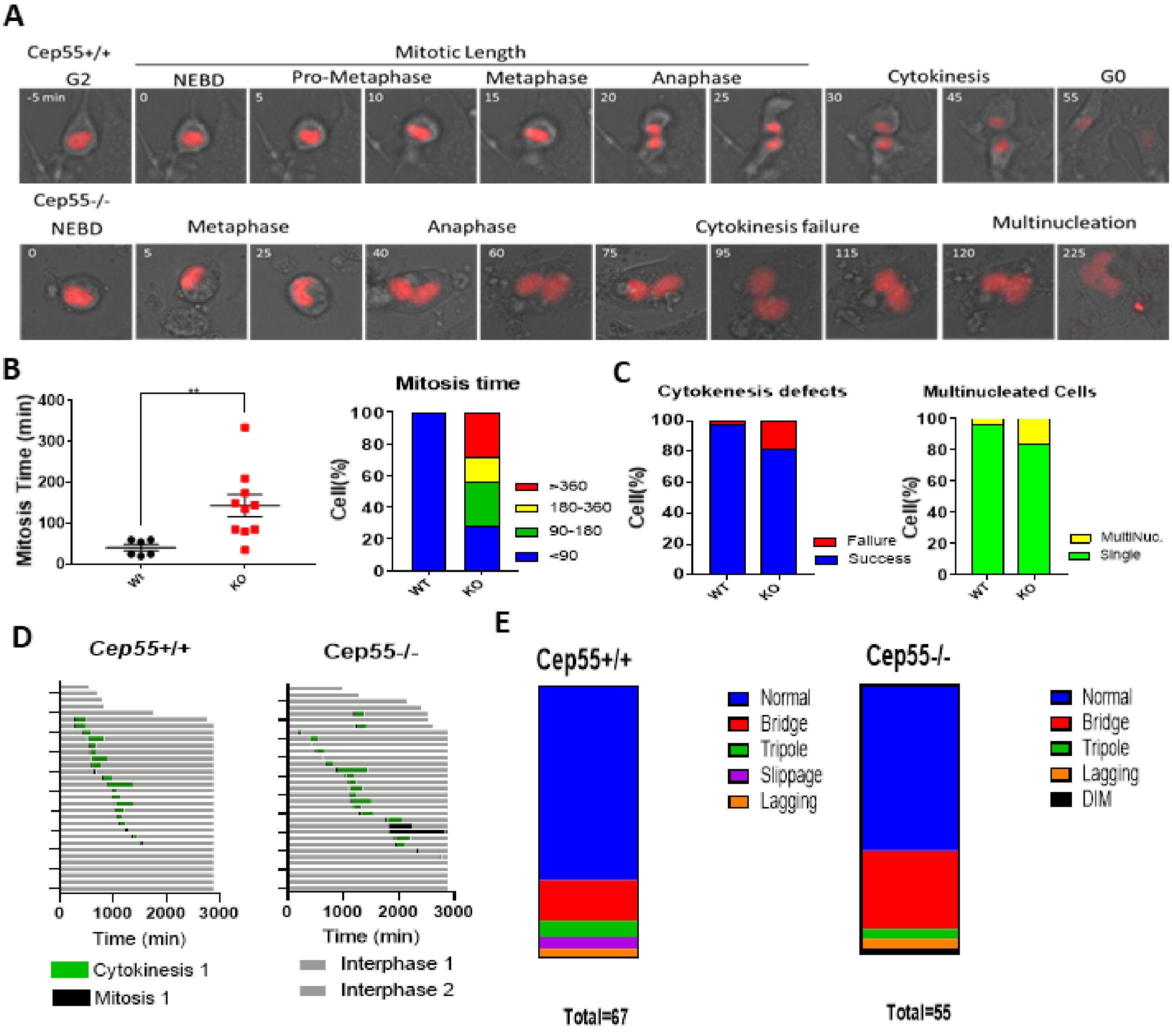

Figure 5.9 ***Cep55***$^{-/-}$ **MEFs exhibit cytokinesis defects.**

(A) Representative images from time-lapse microscopy of *Cep55*$^{+/+}$ (upper panel) and *Cep55*$^{-/-}$ (lower panel) MEFs transfected with Cherry-histone H2B showing different phases of mitosis and cytokinesis; (B) Dot plot showing the time cells took to complete mitosis (left), stacked bar chart showing the average time to complete cell division (right) for *Cep55*$^{+/+}$ and *Cep55*$^{-/-}$ MEFs; (C) Column chart showing percent of cells with (Left) cytokinesis failure or success (Right) multinucleated cells or single cells *for Cep55*$^{+/+}$ and *Cep55*$^{-/-}$. (Mean ± SEM, n=10-25 cells counted from 3 technical repeats Student's t-test, **P < 0.01); (D) Cell fate map shows cellular division events for (left) *Cep55*$^{+/+}$ and (right) *Cep55*$^{-/-}$; (E) Stacked bar chart showing comparison of percentages of different mitotic phenotypes of MEFs transfected with Cherry-histone H2B for *Cep55*$^{+/+}$ (left) and *Cep55*$^{-/-}$ (right), images of the cell captured by time-lapse microscopy (Spinning disk confocal microscopy). (Mean ± SEM, n=55-67 cells counted from 3 technical repeats Student's t-test, **P < 0.01).

5.2.4 Cep55 regulates GSK3β, βCatenin, and Myc downstream of the Akt pathway

In order to define a molecular mechanism underlying the observed phenotypes, we performed detailed signaling analysis in MEFs and E14.5 mouse brains by immunoblotting. Previously, Cep55 has been shown to be an essential regulator of the Akt pathway. Gsk3β is an important downstream regulator of Akt, where Akt controls steady-state levels of Gsk3β through phosphorylation of residue Serine 9 (pGsk3β^{S9}). Conversely, when Akt activity is decreased, pGsk3β^{S9} levels are reduced resulting in its activation. Interestingly, we observed that loss of *Cep55* led to downregulation of pGsk-3β^{S9}, while total levels of GSK-3β remained unchanged. In keeping with this, we also observed that levels of active Akt (measured as Akt phosphorylated on serine 473; pAkt^{s473}) were decreased, but the total protein level of Akt remained unchanged. Activated *Gsk3β* inhibits a number of downstream targets involved in proliferation, including β-catenin and Myc (Fig. 5.10A, B). In keeping with our observations of decreased levels of pGsk3β^{S9} , we also observed reduced levels of both β-catenin and Myc by western blotting. Importantly, we were able to rescue the phosphorylation of Akt and Gsk3β by ectopic expression of *Cep55* in *Cep55*$^{-/-}$ MEFs, confirming the specificity of the observed signal transduction effects (Fig. 5.10C). We also utilized extracts of *Cep55*$^{+/+}$ and *Cep55*$^{-/-}$ E14.5 brains to determine if this signaling defect also manifests in a physiological setting of Cep55 loss. In keeping with our observations in MEFs, we showed similar signaling changes in these tissues, with decreases in pAkt^{s473}, pGSK-3β^{S9}, β-catenin, but not total levels of Akt or Gsk3β. Together, these data reveal an essential role of Cep55 in the regulation of Akt signaling.

Gsk3β controls phosphorylation of β-catenin on S33, S37, and T41, resulting in degradation of this target by the proteasome. Interestingly, we observed downregulated β-catenin levels in *Cep55*$^{-/-}$ embryonic brain samples and a trend of decreased total β-catenin and downregulation of non-phospho β-catenin, (its stabilized form) in *Cep55*$^{-/-}$ MEFs compared to their *Cep55*$^{+/+}$ counterparts. Activated Gsk3β can also destabilize Myc by phosphorylation. Myc degradation was also evident in *Cep55*$^{-/-}$ MEFs, possibly through Gsk3β-mediated phosphorylation of Myc at T58 (Liu and Eisenman, 2012), while there was only a slight change in Myc levels in E14.5 mouse brains.

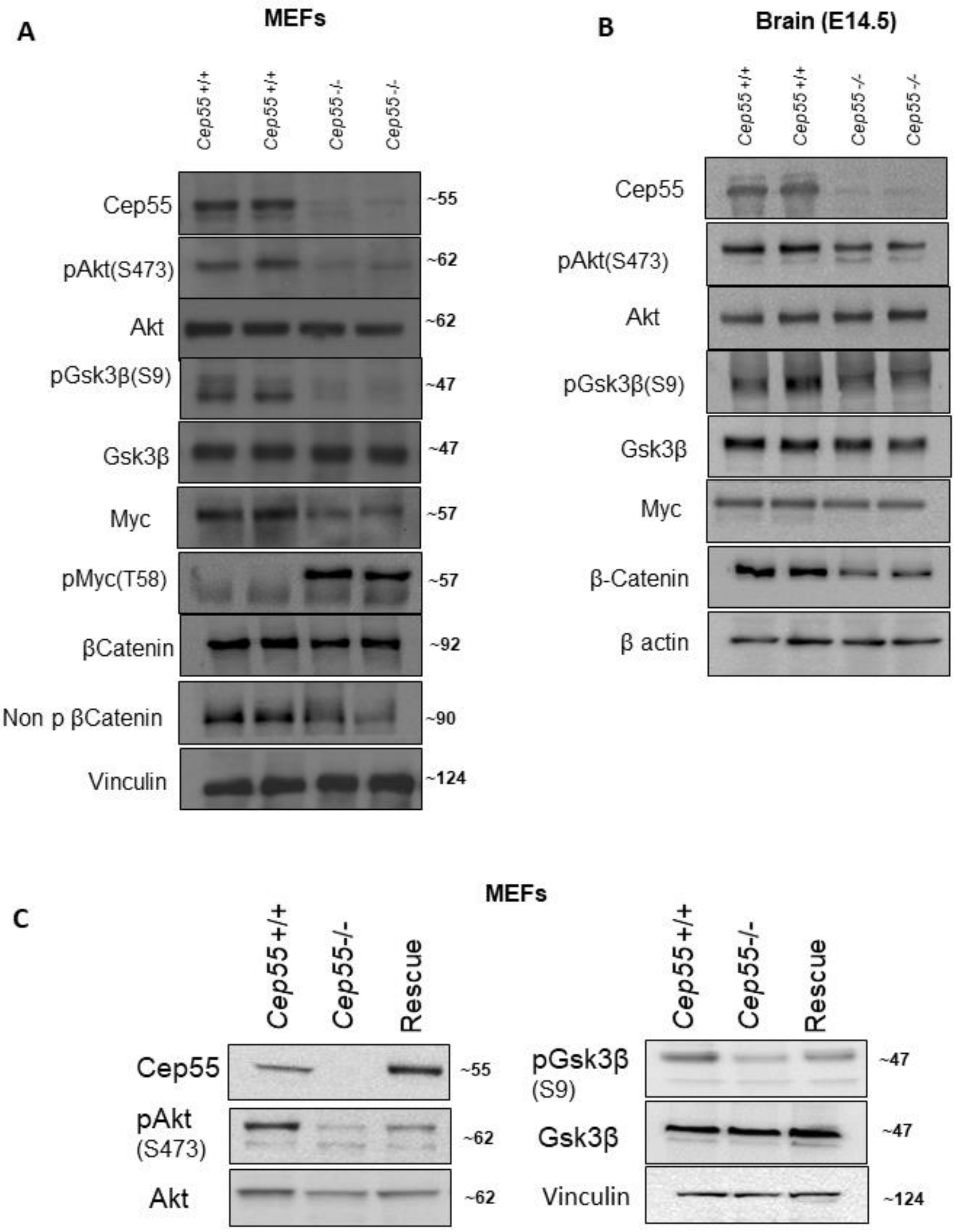

Figure 5.10 ***Cep55*** **regulates Akt/Gsk3β/ β-Catenin/ Myc axis.**

Immunoblot analysis performed on (A) MEFs and (B) E14.5 mouse embryonic brain extracts of *Cep55*$^{+/+}$ and *Cep55*$^{-/-}$ for the indicated proteins. (C) Immunoblot for the indicated proteins in *Cep55*$^{+/+}$ (Wt), *Cep55*$^{-/-}$ (KO), and *Cep55*$^{-/-}$ MEFs with ectopic expression of Cep55 (Rescue). B-actin or Vinculin served as a loading controls.

As *Myc* is also a transcriptional target of the Wnt-β-catenin pathway, we next investigated the role of *Cep55* in regulating *Myc* at the transcription level by qRT-PCR. Notably, *Cep55* loss also reduced the transcript levels of *Myc* ($P<0.05$) and *N-Myc* (a member of the Myc family which is predominantly expressed in neuronal cells) ($P<0.001$) in both MEFs (Fig. 5.11A) and brain samples (Fig. 5.11B). To further explore the role of *CEP55* in the regulation of MYC transcriptional activity, we examined the effect of *CEP55* knockdown and overexpression in transfected HEK293T cells on the expression of a MYC-responsive (E-box) luciferase reporter plasmid. We observed a *CEP55* dose-dependent increase (following overexpression), ($P<0.01$) in expression of the luciferase reporter and concomitant decrease ($P<0.001$) following knockdown of *Cep55* (Fig. 5.11C, left). Moreover, western blot analysis validated these results and confirmed a regulatory effect of *CEP55* on Myc levels upon knockdown and overexpression (Fig. 5.11C, right).

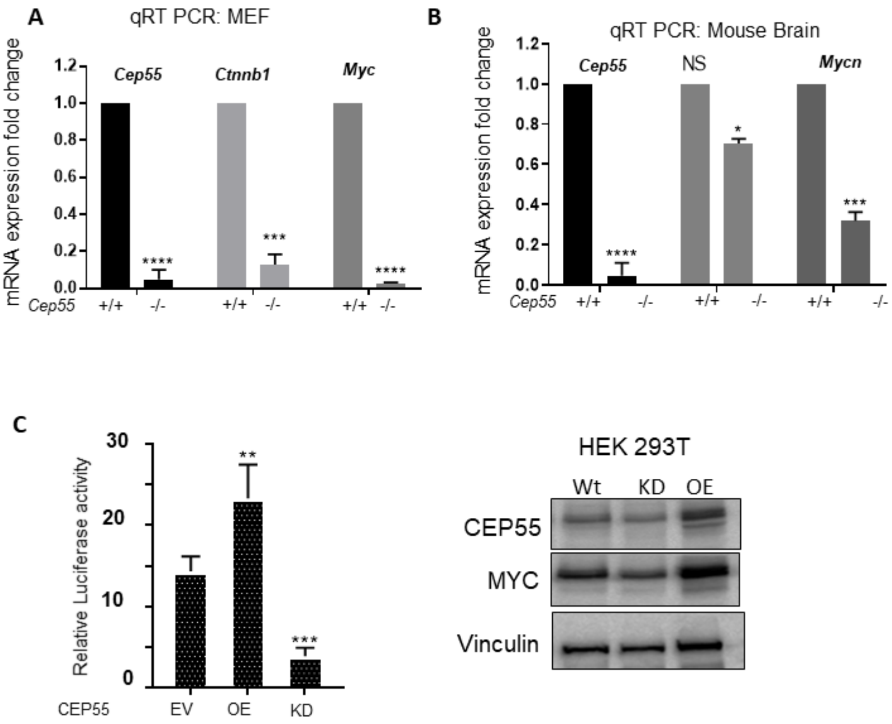

Figure 5.11 Cep55 regulates Ctnnb1 and Myc in MEFs and brain.

Fold change of mRNA expression of *Cep55*$^{+/+}$ and *Cep55*$^{-/-}$ in (A) MEFs (B) brain extract for the indicated transcripts. (Mean ± SEM 2 independent experiments Student's t-test, $*P < 0.05$, $**P < 0.01$, $***P < 0.001$, $****P < 0.0001$); (C) HEK293T cells expressing empty vector (EV), overexpressing lentiviral Flag-Cep55 (OE) or with shRNA-mediated *Cep55* knockdown (KD) were transfected with a construct expressing luciferase under the control of a MYC-responsive E-Box and relative luciferase activity measured (Left); (Mean ± SEM 3 independent experiments Student's t-test, $*P < 0.05$, $**P < 0.01$, $***P < 0.001$, $****P < 0.0001$); Immunoblot for the indicated antibodies in HEK 293T cells transfected with empty vector control (Cep55 Ctrl), a Cep55 expression construct, or shRNA directed against *Cep55*. Vinculin was used as a loading control (right).

To validate our observations regarding Cep55-dependent regulation of β-catenin and Myc levels, we also performed IHC staining of total β-catenin and N-Myc on brain sections. At E18.5, we observed a significant decrease in nuclear β-catenin in *Cep55*$^{-/-}$ neural cells ($P<0.001$) compared to *Cep55*$^{+/+}$ at E18.5, consistent with immunoblot analysis in the embryonic brain (Fig. 5.12A). Similarly, N-Myc levels were significantly decreased ($P<0.05$) in *Cep55*$^{-/-}$ compared to *Cep55*$^{+/+}$ controls (Fig. 5.12B). Together, we conclude that Cep55 loss might inhibit proliferation through a Gsk3β / βcatenin/ Myc axis**.**

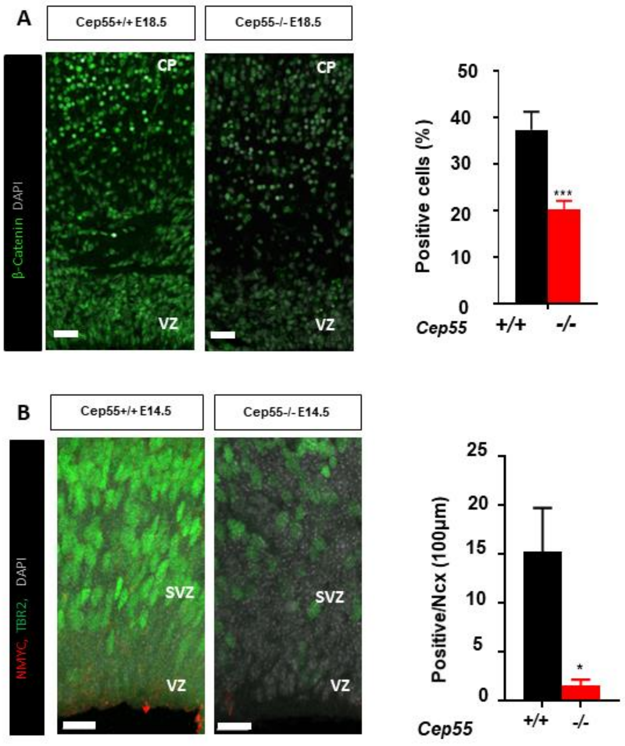
A
Cep55+/+ E18.5
Cep55-/- E18.5
β-Catenin DAPI
CP
CP
VZ
VZ
Positive cells (%)
50
40
30
20
10
0
***
Cep55
+/+
-/-
B
Cep55+/+ E14.5
Cep55-/- E14.5
NMYC, TBR2, DAPI
SVZ
SVZ
VZ
VZ
Positive/Ncx (100µm)
25
20
15
10
5
0
*
Cep55
+/+
-/-

Figure 5.12 Effect of *Cep55* loss on β-catenin and Myc in brain tissue by IHC.

(A) Representative images for *Cep55*$^{+/+}$ (left) and *Cep55*$^{-/-}$ (right) neocortexes stained for β-catenin (green) and nuclei (DAPI, gray) in a 100 µm-width box. Bar chart shows the percent of β-catenin positive cells for *Cep55*$^{+/+}$ and *Cep55*$^{-/-}$. Scale= 50 µm; (B) Representative images for *Cep55*$^{+/+}$ (left) and *Cep55*$^{-/-}$ (right) neocortexes stained for N-Myc (red), TBR2 positive cells (green) and nuclei (DAPI, gray) in a 100 µm-width -width box. Bar chart shows the percent of N-Myc positive cells (Mean ± SEM of four embryos duplicate technical repeats, Student's t-test, *P < 0.05, **P < 0.01, ***P < 0.001, ****P < 0.0001), Scale= 15 µm.

5.2.5 Rescue of Cep55 mutant phenotype by downstream effectors of the PI3K/AKT signaling pathway

Next, we sought to evaluate whether the rescue of Akt signaling would be sufficient to rescue the proliferation and ciliogenesis defects observed in *Cep55*$^{-/-}$ MEFs. To achieve this, we utilized a constitutively-active, myristoylated form of AKT1 (myr-Akt), as previously described (Chan *et al.*, 2019). *Cep55*$^{-/-}$ MEFs were transduced with either myr-AKT1 or an empty plasmid (Fig. 5.13A), and cells were plated for proliferation assay. Incucyte™ analysis revealed that myr-Akt could rescue the proliferation defects observed upon Cep55 loss when compared to control cells (($P<0.0001$); Fig. 5.13B). We also examined whether the myrAKT could rescue the defects in cilia formation, and we observed myrAKT partially rescued the number of ciliated cells ($P<0.05$) Fig. 5.13C, D). We also sought to determine if we could rescue the proliferation and ciliogenesis defects using an inhibitor of activated Gsk3β, as we observe reduced Akt-dependent phosphorylation as a result of *Cep55* loss. While inhibition of GSK3β at all doses examined did not affect ciliogenesis significantly (data not shown), the universal GSK3β inhibitor, CHIR99021, at a low dose (0.1μM) rescued the proliferation defect ($P<0.01$) observed in *Cep55*$^{-/-}$ MEFs, possibly through the inhibition of active GSK3β and circumvention of β-Catenin deregulation as per other reports (Shakoori *et al.*, 2007; Wang *et al.*, 2016). In contrast, in *Cep55*$^{+/+}$ lines (similar to *Cep55* rescued lines where GSK3β is inhibited by Akt activity), CHIR99021 can hinder proliferation in a dose-dependent manner Fig. 5.13E-G). In all lines, however, a higher concentration of CHIR99021 (5 μM) showed cytocidal effects (data not shown).

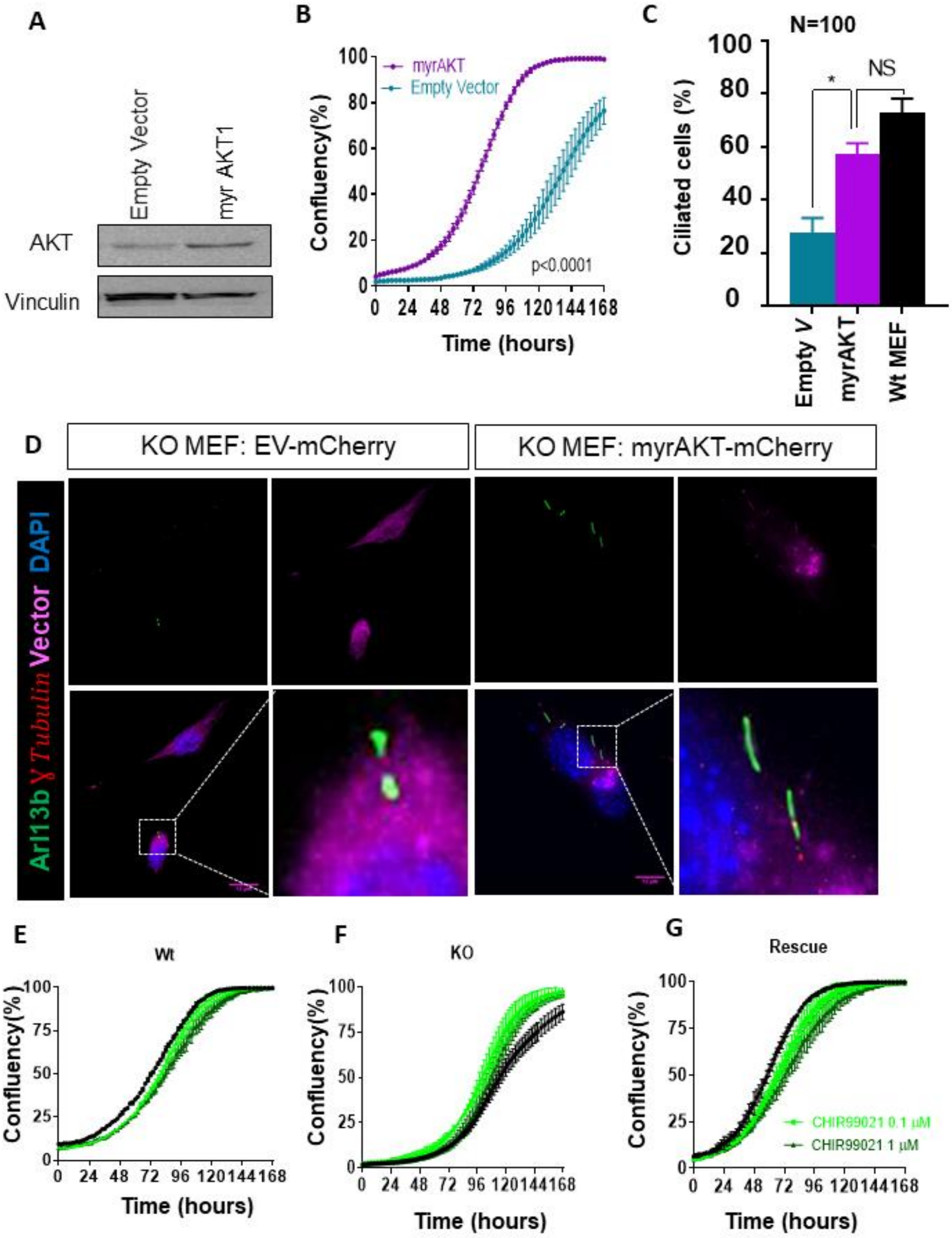

Figure 5.13 Downstream effectors can rescue Cep55 loss.

(A) Immunoblots showing expression of Akt in EV and myr-Akt transfected *Cep55*$^{-/-}$ MEFs. Vinculin was used as a loading control; (B) Proliferation assay showing growth of *Cep55*$^{-/-}$ MEF transiently transfected with EV or myr-Akt (Mean ± SEM, average of 2 biological repeats and 2 independent experiments Student's t-test, ****P < 0.0001); (C) graph showing percent of ciliated cells in *Cep55*$^{+/+}$ (Wt) and *Cep55*$^{-/-}$ (KO) MEFs transfected with EV or myr-Akt. Mean ± SEM, n=100 cells from 3 independent experiments, Student's t-test, *P < 0.05); (D) Representative images of *Cep55*$^{-/-}$ (KO) MEFs reconstituted with EV-mCherry (left panel) or myrAKT-mCherry (right panel) immunostained for cilia (Arl13b; green), basal body (ɣtubulin; red) and nuclei (DAPI). The right lower box shows magnification of the boxed area. Scale=12 µm; Proliferation assay showing growth of (E) *Cep55*$^{+/+}$ (Wt); (F) *Cep55*$^{-/-}$ (KO); and (G) Flag-Cep55 reconstituted *Cep55*$^{-/-}$ MEFs (Rescue) treated with indicated doses of GSK3β inhibitor, CHIR99021 (Mean ± SEM, average of 2 biological repeats and 2 independent experiments Student’s t-test, ****$P < 0.0001$).

These findings strongly validate that *Cep55* regulates cell proliferation in an Akt/Gsk3 β -dependent manner. However, *Cep55*-dependent regulation of ciliogenesis might occur through an Akt downstream effector(s) other than Gsk3β **(Fig. 5.14).**

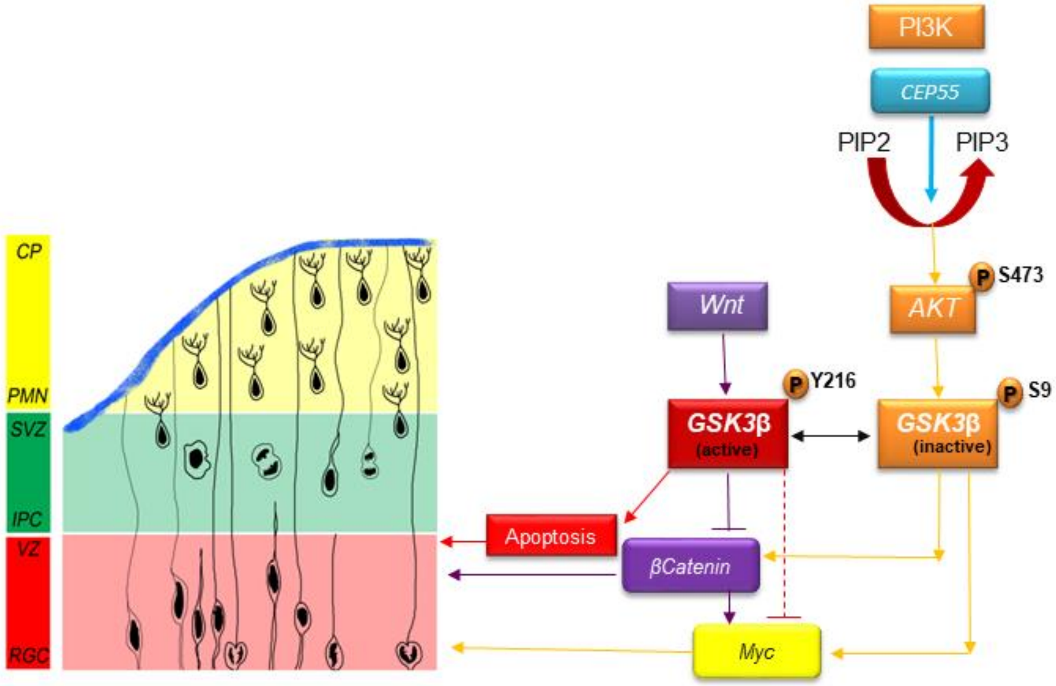

Figure 5.14 Proposed model of Cep55 signaling in neural development.

Schematic showing a proposed model of how *Cep55 might* regulates RGC proliferation or apoptosis (chapter 4) through PI3K/AKT downstream targets *GSK3*β, β*Catenin*, and *Myc (chapter 5). CEP55* binds to the catalytic subunit of PI3K (p110) to facilitate Phosphoinositol 2 (PIP2) to PIP3 conversion and regulate optimal phosphorylation of AKT on S473. Active-AKT inactivates *GSK3*β by phosphorylating S9 and prevents degradation of GSK3β targets *β-Catenin* and Myc resulting in increased proliferative capacity. However, in CEP55 KO downregulation of AKT phosphorylation leads to upregulation of the active form of *GSK3*β (Y216) which can reduce proliferation and activate apoptosis through regulation of β*Catenin* and *Myc*.

5.3 Discussion

In this chapter, we demonstrated that loss of *Cep55* is linked to abnormal cilia formation, causing remnant and shorter cilia. This abnormality is at least partially attributable to disruption of Akt signaling, as the expression of myristoylated AKT was able to partially rescue this phenotype. The Akt pathway and its downstream signaling such as *Gsk3β,* β-Catenin, and Myc have been shown to exhibit cross-talk with other signaling pathways which regulate ciliogenesis, including Shh and Wnt. In addition to the pro-survival role of Akt in regulating proliferation and apoptosis, the dysregulation of *Akt* (Dinsmore and Soriano, 2018; Sittewelle and Monsoro-Burq, 2018) as well as its downstream effectors such as *GSK3β* (Kim *et al.*, 2009) , *MYC* and *CTNNB1* (Zechner *et al.*, 2003; Hirabayashi *et al.*, 2004; Reya and Clevers, 2005) have been reported to have adverse effects on neurodevelopment, predominantly affecting proliferation. *GSK3β,* implicated as a master regulator of NPs, is a central mediator of a wide range of processes in neurodevelopment, including neurogenesis, neurotransmission, synapse formation (Cole, 2012), axon outgrowth and neuronal polarization (Hur and Zhou, 2012). GSK3β is the key bifunctional mediator downstream of both Akt and Wnt pathways and can destabilize β-catenin, which plays a critical role in the crosstalk of these pathways (Yost *et al.*, 1996; Pap and Cooper, 1998; Sineva and Pospelov, 2014). It also controls several additional downstream effectors including N-Myc (Colon *et al.*, 2011), *Myc* (Gregory, Qi and Hann, 2003) and NF-κB by controlling their levels through ubiquitination and the proteasome pathway (Welcker *et al.*, 2003; Moberg *et al.*, 2004). Altogether, *GSK3-β* acts as a hub to regulate proliferation during neurodevelopment to switch on and off critical signaling pathways including Myc and β-catenin. Our data showed reduced AKT phosphorylation and a subsequent reduction in inhibitory phosphorylation on *GSK3β* in the absence of *Cep55*, leading to its activation of *GSK3β* and proteasomal-mediated degradation of *β-Catenin*. The transcriptional activation of β-catenin is known to regulate self-renewal whereas the stabilized β-catenin protein often promotes proliferation (Sineva and Pospelov, 2014). In the *Cep55*$^{-/-}$ brain and MEFs, we observed reduced expression of β-catenin by western blot and immunohistochemistry in the absence of any changes at the level of transcription.

Although Gsk3β can independently regulate Myc, the classic downstream effectors of β-catenin are Myc and Cyclin D1. We identified Myc protein destabilization in MEFs and embryonic brain lysates by western blot and a decrease in Myc and N-Myc transcript levels by qPCR. We also validated these results by IHC analysis, which revealed a decrease in N-Myc protein expressed mostly in the VZ of the mouse neocortex. Moreover, luciferase assays demonstrated that *CEP55* overexpression or knockdown can affect MYC transcriptional activity positively or negatively, respectively, via regulation of MYC levels.

N-Myc as a downstream target of *Wnt/* β-catenin and *GSK3β* promotes neuronal fate, contributing to intermediate progenitor cell (IPC) production and proliferation and blocking differentiation *in vivo* and *in vitro* (Kuwahara *et al.*, 2010). Deficiency in β-catenin and/or N-Myc expression can decrease IPCs numbers in the neocortex (Kuwahara *et al.*, 2010). Interestingly, most of the phenotypes in the *Cep55*$^{-/-}$ brain are associated with either forebrain or hindbrain, which is under the control of N-Myc regulation (Wey and Knoepfler, 2010). Mutation of *N-Myc* in humans is associated with Feingold syndrome, a disorder that affects many parts of the body including brain causing microcephaly, suggesting that common N-Myc-regulated pathways in humans and mice regulate brain development. GSK3β can phosphorylate and degrade N-Myc, and this event in the CNS can lead to either developmental defects during embryogenesis or cerebellar tumorigenesis including neuroblastoma and medulloblastoma (Hahn *et al.*, 2000).

We observed diminished numbers of ciliated cells in *Cep55*$^{-/-}$ embryo brain sections and defective ciliogenesis in *Cep55*$^{-/-}$ MEFs or *Cep55*-depleted RPE cells (a cell line model used widely for the study of ciliogenesis) in line with the described association of *Cep55* with human MKS-like ciliopathy syndrome (Bondeson *et al.,* 2017). The brain is mainly composed neurons and glial cells. It is known that neurons and astrocytes possess a single, non-motile primary cilium. Primary cilia are evident in early progenitor cells, but are lost as these cells differentiate. Additionally, adult neural stem cells in the subventricular zone (SVZ) of the lateral ventricles possess primary cilia, which are essential for Sonic hedgehog (Shh) signaling and adult neurogenesis (Sterpka et al. 2018). Data mining of BIOGRID (Stark *et al.*, 2006) for potential *Cep55* partner proteins in mice revealed interactions with other centrosomal proteins associated with ciliopathy and neural defects including microcephaly. In mice, Cep55 interacts with Cep131 and Cep72, two proteins required for cilia function (Stowe *et al.*, 2012; Hall *et al.*, 2013). In human cell lines, proximity interactions among centrosome components (Firat-Karalar *et al.*, 2014) identified several additional centrosomal proteins apart from the well-defined *CEP55* interaction with TSG101 and ALIX, components of the endosomal sorting complexes required for transport (ESCRT) machinery. These included *CEP162* (associated with the cilia transition zone (Wang *et al.*, 2013)), *CEP120* (the neural progenitors regulator, mutated in Joubert syndrome (Xie *et al.*, 2007; Roosing *et al.*, 2016), *CEP63* (linked with p53-dependent microcephaly through mitotic defects (Marjanović *et al.*, 2015), *CEP128* (regulator of TGF-β at the primary cilium (Breslin *et al.*, no date), *CEP135* (mutations associated with microcephaly) (Hussain *et al.*, 2012)) and finally, *CENPJ* which can cause autosomal recessive primary microcephaly with reduction of the neural progenitor pool when disrupted (Garcez *et al.*, 2015). Consistent with this, we found that *Cep55* predominantly localizes to the basal body of the cilium and can positively regulate cilia growth in MEFs and RPE-1 cells. These data suggest that

Cep55 is a novel player in the regulation of ciliogenesis and its aberrant expression leads to cilia defects; however, how this cellular process contributes to neurodevelopment remains, to a great extent elusive. There is emerging evidence that cilia dysfunction contributes to many neurogenetic disorders such as Meckel-Gruber syndrome (Hartill *et al.*, 2017). In human and mouse, lack of expression of important functional or proliferative genes related to cilia can lead to cortical defects (Fuchs and Schwark, 2004; Han *et al.*, 2008). Abnormal ciliary or basal body function or structure while an embryo is developing can lead to a set of malformations that can occur regardless and independent of the particular causative genetic disorder. Accordingly, ciliary dysfunction can manifest as a collection of features that include renal disease and cerebral anomalies (Fuchs and Schwark, 2004; Han *et al.*, 2008). Ciliopathy can corrupt the function of other evolving organs; therefore, this may cause secondary abnormalities and wide range spectrum of phenotypes regardless and irrelevant to the genetic deviation which originally caused it (Powles-Glover, 2014). Several studies have demonstrated direct or indirect modulation of PI3K/Akt activation in mediating the downstream effects of Shh, a regulator of corticogenesis (Lai *et al.*, 2003) and the main signaling regulator of cilia (Kanda *et al.*, 2003; FU *et al.*, 2006; Riobó *et al.*, 2006)'. It has been reported that pAkt can localize to the primary cilia basal body or to a centrosome-like structure in dividing cells; consequently, Akt knockdown can suppress cilia formation (Suizu *et al.*, 2016). We propose that defective activation of the PI3K-AKT pathway in the absence of *Cep55* leads to defective proliferation and survival of neurons as well as defective cilia formation due to cross-talk between PI3K/AKT and the Shh pathway. Consistent with this, myrAkt was able to rescue both the proliferation and ciliogenesis defects. However, inhibition of activated Gsk3β as a consequence of reduced Akt activation in *Cep55*$^{-/-}$ MEFs could only rescue the defective proliferation defect but not ciliogenesis, suggesting that other downstream effectors of AKT are involved in the regulation of ciliogenesis.

In summary, our study has identified the critical role of *Cep55* during brain development and suggests that defective cilia formation and function due to disrupted PI3K/AKT pathway activation during embryogenesis may be the primary cause of this phenotype.

Chapter 6. *Cep55* loss impedes tumorigenesis *in vivo*

6.1 Introduction

6.1.1 CEP55 overexpression

The *CEP55* gene is overexpressed across a variety of cancers, where it exerts an oncogenic role to promote tumorigenesis. (Waseem *et al.*, 2010; Tao *et al.*, 2014; J. Jeffery *et al.*, 2016; Jiang *et al.*, 2016; M. Li *et al.*, 2018; Yang *et al.*, 2018; Zhou *et al.*, 2019). Our laboratory and others have shown the significance of *CEP55* in cancer development, prognosis, and survival, and *CEP55* has gained significant attention as a therapeutic target. *CEP55* is an abscission component that regulates cytokinesis, chromosome segregation and, subsequently, genome stability (Fabbro, B. *al.*, 2005; Kalimutho *et al.*, 2018). *CEP55* overexpression has also been shown to lead to aneuploidy with increased proliferative potential and confers a survival advantage to cancerous cells. *CEP55* expression can also determine cell fate in response to treatment with anti-mitotic drugs through regulation of interplay between mitotic exit and the cell death network (Kalimutho *et al.*, 2018). *CEP55* can also positively regulate *PI3K/AKT* signaling, which plays a central role in the development of many cancers to promote growth and confer a survival advantage (Chen *et al.*, 2007).

Analysis of *CEP55* expression across TCGA dataset shows overexpression of *CEP55* across multiple tumor types, including breast invasive carcinoma (BRCA), Bladder Urothelial Carcinoma (BLCA), colon adenocarcinoma (COAD), glioblastoma multiforme (GBM), lung adenocarcinoma (LUAD), lung squamous cell carcinoma (LUSC), ovarian serous cystadenocarcinoma (OV), and pancreatic adenocarcinoma (PAAD) (**Fig. 6.1A**). Elevated expression of *CEP55* also correlates with the aggressiveness, metastatic spread, stage of the tumor, prognosis, and poor survival (**Fig. 6.1B**).

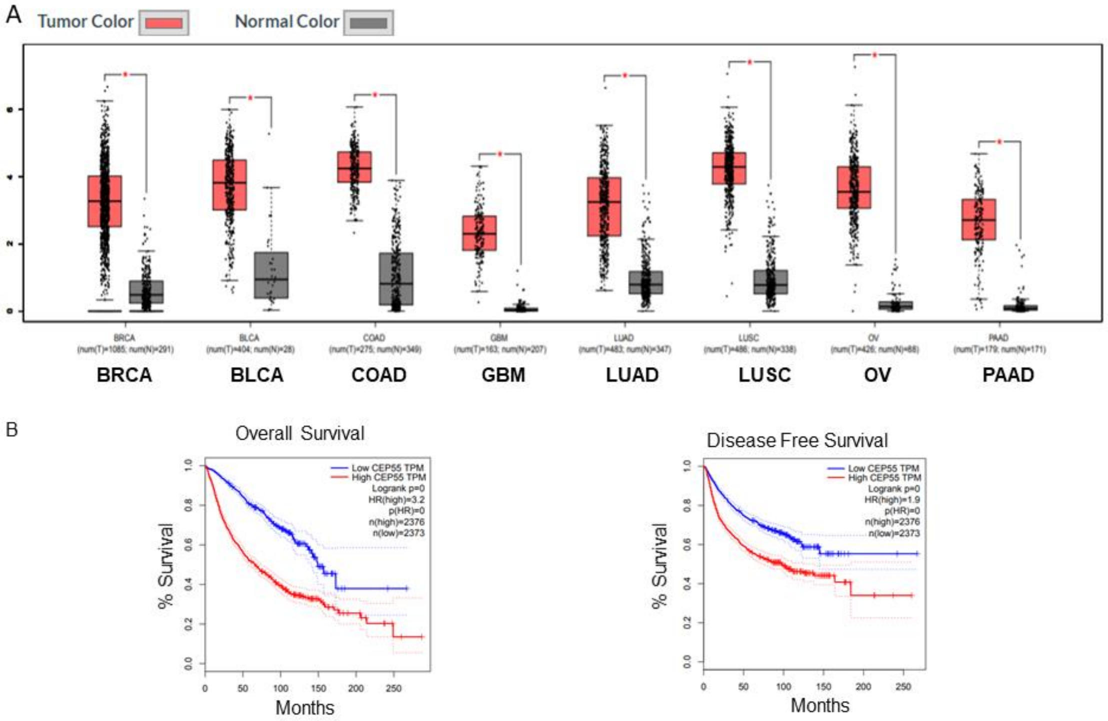

Figure 6.1 *CEP55* is overexpressed across different tumors, and its overexpression is linked to poor survival.

(A) *CEP55* expression levels in normal (gray) and tumor (red) tissues. (GEPIA); (B) Overall survival (left) Disease-free survival (right) comparing low (blue) and high (red) *CEP55* expression.

Despite our understanding of how *Cep55* can promote tumorigenesis *in vitro*, as well as reports showing its overexpression across multiple cancer types, the mechanisms by which *CEP55* promotes malignant transformation in an *in vivo* setting require further characterization.

6.1.2 The PTEN tumor suppressor

The *Phosphatase and Tensin Homolog (PTEN)* gene, identified on human chromosome 10 (10q23.3), has been reported to be mutated or exhibited loss of function in multiple cancers, particularly in prostate and brain tumors including glioblastoma (Li *et al.*, 1997; Teng *et al.*, 1997; Maehama and Dixon, 1998). PTEN has dual protein and lipid phosphatase activity and is a major negative regulator of the *PI3K/AKT/mTOR* pathway (Vivanco and Sawyers, 2002). Mutation of PTEN has been found in a group of autosomal dominant syndromes characterized by developmental disorders, neurological deficits, and syndromes such as Cowden disease, Bannayan–Riley–Ruvalcaba syndrome and Lhermitte–Duclos disease (Liaw *et al.*, 1997; Marsh *et al.*, 1998; Backman *et al.*, 2001). These diseases are characterized by several hamartomatous lesions of different organs, including the central nervous system, skin, intestines, and bone (Marsh *et al.*, 1998; Eng, 2003). This predisposes to malignancy formation and is considered to increase the risk of cancer in the thyroid, breast, and endometrium (Tan *et al.*, 2012). The constitutive loss of one *PTEN* allele is also capable of giving rise to multiple lesions, probably due to loss of heterozygosity (LOH) (Lin *et al.*, 1998; Robertson *et al.*, 1998; Sato *et al.*, 2000; Oki *et al.*, 2005).

Suzuki *et al.* reported that mutation of *Pten* is associated with higher cancer susceptibility and early embryonic lethality using a mouse model (Suzuki *et al.*, 1998). Several additional investigations utilizing inducible or conditional KO of *Pten* have shed light on how *Pten* suppresses tumorigenesis across multiple tissues and organs (Li *et al.*, 2002; Mao *et al.*, 2003; Knobbe *et al.*, 2008; Mirantes *et al.*, 2013). Inducible deletion of *Pten* in most systemic organs using the Cre ERT system leads to the development of a range of malignancies such as lymphoma, prostate, endometrial, intestinal cancers, and squamous cell carcinoma with an overall mean tumor latency of 17 weeks (Lu *et al.*, 2007). Deletion of *Pten* in murine hematopoietic stem cells (HSCs), using a Cre under the control of the polyinosine–polycytidine (pIpC) inducible Mx1 promoter, showed rapid commencement of myeloproliferative malignancies such as acute myeloid leukemia or acute lymphoblastic leukemia within approximately four weeks. Interestingly, Yilmaz et al. concluded the increased HSC proliferation was due to PI3K/Akt signaling hyperactivation; therefore, they could rescue this phenotype upon treatment of rapamycin for seven days after pIpC administration. This treatment could also prolong life-span of these mice even after initiation of leukemia (Yilmaz *et al.*, 2006; Zhang *et al.*, 2006).

6.1.3 Activating mutations in Kras and Tumor development

The *RAS-RAF-MEK-ERK* signaling cascade is one of the most important signaling pathways in proliferation and survival, and its activation leads to activating cell division, proliferation, or survival. The *RAS-RAF-MEK-ERK* signaling pathway involves several proteins, such as mitogen-activated protein kinases (MAPK) or so-called extracellular signal-regulated kinases (ERK). The tyrosine kinase activity initiated by the binding of the receptor (*i.e*., EGFR) with its extracellular ligand (*i.e.*, EGF) and phosphorylation of its cytoplasmic domain via Growth factor receptor-bound protein-2 (GBR2) triggering Ras/Rac Guanine Nucleotide Exchange Factor 1 (SOS). Activated SOS promotes the removal of GDP from RAS to phosphorylate and activate downstream pathways such as *RAF/MEK/ERK* or *PI3K/Akt* (Nandan and Yang, 2011). Downstream, *ERK* signaling regulates the activities of several transcription factors such as NF-κB and Myc, resulting in some biological effects (Campisi *et al.*, 1984). Mutation in any of the three members of the *RAS* distinct yet related family proteins (*K-RAS*, *H-RAS*, and *N-RAS*), as well as any mutation in upstream genes, can promote oncogenesis.

K-RAS is the most frequently mutated member of the RAS family, and its mutation can be found at high levels in leukemias, colorectal cancer (Hänggi and Ruffell, 2019), pancreatic cancer (Waters and Der, 2018) and lung cancer. Lung cancer can be broadly categorized into two types: Non-small cell lung cancer (NSCLC, ~75%) and small cell lung cancer (SCLC, ~15%), and is the leading cause of death by cancer worldwide (1.6 million/year) (Ferlay *et al.*, 2015). NSCLC includes adenocarcinoma, squamous cell lung cancer, and large cell lung cancer (**Fig. 6.2A**) (Travis *et al.*, 2011; Consortium, 2017). KRAS mutations, which are the most frequent mutation in NSCLC, predominantly occur at codon 12 by codon variant incidence of approximately 39% for G12C, 18-21% G12V, and 17–18% for G12D (El Osta *et al.*, 2019). However, in non-smokers, the rate of KRAS G12D mutation is up to 58% (Dogan *et al.*, 2012) (**Fig. 6.2B**).

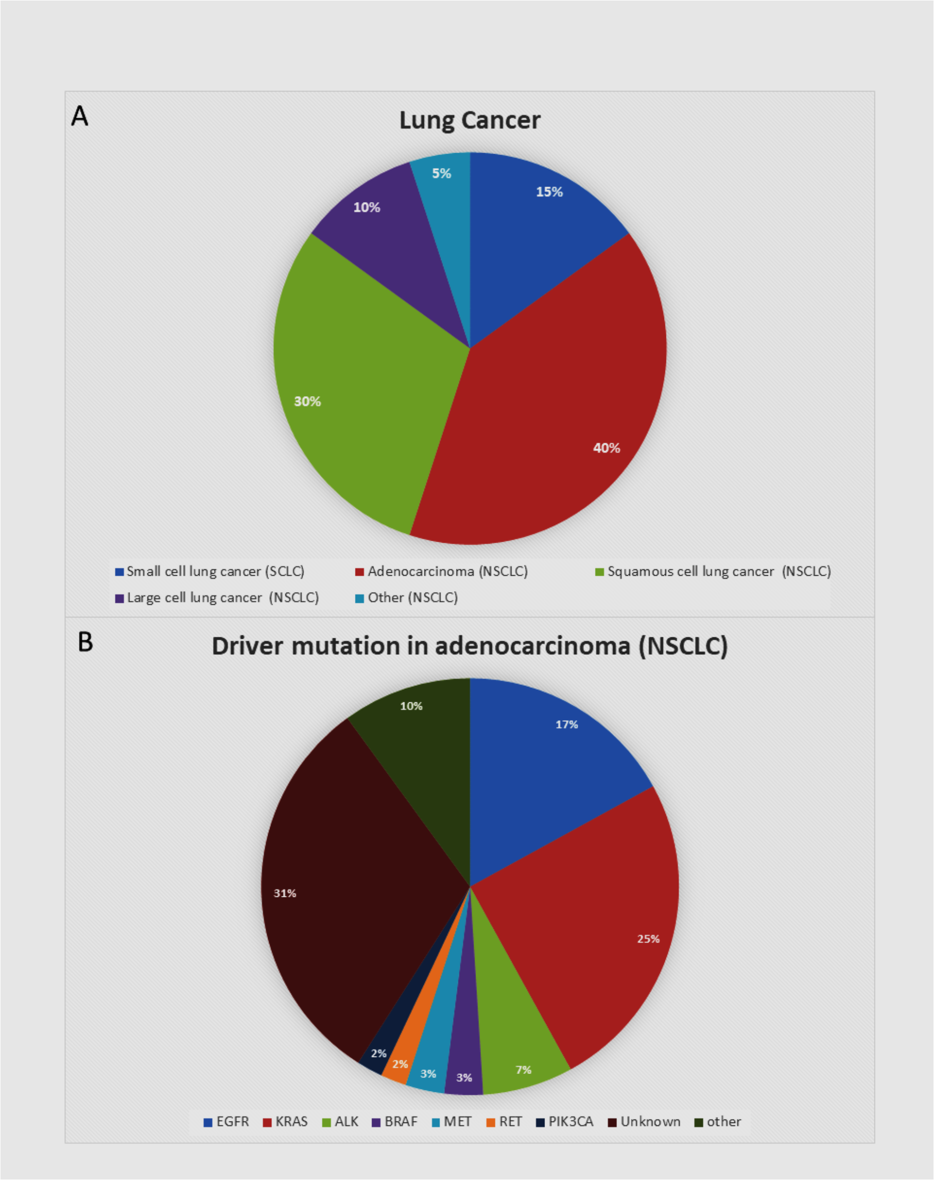

Figure 6.2 Frequent genetic mutations in lung cancer

(A) Lung cancer can be categorized into two main classes, including small cell lung cancer (SCLC) and non-small cell lung cancer (NSCLC), which is further categorized as adenocarcinoma, large cell carcinoma, and squamous cell carcinoma. (B) Percentage of genetic driver mutations in NSCLC.

6.2 Results

6.2.1 A novel mouse model for inducible Cep55 KO

Given the importance of *CEP55* deregulation in cancer, we generated a conditional knockout model of *Cep55* using the inducible *Rosa-Cre ERT2* system, where an inducible Cre transgene in the ubiquitously-expressed *Rosa26* locus can be activated upon tamoxifen administration. We induced a cohort of *RosaCreERT2; Cep55*$^{Fl/Fl}$ mice with either tamoxifen or vehicle control at 8-weeks of age and monitored the mice over a period of 6 months. During this period, we did not observe any phenotypic changes in induced *Cep55* KO mice, indicating *Cep55* is dispensable for adult tissue homeostasis.

6.2.2 Cep55 KO impairs proliferation and transformation in vitro.

We hypothesized that *Cep55* loss might affect tumorigenic or transformative potential in an oncogenic setting. In order to investigate if this was the case, we transformed constitutive *Cep55*$^{+/+}$ and *Cep55*$^{-/-}$ MEFs using a construct expressing E1A/Ras^{V12} (Valente *et al.*, 2015), and performed growth analysis using IncuCyte® live cell analysis (Fig. 6.3A, B).

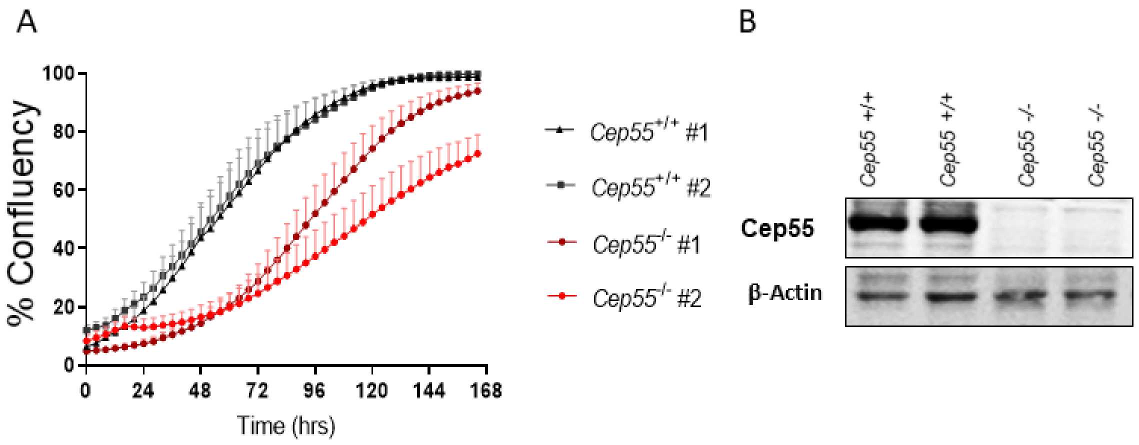

Figure 6.3 Proliferation defects in Cep55-/- MEFs

(A) Proliferation assay showing growth of E1A/Ras-transformed *Cep55*$^{+/+}$ and *Cep55*$^{-/-}$ MEFs (Mean ± SEM, an average of 2 biological repeats, and 2 independent experiments Student's t-test, ****P < 0.0001). (B) Immunoblot analysis of *Cep55* expression from E1A/Ras-transformed *Cep55*$^{+/+}$ and *Cep55*$^{-/-}$ MEFs. Actin served as a loading control.

Next, we sought to determine if *Cep55* loss would perturb colony-forming ability in both a 2D and 3D setting. The colony formation or clonogenic assay is an *in vitro* experiment to determine the ability of single-cell survival to grow into a colony (consisting of at least 50 cells). This method also examined the ability of each cell of a population to undergo unlimited division. Normal cells are prevented from forming a colony because of anoikis, a type of apoptosis, but transformed cells can undergo anchorage-independent growth without binding to a substrate (Franken *et al.*, 2006). Strikingly, we found that the colony-forming ability of E1A/Ras-*Cep55*$^{-/-}$ MEFs was significantly diminished when compared to their E1A/Ras-*Cep55*$^{+/+}$ counterparts. (Fig. 6.4 A, B). This was also the case in a 3D-setting, where E1A/Ras *CEP55*$^{-/-}$ MEF formed colonies approximately one-third the size of their control counterparts (Fig. 6.4 C, D). Although soft-agar assay give an indication of growth potential in a 3D-setting, they do not adequately mimic the extracellular milieu *in vivo*. We, therefore, also sought to replicate these findings using Happy Cell Advanced Suspension Medium® (HCM), a low viscosity liquid reagent matrix that promotes the formation of 3D multicellular structures, enables the cells to grow in a suspension manner to migrate, aggregate and expand from single cells. The suspension system can be inactivated by adding a *stop solution* to facilitate harvesting the cells for downstream analysis (Kulasinghe *et al.*, 2016; Protsenko, 2018; Ryan, 2019). Comparison of E1A/Ras-*Cep55*$^{-/-}$ and E1A/Ras-Cep55$^{+/+}$ MEFs showed that *Cep55*$^{-/-}$ E1A/Ras MEFs formed 2.5 fold-less colonies when compared to control transformed MEFs (Fig. 6.4 E, F).

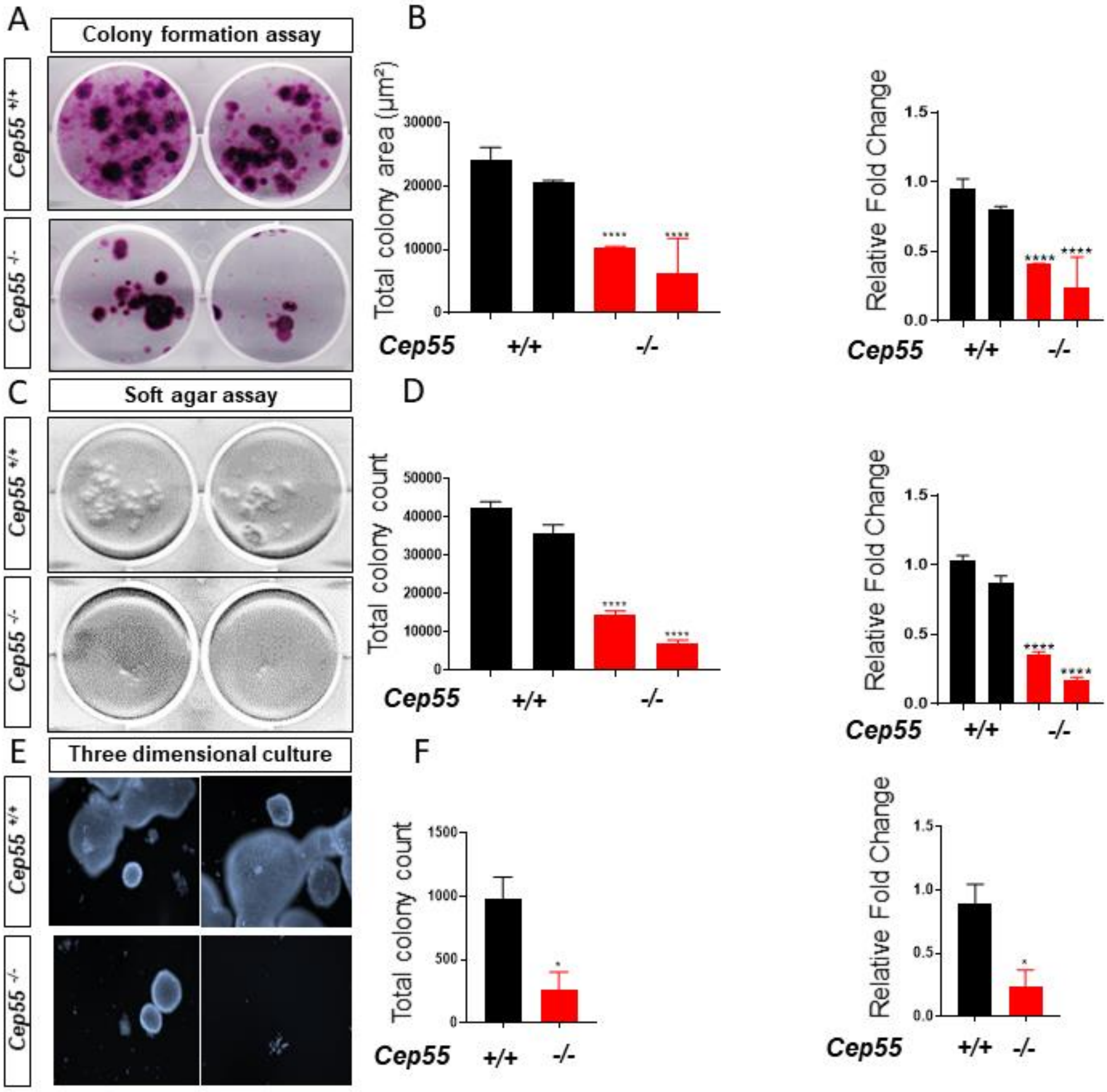

Figure 6.4 2D and 3D colony-forming potential of E1A/Ras-transformed *Cep55*$^{+/+}$ and *Cep55*$^{-/-}$ MEFs

(A) Representative image of colony formation (clonogenic) 2D assay; (B) Bar chart represents (left) : the relative total colony area (μm^2) and (right): Relative fold change; (C) Representative image of soft agar colony formation assay (3D) of E1A/Ras-transformed *Cep55*$^{+/+}$ and *Cep55*$^{-/-}$ MEFs; (D) Bar chart represents (left) : total number of colony count and (right): relative fold change; (E) Representative image of 3D culture of E1A/Ras-transformed *Cep55*$^{+/+}$, and *Cep55*$^{-/-}$ MEFs using HCM; (F) Bar chart represents (left): total colony count and (right): Relative fold change. Data represent the mean ± SEM, n = 2, 3 independent experiments, Student's t-test $^{*}P < 0.05$, $^{**}P < 0.01$, $^{***}P < 0.001$, $^{****}P < 0.0001$).

6.2.3 Delayed tumor progression in Cep55$^{-/-}$ cell-derived xenograft mouse model

To determine if we could recapitulate the effects of Cep55 loss in colony-forming ability in an *in vivo* setting, we next performed cell-line derived xenografts by injecting 1×10^6 cells from each group suspended in Matrigel/ PBS intraperitoneally into 6-10-week old non-obese diabetic/severe combined immunodeficiency (NOD/SCID) mice. In keeping with our *in vitro* observations, while the *Cep55*$^{+/+}$ cohort xenografts took approximately 19 days post-injection for tumors to become palpable, in the *Cep55*$^{-/-}$ E1A/Ras group it took significantly longer, with an average of 30 days. Once tumors established, the time to reach the experimental endpoint was also significantly longer for the *Cep55*$^{-/-}$ cohort compared to *Cep55*$^{+/+}$ cohort (14 days versus 17 days post tumor initiation). Overall, in *Cep55*$^{+/+}$ xenografts, the tumor reached end-stage 33 days on average in contrast to 47 days in *Cep55*$^{-/-}$ xenografts (Fig. 6.5).

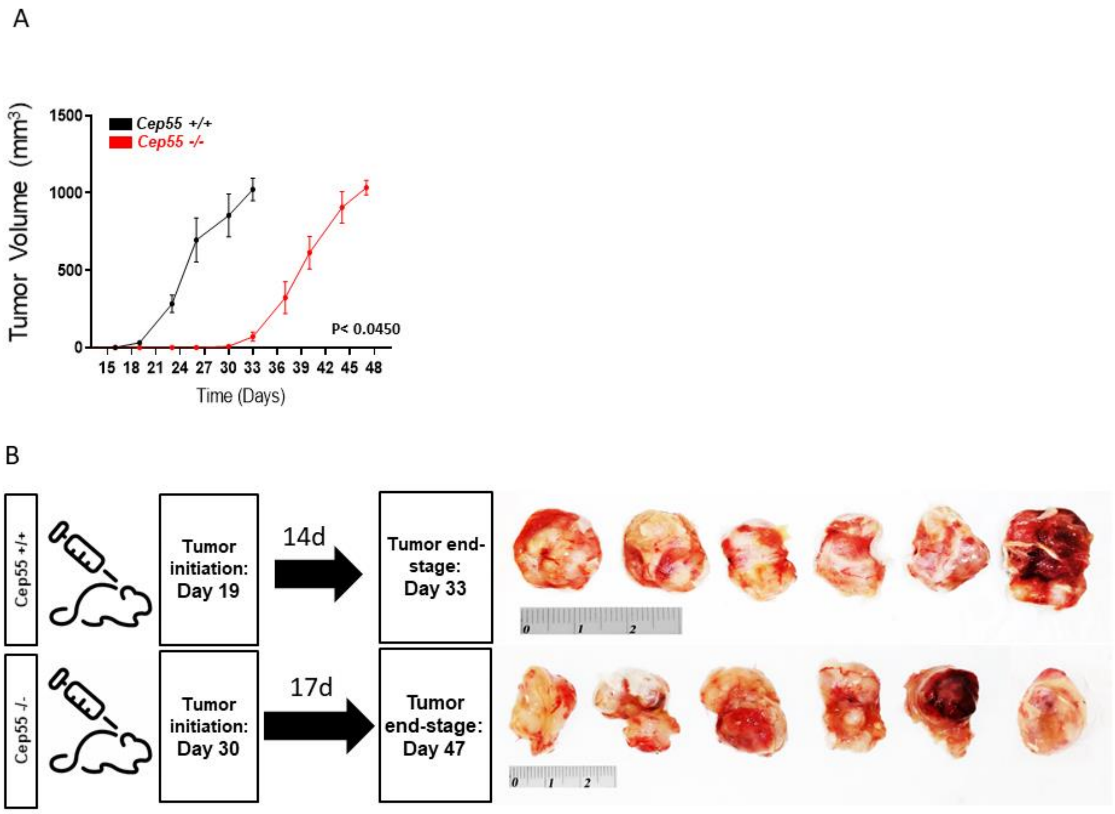

Figure 6.5 Tumors of E1A/Ras-transformed MEFs in NOD/SCID mouse.

(A) Tumor volume (mm^3) comparison of $1x10^6$ E1A/Ras-mediated *Cep55*$^{+/+}$, and *Cep55*$^{-/-}$ MEFs injected into Nod/Scid mice, (Mean ± SEM, n=6 Student's t-test, $*P < 0.05$). (B) Comparison of tumor initiation and development in E1A/Ras-transformed *Cep55*$^{+/+}$ (upper panel) and *Cep55*$^{-/-}$ (lower panel) MEFs injected into Nod/Scid mice and representative images of tumors at experimental end-point for each group.

To further investigate the differences governing these effects, we next performed H&E staining of *Cep55*$^{+/+}$ and *Cep55*$^{-/-}$ tumor xenografts. This staining revealed that although the tumors formed across the two genotypes were morphologically similar, there were much higher levels of tumor necrosis in the *Cep55*$^{-/-}$ tumors (Fig. 6.6A). However, the mitotic rate of the tumors was not significantly different (Fig. 6.6B). Analysis of proliferation (Ki67-positive) and apoptosis (Apoptag) also showed that *Cep55*$^{-/-}$ xenografts had lower levels of proliferating cells and higher levels of apoptosis, respectively (Fig. 6.6C-D). Together, these data suggest that loss of *Cep55* significantly delays tumor formation of E1A/Ras-transformed MEFs *in vivo*.

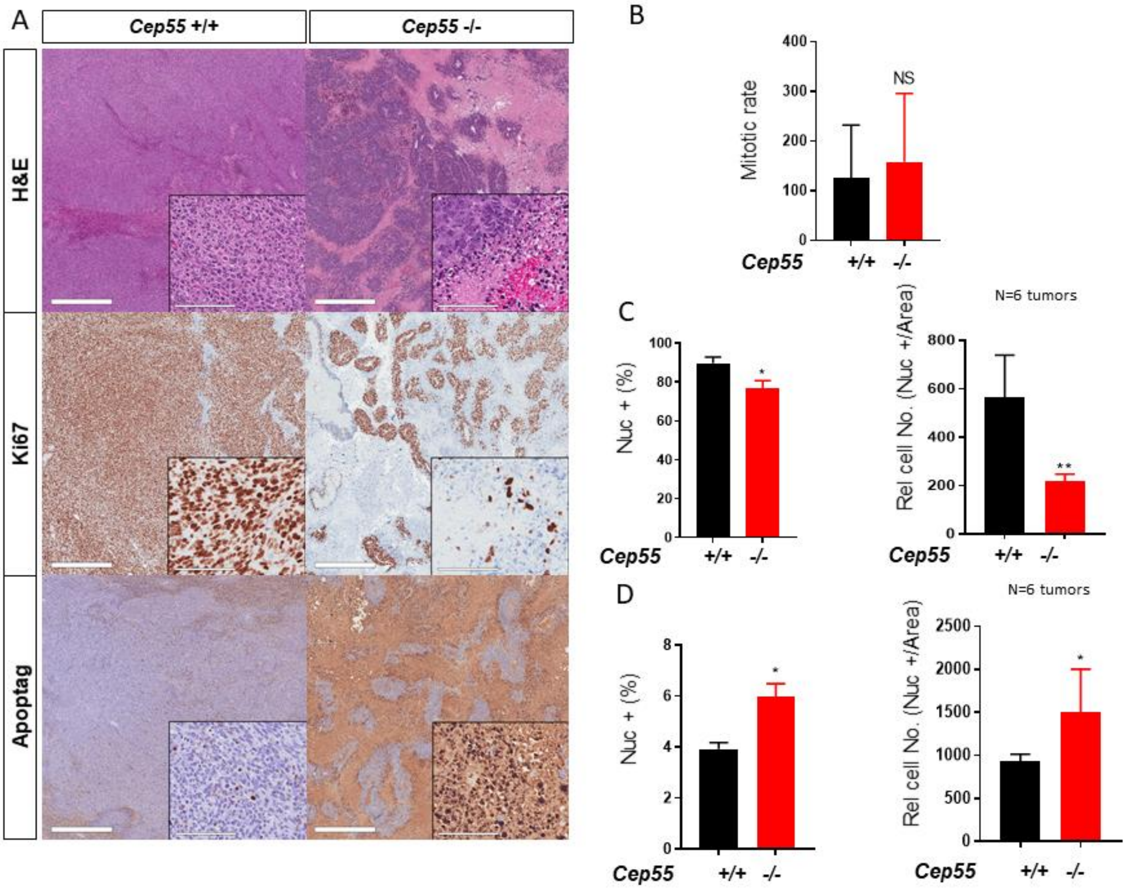
A
Cep55 +/+
Cep55 -/-
H&E
Ki67
Apoptag
B
Mitotic rate
400
300
200
100
0
NS
Cep55
+/+
-/-
C
Nuc + (%)
100
80
60
40
20
0
*
Cep55
+/+
-/-
N=6 tumors
Rel cell No. (Nuc +/Area)
800
600
400
200
0
**
Cep55
+/+
-/-
D
Nuc + (%)
8
6
4
2
0
*
Cep55
+/+
-/-
N=6 tumors
Rel cell No. (Nuc +/Area)
2500
2000
1500
1000
500
0
*
Cep55
+/+
-/-

Figure 6.6 IHC analysis of E1A/Ras-transformed *Cep55*$^{+/+}$, and *Cep55*$^{-/-}$ tumors in mice.

(A) Representative images of tumors from E1A/Ras-transformed *Cep55*$^{+/+}$ (left), and *Cep55*$^{-/-}$(right) MEFs injected into Nod/Scid mice stained for (upper panel): H&E; (middle panel): proliferation marker: Ki67; (lower panel): apoptosis marker: apoptag. Comparison of tumors of E1A/Ras-transformed *Cep55*$^{+/+}$, and *Cep55*$^{-/-}$ MEFs for: (B) mitotic rate; (C) (left): percent of Ki67 positive cells (right): Relative density of Ki67 positive cells; (D) (left): percent of apoptotic cells (right): Relative density of apoptotic cells.

6.2.4 Loss of Cep55 delays tumorigenesis in a Pten-deficient tumor-prone mouse model

Since MEFs with *Cep55*$^{-/-}$ showed delay tumorigenesis when injected into mice, next, we sought to examine whether inducible KO of *Cep55* can restrict tumor incidence or latency in tumor-prone genetically engineered mouse model. *PTEN* is a negative regulator and suppressor of the *PI3K/AKT* pathway, while *CEP55* is a known positive regulator of this signaling, which can hyperactivate this pathway and promote *AKT* activity (Paez and Sellers, 2004; Chen *et al.*, 2007). Analysis of cBioportal also shows that *CEP55* overexpression is mutually exclusive (P< 0.001) with *PTEN* loss in Pan-Cancer Atlas of TCGA data set across many cancers, including invasive breast carcinoma and urothelial carcinoma of the bladder (Fig. 6.7). Given this relationship between these two genes, we sought to understand how Cep55 loss would affect cancer formation in a *Pten*-deficient mouse model as a rationale for targeting of *Cep55* in *Pten*-deficient cancers.

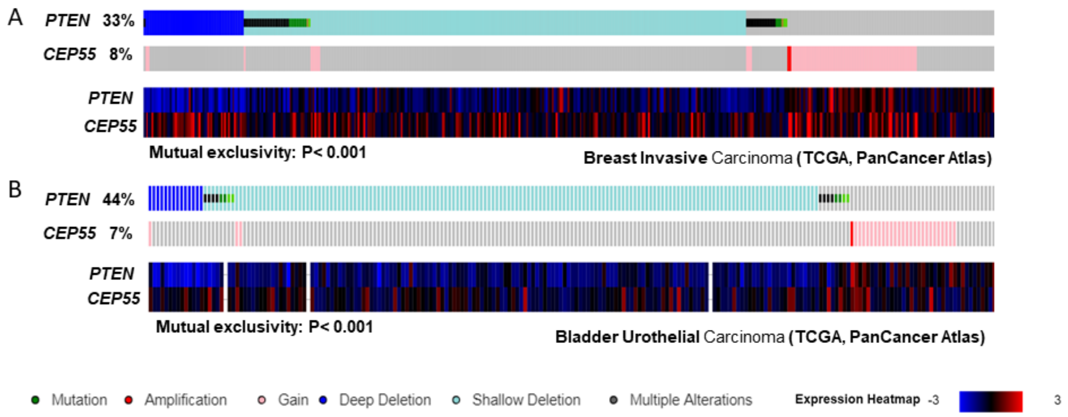

Figure 6.7 OncoPrint of *PTEN* and *CEP55* analyzed from Cancer Genomics cBio-Portal

Overview of genomic alterations (see legend) in PTEN and CEP55 genes (rows). (A) OncoPrint of *Pten* and *Cep55* alterations in Breast cancer across TCGA data set. Genomic alteration events are mutually exclusive (P< 0.001); (B) OncoPrint of *Pten* and *Cep55* alterations in Bladder Urothelial Carcinoma across TCGA data set. Genomic alteration events are mutually exclusive (P< 0.001).

To generate experimental mice to allow co-deletion of both *Cep55* and *Pten*, we utilized our *Cep55*$^{Fl/Fl}$ mice and crossed them against a *Pten*$^{Fl/Fl}$ line, to allow conditional deletion of both genes. As *Cep55* and *Pten* are located on the same chromosome in mice, we calculated there would be an approximate 3% chance of meiotic recombination to obtain both floxed alleles on the one chromosome. After genotyping approximately 200 pups, we found a recombined allele of *Cep55-Pten*^{F}/+ and further crossed this mouse to segregate the allele. *Cep55-Pten*^{F}/+ mice were further crossed against RosaCreERT2 and backcrossed to the *Cep55-Pten*^{F} allele to generate inducible *RosaCreERT2*; *Cep55-Pten*^{F}/*Cep55*$^{-}$*Pten*^{F} offspring. We injected these mice with tamoxifen or vehicle control at 6 weeks of age and monitored them for tumor formation. Four weeks post-injection, the *RosaCreERT2*; *Cep55-Pten*^{F}/*Cep55*$^{-}$*Pten*^{F} and *Pten*$^{Fl/Fl}$ mice began to show signs of morbidity and were sacrificed for the pathological examination of tissues including, but not limited to, bone marrow (BM), thymus, spleen, liver, lymph nodes, whole blood, testis, genital/reproduction organs, lung, intestine, skin, soft tissues, and bone.

Previous studies describing the tumor spectrum of T-cell specific or multiple tissue cKO *Pten*$^{-/-}$ using Rosa-CreERT2 show the predominant tumor formed is lymphoma (Backman *et al.*, 2001; Suzuki *et al.*, 2001; Lu *et al.*, 2007; Hagenbeek and Spits, 2008). Lymphomas are a heterogeneous group of tumors mostly arising in the lymphatic systems and classified into Hodgkin and non-Hodgkin lymphoma (Foon, 1986; Iqbal *et al.*, 2019; X. Wu *et al.*, 2019). BM and thymus are the primary lymphoid organs that are involved in the generation and clonal selection of lymphocyte tissues. While both production and maturation of B-cells occur in BM, T-cells travel to the thymus for further development. Mature T-cells join B-cells to travel to secondary lymphoid organs such as lymph nodes and the spleen to initiate an adaptive immune response (Steinman and Cohn, 1973; De Togni *et al.*, 1994; Elmore, 2018).

In our *Pten* model consistently, we observed splenomegaly in both *Cep55/Pten* (2 folds) and *Pten* (2 folds) groups compared to the corresponding vehicle control group. Rapid and aggressive formation of lymphoid tumors in *Pten* prevents the initiation and development of tumors in other tissues, and thymic or splenic lymphoma were the only tumor types observed. However, in double *Cep55/Pten* mice, a range of pathological abnormalities was found in the collected lymphoid organs (Fig. 6.8 & Tab. 1). Interestingly, these abnormalities appear to be gender-biased because all females died within an average of seven weeks post-injection and only 40% of males died within this period of time. The survived mice exhibited severe phenotypes such as skin papilloma and prostatic hyperplasia. A cohort of tamoxifen-induced *Cep55/Pten* and *Pten* alone monitored for 160 days following injection revealed that the overall survival in mice with loss of *Cep55* and *Pten* is significantly longer than that with *Pten* loss alone. The median survival for *Pten* loss was 21 days, and *Cep55/Pten* was 150 days. Seven mice of the *Pten* group died as early as seven days after injection; however, no signs of toxicity were observed by an independent analysis of organs from a veterinary pathologist. Due to unknown cause of lethality, these mice were excluded from the survival cohort. (Fig. 6.9). Collectively, the data suggest *Cep55* can delay tumorigenesis and tumor latency on a *Pten*-deficient background.

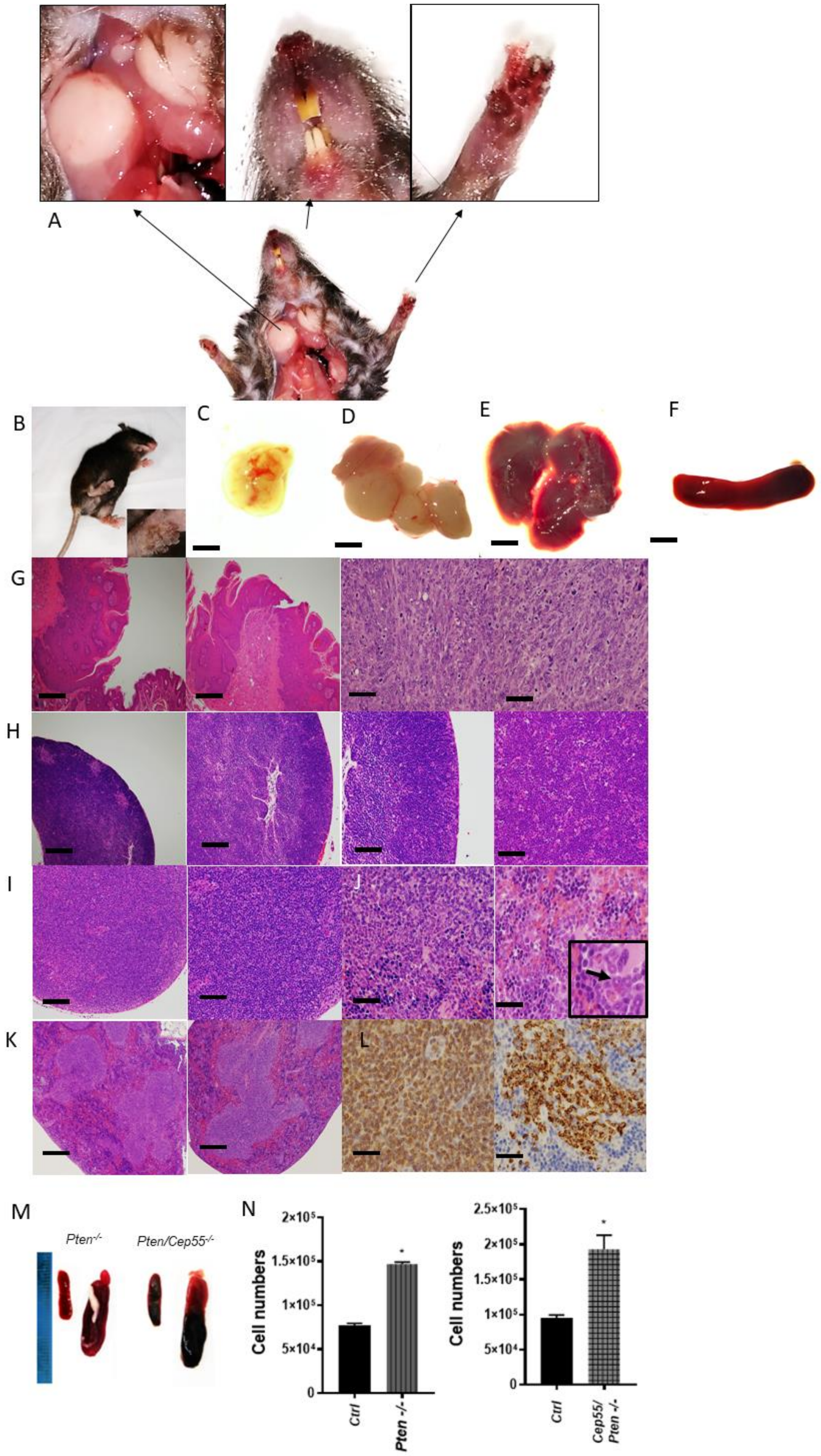
A
B
C
D
E
F
G
H
I
J
K
L
M
Pten-/-
Pten/Cep55-/-
N
Cell numbers
2×10⁵
1.5×10⁵
1×10⁵
5×10⁴
0
*
Ctrl
Pten -/-
Cell numbers
2.5×10⁵
2×10⁵
1.5×10⁵
1×10⁵
5×10⁴
0
*
Ctrl
Cep55/
Pten -/-

Figure 6.8 Analysis of tumor spectrum in Pten and Cep55/Pten mice.

(A) Image of multiple tumors present in the same mouse, note the skin squamous carcinoma around mouth and paw, swollen lymph nodes/thymus. Images of organs as indicated in cKO of *Cep55/Pten*: (B) Skin squamous carcinoma (papilloma) in mouse limb; (C) Thymus; (D) Lymph nodes; (E) Liver; (F) Spleen, Scale bar = 3mm. H&E stain of cKO of Cep55/Pten: (G) Squamous papilloma (right panels), Scale bar = 180 µm; subcutaneous mesenchymal tumor (left panels), Scale bar = 60 µm; (H) Thymus lymphoma, Scale bar = 120 µm; (I) Lymph node lymphoma, Scale bar = 120 µm; (J) Extramedullary haemopoiesis (EMH) in spleen (note "doughnut-shaped" myeloblasts in red pulp), Scale bar = 60 µm; (K) Spleen lymphoma, Scale bar = 180 µm; (L) IHC showing (right panel) the cells are CD3+ for T cell lymphoma (in both groups) and (left panel) B220+ for B cell lymphoma (only in cKO Cep55/Pten), Scale bar = 60 µm; (M) Comparative images of Spleen in Vehicle control (Cre-) and tamoxifen-induced Cre+ *Pten*$^{fl/fl}$ tamoxifen-induced Cre+ [left] and the Vehicle control (Cre-) and *Cep55/Pten*$^{fl/fl}$ Cre+, [right]; Scale in mm; (N) Quantification of cell number from H&E staining of 5µm longitudinal sections of spleens shown in (M).

Genotype	***Cep55*** $^{fl/fl}$**;** ***Pten*** $^{fl/fl}$ **;** ***Cre*** **+**	***Pten*** $^{fl/fl}$ **;** ***Cre*** **+**
Lymphoma	11(16)	6(8)
Extra-medullary hemopoiesis	4(16)	1(8)
Squamous papilloma	4(16)	0
Hematoma	5(16)	1(8)
Hemangio-endothelioma (sarcoma)	2(16)	0
Still alive	5	0

Table 6.1 Tumor burden in cKO Cep55/Pten and cKO Pten mice

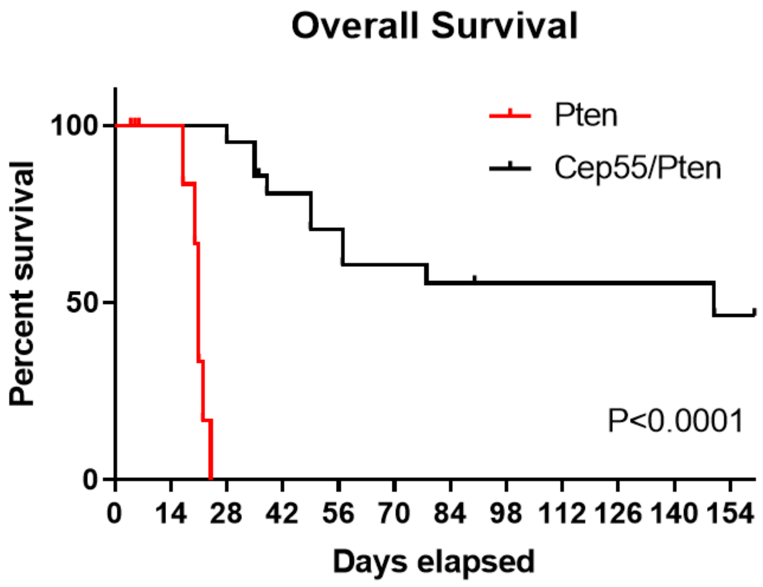

Figure 6.9 Survival of *Cep55/Pten* and *Pten* mice

Kaplan-Meir analysis of Cep55/Pten and Pten mouse cohort survival.

6.2.5 Loss of Cep55 hinders tumorigenesis in a Kras-mutant tumor prone mouse model

Given the significant role of *Cep55* in delaying tumorigenesis in MEFs used as xenografts and *Pten* tumor-prone models, we questioned whether this effect could be reproduced in *Kras* mutant lung-specific tumors which are mainly driven by activation of ERK pathway rather than the PI3K pathway. Cancer genomics analysis through cBioportal shows that *Cep55* overexpression co-occurs (P< 0.003) with *Kras* mutation in a lung cancer setting, leading us to question whether Cep55 potentiates the tumorigenicity of Kras mutation. To test this hypothesis, we utilized a KrasG12D *lox-stop-lox* model, where one of the Kras alleles is replaced with the G12D allele, preceded by a loxP-flanked "stop" cassette. This stop cassette inhibits expression of the mutant protein unless Cre-mediated recombination occurs. The activation of a single allele of oncogenic *Kras* is sufficient to initiate tumorigenesis (Engelman *et al.*, 2008).

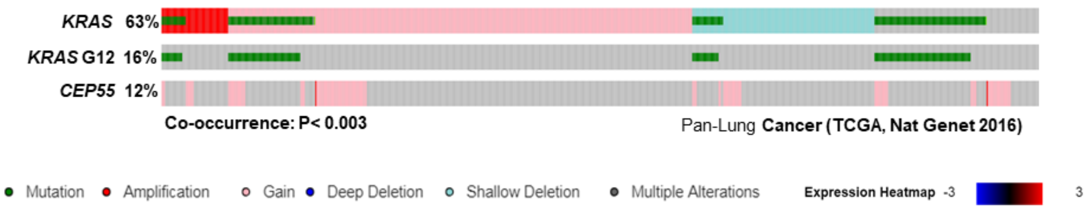

Figure 6.10 OncoPrint of co-occurrence of *KRAS* and *CEP55* alternations analyzed from Cancer Genomics cBio-Portal

OncoPrint of *Kras*, *KrasG12* mutant, and *Cep55* alterations in Lung cancer across TCGA data set. Genomic alteration events are co-occurrence (P< 0.003).

We crossed *Cep55*$^{Fl/Fl}$ mice against *Kras*$^{G12D/+}$ mice to generate *Cep55*$^{Fl/Fl}$; *Kras*$^{G12D/+}$ (hereafter referred to as *Cep55*$^{-/-}$*Kras*$^{m/+}$) or *Cep55*$^{+/+}$; *Kras*$^{G12D/+}$ (*Kras*$^{m/+}$). To induce lung-specific recombination of *the Cep floxed* and Kras *G12D lox-stop-lox* alleles, we administered PBS/Media or Adeno-Cre virus intra-nasally and sacrificed mice at several time-points following induction to monitor lung-tumor formation. *Kras*^{m}/$^{+}$ and *Cep55*$^{-/-}$ *Kras*^{m}/+ mice were initially sacrificed at eight weeks post- Adeno-Cre infection. The lesions identified at this time-point mostly consisted of atypical adenomatous hyperplasia (AAH, Fig. 6.11A) and adenomas (Fig. 6.11B, C). To a lesser degree, alveolar-bronchiolar early carcinomas were also observed at this stage (Fig. 6.11D, E). Classification of early carcinoma was based on sufficient cellular atypia to be classified as a carcinoma rather than adenoma (Fig. 6.11F); however, in well-established carcinoma, reasonably well differentiated pleomorphic nuclei and mixed cellular phenotypes are evidenced (Fig. 6.11G). As expected, at 8 weeks post-infection the *Kras* control group (Vehicle-treated or *Kras Wt* regardless of *Cep55* status, Wt/Het/KO) did not form any tumors (Fig. 6.11H); however, in both *Kras*^{m}/+ (Fig. 6.11I) and *Cep55*$^{-/-}$*Kras*^{m}/+ (Fig. 6.11J) groups tumors were identified. At 16 weeks post-infection, the number, size and percentage of adenocarcinomas formed compared to earlier time points also increased (Fig. 6.11K). At 20 weeks post-infection, increased tumor growth was observed, without metastasis (Fig. 6.11L, M).

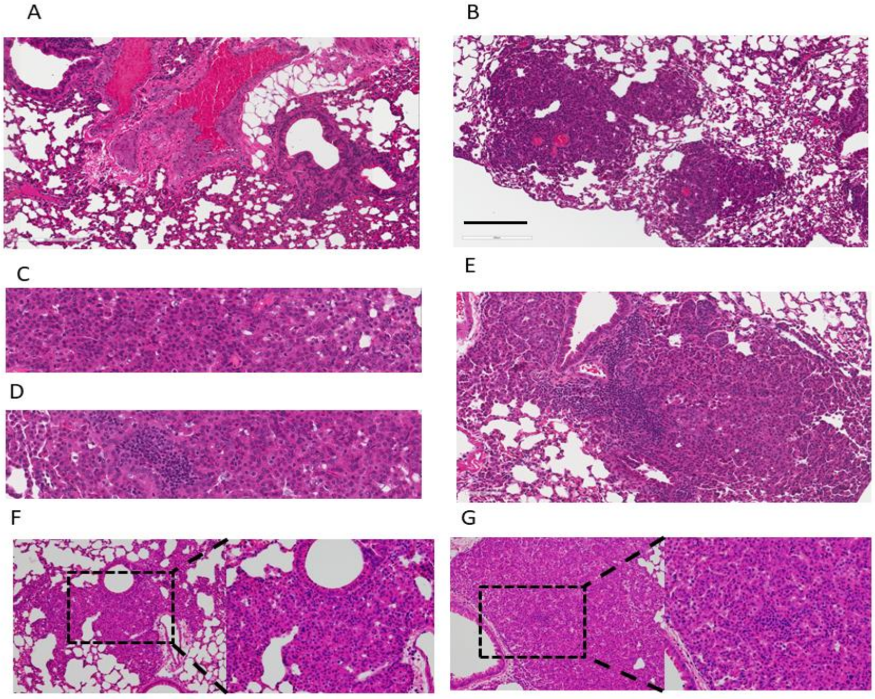

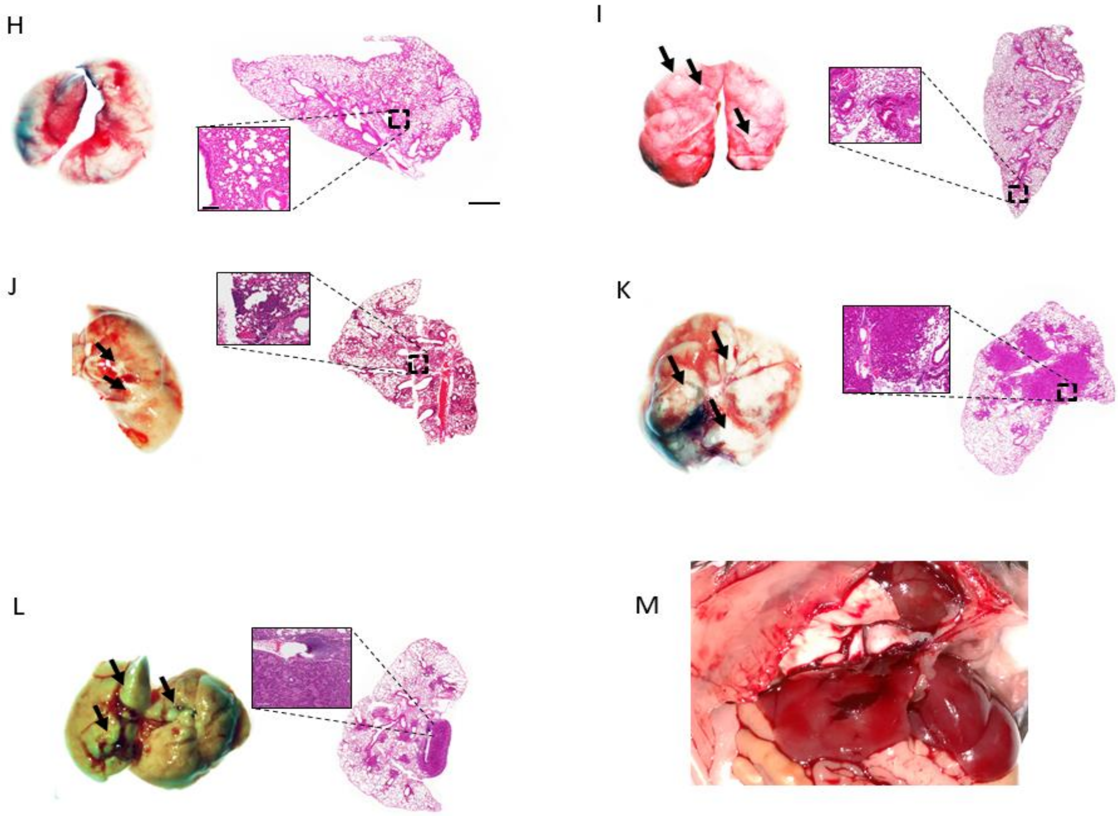

Figure 6.11. Tumor spectrum in *Kras G12D*-driven lung cancer

(A) Grade 1 lesion of an AAH progressing to a small adenoma; (B) Grade 2 adenoma; (C) Uniform nuclei in a grade 2 adenoma; (D) Pleomorphic nuclei in a Grade 3 adenocarcinoma; (E) Grade 3 adenocarcinoma displaying mixed cellular phenotypes; (F) Early alveolar-bronchiolar carcinoma;(G) Alveolar-bronchiolar carcinoma; Representative image of lung and H&E, boxed area is zoomed, (arrows show tumors), Scale bar = 60 µm:(H) *Cep55*$^{+/+}$*; Kras*$^{+/+}$ at 8 weeks; (I) *Cep55*$^{+/+}$*; Kras*$^{m/+}$at 8 weeks; (J) *Cep55*$^{-/-}$*; Kras*$^{m/+}$ at 8 weeks; (K) *Cep55*$^{+/+}$*; Kras*$^{m/+}$ at 16 weeks; (L) *Cep55*$^{+/+}$*; Kras*$^{m/+}$ at 20 weeks; (M) Photographs of lungs and adjacent organs from mice sacrificed 20 weeks following intranasal inhalation of AdCre of lung *Cep55*$^{+/+}$; *Kras*$^{m/+}$, no metastasis observed.

After initial observation and characterization, next, I infected a cohort of *Cep55*$^{-/-}$ *Kras*$^{m/+}$ and *Kras*$^{m/+}$ to be sacrificed at eight weeks post-infection and examined for histopathological grading and quantification of tumor burden. The tumor incidence at this time point in *Cep55*$^{-/-}$*Kras*$^{m/+}$ mice was 68%, compared to 100% of *Kras*$^{m/+}$ mice. The percent of tumor area to the total lung area had reduced significantly (Fig. 6.12A-D). *Cep55*$^{-/-}$*Kras*$^{m/+}$ mice exhibited 28.5% adenocarcinoma, and 28.5% adenoma and 43% were tumor-free. However, *Kras*$^{m/+}$ mice formed 33.4% adenocarcinoma and 66.6%

adenoma at 8 weeks post-infection. Collectively, our data show that *Cep55*$^{-/-}$*Kras*$^{m/+}$ mice exhibited decreased tumor formation compared to *Kras*$^{m/+}$ mice (Fig. 6.12E).

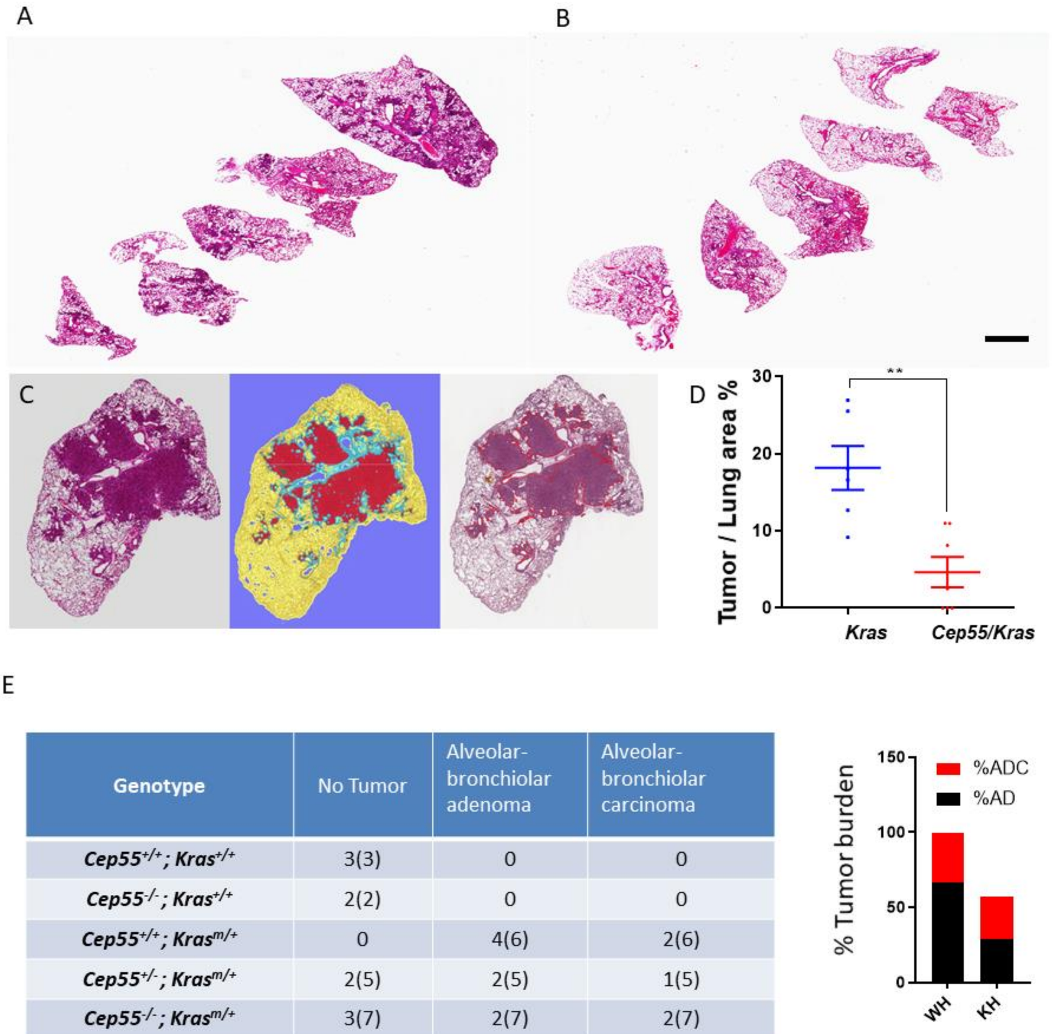

Genotype	No Tumor	Alveolar-bronchiolar adenoma	Alveolar-bronchiolar carcinoma
$Cep55^{+/+}$; $Kras^{+/+}$	3(3)	0	0
$Cep55^{-/-}$; $Kras^{+/+}$	2(2)	0	0
$Cep55^{+/+}$; $Kras^{m/+}$	0	4(6)	2(6)
$Cep55^{+/-}$; $Kras^{m/+}$	2(5)	2(5)	1(5)
$Cep55^{-/-}$; $Kras^{m/+}$	3(7)	2(7)	2(7)

Figure 6.12 Tumor quantification and tumor burden in *Kras*-driven lung cancer

(A) lung lobes showing tumors from *Cep55*$^{+/+}$; *Kras* $^{m/+}$ mice; (B) lung lobes showing tumors from *Cep55*$^{-/-}$; *Kras*$^{m/+}$ mice; (C) Representative image showing H&E staining of lung and tumor area (right), representative image of automatic detection of tumor based on machine learning algorithm after training the software for 5 regions by HALO™ (middle), representative image of manual detection of tumor area by QuPath™ (left); (D) Chart showing percent of tumor relative to lung area; (E) Table showing tumor burden of adenoma and adenocarcinoma among different genotypes right-hand chart shows percent of tumor burden in lung cancer model.

In order to further understand the histological differences between *Cep55-Kras*^{m}/+ and *Kras*^{m}/$^{+}$, we performed Masson's trichrome staining to detect and analyze tumors for keratin (red-stained) and collagen (blue-stained) formation. This staining is used to identify desmoplastic growth of fibrous tissue, and in the lungs, it can also be used to calculate a lung fibrosis score based on comparison of keratin and collagen formation (O'connor and Valle, 1982; Elsum *et al.*, 2014; Brooks *et al.*, 2018). It is widely accepted that during carcinogenesis, the extracellular matrix (ECM) is remodeled (Fang *et al.*, 2019). Collagen Type-I, is secreted by fibroblasts or cancer cells, and it is an essential compartment of ECM. It is vital for tumor growth and epithelial-mesenchymal transition (EMT) and endogenously produced by non-small cell lung cancer (NSCLC) and esophageal squamous cell carcinoma (ESCC) cells (Poltavets *et al.*, 2018). Cancer-derived Type I collagen has a potential function in cancer development and associated with overall survival and cancer cell differentiation (Nissen, Karsdal and Willumsen, 2019). However, although we observed diminished tumor incidence in *Cep55*$^{-/-}$*Kras*$^{m/+}$ *vs Kras*$^{m/+}$, we did not observe any differences in the staining pattern between the two groups (Fig. 6.13A). Moreover, whether *Cep55* can modulate ECM remodelling and/or EMT requires further experiments.

Next, we performed IHC for pAkt and pErk1/2, which can be activated by Kras signaling (Lai *et al.*, 2018). Interestingly, we observed that there were less immunopositive cells for these markers in *Cep55-Kras*$^{m/+}$ tumors compared to *Kras*$^{m/+}$ tumors indicating that *Cep55*-deficient cancerous cells may be unable to activate fully *Akt* and *Erk* as well as their downstream targets which may be a mechanism of impeding tumorigenesis in these tumors (Fig. 6.13B, C). Immunoblot analysis of our MEFs also confirmed that pAkt (S473) and pErk1/2 (Phospho-p44/42 MAPK (Erk1/2, Thr202/Tyr204) were downregulated in a Cep55-dosage-dependent manner. However, the expression of Kras, Egfr and Pdgfr is steady suggesting that these defects are downstream at the level of PI3K/*Akt* and *Mek/Erk* pathways (Fig. 6.13D).

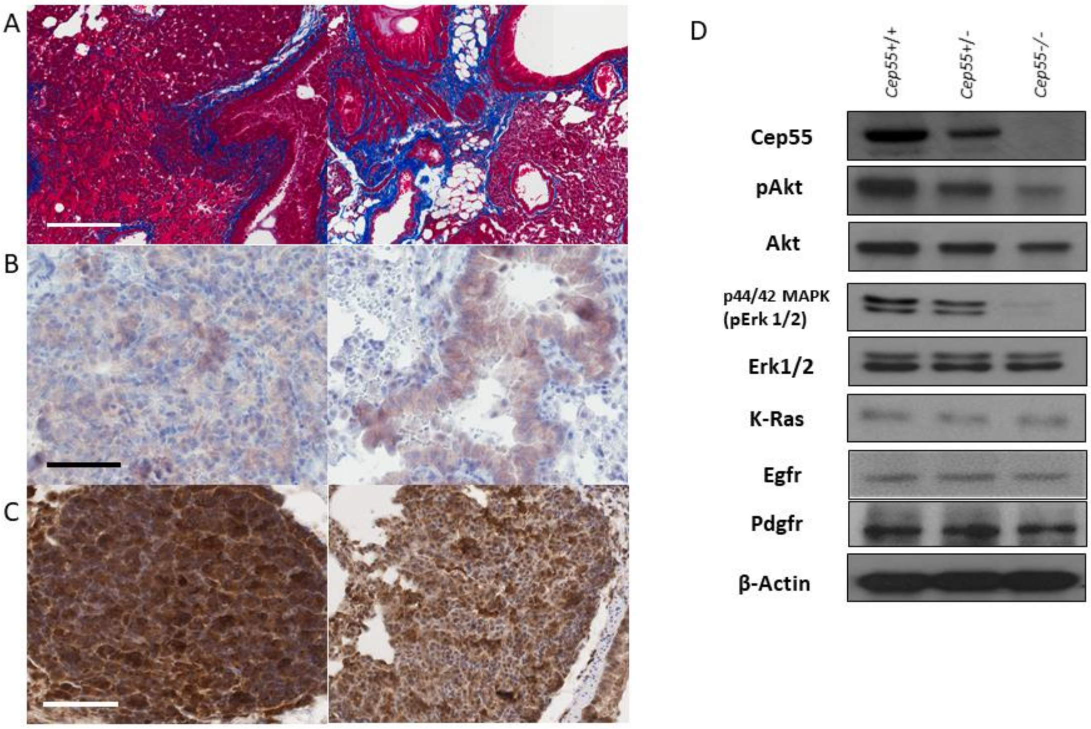

Figure 6.13 Tumor quantification and tumor burden in *Kras*-driven lung cancer

Representative images for staining of *Kras*$^{m/+}$ (left) and *Cep55-Kras*$^{m/+}$ (right), images are taken from central regions of tumors, Scale bar = 60 µm; (A) Masson trichrome: keratin (red), collagen (blue or green), cytoplasm (light red or pink), and cell nuclei (dark brown); (B) pAkt Ser473; (C) Phospho-p44/42 MAPK (Erk1/2) (Thr202/Tyr204); (D) Immunoblot analysis of *Cep55*+/+, *Cep55*+/-, and *Cep55*-/- MEFs. Actin served as a loading control.

In conclusion, these results demonstrate that *Cep55* can reduce tumorigenesis in a *Kras* mutant tumor prone model, likely due to its role in *Akt* and *Erk* signaling. Although *Cep55* loss could not prevent tumor development in the *Pten* knockout or *Kras G12D* model, it did significantly delay tumor development and alter its progression in both tumor- prone mouse models (Fig. 6.14)

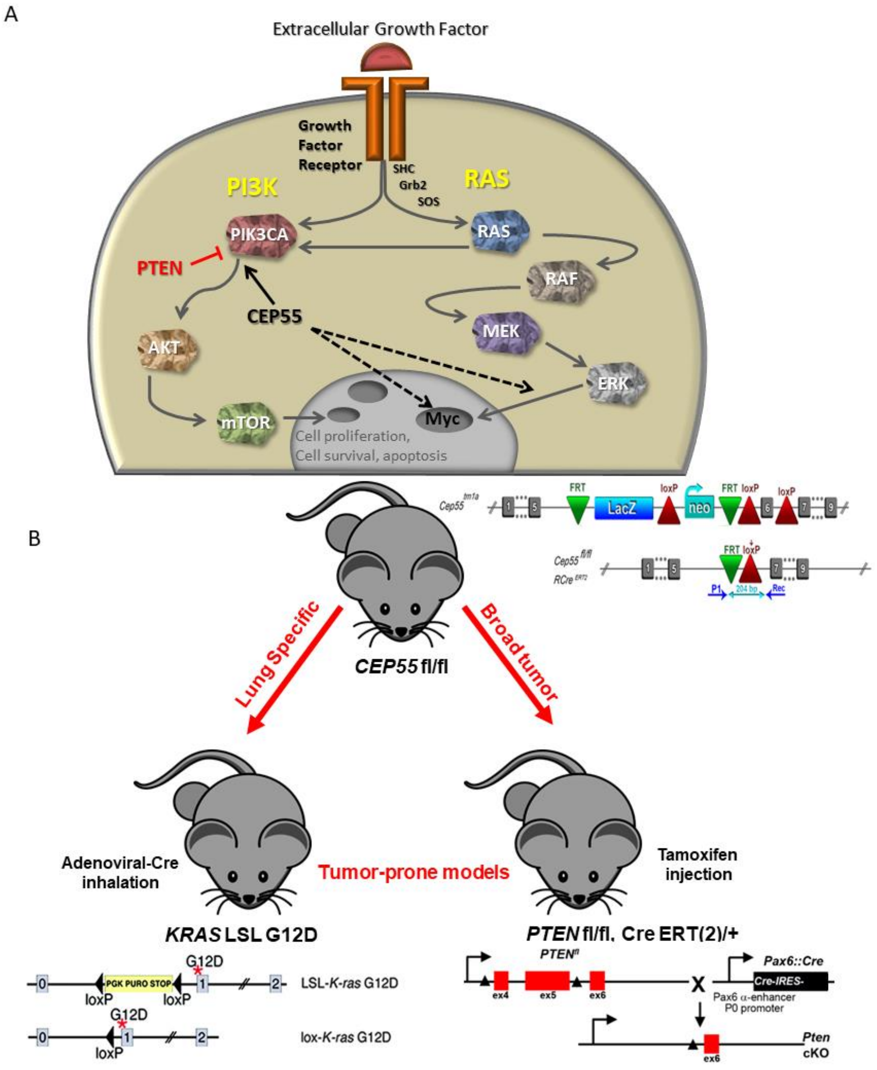
A
Extracellular Growth Factor
Growth Factor Receptor
SHC
Grb2
SOS
PI3K
RAS
PIK3CA
RAS
PTEN
RAF
CEP55
MEK
AKT
ERK
mTOR
Myc
Cell proliferation,
Cell survival, apoptosis
B
Cep55 tm1a
FRT
LacZ
loxP
neo
FRT
loxP
loxP
Cep55 fl/fl
RCre ERT2
FRT
loxP
P1
204 bp
Rec
CEP55 fl/fl
Lung Specific
Broad tumor
Adenoviral-Cre inhalation
Tumor-prone models
Tamoxifen injection
KRAS LSL G12D
PTEN fl/fl, Cre ERT(2)/+
G12D
PGK PURO STOP
loxP
loxP
LSL-K-ras G12D
G12D
loxP
lox-K-ras G12D
PTEN fl
ex4
ex5
ex6
Pax6::Cre
Cre-IRES-
Pax6 α-enhancer
P0 promoter
ex6
Pten cKO

Figure 6.14 Schematic model of Cep55 modulation of tumorigenesis.

(A) The diagram shows *Cep55* involvement in the PI3K/AKT - Ras pathways; (B) Schematic of *Cep55* tumor prone models.

6.3 Discussion

Overexpression of *CEP55* has been linked to tumorigenesis across multiple cancers, including T-cell lymphoma, breast, lung, colorectal cancer and hepatocellular carcinoma (Inoda *et al.*, 2009, 2011; Waseem *et al.*, 2010; Tao *et al.*, 2014; Singh *et al.*, 2015; Xu *et al.*, 2018). Mechanistically, CEP55 stabilizes p110, the catalytic subunit of PIK3CA, and promotes *AKT* signaling activation (Jeffery *et al.*, 2016). To have a better understanding of the functional roles of *Cep55* in tumorigenesis and the mechanisms by which tumors may rely upon *Cep55* for survival and proliferation, we generated a novel *Cep55* conditional KO mouse model.

Initially, we used MEFs as an *in vitro* model system to evaluate the structural and functional differences between *Cep55*$^{+/+}$ and *Cep55*$^{-/-}$. As primary MEFs are neither immortalized nor transformed, we utilized oncogenic *Ras* together with Adenoviral E1A to bypass senescence and to transform *Cep55*$^{+/+}$ and *Cep55*$^{-/-}$ MEFs. We found that *Cep55*$^{-/-}$E1A/Ras MEFs exhibited lower tumorigenic potential compared to their *Cep55*$^{+/+}$E1A/Ras counterparts, as evidenced by proliferation defects and clonogenic deficiency in 2D and 3D cultures. Next, we examined the tumorigenicity of these lines in a xenograft model. The results demonstrated delayed tumor progression in NOD/SCID mice injected with the *Cep55*$^{-/-}$E1A/Ras line compared to *Cep55*$^{+/+}$E1A/Ras. Then, based on cancer genomics analysis, we selected *Pten* and *Kras* tumor prone models to further study the contribution of *Cep55* loss to tumorigenic potential in these genetically engineered models.

Pten is a well-documented tumor suppressor gene, and the tumorigenesis events which occur due to its loss of function have been extensively characterized. The aim of this chapter was to evaluate how the loss of *Cep55* may impact tumor latency or tumor incidence. We utilized the previously described *Pten*$^{\mathrm{Fl/Fl}}$ tumor-prone model. This system was previously used in combination with *Rosa26*CreER(T) to examine the effects of ubiquitous, conditional *Pten* loss. In this analysis, six-week-old *ROSA26* Cre ER(T); *Pten*$^{\mathrm{Fl/Fl}}$ mice were injected three times with 100 micrograms of tamoxifen. The results revealed the development of various gender-biased malignancies. Mainly, these malignancies included lymphoma (40.0% in males, 76.9% in females), prostate (20.0% in males), endometrial cancer (46.1%), intestinal cancer (35.0 % in males) and squamous cell carcinoma (10.0% in males, 15.4% in females). While the tumor mean latency in female *Pten*-deficient mice was 10–11 weeks, in mutant males, the malignancies developed more slowly with an on average of 21 weeks, and the overall tumor mean latency for both genders was 17 weeks. These report also found high tumor susceptibility in lymphoid organs, the epithelium of the prostate, endometrium, intestine, and epidermis (Lu *et al.*, 2007). In our experimental design, I used a single 3 mg dose of Tamoxifen, a dose that we have previously utilized for recombination (Shi *et al.*, 2013). However, our data revealed an acceleration in tumorigenesis, decreasing the average of survival to 10 weeks and overall tumor mean latency to four weeks post tamoxifen injection. Interestingly, *Cep55* loss was able to increase this latency significantly in line with our hypothesis. The differences between our observations and those of Lu et al. could be due to several factors. One is that there are subtle differences between the CreERT and CreERT2 systems, and recombination may be more efficient in the CreERT2 system (Feil et al., 2009). Other possibilities are that differences in the mouse strain background, tamoxifen dosing or animal house environment have contributed to these differences.

The wide tumor spectrum and rapid tumor development of the *Pten* deficient mouse model using Cre ERT2 system was a limitation of this study, as it caused difficulty in determining the mechanism through which *Cep55* loss can delay *Pten* deficient tumorigenesis. As the dominant malignancy and the most probable cause of lethality, according to the literature, was lymphoma, we concentrated on this neoplasm for further analysis. However, the spectrum of additional tumors across multiple organs in the *Pten*-deficient mouse model has added complexity to our analyses. However, this investigation provides a valuable understanding towards the advantages of overall targeting of *Cep55* in *Pten*-deficient cancers across multiple tissue lineages and cells as a potential pre-clinical model.

In addition to ubiquitous *Pten* deletion, several other model systems have investigated the effects of Pten loss using tissue-specific Cre systems. Conditional *Pten* loss using transgenic mice with a Cre under the control of the keratin 5(k5Cre) induced hyperplasia of both skin and esophageal squamous epithelium (Suzuki *et al.*, 2003). One of the earliest symptoms frequently reported after *Pten* loss or mutation is hamartomatous lesions, such as oral papillomatosis, trichilemmomas, and cutaneous keratoses associated with Cowden syndrome (Pilarski *et al.*, 2013). Meanwhile, dominant cancer in constitutive *Pten* heterozygous mice was lymphoid hyperplasia, Suzuki *et al.*, and others, showed conditional T-cell specific *Pten* depletion using Lck Cre leads to T-cell lymphoma, splenomegaly, enlarged thymus as well as increased proliferation and decreased apoptosis (Suzuki *et al.*, 2001; Hagenbeek *et al.*, 2004; Hagenbeek and Spits, 2008). In Lck *Pten*$^{fl/-}$ mice, lymphadenopathy, splenomegaly, and an enlarged thymus were observed at 6–8 weeks of age, followed by tumor formation from 10 weeks. All mice reached the end-stage of T-cell lymphoma by week 17.

Regarding the phenotype and tumor spectrum of *Pten* and *Cep55/Pten* models, we found splenomegaly with a 3-fold enlargement of the spleen in Cep55/Pten and a 2-fold enlargement in *Pten* alone. Thymic and splenic lymphoma were the dominant malignancies followed by other pathologic lesions such as extramedullary hematopoiesis, squamous papilloma, hemangioendothelioma (sarcoma), prostatic hyperplasia and hematoma. Detailed analysis of the tumor spectrum requires a tissue-by-tissue inquiry to find the exact percentage of each neoplasm across all organs. However, this was not the aim of our preliminary analysis, and we therefore solely focused on the comparison of lymphoma in lymphoid organs.

To investigate the contribution of *Cep55* to tumorigenic potential in *Kras*-mutant-driven lung tumors, for the second model system, we utilized the *Kras G12D LSL* system.

DuPage *et al.,* who developed the inoculation technique to deliver Cre virus to the lung, revealed that the median survival of Ad Cre activated *Kras G12D LSL* mice was 185 days, and these mice can have the presence of more than 200 tumors in their lungs. They also categorized the tumorigenesis of this mouse model into three grades. The first grade, which can appear as early as two weeks of post-viral infection, is classified by atypical adenomatous hyperplasia (AAH) lesions that feature uniform nuclei. After about six weeks post-inoculation, the lesions become visible on the surface of the lung and tumors turn into grade 2 where the larger adenomas, with slightly enlarged nuclei with prominent nucleoli, can be observed. The well-differentiated cellular atypia and nuclear pleomorphism in adenocarcinomas are classified as grade 3, which is the final stage of disease in this mouse model. However, in *Kras* coupled with *p53* mutation, the invasive adenocarcinomas form grade 4 of disease, with metastatic features appearing after 18 weeks and invasion of lung adenocarcinoma to bordering lymphatic vessels, blood vessels, or the pleura cavity. The distant metastases then can be observed in the liver or the kidneys after 20 weeks post-infection in some mice (DuPage, Dooley and Jacks, 2009).

Our data suggest that *Cep55* can decrease the size or number of tumors, tumor incidence, and tumor latency; however, it cannot change the lung tumor spectrum. At eight weeks post-inoculation, both groups of $Kras^{G12D/+}$ and $Cep55^{-/-}$;$Kras^{G12D/+}$ formed early carcinoma with higher proportion and numbers in $Kras^{G12D/+}$ compared to $Cep55^{-/-}$, $Kras^{G12D/+}$.

Activation of *Kras* results in hyperactivity of downstream *PI3K/AKT,* however inhibition of *AKT* in the clinic has thus far been inadequate for treatment of KRAS-mutant, and tumor progression due to various alternative activated downstream pathways (Ihle *et al.*, 2009; Dan *et al.*, 2010). Although our data suggest that *Cep55* can downregulate pErk1/2 as evidenced by IHC staining and validated by WB, it will be important to investigate the effects that Cep55 has on this pathway in more detail to better understand the additional mechanism by which it may increase tumor latency.

Kim *et al.*, using a multi-genomic, data-driven approach, suggested that the nuclear transport machinery (NTM) was the only cellular process that can be targeted in a cell-independent addiction of *KRAS*-mutant of NSCLC. Synthetic-lethal interactions of oncogenic addicted NTM components, which are selectively essential for the survival of KRAS-mutant cells, were revealed to be robust in targeting cancer cells and displayed unexpected resistance mechanisms. These results propose that variations in the subcellular localization of NTM components could promote KRAS mutant oncogenic growth. Consequently, components of the NTM, such as activate nuclear factor-κB (NF-κB) and Yes-associated protein (YAP), could be promising targets for the treatment of KRAS-mutant cancers (Cully, 2016; Kim *et al.*, 2016). Multiple transport signals, adaptors, and receptors mediate the transport of cargo proteins, which interact with components of the nuclear pore complex (NPC) and with the Ras family GTPase Ran (Cautain *et al.*, 2015). *CEP55* engages the endosomal sorting complex required for transport machinery (ESCRT) in cellular procedures, and it plays a role in protein cargo trafficking, especially by interacting with asparagine-linked glycosylation 2–interacting X (ALIX) and tumor susceptibility gene 101 (TSG101)(Lee *et al.*, 2008). Furthermore, *CEP55* upregulation via an unknown mechanism increases the activity of NF-κB which is an NTM component. Interestingly, inhibition of the NF-κB signaling also suppresses the *CEP55*-induced aggressiveness in pancreatic cancer cells (Peng *et al.*, 2017). The emerging, direct or mediated roles of *CEP55* in protein trafficking and related signaling suggests another complementary mechanism that justifies *CEP55's* contribution to tumorigenesis. This aspect of functional cellular interplay of *CEP55* and how it can regulate protein trafficking adds another dimension to this target that requires further investigation.

Chapter 7. General discussion and future direction

7.1 General Discussion

CEP55 was initially described as an abscission component serving to regulate cellular segregation during cytokinesis. Later, the finding of a regulatory role for *CEP55* in *PI3K/AKT* survival signaling illustrated the importance of this gene, especially in cancer where *CEP55* overexpression widely contributes to its progression (Jeffery *et al.*, 2015). Recently, three reports linked homozygous *CEP55* mutations that truncate the protein to lethal fetal syndromes, demonstrating the importance of *CEP55* in embryogenesis and especially in neuronal development (Bondeson *et al.*, 2017; Frosk *et al.*, 2017; Rawlins *et al.*, 2019). However, to date, the exact molecular mechanism underlying these disorders has remained elusive. Our *Cep55*$^{-/-}$ mouse model, which is the first such model to our knowledge, sheds light on the pathophysiological role of *Cep55*. The lethal phenotypes observed in these mice, including the forebrain and hindbrain abnormalities and overall lack of proper cerebral development, show significant overlap with the human disorders. Furthermore, multinucleation of neurons was a key observation in the report of CEP55-associated MARCH syndrome (Frosk *et al.*, 2017). Similar to this study, we also observed a higher proportion of multinucleated neurons in E14.5 *Cep55*$^{-/-}$ brains when compared to controls. Moreover, a significant proportion of MEFs exhibited multinucleation upon both constitutive and conditional loss of *Cep55*.

To evaluate neurodevelopmental defects upon loss of *Cep55*, in this study we have concentrated on the development of the neocortex. Corticogenesis is a consequence of three successive phases including neurogenesis, neural morphogenesis and synaptogenesis (Hur and Zhou, 2012). Neurogenesis is typically dependent upon synchronized proliferation and lineage-specific differentiation events, while asymmetric and symmetric cell division, as well as migration, contribute mostly to morphogenesis

(Dwyer *et al.*, 2016). Neurogenesis investigations have revealed that a decrease in the population of the neurons is responsible for a decline in the thickness of the cortex and consequent defects in corticogenesis. Various cell cycle regulators and related signaling facilitate cell division to delaminate different NP layers and subsequently mature neurons to control the overall brain size (Hur and Zhou, 2010). The brain size of *Cep55*-deficient embryos was significantly reduced compared to control due to hypocellularity. Analysis of the overall distribution of neurons across the neocortex revealed a decreased population of neuroprogenitors and neurons in *Cep55*$^{-/-}$ brains including RGCs, IPCs, and PMNs. Deficiency in proliferation of *Cep55*$^{-/-}$ brain cells, as well as the significant increase of apoptosis in both NPs and PMNs, are likely to be due to the pro-survival role of Akt where its activation is significantly compromised in *Cep55*$^{-/-}$ brain cells. This finding is in line with the time-lapse data showing that cell death is not due to mitotic catastrophe because of aberrant cytokinesis but that cells are mainly dying during interphase. However, differentiation and cell migration are cellular events that require more investigation to be characterized.

Our data focused on the proliferation defects associated with loss of Cep55 in both E14.5 embryonic brains by Ki67 quantitation as well as *in vitro* in MEF models with both constitutive and conditional Cep55 loss. This proliferation defect could be rescued in *Cep55*$^{-/-}$ MEFs by ectopic expression of *Cep55*. We also observed increased levels of cleaved caspase-3, a marker of apoptotic cell death by WB in *Cep55*$^{-/-}$ E14.5 embryonic brain tissue consistent with increased apoptosis as assessed by TUNEL staining of brain sections by IHC. However, in MEFs, the induction of apoptosis was negligible, likely due to SV40-mediated immortalization. Nevertheless, primary *Cep55*$^{-/-}$ MEFs could not immortalize spontaneously unlike the *Cep55*$^{+/+}$ and *Cep55*$^{+/-}$ MEFs which may be indicative of an important role for *Cep55* in mediating cellular survival.

To further define the molecular mechanisms underpinning the morphological defects of *Cep55*$^{-/-}$ embryos, we assessed for defects in cell signaling during embryogenesis. We confirmed a requirement for Cep55 in activation of the PI3K/AKT pathway which has previously been shown to play a key role in the regulation of stem (progenitor) cells by promoting β-catenin activity (Jason and Cui, 2016). One of the most important signaling sensors during neurogenesis is *Glycogen Synthase Kinase-3β* (*GSK3β*) which is implicated as a master regulator of NPs (Kim *et al.*, 2009). Remarkably, *GSK3β* is an important mediator of wide range of processes in neurodevelopment including neurogenesis, neurotransmission and synapse formation (Cole, 2012), axon outgrowth and neuronal polarization (Hur and Zhou, 2012). This gene is also associated with modulating microtubule dynamics through regulating multiple microtubule-associated proteins (Goold, Owen and Gordon-Weeks, 1999). *GSK3β* controls levels of its downstream targets including *N-Myc* (Colon *et al.*, 2011), *Myc* (Gregory, Qi and Hann, 2003) and β-catenin (Sineva and Pospelov, 2014) by promoting protein degradation through the ubiquitination proteasome pathway (Moberg, et al 2004;Welcker et al., 2003). *GSK3β* is a key bifunctional effector downstream of both Akt and Wnt pathways and plays a critical role in crosstalk of these pathways. Altogether, *GSK3*β acts as a central regulator during neurodevelopment to switch between important signaling pathways to regulate neural progenitors primarily through Myc and β-catenin levels. Our data suggest that *Gsk3*β is activated and its effectors Myc and β-catenin are downregulated following *Cep55* loss due to a reduction in levels of phospho-Akt (active form of Akt).

In this thesis, we were able to partially rescue the ciliogenesis and proliferation defects of *Cep55* loss with the expression of an active form of Akt, myristoylated-Akt. Although the mechanism by which *AKT* regulates cilia formation or function remains poorly defined, at least one report has shown phospho-AKT to localize to the basal body (Suizu *et al.*, 2016). Interestingly, however, inhibition of GSK3β was only able to partially rescue the proliferation, but not the ciliogenesis defect. These data are interesting, as they suggest that the effect of *Cep55* on promoting ciliogenesis occurs through *Akt* but not through its major effector Gsk3β. It is possible that this effect is therefore mediated via cross-talk with another signaling pathway in parallel or upstream of Gsk3β. It is, however, important to note that these rescue experiments were only done in MEFs, and maybe cell-line specific effects. It will, therefore, be interesting to evaluate the effects of *Gsk3β* inhibition or expression of active *Akt in vivo*. To do this, embryonic electroporation or cortical organoid culture could serve as model systems to investigate these effects following loss of *Cep55* on neuronal development and cortical neurogenesis.

PI3-Kinase/Akt signaling has been shown to play a key role in the regulation of stem (progenitor) cells by promoting β-catenin activity. β-catenin also acts downstream of the PI3K/AKT and Wnt signaling pathways. Wnt is a vital conserved gene involved across multiple signaling pathways identified in embryonic development as well as carcinogenesis (Nusse *et al.*, 1991). Elevated β-catenin expression is linked to poor prognosis in BC patients especially through epithelial-mesenchymal transition (EMT)-related metastasis (DiMeo *et al.*, 2009). Moreover, β-catenin dysregulation is implicated across multiple malignancies including melanoma, glioblastoma, colorectal, prostate, lung, oesophageal, and ovarian cancers (Anastas and Moon, 2013). These findings show the importance of β-catenin dysregulation in the cancer setting. Our data confirm that hyperactive *Gsk3*β that suppressed β-catenin/Myc levels in an *in vitro* model of *Cep55* loss might be a mechanism that led to reduced colony formation, anchorage-independent growth in 3D culture and a delay in formation of xenograft tumors of EIA/RAS transformed *Cep55*-knockout MEFs compared to control MEFs.

Previously, our laboratory showed that knock-down of *CEP55* in TNBC lines hinders cell proliferation, colony formation and tumor-forming capability in athymic nude mice in a dose-dependent manner (Kalimutho *et al.*, 2018). This study reported no tumor formation in mice when *CEP55* was depleted in these cells. In contrast, in this thesis, we showed that although *Cep55* loss is unable to prevent tumorigenesis in NOD/SCID mice injected with E1A/Ras-transformed *Cep55*$^{-/-}$ MEFs, tumorigenesis can be impeded significantly in these lines. This delay in tumorigenesis was concomitant with increased necrosis and apoptosis in tumors, consistent with our previous report on activation of cell death pathways in the tumorigenesis of *CEP55*-depleted cells (Kalimutho *et al.*, 2018).

In this thesis, we also sought to determine whether tumorigenesis could be delayed upon *Cep55* loss in tumor prone models by investigation of *Pten* and *Ras*-driven tumors. This data showed that inhibition of *Cep55* might be a promising target for a wide range of cancer including *Pten* and *Ras*-driven cancers. The ability of loss of *Cep55* to delay *Ras*-driven tumorigenesis is interesting, as it may indicate a regulatory ability of *Cep55* beyond its effects on the PI3K/AKT pathway as *RAS* can promote RAF/MEK/ERK signaling independent of AKT. Our data in MEFs and tumors showing that *Cep55* loss is associated with downregulation of pErk1/2 is another interesting regulatory mechanism requiring further investigations.

7.2 Conclusions and Future Directions

In this thesis, we have provided a comprehensive characterization of the first KO model of *Cep55*. We showed that *Cep55* is essential for embryonic viability, corticogenesis and showed for the first time that *Cep55* localizes in the vicinity of basal body of the cilium and regulates its growth. Moreover, we demonstrated that loss of *Cep55* using a conditional mouse model is able to impede tumor growth in a cell-line-derived xenograft as well as in tumor-prone *Pten*-deficient and *Ras*-mutant mouse models.

The novel role of *Cep55* in neurogenesis requires further characterization to shed light on the exact molecular mechanisms perturbed. It will also be interesting to determine its involvement in the development of other regions of the brain such as the cerebellum, as well as specific neural populations like glia and to further understand its role in neural migration in a more cell-autonomous manner. To achieve this, we would utilize a conditional Cre system such as Nestin-Cre which is expressed in the central and peripheral nervous system, including neuronal and glial cell precursors. Moreover, it will be of interest to further determine the role of *Cep55* in regulation of ciliogenesis, and extend our mechanistic studies to characterizing the potential roles of *Cep55* in localization and expression of intraflagellar transport (IFT) components and interactions with other proteins of the basal body.

We found that the mouse model of *Cep55* phenocopies some of the symptoms of human genetic syndromes caused by loss of function of *CEP55*. Our *in vitro* data confirmed that downstream pathways such as Akt activation or *Gsk3β* inhibition could partially rescue the cellular defects in ciliogenesis and signaling. However, to further understand whether this rescue can occur in a physiological setting, it would be useful to test in another model system such as cortical organoid culture to investigate whether these down-stream targets can compensate the phenotypes of *Cep55* depletion. The validation of this hypothesis may lead to the development of therapeutics such as *Gsk3β* inhibitors against the neurodegenerative/ciliopathic syndromes caused by loss of *Cep55* for preclinical studies.

Our studies in this thesis have demonstrated that *Cep55* may be a suitable cancer target. Unfortunately, due to the coiled-coil nature of CEP55, targeting this protein is difficult (Cox *et al.,* 2014; Whitfield, Beaulieu and Soucek, 2017). Alternative approaches to target CEP55 will, therefore, be required if this protein is to be investigated as a therapeutic option. Targeting will require innovative approaches beyond classic strategies such as using small molecule inhibitors. One new therapeutic strategy relies on induction of protein degradation with heterofunctional molecules to degrade the protein of interest (Miyata, Nakamoto and Neckers, 2013). Based on this strategy, the proteolysis targeting chimera (PROTAC), a small molecule inducing selective intracellular proteolysis of their targets has been developed (DeMars *et al.*, 2018; Zoppi *et al.*, 2018; Han *et al.*, 2019; Zhao *et al.*, 2019). PROTAC has two domains for binding to the target protein and the E3 ubiquitin ligase which results in ubiquitination and subsequently proteasomal degradation of the target. This targeting strategy can be applicable to CEP55 as the exact sequence in its partner proteins (TSG101 and ALIX) required for CEP55 binding has been mapped at peptide level and this peptide can be used as CEP55 recruiting ligand (Lee *et al.*, 2008).

Finally, we are interested to better understand the role of *Cep55* at the molecular level. We have recently performed detailed proteomics analysis of total protein, phosphoprotein and exosome vesicles from *Cep55* knockout compared to wild-type MEFs but detailed analysis and characterization were not within the scope of this thesis. These analyses will hopefully shed light upon novels ways to target *Cep55* in tumorigenesis.

References

Abdelhamed, Z. A. *et al.* (2013) 'Variable expressivity of ciliopathy neurological phenotypes that encompass Meckel–Gruber syndrome and Joubert syndrome is caused by complex de-regulated ciliogenesis, Shh and Wnt signalling defects', *Human Molecular Genetics*, 22(7), pp. 1358–1372. doi: 10.1093/hmg/dds546.

Adams, M. *et al.* (2008) 'Recent advances in the molecular pathology, cell biology and genetics of ciliopathies', *Journal of Medical Genetics*, 45(5), pp. 257–267. doi: 10.1136/jmg.2007.054999.

Addi, C., Bai, J. and Echard, A. (2018) 'Actin, microtubule, septin and ESCRT filament remodeling during late steps of cytokinesis', *Current opinion in cell biology*. Elsevier, 50, pp. 27–34.

Al-Ejeh, F. *et al.* (2014a) 'Kinome profiling reveals breast cancer heterogeneity and identifies targeted therapeutic opportunities for triple negative breast cancer', *Oncotarget*. Impact Journals LLC, 5(10), pp. 3145–3158. doi: 10.18632/oncotarget.1865.

Al-Ejeh, F. *et al.* (2014b) 'Kinome profiling reveals breast cancer heterogeneity and identifies targeted therapeutic opportunities for triple negative breast cancer', *Oncotarget*. Impact Journals LLC, 5(10), pp. 3145–3158. doi: 10.18632/oncotarget.1865.

Alizadeh, A. A. (2000) 'Web Document 11.4. Two-way clustering of microarray gene expression data. Two-way clustering of both genes and samples is used to define patterns of genes that are expressed across a variety of samples. A dramatic example is provided by Alizadeh et al.(20', *Nature,* 403, pp. 503–511.

Arellano, J. I. *et al.* (2012) 'Development and distribution of neuronal cilia in mouse neocortex', *Journal of Comparative Neurology*. Wiley Online Library, 520(4), pp. 848–873.

Ashkenazi, A. and Dixit, V. M. (1999) 'Apoptosis control by death and decoy receptors', *Current opinion in cell biology*. Elsevier, 11(2), pp. 255–260.

AU - Borowicz, S. *et al.* (2014) 'The Soft Agar Colony Formation Assay', *JoVE*. MyJoVE Corp, (92), p. e51998. doi: doi:10.3791/51998.

Avidor-Reiss, T. and Gopalakrishnan, J. (2013) 'Cell Cycle Regulation of the Centrosome and Cilium', *Drug discovery today. Disease mechanisms*, 10(3–4), pp. e119–e124. doi: 10.1016/j.ddmec.2013.03.002.

Azmi, A. S., Bao, B. and Sarkar, F. H. (2013) 'Exosomes in cancer development, metastasis, and drug resistance: a comprehensive review', *Cancer and Metastasis Reviews*. Springer, 32(3–4), pp. 623–642.

Backman, S. A. *et al.* (2001) 'Deletion of Pten in mouse brain causes seizures, ataxia and defects in soma size resembling Lhermitte-Duclos disease', *Nature genetics*. Nature Publishing Group, 29(4), p. 396.

Badano, J. L., Teslovich, T. M. and Katsanis, N. (2005a) 'The centrosome in human genetic disease', *Nature Reviews Genetics*, 6(3), pp. 194–205. doi: 10.1038/nrg1557.

Badano, J. L., Teslovich, T. M. and Katsanis, N. (2005b) 'The centrosome in human genetic disease', *Nature Reviews Genetics*, 6(3), pp. 194–205. doi: 10.1038/nrg1557.

Bahrami, A. *et al.* (2018) 'The therapeutic potential of PI3K/Akt/mTOR inhibitors in breast cancer: rational and progress', *Journal of cellular biochemistry*. Wiley Online Library, 119(1), pp. 213–222.

Ballew, O. and Lacefield, S. (2019) 'The DNA damage checkpoint and the spindle position checkpoint: guardians of meiotic commitment', *Current genetics*. Springer, pp. 1–6.

Barr, F. A. and Gruneberg, U. (2007) 'Cytokinesis: placing and making the final cut', *Cell*. Elsevier, 131(5), pp. 847–860.

Bartkova, J. *et al.* (2005) 'DNA damage response as a candidate anti-cancer barrier in early human tumorigenesis', *Nature*. Nature Publishing Group, 434(7035), pp. 864–870.

Baserga, R. (1968) 'Biochemistry of the cell cycle: a review', *Cell proliferation*. Wiley Online Library, 1(2), pp. 167–191.

Bastos, R. N. and Barr, F. A. (2010) 'Plk1 negatively regulates Cep55 recruitment to the midbody to ensure orderly abscission', *The Journal of cell biology*. The Rockefeller University Press, 191(4), pp. 751–760. doi: 10.1083/jcb.201008108.

Bendon, R. W. *et al.* (1987) 'Recurrent developmental anomalies: 1. Syndrome of hydranencephaly with renal aplastic dysplasia; 2. Polyvalvular developmental heart defect', *American journal of medical genetics*. Wiley Online Library, 28(S3), pp. 357–365.

Berns, K. *et al.* (2007) 'A functional genetic approach identifies the PI3K pathway as a major determinant of trastuzumab resistance in breast cancer', *Cancer cell*. Elsevier, 12(4), pp. 395–402.

Bhat, M. *et al.* (2015) 'Targeting the translation machinery in cancer', *Nature reviews Drug discovery*. Nature Publishing Group, 14(4), p. 261.

Binarová, P. *et al.* (2006) 'γ-Tubulin Is Essential for Acentrosomal Microtubule Nucleation and Coordination of Late Mitotic Events in Arabidopsis ', *The Plant Cell* . ROCKVILLE : American Society of Plant Biologists , pp. 1199–1212. doi: 10.1105/tpc.105.038364.

Bischoff, J. R. *et al.* (1998) 'A homologue of Drosophila aurora kinase is oncogenic and amplified in human colorectal cancers', *The EMBO journal*. EMBO Press, 17(11), pp. 3052–3065.

Bodine, S. C. *et al.* (2001) 'Akt/mTOR pathway is a crucial regulator of skeletal muscle hypertrophy and can prevent muscle atrophy in vivo', *Nature cell biology*. Nature

Publishing Group, 3(11), p. 1014.

Bondeson, M. *et al.* (2017) ‘A nonsense mutation in CEP55 defines a new locus for a Meckel-like syndrome, an autosomal recessive lethal fetal ciliopathy’, *Clinical Genetics*. Wiley Online Library.

Bouck, N., Stellmach, V. and Hsu, S. C. (1996) ‘How tumors become angiogenic’, *Advances in cancer research*. Elsevier, 69, pp. 135–174.

Boulikas, T. (1995) ‘Phosphorylation of transcription factors and control of the cell cycle.’, *Critical reviews in eukaryotic gene expression*, 5(1), pp. 1–77.

Boward, B., Wu, T. and Dalton, S. (2016) ‘Concise review: control of cell fate through cell cycle and pluripotency networks’, *Stem cells*. Wiley Online Library, 34(6), pp. 1427–1436.

Braga, A. B. *et al.* (2012) ‘Comparison of static postural balance between healthy subjects and those with low back pain’, *Acta ortopedica brasileira*. Brazilian Society of Orthopedics and Traumatology, 20(4), p. 210.

Bray, F. *et al.* (2018) ‘Global cancer statistics 2018: GLOBOCAN estimates of incidence and mortality worldwide for 36 cancers in 185 countries’, *CA: a cancer journal for clinicians*. Wiley Online Library, 68(6), pp. 394–424.

Breslin, L. *et al.* (no date) ‘CEP128 Localizes to the Subdistal Appendages of the Mother Centriole and Regulates TGF-b/BMP Signaling at the Primary Cilium’.

Brooks, D. *et al.* (2018) ‘Limited fibrosis accompanies triple-negative breast cancer metastasis in multiple model systems and is not a preventive target’, *Oncotarget*. Impact Journals LLC, 9(34), pp. 23462–23481. doi: 10.18632/oncotarget.25231.

Brown, N. J. *et al.* (2013) ‘Cep63 and cep152 cooperate to ensure centriole duplication’, *PloS one*. Public Library of Science, 8(7), pp. e69986–e69986. doi: 10.1371/journal.pone.0069986.

Burn, S. F. (2012) ‘Detection of β-Galactosidase Activity: X-gal Staining BT - Kidney Development: Methods and Protocols’, in Michos, O. (ed.). Totowa, NJ: Humana Press, pp. 241–250. doi: 10.1007/978-1-61779-851-1_21.

Cahill, D. P. *et al.* (1998) ‘Mutations of mitotic checkpoint genes in human cancers’, *Nature*. Nature Publishing Group, 392(6673), pp. 300–303.

Campisi, J. *et al.* (1984) ‘Cell-cycle control of c-myc but not c-ras expression is lost following chemical transformation’, *Cell*. Elsevier, 36(2), pp. 241–247.

Cantley, L. C. (2002) ‘The phosphoinositide 3-kinase pathway’, *Science*. American Association for the Advancement of Science, 296(5573), pp. 1655–1657.

Cantley, L. C. and Neel, B. G. (1999) ‘New insights into tumor suppression: PTEN suppresses tumor formation by restraining the phosphoinositide 3-kinase/AKT pathway’, *Proceedings of the National Academy of Sciences*. National Acad Sciences, 96(8), pp. 4240–4245.

Carter, J. J. *et al.* (2006) ‘Perioperative immunomodulation with Flt3 kinase ligand or a whole tumor cell vaccine is associated with a reduction in lung metastasis formation after laparotomy in mice', *Surgical innovation*. Westminster Publications, Inc. 708 Glen Cove Avenue, Glen Head, NY 11545, USA, 13(1), pp. 41–47.

Cautain, B. *et al.* (2015) 'Components and regulation of nuclear transport processes', *The FEBS journal*. Wiley Online Library, 282(3), pp. 445–462.

Caviness Jr, V. S. (1982) 'Neocortical histogenesis in normal and reeler mice: a developmental study based upon [3H] thymidine autoradiography', *Developmental Brain Research*. Elsevier, 4(3), pp. 293–302.

Chan, K. T. *et al.* (2019) 'A functional genetic screen defines the AKT-induced senescence signaling network.', *Cell death and differentiation*.

Chang, Y.-C. *et al.* (2012) 'Centrosomal protein 55 (Cep55) stability is negatively regulated by p53 protein through Polo-like kinase 1 (Plk1)', *Journal of Biological Chemistry*. ASBMB, 287(6), pp. 4376–4385.

Chemudupati, M., Johns, M. and Osmani, S. A. (2019) 'The mode of mitosis is dramatically modified by deletion of a single nuclear pore complex gene in Aspergillus nidulans', *Fungal Genetics and Biology*. Elsevier, 130, pp. 72–81.

Chen, C.-H. *et al.* (2009) 'Expression of FLJ10540 is correlated with aggressiveness of oral cavity squamous cell carcinoma by stimulating cell migration and invasion through increased FOXM1 and MMP-2 activity', *Oncogene*. Nature Publishing Group, 28(30), p. 2723.

Chen, C.-H. (2010) 'Insulation displacement contact (IDC) and IDC mounting system'. Google Patents.

Chen, C. H. *et al.* (2007) 'FLJ10540-elicited cell transformation is through the activation of PI3-kinase/AKT pathway', *Oncogene*, 26(29), pp. 4272–4283. doi: 10.1038/sj.onc.1210207.

Chen, C. H. *et al.* (2009) 'VEGFA upregulates FLJ10540 and modulates migration and invasion of lung cancer via PI3K/AKT pathway', *PLoS ONE*, 4(4). doi: 10.1371/journal.pone.0005052.

Chen, C. H. *et al.* (2012) 'FLJ10540 is associated with tumor progression in nasopharyngeal carcinomas and contributes to nasopharyngeal cell proliferation, and metastasis via osteopontin/CD44 pathway', *Journal of Translational Medicine*, 10(1), pp. 1–16. doi: 10.1186/1479-5876-10-93.

Chen, J.-L., Chang, C.-H. and Tsai, J.-W. (2018) 'Gli2 rescues delays in brain development induced by Kif3a dysfunction', *Cerebral Cortex*. Oxford University Press, 29(2), pp. 751–764.

Chieffi, P. *et al.* (2006) 'Aurora B expression directly correlates with prostate cancer malignancy and influence prostate cell proliferation', *The Prostate*. Wiley Online Library, 66(3), pp. 326–333.

Chiodi, I. and Mondello, C. (2016) 'Telomere and telomerase stability in human diseases and cancer', *Front Biosci (Landmark Ed)*, 21, pp. 203–224.

Chu, G. *et al.* (1998) ‘Hydranencephaly with binucleate neurons-renal dysplasia-syndactyly syndrome in three siblings’, *Journal of Neuropathology and Experimental Neurology*, 57(5).

Clancy, B., Teague-Ross, T. J. and Nagarajan, R. (2009) ‘Cross-species analyses of the cortical GABAergic and subplate neural populations’, *Frontiers in neuroanatomy*. Frontiers Research Foundation, 3, p. 20. doi: 10.3389/neuro.05.020.2009.

Colak, D. *et al.* (2013) ‘Age-specific gene expression signatures for breast tumors and cross-species conserved potential cancer progression markers in young women’, *PloS one*. Public Library of Science, 8(5), p. e63204.

Cole, A. R. (2012) ‘GSK3 as a Sensor Determining Cell Fate in the Brain’, *Frontiers in Molecular Neuroscience*, 5(February), pp. 1–10. doi: 10.3389/fnmol.2012.00004.

Colman, H. *et al.* (2006) ‘Assessment and prognostic significance of mitotic index using the mitosis marker phospho-histone H3 in low and intermediate-grade infiltrating astrocytomas’, *The American journal of surgical pathology*. LWW, 30(5), pp. 657–664.

Colon, N. C. *et al.* (2011) ‘Aurora A kinase regulates N-myc activity through phosphorylation of GSK3-beta and beta-catenin’, *Journal of the American College of Surgeons*. Elsevier, 213(3), pp. S82–S83.

Conduit, S. E. *et al.* (2017) ‘A compartmentalized phosphoinositide signaling axis at cilia is regulated by INPP5E to maintain cilia and promote Sonic Hedgehog medulloblastoma’, *Oncogene*. Nature Publishing Group, 36(43), p. 5969.

Consortium, A. P. G. (2017) ‘AACR Project GENIE: powering precision medicine through an international consortium’, *Cancer discovery*. AACR, 7(8), pp. 818–831.

Cruz, L. *et al.* (2018) ‘Evidence of extracellular vesicles biogenesis and release in mouse embryonic stem cells’, *Stem Cell Reviews and Reports*. Springer, 14(2), pp. 262–276.

Cully, M. (2016) ‘Cancer: closing the door on KRAS-mutant lung cancer’, *Nature Reviews Drug Discovery*. Nature Publishing Group, 15(11), p. 747.

Cuzick, J. *et al.* (2012) ‘Prognostic value of a cell cycle progression signature for prostate cancer death in a conservatively managed needle biopsy cohort’, *British journal of cancer*. Nature Publishing Group, 106(6), p. 1095.

Cuzick, J. (2014) ‘Prognostic value of a cell cycle progression score for men with prostate cancer’, in *Prostate Cancer Prevention*. Springer, pp. 133–140.

D’Avino, P. P., Giansanti, M. G. and Petronczki, M. (2015) ‘Cytokinesis in animal cells’, *Cold Spring Harbor perspectives in biology*. Cold Spring Harbor Lab, 7(4), p. a015834.

Dan, S. *et al.* (2010) ‘Correlating phosphatidylinositol 3-kinase inhibitor efficacy with signaling pathway status: in silico and biological evaluations’, *Cancer research*. AACR, 70(12), pp. 4982–4994.

Datta, S. R. *et al.* (1997) ‘Akt phosphorylation of BAD couples survival signals to the cell-intrinsic death machinery’, *Cell*. Elsevier, 91(2), pp. 231–241.

Deeraksa, A. *et al.* (2013) ‘Plk1 is upregulated in androgen-insensitive prostate cancer cells and its inhibition leads to necroptosis’, *Oncogene*. Nature Publishing Group, 32(24), pp. 2973–2983.

Denko, N. C. *et al.* (1994) ‘The human Ha-ras oncogene induces genomic instability in murine fibroblasts within one cell cycle’, *Proceedings of the National Academy of Sciences*. National Acad Sciences, 91(11), pp. 5124–5128.

Dinsmore, C. J. and Soriano, P. (2018) ‘MAPK and PI3K signaling: At the crossroads of neural crest development’, *Developmental biology*. Elsevier.

Dobbelstein, M. and Moll, U. (2014) ‘Targeting tumour-supportive cellular machineries in anticancer drug development.’, *Nature reviews. Drug discovery*. Nature Publishing Group, 13(3), pp. 179–96. doi: 10.1038/nrd4201.

Dogan, S. *et al.* (2012) ‘Molecular epidemiology of EGFR and KRAS mutations in 3,026 lung adenocarcinomas: higher susceptibility of women to smoking-related KRAS-mutant cancers’, *Clinical cancer research*. AACR, 18(22), pp. 6169–6177.

DuPage, M., Dooley, A. L. and Jacks, T. (2009) ‘Conditional mouse lung cancer models using adenoviral or lentiviral delivery of Cre recombinase’, *Nature protocols*. Nature Publishing Group, 4(7), p. 1064.

Dupuy, L., Mackenzie, J. and Haseloff, J. (2010) ‘Coordination of plant cell division and expansion in a simple morphogenetic system’, *Proceedings of the National Academy of Sciences*. National Acad Sciences, 107(6), pp. 2711–2716.

Dymecki, S. M. (1996) ‘Flp recombinase promotes site-specific DNA recombination in embryonic stem cells and transgenic mice’, *Proceedings of the National Academy of Sciences*. National Acad Sciences, 93(12), pp. 6191–6196.

Eggert, U. S., Mitchison, T. J. and Field, C. M. (2006) ‘Animal cytokinesis: from parts list to mechanisms’, *Annu. Rev. Biochem.* Annual Reviews, 75, pp. 543–566.

Elmore, S. A. (2018) ‘Enhanced histopathology evaluation of lymphoid organs’, in *Immunotoxicity Testing*. Springer, pp. 147–168.

Elsum, I. A. *et al.* (2014) ‘Scrib heterozygosity predisposes to lung cancer and cooperates with KRas hyperactivation to accelerate lung cancer progression in vivo’, *Oncogene*. Nature Publishing Group, 33(48), p. 5523.

Eng, C. (2003) ‘PTEN: one gene, many syndromes’, *Human mutation*. Wiley Online Library, 22(3), pp. 183–198.

Engeland, K. (2018) ‘Cell cycle arrest through indirect transcriptional repression by p53: I have a DREAM’, *Cell death and differentiation*. Nature Publishing Group, 25(1), p. 114.

Engelman, J. A. *et al.* (2008) ‘Effective use of PI3K and MEK inhibitors to treat mutant Kras G12D and PIK3CA H1047R murine lung cancers’, *Nature medicine*. Nature Publishing Group, 14(12), p. 1351.

Englund, C. (2005) ‘Pax6, Tbr2, and Tbr1 Are Expressed Sequentially by Radial Glia, Intermediate Progenitor Cells, and Postmitotic Neurons in Developing Neocortex’, *Journal of Neuroscience*, 25(1), pp. 247–251. doi: 10.1523/JNEUROSCI.2899-04.2005.

Enomoto, H. *et al.* (2001) ‘RET signaling is essential for migration, axonal growth and axon guidance of developing sympathetic neurons’, *Development*. The Company of Biologists Ltd, 128(20), pp. 3963–3974.

Eppig, J. T. *et al.* (2015) ‘The Mouse Genome Database (MGD): facilitating mouse as a model for human biology and disease’, *Nucleic acids research*. 2014/10/27. Oxford University Press, 43(Database issue), pp. D726–D736. doi: 10.1093/nar/gku967.

Ettinger, A. W. *et al.* (2011) ‘Proliferating versus differentiating stem and cancer cells exhibit distinct midbody-release behaviour’, *Nature communications*. Nature Research, 2, p. 503.

Evan, G. and Littlewood, T. (1998) ‘A matter of life and cell death’, *Science*. American Association for the Advancement of Science, 281(5381), pp. 1317–1322.

Fabbro, M., Zhou, B. B., *et al.* (2005) ‘Cdk1/Erk2- and Plk1-dependent phosphorylation of a centrosome protein, Cep55, is required for its recruitment to midbody and cytokinesis’, *Developmental Cell*, 9(4), pp. 477–488. doi: 10.1016/j.devcel.2005.09.003.

Fabbro, M., Zhou, B.-B., *et al.* (2005) ‘Cdk1/Erk2-and Plk1-dependent phosphorylation of a centrosome protein, Cep55, is required for its recruitment to midbody and cytokinesis’, *Developmental cell*. Elsevier, 9(4), pp. 477–488.

Faes, S. and Dormond, O. (2015) ‘PI3K and AKT: Unfaithful partners in cancer’, *International journal of molecular sciences*. Multidisciplinary Digital Publishing Institute, 16(9), pp. 21138–21152.

Fagerberg, L. *et al.* (2014) ‘Analysis of the human tissue-specific expression by genome-wide integration of transcriptomics and antibody-based proteomics’, *Molecular & Cellular Proteomics*. ASBMB, 13(2), pp. 397–406.

Fang, S. *et al.* (2019) ‘Clinical significance and biological role of cancer-derived Type I collagen in lung and esophageal cancers’, *Thoracic cancer*. 2019/01/03. John Wiley & Sons Australia, Ltd, 10(2), pp. 277–288. doi: 10.1111/1759-7714.12947.

Feil, S., Valtcheva, N. and Feil, R. (2009) ‘Inducible cre mice’, in *Gene knockout protocols*. Springer, pp. 343–363.

Ferlay, J. *et al.* (2015) ‘Cancer incidence and mortality worldwide: sources, methods and major patterns in GLOBOCAN 2012’, *International journal of cancer*. Wiley Online Library, 136(5), pp. E359–E386.

Finlay, B. L. and Darlington, R. B. (1995) ‘Linked regularities in the development and evolution of mammalian brains’, *Science*. American Association for the Advancement of Science, 268(5217), pp. 1578–1584.

Firat-Karalar, E. N. *et al.* (2014) ‘Proximity interactions among centrosome components identify regulators of centriole duplication’, *Current Biology*. Elsevier, 24(6), pp. 664–670.

Flavahan, W. A., Gaskell, E. and Bernstein, B. E. (2017) ‘Epigenetic plasticity and the hallmarks of cancer', *Science*. American Association for the Advancement of Science, 357(6348), p. eaal2380.

Foerster, P. *et al.* (2017) 'mTORC1 signaling and primary cilia are required for brain ventricle morphogenesis', *Development*. Oxford University Press for The Company of Biologists Limited, 144(2), pp. 201–210.

Foon, K. A. (1986) 'Immunologic classification of leukemia and lymphoma', *Blood*. Am Soc Hematology, 68(1), pp. 1–31.

Forsythe, E. and Beales, P. L. (2013) 'Bardet-Biedl syndrome', *European journal of human genetics : EJHG*. 2012/06/20. Nature Publishing Group, 21(1), pp. 8–13. doi: 10.1038/ejhg.2012.115.

Franken, N. A. P. *et al.* (2006) 'Clonogenic assay of cells in vitro', *Nature protocols*. Nature Publishing Group, 1(5), p. 2315.

Fratta, E. *et al.* (2011) 'The biology of cancer testis antigens: putative function, regulation and therapeutic potential', *Molecular oncology*. Elsevier, 5(2), pp. 164–182.

Frosk, P. *et al.* (2017) 'A truncating mutation in CEP55 is the likely cause of MARCH, a novel syndrome affecting neuronal mitosis', *Journal of Medical Genetics*. BMJ Publishing Group Ltd, p. jmedgenet-2016.

FU, J. *et al.* (2006) 'Sonic hedgehog protein promotes bone marrow-derived endothelial progenitor cell proliferation, migration and VEGF production via PI 3-kinase/Akt signaling pathways 1', *Acta Pharmacologica Sinica*. Wiley Online Library, 27(6), pp. 685–693.

Fuchs, J. L. and Schwark, H. D. (2004) 'Neuronal primary cilia: a review', *Cell biology international*. Wiley Online Library, 28(2), pp. 111–118.

Gagan, J. and Van Allen, E. M. (2015) 'Next-generation sequencing to guide cancer therapy', *Genome medicine*. BioMed Central, 7(1), p. 80.

Ganem, N. J., Storchova, Z. and Pellman, D. (2007) 'Tetraploidy, aneuploidy and cancer', *Current opinion in genetics & development*. Elsevier, 17(2), pp. 157–162.

Garcez, P. P. *et al.* (2015) 'Cenpj/CPAP regulates progenitor divisions and neuronal migration in the cerebral cortex downstream of Ascl1', *Nature communications*. Nature Publishing Group, 6, p. 6474.

Gavande, N. S. *et al.* (2016) 'DNA repair targeted therapy: The past or future of cancer treatment?', *Pharmacology & therapeutics*. The Authors, 160, pp. 65–83. doi: 10.1016/j.pharmthera.2016.02.003.

Gemenetzidis, E. *et al.* (2009) 'FOXM1 upregulation is an early event in human squamous cell carcinoma and it is enhanced by nicotine during malignant transformation', *PloS one*. Public Library of Science, 4(3), p. e4849.

Gemma, A. *et al.* (2000) 'Somatic mutation of the hBUB1 mitotic checkpoint gene in primary lung cancer', *Genes, Chromosomes and Cancer*. Wiley Online Library, 29(3), pp. 213–218.

Ghosh, A., Ghartimagar, D. and Thapa, S. (2016) 'Oncogenes-the basics', *Journal of Biomedical Sciences*, 3(4), pp. 35–37.

Gil, E. M. C. (2014) 'Targeting the PI3K/AKT/mTOR pathway in estrogen receptor-positive breast cancer', *Cancer treatment reviews*. Elsevier, 40(7), pp. 862–871.

Goel, H. L. and Mercurio, A. M. (2013) 'VEGF targets the tumour cell', *Nature Reviews Cancer*. Nature Research, 13(12), pp. 871–882.

Grandage, V. L. *et al.* (2005) 'PI3-kinase/Akt is constitutively active in primary acute myeloid leukaemia cells and regulates survival and chemoresistance via NF-kB, MAPkinase and p53 pathways', *Leukemia*. Nature Publishing Group, 19(4), p. 586.

Greenberg, R. A. *et al.* (1999) 'Short dysfunctional telomeres impair tumorigenesis in the INK4a Δ2/3 cancer-prone mouse', *Cell*. Elsevier, 97(4), pp. 515–525.

Gregory, M. A., Qi, Y. and Hann, S. R. (2003) 'Phosphorylation by Glycogen Synthase Kinase-3 Controls c-Myc Proteolysis and Subnuclear Localization', *Journal of Biological Chemistry*, 278(51), pp. 51606–51612. doi: 10.1074/jbc.M310722200.

Gschwendtner, A. *et al.* (1997) 'Hydranencephaly with Renal Dysgenesis: A Coincidental Finding?', *Gynecologic and obstetric investigation*. Karger Publishers, 44(3), pp. 206–210.

Gu, T. *et al.* (2011) 'CREB is a novel nuclear target of PTEN phosphatase', *Cancer research*. AACR, 71(8), pp. 2821–2825.

Guo, B. B. *et al.* (2019) 'Platelets in myeloproliferative neoplasms have a distinct transcript signature in the presence of marrow fibrosis', *British journal of haematology*. Wiley Online Library.

Guo, J. *et al.* (2015) 'Developmental disruptions underlying brain abnormalities in ciliopathies', *Nature communications*. Nature Publishing Group, 6, p. 7857.

Hagenbeek, T. J. *et al.* (2004) 'The loss of PTEN allows TCR αβ lineage thymocytes to bypass IL-7 and Pre-TCR–mediated signaling', *Journal of Experimental Medicine*. Rockefeller University Press, 200(7), pp. 883–894.

Hagenbeek, T. J. and Spits, H. (2008) 'T-cell lymphomas in T-cell-specific Pten-deficient mice originate in the thymus', *Leukemia*. Nature Publishing Group, 22(3), p. 608.

Hahn, H. *et al.* (2000) 'Patched target Igf2 is indispensable for the formation of medulloblastoma and rhabdomyosarcoma', *Journal of Biological Chemistry*. ASBMB, 275(37), pp. 28341–28344.

Halazonetis, T. D., Gorgoulis, V. G. and Bartek, J. (2008) 'An oncogene-induced DNA damage model for cancer development', *science*. American Association for the Advancement of Science, 319(5868), pp. 1352–1355.

Hall, E. A. *et al.* (2013) 'Acute versus chronic loss of mammalian Azi1/Cep131 results in distinct ciliary phenotypes', *PLoS genetics*. Public Library of Science, 9(12), p. e1003928.

Hallinan, N. *et al.* (2016) ‘Targeting the fibroblast growth factor receptor family in cancer’, *Cancer treatment reviews*. Elsevier, 46, pp. 51–62.

Hamby, W. B., Krauss, R. F. and Beswick, W. F. (1950) ‘Hydranencephaly: clinical diagnosis: presentation of seven cases’, *Pediatrics*. Am Acad Pediatrics, 6(3), pp. 371–383.

Han, S. *et al.* (2000) ‘Clinical implication of altered expression of Mad1 protein in human breast carcinoma’, *Cancer*. Wiley Online Library, 88(7), pp. 1623–1632.

Han, Y.-G. *et al.* (2008) ‘Hedgehog signaling and primary cilia are required for the formation of adult neural stem cells’, *Nature Neuroscience*, 11(3), pp. 277–284. doi: 10.1038/nn2059.

Hanahan, D. and Weinberg, R. A. (2000) ‘The hallmarks of cancer’, *cell*. Elsevier, 100(1), pp. 57–70.

Hanahan, D. and Weinberg, R. A. (2011) ‘Hallmarks of cancer: the next generation’, *cell*. Elsevier, 144(5), pp. 646–674.

Hänggi, K. and Ruffell, B. (2019) ‘Oncogenic KRAS Drives Immune Suppression in Colorectal Cancer’, *Cancer cell*. Elsevier, 35(4), pp. 535–537.

Harley, C. B. (2008) ‘Telomerase and cancer therapeutics’, *Nature Reviews Cancer*. Nature Publishing Group, 8(3), p. 167.

Harris, L. *et al.* (2016) ‘Transcriptional regulation of intermediate progenitor cell generation during hippocampal development’, *Development (Cambridge, England)*. The Company of Biologists Ltd, 143(24), pp. 4620–4630. doi: 10.1242/dev.140681.

Hartill, V. *et al.* (2017) ‘Meckel–Gruber syndrome: An update on diagnosis, clinical management, and research advances’, *Frontiers in pediatrics*. Frontiers, 5, p. 244.

Hartwell, L. H. and Kastan, M. B. (1994) ‘Cell cycle control and cancer’, *Science*. The American Association for the Advancement of Science, 266(5192), p. 1821.

Heikaus, C. C., Pandit, J. and Klevit, R. E. (2009) ‘Cyclic nucleotide binding GAF domains from phosphodiesterases: structural and mechanistic insights’, *Structure*. Elsevier, 17(12), pp. 1551–1557.

Hemmings, B. A. and Restuccia, D. F. (2012) ‘Pi3k-pkb/akt pathway’, *Cold Spring Harbor perspectives in biology*. Cold Spring Harbor Lab, 4(9), p. a011189.

Hempen, P. M. *et al.* (2003) ‘A double missense variation of the BUB1 gene and a defective mitotic spindle checkpoint in the pancreatic cancer cell line Hs766T’, *Human mutation*. Wiley Online Library, 21(4), p. 445.

Hengeveld, R. C. C. *et al.* (2017) ‘Inner centromere localization of the CPC maintains centromere cohesion and allows mitotic checkpoint silencing’, *Nature communications*. Nature Publishing Group, 8, p. 15542.

Hirabayashi, Y. *et al.* (2004) ‘The Wnt/β-catenin pathway directs neuronal differentiation of cortical neural precursor cells’, *Development*. The Company of Biologists Ltd, 131(12), pp. 2791–2801.

Holder, J., Poser, E. and Barr, F. A. (2019) ‘Getting out of mitosis: spatial and temporal control of mitotic exit and cytokinesis by PP1 and PP2A’, *FEBS letters*. Wiley Online Library.

van der Horst, A. and Khanna, K. K. (2009) ‘The peptidyl-prolyl isomerase Pin1 regulates cytokinesis through Cep55’, *Cancer research*. AACR, 69(16), pp. 6651–6659.

Hsieh, Y. *et al.* (2014) ‘NFIX Regulates Neural Progenitor Cell Differentiation During Hippocampal Morphogenesis’, (January), pp. 261–279. doi: 10.1093/cercor/bhs307.

Hu, C.-K. *et al.* (2012) ‘Plk1 negatively regulates PRC1 to prevent premature midzone formation before cytokinesis’, *Molecular biology of the cell*. Am Soc Cell Biol, 23(14), pp. 2702–2711.

Huang, S., Murphy, L. and Xu, W. (2018) ‘Genes and functions from breast cancer signatures’, *BMC cancer*. BioMed Central, 18(1), p. 473. doi: 10.1186/s12885-018-4388-4.

Hur, E.-M. and Zhou, F.-Q. (2012) ‘GSK3 signaling in neural development’, *Nature Reviews Neuroscience*, 11(8), pp. 539–551. doi: 10.1038/nrn2870.GSK3.

Hussain, M. S. *et al.* (2012) ‘A truncating mutation of CEP135 causes primary microcephaly and disturbed centrosomal function’, *The American Journal of Human Genetics*. Elsevier, 90(5), pp. 871–878.

Hwang, C.-F. *et al.* (2013) ‘Oncogenic fibulin-5 promotes nasopharyngeal carcinoma cell metastasis through the FLJ10540/AKT pathway and correlates with poor prognosis’, *PloS one*. Public Library of Science, 8(12), p. e84218.

Hyman, D. M. *et al.* (2017) ‘AKT inhibition in solid tumors with AKT1 mutations’, *Journal of Clinical Oncology*. American Society of Clinical Oncology, 35(20), p. 2251.

Ihle, N. T. *et al.* (2009) ‘Mutations in the phosphatidylinositol-3-kinase pathway predict for antitumor activity of the inhibitor PX-866 whereas oncogenic Ras is a dominant predictor for resistance’, *Cancer research*. AACR, 69(1), pp. 143–150.

Imai, Y. *et al.* (1999) ‘Mutational inactivation of mitotic checkpoint genes, hsMAD2 and hBUB1, is rare in sporadic digestive tract cancers’, *Japanese journal of cancer research*. Wiley Online Library, 90(8), pp. 837–840.

Innocente, S. A. *et al.* (1999) ‘p53 regulates a G2 checkpoint through cyclin B1’, *Proceedings of the National Academy of Sciences*. National Acad Sciences, 96(5), pp. 2147–2152.

Inoda, S. *et al.* (2009) ‘Cep55/c10orf3, a tumor antigen derived from a centrosome residing protein in breast carcinoma’, *Journal of Immunotherapy*, 32(5), pp. 474–485. doi: 10.1097/CJI.0b013e3181a1d109.

Inoda, S. *et al.* (2011) ‘The feasibility of Cep55/c10orf3 derived peptide vaccine therapy for colorectal carcinoma’, *Experimental and molecular pathology*. Elsevier, 90(1), pp. 55–60.

Iqbal, J. *et al.* (2019) ‘Molecular and Genomic Landscape of Peripheral T-Cell Lymphoma’, in *T-Cell and NK-Cell Lymphomas*. Springer, pp. 31–68.

Janus, J. R. *et al.* (2011) ‘Linking expression of FOXM1, CEP55 and HELLS to tumorigenesis in oropharyngeal squamous cell carcinoma’, *The Laryngoscope*. Wiley Online Library, 121(12), pp. 2598–2603.

Jeffery, J., Neyt, C., Moore, W., Paterson, S., Bower, Neil I., *et al.* (2015) ‘Cep55 regulates embryonic growth and development by promoting Akt stability in zebrafish’, *FASEB Journal*, 29(5), pp. 1999–2009. doi: 10.1096/fj.14-265090.

Jeffery, J., Neyt, C., Moore, W., Paterson, S., Bower, Neil I, *et al.* (2015) ‘Cep55 regulates embryonic growth and development by promoting Akt stability in zebrafish’, *The FASEB Journal*. FASEB, 29(5), pp. 1999–2009.

Jeffery, J *et al.* (2016) ‘Beyond cytokinesis: the emerging roles of CEP55 in tumorigenesis’, *Oncogene*. Nature Publishing Group, 35(6), pp. 683–690.

Jeffery, J. *et al.* (2016) ‘Beyond cytokinesis: The emerging roles of CEP55 in tumorigenesis’, *Oncogene*. Nature Publishing Group, 35(6), pp. 683–6390. doi: 10.1038/onc.2015.128.

Jeggo, P. A., Pearl, L. H. and Carr, A. M. (2016) ‘DNA repair, genome stability and cancer: a historical perspective’, *Nature Reviews Cancer*. Nature Publishing Group, 16(1), p. 35.

Jiang, W. *et al.* (2016) ‘Prognostic significance of centrosomal protein 55 in stage I pulmonary adenocarcinoma after radical resection’, *Thoracic cancer*. Wiley Online Library, 7(3), pp. 316–322.

Jones, C. *et al.* (2008) ‘Ciliary proteins link basal body polarization to planar cell polarity regulation’, *Nature genetics*. Nature Publishing Group, 40(1), p. 69.

Jones, J. *et al.* (2005) ‘Gene signatures of progression and metastasis in renal cell cancer’, *Clinical Cancer Research*. AACR, 11(16), pp. 5730–5739.

Juanes, M. A. and Piatti, S. (2016) ‘The final cut: cell polarity meets cytokinesis at the bud neck in S. cerevisiae’, *Cellular and Molecular Life Sciences*. Springer, 73(16), pp. 3115–3136.

Kaas, J. H., Gharbawie, O. A. and Stepniewska, I. (2013) ‘Cortical networks for ethologically relevant behaviors in primates’, *American journal of primatology*. Wiley Online Library, 75(5), pp. 407–414.

Kalimutho, M., Sinha, D., Jeffery, J., Nones, K., Srihari, S., Fernando, W. C., Duijf, P. H. G., *et al.* (2018) ‘CEP 55 is a determinant of cell fate during perturbed mitosis in breast cancer’, pp. 1–22. doi: 10.15252/emmm.201708566.

Kalimutho, M., Sinha, D., Jeffery, J., Nones, K., Srihari, S., Fernando, W. C., Duijf, P. H., *et al.* (2018) ‘CEP55 is a determinant of cell fate during perturbed mitosis in breast cancer’, *EMBO molecular medicine*. 2018/08/14. John Wiley and Sons Inc., 10(9), p. e8566. doi: 10.15252/emmm.201708566.

Kanda, S. *et al.* (2003) ‘Sonic hedgehog induces capillary morphogenesis by endothelial cells through phosphoinositide 3-kinase’, *Journal of Biological Chemistry*. ASBMB, 278(10), pp. 8244–8249.

Karimian, A., Ahmadi, Y. and Yousefi, B. (2016) ‘Multiple functions of p21 in cell cycle, apoptosis and transcriptional regulation after DNA damage’, *DNA repair*. Elsevier, 42, pp. 63–71.

Katayama, H. *et al.* (1999) ‘Mitotic kinase expression and colorectal cancer progression’, *Journal of the National Cancer Institute*. Oxford University Press, 91(13), pp. 1160–1162.

Katsnelson, A. (2013) ‘Momentum grows to make’personalized’medicine more’precise’’. Nature Publishing Group.

Kenney, A. M., Widlund, H. R. and Rowitch, D. H. (2004) ‘Hedgehog and PI-3 kinase signaling converge on Nmyc1 to promote cell cycle progression in cerebellar neuronal precursors’, *Development*. The Company of Biologists Ltd, 131(1), pp. 217–228.

Kim, J. *et al.* (2016) ‘XPO1-dependent nuclear export is a druggable vulnerability in KRAS-mutant lung cancer’, *Nature*. Nature Publishing Group, 538(7623), p. 114.

Kim, S. and Dynlacht, B. D. (2013) ‘Assembling a primary cilium’, *Current opinion in cell biology*. Elsevier, 25(4), pp. 506–511.

Kim, W.-Y. *et al.* (2009) ‘GSK-3 is a master regulator of neural progenitor homeostasis’, *Nature neuroscience*. Nature Publishing Group, 12(11), p. 1390.

Kim, W. Y. and Sharpless, N. E. (2006) ‘The regulation of INK4/ARF in cancer and aging’, *Cell*. Elsevier, 127(2), pp. 265–275.

Knobbe, C. B. *et al.* (2008) ‘The roles of PTEN in development, physiology and tumorigenesis in mouse models: a tissue-by-tissue survey’, *Oncogene*. Nature Publishing Group, 27(41), p. 5398.

Kramer, E. R. *et al.* (2006) ‘Cooperation between GDNF/Ret and ephrinA/EphA4 signals for motor-axon pathway selection in the limb’, *Neuron*. Elsevier, 50(1), pp. 35–47.

Kramer, E. R. *et al.* (2007) ‘Absence of Ret signaling in mice causes progressive and late degeneration of the nigrostriatal system’, *PLoS biology*. Public Library of Science, 5(3), p. e39.

Kulasinghe, A. *et al.* (2016) ‘Short term ex-vivo expansion of circulating head and neck tumour cells’, *Oncotarget*. Impact Journals, LLC, 7(37), p. 60101.

Kumar, A. *et al.* (2013) ‘CEP proteins: the knights of centrosome dynasty’, *Protoplasma*. Springer, 250(5), pp. 965–983.

Kumar, T. R. *et al.* (2009) ‘Transgenic mouse technology: principles and methods’, in *Molecular Endocrinology*. Springer, pp. 335–362.

Kuo, T.-C. *et al.* (2011) ‘Midbody accumulation through evasion of autophagy contributes to cellular reprogramming and tumorigenicity’, *Nature cell biology*. Nature Publishing Group, 13(10), p. 1214.

Kuo, T. *et al.* (2014) ‘Midbody accumulation through evasion of autophagy contributes to cellular reprogramming and tumorigenicity’, *Nat Cell Biol.*, 13(10), pp. 1214–1223.

doi: 10.1038/ncb2332.Midbody.

Kuwahara, A. *et al.* (2010) ‘Wnt signaling and its downstream target N-myc regulate basal progenitors in the developing neocortex’, *Development*, 137(7), pp. 1035–1044. doi: 10.1242/dev.046417.

Kuwahara, K. *et al.* (2000) ‘Cardiotrophin-1 phosphorylates akt and BAD, and prolongs cell survival via a PI3K-dependent pathway in cardiac myocytes’, *Journal of molecular and cellular cardiology*. Elsevier, 32(8), pp. 1385–1394.

Lachmann, A. *et al.* (2018) ‘Massive mining of publicly available RNA-seq data from human and mouse’, *Nature communications*. Nature Publishing Group, 9(1), p. 1366.

Lai, H. *et al.* (2018) ‘Krukovine Suppresses KRAS-Mutated Lung Cancer Cell Growth and Proliferation by Inhibiting the RAF-ERK Pathway and Inactivating AKT Pathway’, *Frontiers in pharmacology*. Frontiers Media S.A., 9, p. 958. doi: 10.3389/fphar.2018.00958.

Lai, K. *et al.* (2003) ‘Sonic hedgehog regulates adult neural progenitor proliferation in vitro and in vivo’, *Nature neuroscience*. Nature Publishing Group, 6(1), p. 21.

Lamballe, F., Klein, R. and Barbacid, M. (1991) ‘The trk family of oncogenes and neurotrophin receptors.’, in *Princess Takamatsu symposia*, pp. 153–170.

Lambert, A. W., Pattabiraman, D. R. and Weinberg, R. A. (2017) ‘Emerging biological principles of metastasis’, *Cell*. Elsevier, 168(4), pp. 670–691.

Lampreht Tratar, U., Horvat, S. and Cemazar, M. (2018) ‘Transgenic Mouse Models in Cancer Research’, *Frontiers in oncology*. Frontiers Media S.A., 8, p. 268. doi: 10.3389/fonc.2018.00268.

Laoukili, J. *et al.* (2005) ‘FoxM1 is required for execution of the mitotic programme and chromosome stability’, *Nature cell biology*. Nature publishing group, 7(2), p. 126.

Laoukili, J., Stahl, M. and Medema, R. H. (2007) ‘FoxM1: at the crossroads of ageing and cancer’, *Biochimica et Biophysica Acta (BBA)-Reviews on Cancer*. Elsevier, 1775(1), pp. 92–102.

Lee, H. H. *et al.* (2008) ‘Midbody targeting of the ESCRT machinery by a noncanonical coiled coil in CEP55’, *Science*. American Association for the Advancement of Science, 322(5901), pp. 576–580.

Lee, J. H., Park, S. M. and Jang, H. J. (2019) ‘Roles of primary cilia in the developing brain’, *Frontiers in cellular neuroscience*. Frontiers, 13, p. 218.

Lee, J. Y. *et al.* (2015) ‘Patient-derived cell models as preclinical tools for genome-directed targeted therapy’, *Oncotarget*. Impact Journals, LLC, 6(28), p. 25619.

Léger, B. *et al.* (2006) ‘Akt signalling through GSK-3β, mTOR and Foxo1 is involved in human skeletal muscle hypertrophy and atrophy’, *The Journal of physiology*. Wiley Online Library, 576(3), pp. 923–933.

Li, D. *et al.* (2003) ‘Overexpression of oncogenic STK15/BTAK/Aurora A kinase in human pancreatic cancer’, *Clinical cancer research*. AACR, 9(3), pp. 991–997.

Li, F. *et al.* (2018) 'CEP55 promotes cell proliferation and inhibits apoptosis via the PI3K/Akt/p21 signaling pathway in human glioma U251 cells', *Oncology letters*. Spandidos Publications, 15(4), pp. 4789–4796.

Li, G. *et al.* (2002) 'Conditional loss of PTEN leads to precocious development and neoplasia in the mammary gland', *Development*. The Company of Biologists Ltd, 129(17), pp. 4159–4170.

Li, H., Kwak, I. and DeMayo, F. J. (2005) 'Genetically engineered mouse models for lung cancer', *Drug Discovery Today: Disease Models*. Elsevier, 2(1), pp. 35–40.

Li, J. *et al.* (1997) 'PTEN, a putative protein tyrosine phosphatase gene mutated in human brain, breast, and prostate cancer', *science*. American Association for the Advancement of Science, 275(5308), pp. 1943–1947.

Li, M. *et al.* (2018) 'CEP55 Promotes Cell Motility via JAK2–STAT3–MMPs Cascade in Hepatocellular Carcinoma', *Cells*, 7(8), p. 99. doi: 10.3390/cells7080099.

Li, Y. *et al.* (2012) 'Targeting the Hedgehog signaling pathway for cancer therapy', *Expert opinion on therapeutic targets*. Taylor & Francis, 16(1), pp. 49–66.

Liaw, D. *et al.* (1997) 'Germline mutations of the PTEN gene in Cowden disease, an inherited breast and thyroid cancer syndrome', *Nature genetics*. Nature Publishing Group, 16(1), p. 64.

Lien, E. C., Dibble, C. C. and Toker, A. (2017) 'PI3K signaling in cancer: beyond AKT', *Current opinion in cell biology*. Elsevier, 45, pp. 62–71.

Lin, W. M. *et al.* (1998) 'Loss of heterozygosity and mutational analysis of the PTEN/MMAC1 gene in synchronous endometrial and ovarian carcinomas.', *Clinical Cancer Research*. AACR, 4(11), pp. 2577–2583.

Liu, L. and Eisenman, R. N. (2012) 'Regulation of c-Myc Protein Abundance by a Protein Phosphatase 2A-Glycogen Synthase Kinase 3β-Negative Feedback Pathway', *Genes & cancer*. SAGE Publications, 3(1), pp. 23–36. doi: 10.1177/1947601912448067.

Loo, L. *et al.* (2019) 'Single-cell transcriptomic analysis of mouse neocortical development', *Nature communications*. Nature Publishing Group, 10(1), p. 134.

Lu, T.-L. *et al.* (2007) 'Tumor spectrum, tumor latency and tumor incidence of the Pten-deficient mice', *PLoS One*. Public Library of Science, 2(11), p. e1237.

Luo, J., Manning, B. D. and Cantley, L. C. (2003) 'Targeting the PI3K-Akt pathway in human cancer: rationale and promise', *Cancer cell*. Elsevier, 4(4), pp. 257–262.

Luo, J., Solimini, N. L. and Elledge, S. J. (2009) 'Principles of cancer therapy: oncogene and non-oncogene addiction', *Cell*. Elsevier, 136(5), pp. 823–837.

Luo, W. *et al.* (2009) 'Molecular identification of rapidly adapting mechanoreceptors and their developmental dependence on ret signaling', *Neuron*. Elsevier, 64(6), pp. 841–856.

Maehama, T. and Dixon, J. E. (1998) 'The tumor suppressor, PTEN/MMAC1, dephosphorylates the lipid second messenger, phosphatidylinositol 3, 4, 5-trisphosphate', *Journal of Biological Chemistry*. ASBMB, 273(22), pp. 13375–13378.

Mahmood, T. and Yang, P.-C. (2012) 'Western blot: technique, theory, and trouble shooting', *North American journal of medical sciences*. Medknow Publications & Media Pvt Ltd, 4(9), pp. 429–434. doi: 10.4103/1947-2714.100998.

Manning, B. D. and Cantley, L. C. (2007) 'AKT/PKB signaling: navigating downstream', *Cell*. Elsevier, 129(7), pp. 1261–1274.

Manuel, M. N. *et al.* (2015) 'Regulation of cerebral cortical neurogenesis by the Pax6 transcription factor ', *Frontiers in Cellular Neuroscience* , p. 70. Available at: https://www.frontiersin.org/article/10.3389/fncel.2015.00070.

Mao, J.-H. *et al.* (2003) 'Genetic interactions between Pten and p53 in radiation-induced lymphoma development', *Oncogene*. Nature Publishing Group, 22(52), p. 8379.

Marjanović, M. *et al.* (2015) 'CEP63 deficiency promotes p53-dependent microcephaly and reveals a role for the centrosome in meiotic recombination', *Nature communications*. Nature Publishing Group, 6, p. 7676.

Marsh, D. J. *et al.* (1998) 'Mutation spectrum and genotype-phenotype analyses in Cowden disease and Bannayan-Zonana syndrome, two hamartoma syndromes with germline PTEN mutation', *Human molecular genetics*. Oxford University Press, 7(3), pp. 507–515.

Marshall, W. F. (2008) 'Basal bodies: platforms for building cilia', *Current topics in developmental biology*. Elsevier, 85, pp. 1–22.

Martelli, A. M. *et al.* (2012) 'The emerging multiple roles of nuclear Akt', *Biochimica et Biophysica Acta (BBA)-Molecular Cell Research*. Elsevier, 1823(12), pp. 2168–2178.

Martinez-Garay, I. *et al.* (2006) 'The novel centrosomal associated protein CEP55 is present in the spindle midzone and the midbody', *Genomics*. Elsevier, 87(2), pp. 243–253.

Martínez-Garay, I. *et al.* (2007) 'A two base pair deletion in the PQBP1 gene is associated with microphthalmia, microcephaly, and mental retardation', *European Journal of Human Genetics*. Nature Publishing Group, 15(1), p. 29.

Mathivanan, S. *et al.* (2010) 'Proteomics analysis of A33 immunoaffinity-purified exosomes released from the human colon tumor cell line LIM1215 reveals a tissue-specific protein signature', *Molecular & Cellular Proteomics*. ASBMB, 9(2), pp. 197–208.

Matsuoka, S. *et al.* (2007) 'ATM and ATR substrate analysis reveals extensive protein networks responsive to DNA damage', *science*. American Association for the Advancement of Science, 316(5828), pp. 1160–1166.

Mayer, I. A. and Arteaga, C. L. (2016) 'The PI3K/AKT pathway as a target for cancer treatment', *Annual review of medicine*. Annual Reviews, 67, pp. 11–28.

Mayo, L. D. and Donner, D. B. (2001) 'A phosphatidylinositol 3-kinase/Akt pathway promotes translocation of Mdm2 from the cytoplasm to the nucleus', *Proceedings of the National Academy of Sciences*. National Acad Sciences, 98(20), pp. 11598–11603.

McRee, S. K. *et al.* (2018) 'AKT2 loss impairs BRAF mutant melanoma metastasis'. AACR.

Metzger, D. and Chambon, P. (2001) 'Site-and time-specific gene targeting in the mouse', *Methods*. Elsevier, 24(1), pp. 71–80.

Mierzwa, B. and Gerlich, D. W. (2014) 'Cytokinetic abscission: molecular mechanisms and temporal control', *Developmental cell*. Elsevier, 31(5), pp. 525–538.

Mill, P. *et al.* (2005) 'Shh controls epithelial proliferation via independent pathways that converge on N-Myc', *Developmental Cell*, 9(2), pp. 293–303. doi: 10.1016/j.devcel.2005.05.009.

Minamoto, T., Mai, M. and Ronai, Z. (1999) 'Environmental factors as regulators and effectors of multistep carcinogenesis', *Carcinogenesis*. Oxford University Press, 20(4), pp. 519–527.

Ming, G. and Song, H. (2005) 'Adult neurogenesis in the mammalian central nervous system', *Annu. Rev. Neurosci.* Annual Reviews, 28, pp. 223–250.

Mirantes, C. *et al.* (2013) 'An inducible knockout mouse to model the cell-autonomous role of PTEN in initiating endometrial, prostate and thyroid neoplasias', *Disease models & mechanisms*. The Company of Biologists Ltd, 6(3), pp. 710–720.

Miyoshi, K. *et al.* (2006) 'Embryonic expression of pericentrin suggests universal roles in ciliogenesis', *Development genes and evolution*. Springer, 216(9), pp. 537–542.

Moberg, K. H. *et al.* (2004) 'The Drosophila F box protein archipelago regulates dMyc protein levels in vivo', *Current biology*. Elsevier, 14(11), pp. 965–974.

Molyneaux, B. J. *et al.* (2007) 'Neuronal subtype specification in the cerebral cortex', *Nature reviews neuroscience*. Nature Publishing Group, 8(6), p. 427.

Mondal G, Rowley M, Guidugli L, Wu J, Pankratz VS, C. F. (2012) 'BRCA2 localization to the midbody by filamin A regulates cep55 signaling and completion of cytokinesis.', *Dev Cell*, 23, pp. 137–152.

Montero-Conde, C. *et al.* (2008) 'Molecular profiling related to poor prognosis in thyroid carcinoma. Combining gene expression data and biological information', *Oncogene*. Nature Publishing Group, 27(11), pp. 1554–1561.

Mori, S. and Leblond, C. P. (1969) 'Electron microscopic features and proliferation of astrocytes in the corpus callosum of the rat', *Journal of Comparative Neurology*. Wiley Online Library, 137(2), pp. 197–225.

Mühlhans, J., Brandstätter, J. H. and Gießl, A. (2011) 'The centrosomal protein pericentrin identified at the basal body complex of the connecting cilium in mouse photoreceptors', *PLoS One*. Public Library of Science, 6(10), p. e26496.

Mullins, J. and Biesele, J. J. (1977) 'Terminal phase of cytokinesis in D-98s cells', *The Journal of cell biology*. The Rockefeller University Press, 73(3), p. 672.

Myatt, S. S. and Lam, E. W.-F. (2008) ‘Targeting foxm1’, *Nature reviews Cancer*. Nature Publishing Group, 8(3), p. 242.

Nakad, R. and Schumacher, B. (2016) ‘DNA damage response and immune defense: links and mechanisms’, *Frontiers in genetics*. Frontiers, 7, p. 147.

Nandan, M. O. and Yang, V. W. (2011) ‘An update on the biology of RAS/RAF mutations in colorectal cancer’, *Current colorectal cancer reports*. Springer, 7(2), pp. 113–120.

Nasmyth, K. (1995) ‘Evolution of the cell cycle’, *Philosophical Transactions of the Royal Society of London B: Biological Sciences*. The Royal Society, 349(1329), pp. 271–281.

Naughton, C. K. *et al.* (2006) ‘Glial cell-line derived neurotrophic factor-mediated RET signaling regulates spermatogonial stem cell fate’, *Biology of reproduction*. Oxford University Press, 74(2), pp. 314–321.

Neto, H. *et al.* (2013) ‘Syntaxin 16 is a master recruitment factor for cytokinesis’, *Molecular biology of the cell*. Am Soc Cell Biol, 24(23), pp. 3663–3674.

Nissen, N. I., Karsdal, M. and Willumsen, N. (2019) ‘Collagens and Cancer associated fibroblasts in the reactive stroma and its relation to Cancer biology’, *Journal of experimental & clinical cancer research : CR*. BioMed Central, 38(1), p. 115. doi: 10.1186/s13046-019-1110-6.

O’Connor, M. J. (2015) ‘Targeting the DNA damage response in cancer’, *Molecular cell*. Elsevier, 60(4), pp. 547–560.

O’connor, W. N. and Valle, S. (1982) ‘A combination Verhoeffs elastic and Masson’s trichrome stain for routine histology’, *Stain technology*. Taylor & Francis, 57(4), pp. 207–210.

Ohtani, N. and Hara, E. (2013) ‘Roles and mechanisms of cellular senescence in regulation of tissue homeostasis’, *Cancer science*. Wiley Online Library, 104(5), pp. 525–530.

Oki, E. *et al.* (2005) ‘Akt phosphorylation associates with LOH of PTEN and leads to chemoresistance for gastric cancer’, *International journal of cancer*. Wiley Online Library, 117(3), pp. 376–380.

Orzáez, M., Medina, M. S. and Pérez-Payá, E. (2016) *Cyclin-dependent Kinase (CDK) Inhibitors: Methods and Protocols*. Springer.

El Osta, B. *et al.* (2019) ‘Characteristics and outcomes of patients with metastatic KRAS mutant lung adenocarcinomas: The Lung Cancer Mutation Consortium experience’, *Journal of Thoracic Oncology*. Elsevier.

Ozenne, P. *et al.* (2010) ‘The ARF tumor suppressor: structure, functions and status in cancer’, *International journal of cancer*. Wiley Online Library, 127(10), pp. 2239–2247.

Paez-Ribes, M. *et al.* (2016) ‘Development of patient derived xenograft models of overt spontaneous breast cancer metastasis: a cautionary note’, *PloS one*. Public Library of

Science, 11(6), p. e0158034.

Paez, J. and Sellers, W. R. (2004) ‘PI3K/PTEN/Akt Pathway’, in *Signal transduction in cancer*. Springer, pp. 145–167.

Pap, M. and Cooper, G. M. (1998) ‘Role of glycogen synthase kinase-3 in the phosphatidylinositol 3-kinase/Akt cell survival pathway’, *Journal of Biological Chemistry*. ASBMB, 273(32), pp. 19929–19932.

Parsa, N. (2012) ‘Environmental factors inducing human cancers’, *Iranian journal of public health*. Tehran University of Medical Sciences, 41(11), p. 1.

Pedersen, R. S. *et al.* (2016) ‘Profiling DNA damage response following mitotic perturbations’, *Nature communications*. Nature Publishing Group, 7, p. 13887.

Peng, T. *et al.* (2017) ‘Centrosomal protein 55 activates NF-κB signalling and promotes pancreatic cancer cells aggressiveness’, *Scientific reports*. Nature Publishing Group, 7(1), p. 5925.

Perou, C. M. *et al.* (2000) ‘Molecular portraits of human breast tumours.’, *Nature*, 406(6797), pp. 747–752. doi: 10.1038/35021093.

Pierotti, M. A. *et al.* (2016) ‘Oncogenes’, *Holland-Frei Cancer Medicine*. Wiley Online Library, pp. 1–22.

Pilarski, R. *et al.* (2013) ‘Cowden Syndrome and the PTEN Hamartoma Tumor Syndrome: Systematic Review and Revised Diagnostic Criteria ’, *JNCI: Journal of the National Cancer Institute*, 105(21), pp. 1607–1616. doi: 10.1093/jnci/djt277.

Poltavets, V. *et al.* (2018) ‘The Role of the Extracellular Matrix and Its Molecular and Cellular Regulators in Cancer Cell Plasticity’, *Frontiers in oncology*. Frontiers Media S.A., 8, p. 431. doi: 10.3389/fonc.2018.00431.

Powles-Glover, N. (2014) ‘Cilia and ciliopathies: Classic examples linking phenotype and genotype-An overview’, *Reproductive Toxicology*. Elsevier Inc., 48, pp. 98–105. doi: 10.1016/j.reprotox.2014.05.005.

Protsenko, A. (2018) ‘The role of EphB4 and ephrin-B2 interactions in prostate cancer models of intravasation and extravasation’. Queensland University of Technology.

Rabellino, A. *et al.* (2016) ‘PIAS1 Promotes Lymphomagenesis through MYC Upregulation’, *Cell reports*. 2016/05/26, 15(10), pp. 2266–2278. doi: 10.1016/j.celrep.2016.05.015.

Raiborg, C. and Stenmark, H. (2009) ‘The ESCRT machinery in endosomal sorting of ubiquitylated membrane proteins’, *Nature*. Nature Publishing Group, 458(7237), p. 445.

Ramos, A. D. *et al.* (2013) ‘Integration of genome-wide approaches identifies lncRNAs of adult neural stem cells and their progeny in vivo’, *Cell stem cell*. Elsevier, 12(5), pp. 616–628.

Rao, G. *et al.* (2004) ‘Sonic hedgehog and insulin-like growth factor signaling synergize to induce medulloblastoma formation from nestin-expressing neural progenitors in mice’, *Oncogene*. Nature Publishing Group, 23(36), p. 6156.

Rawlins, L. E. *et al.* (2019) ‘An Amish founder variant consolidates disruption of CEP55 as a cause of hydranencephaly and renal dysplasia’, *European Journal of Human Genetics*. doi: 10.1038/s41431-018-0306-0.

Regad, T. (2015) ‘Targeting RTK signaling pathways in cancer’, *Cancers*. Multidisciplinary Digital Publishing Institute, 7(3), pp. 1758–1784.

Reiter, J. F. and Leroux, M. R. (2017) ‘Genes and molecular pathways underpinning ciliopathies’, *Nature reviews Molecular cell biology*. Nature Publishing Group, 18(9), p. 533.

Reya, T. and Clevers, H. (2005) ‘Wnt signalling in stem cells and cancer’, *Nature*. Nature Publishing Group, 434(7035), p. 843.

Rieder, C. L., Faruki, S. and Khodjakov, A. (2001a) ‘The centrosome in vertebrates: more than a microtubule-organizing center ’, *Trends in Cell Biology* . LONDON : Elsevier Ltd , pp. 413–419. doi: 10.1016/S0962-8924(01)02085-2.

Rieder, C. L., Faruki, S. and Khodjakov, A. (2001b) ‘The centrosome in vertebrates: more than a microtubule-organizing center ’, *Trends in Cell Biology* . LONDON : Elsevier Ltd , pp. 413–419. doi: 10.1016/S0962-8924(01)02085-2.

Rigueur, D. and Lyons, K. M. (2014) ‘Whole-mount skeletal staining’, *Methods in molecular biology (Clifton, N.J.)*, 1130, pp. 113–121. doi: 10.1007/978-1-62703-989-5_9.

Riobó, N. A. *et al.* (2006) ‘Phosphoinositide 3-kinase and Akt are essential for Sonic Hedgehog signaling.’, *Proceedings of the National Academy of Sciences of the United States of America*, 103(12), pp. 4505–10. doi: 10.1073/pnas.0504337103.

Riobo, N. A., Lu, K. and Emerson, C. P. (2006) ‘Hedgehog signal transduction: Signal integration and cross talk in development and cancer’, *Cell Cycle*, 5(15), pp. 1612–1615. doi: 10.4161/cc.5.15.3130.

Robertson, G. P. *et al.* (1998) ‘In vitro loss of heterozygosity targets the PTEN/MMAC1 gene in melanoma’, *Proceedings of the National Academy of Sciences*. National Acad Sciences, 95(16), pp. 9418–9423.

Rockland, K. S., Kaas, J. H. and Peters, A. (2013) *Cerebral Cortex: Volume 12: Extrastriate Cortex in Primates*. Springer Science & Business Media.

Roos, W. P. and Kaina, B. (2006) ‘DNA damage-induced cell death by apoptosis’, *Trends in molecular medicine*. Elsevier, 12(9), pp. 440–450.

Roosing, S. *et al.* (2016) ‘Mutations in CEP120 cause Joubert syndrome as well as complex ciliopathy phenotypes’, *Journal of medical genetics*. BMJ Publishing Group Ltd, p. jmedgenet-2016.

Rotheneichner, P. *et al.* (2017) ‘Tamoxifen Activation of Cre-Recombinase Has No Persisting Effects on Adult Neurogenesis or Learning and Anxiety’, *Frontiers in neuroscience*. Frontiers Media S.A., 11, p. 27. doi: 10.3389/fnins.2017.00027.

Ruchaud, S., Carmena, M. and Earnshaw, W. C. (2007) ‘Chromosomal passengers: conducting cell division’, *Nature reviews Molecular cell biology*. Nature Publishing

Group, 8(10), p. 798.

Ryan, S.-L. (2019) ‘Targeting the nuclear factor kappa-light-chain-enhancer of activated b cells (NF-kb) pathway to overcome cisplatin-resistance in non-small cell lung cancer’. Queensland University of Technology.

Sachdeva, M. *et al.* (2009) ‘p53 represses c-Myc through induction of the tumor suppressor miR-145’, *Proceedings of the National Academy of Sciences*. National Acad Sciences, 106(9), pp. 3207–3212.

Sakai, M. *et al.* (2006) ‘Elevated expression of C10orf3 (chromosome 10 open reading frame 3) is involved in the growth of human colon tumor’, *Oncogene*, 25(3), pp. 480–486. doi: 10.1038/sj.onc.1209051.

Sanchez-Martinez, C. *et al.* (2015) ‘Cyclin dependent kinase (CDK) inhibitors as anticancer drugs’, *Bioorganic & medicinal chemistry letters*. Elsevier, 25(17), pp. 3420–3435.

Sánchez-Martínez, C. *et al.* (2019) ‘Cyclin Dependent Kinase (CDK) inhibitors as anticancer drugs: Recent Advances (2015-2019)’, *Bioorganic & medicinal chemistry letters*. Elsevier, p. 126637.

Sato, N. *et al.* (2000) ‘Loss of heterozygosity on 10q23. 3 and mutation of the tumor suppressor gene PTEN in benign endometrial cyst of the ovary: possible sequence progression from benign endometrial cyst to endometrioid carcinoma and clear cell carcinoma of the ovary’, *Cancer research*. AACR, 60(24), pp. 7052–7056.

Schorey, J. S. and Bhatnagar, S. (2008) ‘Exosome function: from tumor immunology to pathogen biology’, *Traffic*. Wiley Online Library, 9(6), pp. 871–881.

Schrøder, J. M. *et al.* (2011) ‘EB1 and EB3 promote cilia biogenesis by several centrosome-related mechanisms’, *J Cell Sci*. The Company of Biologists Ltd, 124(15), pp. 2539–2551.

Schuchardt, A. *et al.* (1994) ‘Defects in the kidney and enteric nervous system of mice lacking the tyrosine kinase receptor Ret’, *Nature*. Nature Publishing Group, 367(6461), p. 380.

Sever, R. and Brugge, J. S. (2015) ‘Signal transduction in cancer’, *Cold Spring Harbor perspectives in medicine*. Cold Spring Harbor Laboratory Press, 5(4), p. a006098.

Seyedabadi, S. *et al.* (2018) ‘Assessment of CEP55, PLK1 and FOXM1 expression in patients with bladder cancer in comparison with healthy individuals’, *Cancer Investigation*. Taylor & Francis, 36(8), pp. 407–414. doi: 10.1080/07357907.2018.1514504.

Shakoori, A. *et al.* (2007) ‘Inhibition of GSK-3β activity attenuates proliferation of human colon cancer cells in rodents’, *Cancer science*. Wiley Online Library, 98(9), pp. 1388–1393.

Shay, J. W. (2016) ‘Role of telomeres and telomerase in aging and cancer’, *Cancer discovery*. AACR, 6(6), pp. 584–593.

Shen, E. H., Overly, C. C. and Jones, A. R. (2012) ‘The Allen Human Brain Atlas:

comprehensive gene expression mapping of the human brain', *Trends in neurosciences*. Elsevier, 35(12), pp. 711–714.

Sherr, C. J. (1996) 'Cancer cell cycles', *Science*. American Association for the Advancement of Science, 274(5293), pp. 1672–1677.

Sherr, C. J. and McCormick, F. (2002) 'The RB and p53 pathways in cancer', *Cancer cell*. Elsevier, 2(2), pp. 103–112.

Shi, D. and Gu, W. (2012) 'Dual Roles of MDM2 in the Regulation of p53: Ubiquitination Dependent and Ubiquitination Independent Mechanisms of MDM2 Repression of p53 Activity', *Genes & cancer*. SAGE Publications, 3(3–4), pp. 240–248. doi: 10.1177/1947601912455199.

Shi, W. *et al.* (2013) 'Essential developmental, genomic stability, and tumour suppressor functions of the mouse orthologue of hSSB1/NABP2', *PLoS Genet*. Public Library of Science, 9(2), p. e1003298.

Shiraishi, T. *et al.* (2011) 'Cancer/Testis antigens as potential predictors of biochemical recurrence of prostate cancer following radical prostatectomy', *Journal of Translational Medicine*. BioMed Central Ltd, 9(1), p. 153. doi: 10.1186/1479-5876-9-153.

Shruthi, B. S. and Palani Vinodhkumar, S. (2016) 'Proteomics: A new perspective for cancer', *Advanced biomedical research*. Wolters Kluwer--Medknow Publications, 5.

Simms, R. J. *et al.* (2011) 'Nephronophthisis: a genetically diverse ciliopathy', *International journal of nephrology*. 2011/05/15. SAGE-Hindawi Access to Research, 2011, p. 527137. doi: 10.4061/2011/527137.

Sineva, G. S. and Pospelov, V. A. (2014) 'β-Catenin in pluripotency: adhering to self-renewal or Wnting to differentiate?', in *International review of cell and molecular biology*. Elsevier, pp. 53–78.

Singh, P. K. *et al.* (2015) 'Expression and clinical significance of Centrosomal protein 55 (CEP55) in human urinary bladder transitional cell carcinoma', *Immunobiology*. Elsevier, 220(1), pp. 103–108.

Sinha, D. *et al.* (2018) 'Cep55 overexpression causes male-specific sterility in mice by suppressing Foxo1 nuclear retention through sustained activation of PI3K / Akt signaling', *The FASEB Journal*, 0(0). doi: 10.1096/fj.201701096RR.

Sinha, D. *et al.* (2019) 'Cep55 overexpression promotes genomic instability and tumorigenesis in mice', *bioRxiv*. Cold Spring Harbor Laboratory, p. 780775.

Sir, J.-H. *et al.* (2011) 'A primary microcephaly protein complex forms a ring around parental centrioles', *Nature genetics*, 43(11), pp. 1147–1153. doi: 10.1038/ng.971.

Sittewelle, M. and Monsoro-Burq, A. H. (2018) 'AKT signaling displays multifacet functions in Neural Crest development', *Developmental biology*. Elsevier.

Slamon, D. J. (1987) 'Human breast cancer: correlation of relapse and', *Science*, 3798106(177), p. 235.

Sontag, E. *et al.* (1995) 'A novel pool of protein phosphatase 2A is associated with microtubules and is regulated during the cell cycle.', *The Journal of Cell Biology*, 128(6), pp. 1131 LP – 1144. doi: 10.1083/jcb.128.6.1131.

Spalluto, C., Wilson, D. I. and Hearn, T. (2013) 'Evidence for reciliation of RPE1 cells in late G1 phase, and ciliary localisation of cyclin B1', *FEBS open bio*. Elsevier, 3, pp. 334–340.

Stahl, P. D. and Raposo, G. (2019) 'Extracellular vesicles: exosomes and microvesicles, integrators of homeostasis', *Physiology*. American Physiological Society Bethesda, MD, 34(3), pp. 169–177.

Stark, A.-K. *et al.* (2015) 'PI3K inhibitors in inflammation, autoimmunity and cancer', *Current opinion in pharmacology*. Elsevier, 23, pp. 82–91.

Stark, C. *et al.* (2006) 'BioGRID: a general repository for interaction datasets', *Nucleic acids research*. Oxford University Press, 34(suppl_1), pp. D535–D539.

Steeg, P. S. (2016) 'Targeting metastasis', *Nature reviews cancer*. Nature Publishing Group, 16(4), p. 201.

Steigemann, P. and Gerlich, D. W. (2009) 'Cytokinetic abscission: cellular dynamics at the midbody', *Trends in cell biology*. Elsevier, 19(11), pp. 606–616.

Steinman, R. M. and Cohn, Z. A. (1973) 'Identification of a novel cell type in peripheral lymphoid organs of mice: I. Morphology, quantitation, tissue distribution', *Journal of Experimental Medicine*. Rockefeller University Press, 137(5), pp. 1142–1162.

Stewart, B. W. and Wild, C. P. (2014) *World Cancer Report 2014, World Health Organization: Geneva*. doi: 9283204298.

Stoscheck, C. M. and King, L. E. (1986) 'Role of epidermal growth factor in carcinogenesis', *Cancer research*. AACR, 46(3), pp. 1030–1037.

Stowe, T. R. *et al.* (2012) 'The centriolar satellite proteins Cep72 and Cep290 interact and are required for recruitment of BBS proteins to the cilium', *Molecular biology of the cell*. Am Soc Cell Biol, 23(17), pp. 3322–3335.

Strauss, S. *et al.* (1984) 'Antenatal ultrasound diagnosis of an unusual case of hydranencephaly', *Journal of clinical ultrasound*. Wiley Online Library, 12(7), pp. 420–422.

Subramanian, A. *et al.* (2005) 'Gene set enrichment analysis: a knowledge-based approach for interpreting genome-wide expression profiles', *Proceedings of the National Academy of Sciences*. National Acad Sciences, 102(43), pp. 15545–15550.

Suizu, F. *et al.* (2016) 'Phosphorylation-dependent Akt-Inversin interaction at the basal body of primary cilia', *The EMBO journal*. 2016/05/24. John Wiley and Sons Inc., 35(12), pp. 1346–1363. doi: 10.15252/embj.201593003.

Sun, Z. *et al.* (2018) 'Emerging role of exosome signalling in maintaining cancer stem cell dynamic equilibrium', *Journal of cellular and molecular medicine*. Wiley Online Library, 22(8), pp. 3719–3728.

Suzuki, A. *et al.* (1998) 'High cancer susceptibility and embryonic lethality associated with mutation of the PTEN tumor suppressor gene in mice’, *Current Biology*. Elsevier, 8(21), pp. 1169–1178.

Suzuki, A. *et al.* (2001) ‘T cell-specific loss of Pten leads to defects in central and peripheral tolerance’, *Immunity*. Elsevier, 14(5), pp. 523–534.

Suzuki, A. *et al.* (2003) ‘Keratinocyte-specific Pten deficiency results in epidermal hyperplasia, accelerated hair follicle morphogenesis and tumor formation’, *Cancer research*. AACR, 63(3), pp. 674–681.

Tan, M.-H. *et al.* (2012) ‘Lifetime cancer risks in individuals with germline PTEN mutations’, *Clinical Cancer Research*. AACR, 18(2), pp. 400–407.

Tang, E. D. *et al.* (1999) ‘Negative regulation of the forkhead transcription factor FKHR by Akt’, *Journal of Biological Chemistry*. ASBMB, 274(24), pp. 16741–16746.

Tao, J. *et al.* (2014) ‘CEP55 contributes to human gastric carcinoma by regulating cell proliferation’, *Tumor Biology*. Springer, 35(5), pp. 4389–4399.

Taverna, E., Götz, M. and Huttner, W. B. (2014) ‘The cell biology of neurogenesis: toward an understanding of the development and evolution of the neocortex’, *Annual review of cell and developmental biology*. Annual Reviews, 30, pp. 465–502.

Teng, D. H. F. *et al.* (1997) ‘MMAC1/PTEN mutations in primary tumor specimens and tumor cell lines’, *Cancer research*. AACR, 57(23), pp. 5221–5225.

Thompson, S. L., Bakhoum, S. F. and Compton, D. A. (2010) ‘Mechanisms of chromosomal instability’, *Current biology*. Elsevier, 20(6), pp. R285–R295.

Thorpe, L. M., Yuzugullu, H. and Zhao, J. J. (2015) ‘PI3K in cancer: divergent roles of isoforms, modes of activation and therapeutic targeting’, *Nature Reviews Cancer*. Nature Publishing Group, 15(1), p. 7.

Tian, H. *et al.* (2015) ‘DNA damage response–a double-edged sword in cancer prevention and cancer therapy’, *Cancer letters*. Elsevier, 358(1), pp. 8–16.

De Togni, P. *et al.* (1994) ‘Abnormal development of peripheral lymphoid organs in mice deficient in lymphotoxin’, *Science*. American Association for the Advancement of Science, 264(5159), pp. 703–707.

de Torres, C. *et al.* (1997) ‘Identification of necrotic cell death by the TUNEL assay in the hypoxic-ischemic neonatal rat brain’, *Neuroscience letters*. Elsevier, 230(1), pp. 1–4.

Travis, W. D. *et al.* (2011) ‘International association for the study of lung cancer/american thoracic society/european respiratory society international multidisciplinary classification of lung adenocarcinoma’, *Journal of thoracic oncology : official publication of the International Association for the Study of Lung Cancer*, 6(2), pp. 244–285. doi: 10.1097/JTO.0b013e318206a221.

Travis, W. D. *et al.* (2015) ‘The 2015 World Health Organization classification of lung tumors: impact of genetic, clinical and radiologic advances since the 2004 classification’, *Journal of thoracic oncology*. Elsevier, 10(9), pp. 1243–1260.

Tsafrir, D. *et al.* (2006) 'Relationship of gene expression and chromosomal abnormalities in colorectal cancer', *Cancer research*. AACR, 66(4), pp. 2129–2137.

Valente, D. *et al.* (2015) 'HIPK2 deficiency causes chromosomal instability by cytokinesis failure and increases tumorigenicity', *Oncotarget*, 6(12). doi: 10.18632/oncotarget.3583.

Vied, C. M. *et al.* (2014) 'A multi-resource data integration approach: identification of candidate genes regulating cell proliferation during neocortical development', *Frontiers in neuroscience*. Frontiers, 8, p. 257.

Vivanco, I. and Sawyers, C. L. (2002) 'The phosphatidylinositol 3-kinase–AKT pathway in human cancer', *Nature Reviews Cancer*. Nature Publishing Group, 2(7), p. 489.

Wala, J. and Beroukhim, R. (2016) 'The oncogene makes its escape', *Science*. American Association for the Advancement of Science, 351(6280), pp. 1398–1399.

Wang, D. C. and Wang, X. (2017) 'Tomorrow's genome medicine in lung cancer', in *Seminars in cancer biology*. Elsevier, pp. 39–43.

Wang, L.-H. *et al.* (2018) 'Loss of Tumor Suppressor Gene Function in Human Cancer: An Overview', *Cellular Physiology and Biochemistry*. Karger Publishers, 51(6), pp. 2647–2693.

Wang, Q., Chen, X. and Hay, N. (2017) 'Akt as a target for cancer therapy: more is not always better (lessons from studies in mice)', *British journal of cancer*. Nature Publishing Group, 117(2), p. 159.

Wang, S. *et al.* (2016) 'GSK-3β inhibitor CHIR-99021 promotes proliferation through upregulating β-catenin in neonatal atrial human cardiomyocytes', *Journal of cardiovascular pharmacology*. Wolters Kluwer, 68(6), pp. 425–432.

Wang, W.-J. *et al.* (2013) 'CEP162 is an axoneme-recognition protein promoting ciliary transition zone assembly at the cilia base', *Nature cell biology*. Nature Publishing Group, 15(6), p. 591.

Waseem, A. *et al.* (2010) 'Downstream targets of FOXM1: CEP55 and HELLS are cancer progression markers of head and neck squamous cell carcinoma', *Oral oncology*. Elsevier, 46(7), pp. 536–542.

Waters, A. M. and Der, C. J. (2018) 'KRAS: the critical driver and therapeutic target for pancreatic cancer', *Cold Spring Harbor perspectives in medicine*. Cold Spring Harbor Laboratory Press, 8(9), p. a031435.

Weinberg, R. A. (1991) 'Tumor suppressor genes', *Science*. American Association for the Advancement of Science, 254(5035), pp. 1138–1146.

Welcker, M. *et al.* (2003) 'Multisite phosphorylation by Cdk2 and GSK3 controls cyclin E degradation', *Molecular cell*. Elsevier, 12(2), pp. 381–392.

Wey, A. and Knoepfler, P. S. (2010) 'C-myc and N-myc in the developing brain', *Aging*, 2(5), pp. 261–262. doi: 10.18632/aging.100151.

White, R. J. (2005) 'RNA polymerases I and III, growth control and cancer.', *Nature reviews. Molecular cell biology*, 6(1), pp. 69–78. doi: 10.1038/nrm1551.

Wingren, A. G. and Nyesiga, B. (2018) 'CDK2 (cyclin dependent kinase 2)', *Atlas of Genetics and Cytogenetics in Oncology and Haematology*. ARMGHM-Atlas Génétique des Cancers.

Wright, W. E., Pereira-Smith, O. M. and Shay, J. W. (1989) 'Reversible cellular senescence: implications for immortalization of normal human diploid fibroblasts.', *Molecular and cellular biology*. Am Soc Microbiol, 9(7), pp. 3088–3092.

Wu, S. *et al.* (2019) 'Correlation between EZH2 and CEP55 and lung adenocarcinoma prognosis', *Pathology-Research and Practice*. Elsevier, 215(2), pp. 292–301.

Wu, X. *et al.* (2019) 'Targeting glycogen synthase kinase 3 for therapeutic benefit in lymphoma', *Blood*. Am Soc Hematology, p. blood-2018874560.

Xia, Y.-P. *et al.* (2012) 'The protective effect of sonic hedgehog is mediated by the propidium iodide 3-kinase/AKT/Bcl-2 pathway in cultured rat astrocytes under oxidative stress', *Neuroscience*. Elsevier, 209, pp. 1–11.

Xie, J. *et al.* (2013) 'Targeting hedgehog signaling in cancer: research and clinical developments', *OncoTargets and therapy*. Dove Press, 6, p. 1425.

Xie, Z. *et al.* (2007) 'Cep120 and TACCs control interkinetic nuclear migration and the neural progenitor pool', *Neuron*. Elsevier, 56(1), pp. 79–93.

Xu, Y. *et al.* (2018) 'Expression and clinical significance of centrosomal protein 55 in T-cell lymphoma', *Journal of cancer research and therapeutics*. Medknow Publications, 14(1), p. 94.

Xu, Z.-Y. *et al.* (2015) 'Cep55 regulates spindle organization and cell cycle progression in meiotic oocyte', *Scientific reports*. Nature Publishing Group, 5, p. 16978.

Yanagisawa, H., Schluterman, M. K. and Brekken, R. A. (2009) 'Fibulin-5, an integrin-binding matricellular protein: its function in development and disease', *Journal of cell communication and signaling*. Springer, 3(3–4), pp. 337–347.

Yang, M. and Huang, C.-Z. (2015) 'Mitogen-activated protein kinase signaling pathway and invasion and metastasis of gastric cancer', *World journal of gastroenterology*. Baishideng Publishing Group Inc, 21(41), p. 11673.

Yang, Y.-F. *et al.* (2018) 'SPAG5 interacts with CEP55 and exerts oncogenic activities via PI3K/AKT pathway in hepatocellular carcinoma', *Molecular cancer*. BioMed Central, 17(1), p. 117.

Yilmaz, Ö. H. *et al.* (2006) 'Pten dependence distinguishes haematopoietic stem cells from leukaemia-initiating cells', *Nature*. Nature Publishing Group, 441(7092), p. 475.

Yost, C. *et al.* (1996) 'The axis-inducing activity, stability, and subcellular distribution of beta-catenin is regulated in Xenopus embryos by glycogen synthase kinase 3.', *Genes & development*. Cold Spring Harbor Lab, 10(12), pp. 1443–1454.

Zambetti, G. P. *et al.* (1992) 'Wild-type p53 mediates positive regulation of gene expression through a specific DNA sequence element.', *Genes & Development*. Cold Spring Harbor Lab, 6(7), pp. 1143–1152.

Zardavas, D., Phillips, W. A. and Loi, S. (2014) 'PIK3CA mutations in breast cancer: reconciling findings from preclinical and clinical data', *Breast cancer research*. BioMed Central, 16(1), p. 201.

Zechner, D. *et al.* (2003) 'β-Catenin signals regulate cell growth and the balance between progenitor cell expansion and differentiation in the nervous system', *Developmental biology*. Elsevier, 258(2), pp. 406–418.

Zhang, H.-G. and Grizzle, W. E. (2011) 'Exosomes and cancer: a newly described pathway of immune suppression', *Clinical Cancer Research*. AACR, 17(5), pp. 959–964.

Zhang, J. *et al.* (2006) 'PTEN maintains haematopoietic stem cells and acts in lineage choice and leukaemia prevention', *Nature*. Nature Publishing Group, 441(7092), p. 518.

Zhang, W. *et al.* (2016) 'Upregulation of centrosomal protein 55 is associated with unfavorable prognosis and tumor invasion in epithelial ovarian carcinoma', *Tumor Biology*. Tumor Biology, 37(5), pp. 6239–6254. doi: 10.1007/s13277-015-4419-6.

Zhao, L. and Vogt, P. K. (2008) 'Class I PI3K in oncogenic cellular transformation', *Oncogene*. Nature Publishing Group, 27(41), p. 5486.

Zhao, W., Seki, A. and Fang, G. (2006) 'Cep55, a microtubule-bundling protein, associates with centralspindlin to control the midbody integrity and cell abscission during cytokinesis', *Molecular biology of the cell*. Am Soc Cell Biol, 17(9), pp. 3881–3896.

Zhao, Y. and Adjei, A. A. (2015) 'Targeting angiogenesis in cancer therapy: moving beyond vascular endothelial growth factor', *The oncologist*. AlphaMed Press, 20(6), pp. 660–673.

Zhou, J. *et al.* (2013) 'MicroRNA-155 promotes glioma cell proliferation via the regulation of MXI1', *PloS one*. Public Library of Science, 8(12), p. e83055.

Zhou, L. *et al.* (2019) 'Diagnostic and prognostic value of CEP55 in clear cell renal cell carcinoma as determined by bioinformatics analysis', *Molecular medicine reports*. Spandidos Publications, 19(5), pp. 3485–3496.

Zopf, C. J. *et al.* (2013) 'Cell-cycle dependence of transcription dominates noise in gene expression', *PLoS computational biology*. Public Library of Science, 9(7), p. e1003161.

Zou, M. *et al.* (2015) 'KRAS G12D-mediated oncogenic transformation of thyroid follicular cells requires long-term TSH stimulation and is regulated by SPRY1', *Laboratory Investigation*. Nature Publishing Group, 95(11), p. 1269.

Received: 16 August 2018 | Revised: 20 January 2019 | Accepted: 24 January 2019
DOI: 10.1002/jcb.28575

RESEARCH ARTICLE

WILEY Journal of Cellular Biochemistry

Interaction and molecular dynamics simulation study of Osimertinib (AstraZeneca 9291) anticancer drug with the EGFR kinase domain in native protein and mutated L844V and C797S

Vahideh Assadollahi[1] | **Behnam Rashidieh**[2,3] | **Masoud Alasvand**[4] | **Alina Abdolahi**[5] | **J. Alejandro Lopez**[2,6]

[1]Cellular and Molecular Research Center, Research Institute for Health Development, Kurdistan University of Medical Sciences, Sanandaj, Iran

[2]School of Environment and Sciences, Griffith University, Nathan, Queensland, Australia

[3]Signal Transduction Laboratory, QIMR Berghofer Medical Research Institute, Herston, Queensland, Australia

[4]Department of Medical Physiology and Pharmacology, Faculty of Medicine, Kurdistan University of Medical Sciences, Sanandaj, Iran

[5]Student Research Committee, Kurdistan University of Medical Sciences, Sanandaj, Iran

[6]Tumour Immunology Laboratory, QIMR Berghofer Medical Research Institute, Brisbane, Queensland, Australia

Correspondence
Rashidieh, B, Lopez, JA, School of Environment and Sciences, Griffith University, Nathan, QLD 4111, Australia.
Email: Behnam.Rashidieh@griffithuni.edu.au

Funding information
BR was a recipient of the GUIPRS and GUPRS by Griffith University for the financial support.

Abstract

Background: Targeted therapy is a novel, promising approach to anticancer treatment that endeavors to overcome drug resistance to traditional chemotherapies. Patients with the L858R mutation in epidermal growth factor receptor (EGFR) respond to the first generation tyrosine kinase inhibitors (TKIs); however, after one year of treatment, they may become resistant. The T790M mutation is the most probable cause for drug resistance. Third generation drugs, including Osimertinib (AZD9291), are more effective against T790M and other sensitive mutations. Osimertinib is effective against the L844V mutation, has conditional effectiveness for the L718Q mutation, and is ineffective for the Cys797Ser (C797S) mutation. Cells that have both the T790M and C797 mutations are more resistant to third generation drugs. Although research has shown that Osimertinib is an effective treatment for EGFR L844V cells, this has not been shown for cells that have the C797S mutation. This molecular mechanism has not been well-studied.

Methods: In the present study, we used the GROMACS software for molecular dynamics simulation to identify interactions between Osimertinib and the kinase part of EGFR in L844V and C797S mutants.

Results: We evaluated native EGFR protein and the L844V and C797S mutations' docking and binding energy, kI, intermolecular, internal, and torsional energy parameters. Osimertinib was effective for the EGFR L844V mutation, but not for EGFR C797S. All simulations were validated by root-mean-square deviation (RMSD), root-mean square fluctuation (RMSF), and radius of gyration (ROG).

Abbreviations: EGFR, Epidermal growth factor receptor; NSCLC, Non-small-cell lung cancer; RMSD, Root-mean square deviation; RMSF, Root-mean square fluctuation; ROG, Radius of gyration; TKIs, Tyrosine kinase inhibitors.

Assadollahi and Rashidieh have contributed equally into this study.

J Cell Biochem. 2019;1-10. wileyonlinelibrary.com/journal/jcb © 2019 Wiley Periodicals, Inc.

Conclusion: According to our computational simulation, the results supported the experimental models and, therefore, could confirm and predict the molecular mechanism of drug efficacy.

KEYWORDS

EGFR, MD simulation, mutants of L844V and C797S, non-small-cell lung cancer (NSCLC), osimertinib (AZD 9291)

1 | INTRODUCTION

The epidermal growth factor receptor (*EGFR*) gene, also referred to as *ERBB*, *ERBB1,* or *HER1,* is a tyrosine kinase receptor.[1,2] Its aberrant activation or mutation promotes the growth of non-small-cell lung cancer (NSCLC), in addition to liver, stomach, breast, colorectal, and esophageal cancers.[3-6] AstraZeneca has developed a new series of irreversible, selective small-molecule inhibitors that target the sensitizing and T790M-resistant mutant forms of EGFR tyrosine kinase instead of the wild-type EGFR. These compounds target the cysteine-797 (Cys797) residue when they form a covalent, irreversible bond with EGFR kinase at the ATP site.[7] Favorable drug-like properties have been attained with this chemotype as the target potency was enhanced by discovering additional structure-activity relationships (SARs) without increased lipophilicity.[8]

Osimertinib (TAGRISSO™ or AZD9291) is an FDA approved drug for the treatment of patients with metastatic EGFR T790M mutation-positive NSCLC, as a new and fast developed EGFR tyrosine kinase inhibitor (TKI) therapy.[9] The unique design of Osimertinib, a novel mono-anilino-pyrimidine compound, makes it structurally and pharmacologically different from other TKIs, such as CO-1686 and WZ4002.[10] Amongst the improvements achieved, it exhibits augmented kinase selectivity. CO-1686 and WZ4002 provide an electrophilic functionality because of their reaction with a conserved cysteine residue that is present in EGFR (Cys797), a heteroatom-linked pyrimidine with four substituents, and a pyrimidine that contains five substituents. Other differences are related to the electrophilic functionality on the C-2 substituent ring of pyrimidine, including the 4-substituent of pyrimidine being C-linked and heterocyclic, and nonsubstitution of the pyrimidine 5-position. Mass spectrometry (MS) analysis of the chymotrypsin digests has verified that Osimertinib could covalently modify recombinant EGFR (L858R/T790M) at the 797 amino acid of the target Cys.[8]

Osimertinib, a new irreversible EGFR TKI, provides selectivity against mutant versus wild-type forms of EGFR. Osimertinib has a unique third-generation TKI profile compared with the first generation EGFR inhibitors (Gefitinib and Erlotinib) and second generation EGFR inhibitors (Afatinib and Dacomitinib). By inhibiting EGFR phosphorylation in EGFR cells and harboring sensitizing EGFR mutants, such as PC-9 and H1650 (ex19del) and H3255 (L858R), Osimertinib is similarly potent against early generation TKIs.[8] Osimertinib activity against EGFR has been profiled because of its active circulating metabolites. The potential mechanism of EGFR Cys797Ser (C797S) resistance to irreversible EGFR inhibitors Osimertinib, HM61713, WZ4002, and CO-1686 is reportedly from a mutation within the tyrosine kinase domain in T790M-positive patients.[11-15] A predicted mechanism of resistance to irreversible EGFR inhibitors is from mutations that occur at the EGFR C797 codon within the kinase-binding site.[16] The cellular potency of this class of TKIs is significantly reduced by a C797S missense mutation when they lose the potential for covalent bond formation at position 797.[17] Acquired resistance to third-generation TKIs is a novel mechanism of the C797S mutation in EGFR.[11] The development of this resistance has been recently reported by several studies. Furthermore, C797S tertiary point mutation occurs in 40% of Osimertinib-treated patients.[18] Figure 1 shows the EGFR activation and inhibition of related signaling pathways by drug binding. EGFR is a transmembrane tyrosine kinase which is activated by a mechanism so-called ligand-induced dimerization. This receptor is a crucial regulator of some cellular process such as proliferation, survival, differentiation, and migration. Any dysfunction or aberrant regulation in downstream signaling pathways such as PI3K/Akt, Jak1/2 STAT3, and RAS/MEK/ERK can lead to cancer. Targeting this receptor by the drug can inhibit the abnormal activation of these signaling pathways which most of the cancerous cells adopting adopt for proliferation, survival, and avoidance of apoptosis or cell death.

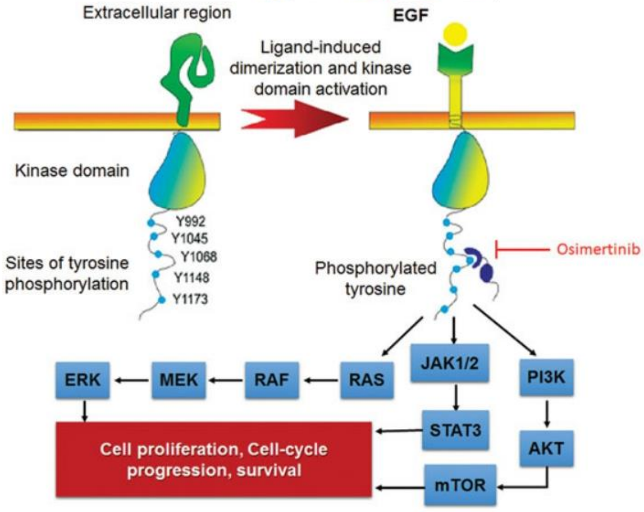
Extracellular region
EGF
Ligand-induced dimerization and kinase domain activation
Kinase domain
Y992
Y1045
Y1068
Y1148
Y1173
Sites of tyrosine phosphorylation
Osimertinib
Phosphorylated tyrosine
ERK
MEK
RAF
RAS
JAK1/2
PI3K
STAT3
AKT
mTOR
Cell proliferation, Cell-cycle progression, survival

FIGURE 1 General view of the ligand-induced dimerization and activation process of EGFR and inhibition of general oncogenic signaling pathways. EGFR, epidermal growth factor receptor

Despite Osimertinib being an FDA approved drug, no molecular dynamics simulation (MDS) is available for it to the best of our knowledge. This MDS study especially for a successful drug not only clarifies and explains the molecular interaction between drug and ligand but also validates the drug discovery process to utilize the same procedure for the new targets.

2 | METHODOLOGY

2.1 | Creation of input files

2.1.1 | Protein preparation

We obtained the crystallographic structure of the target protein from the Protein Data Bank (www.rcsb.org/PDB ID:4zau). Chain A was used for simulation (Supporting Information Figure S1A). For the docking procedure, we first removed the water molecules and ligands from the native structure of the protein and then added charges and hydrogen atoms to the protein. A missing residue was added to the structure by Modeller 9.16 and 10 loop optimized models were created for use according to energy ranks. Energy minimization was performed on the molecules in a vacuum with GROMACS. This stage was necessary to avoid false van der Waals interactions and to achieve better conformational status.

2.1.2 | Ligand preparation

Osimertinib or N-(2-{[2-(dimethylamino)ethyl](methyl)amino}-4-methoxy-5-{[4-(1-methyl-1H-indol-3-yl)pyrimidin-2-yl]amino}phenyl)prop-2-enamide C28 H33 N7 C797S O2, as the ligand, was downloaded from ChemSpider (www.chemspider.com/ID: 31042598). Its parameters were calculated and minimized by AMBER (ff99SB) and AnteChamber PYthon Parser InterfacE (ACPYPE; Supporting Information Figure S1B).

2.2 | Docking

The AutoDock software package is an automated docking tool which provides quality protein-ligand docking results. We used AutoDock 4.2.6 to predict binding properties of small molecules, like drugs, to their target proteins and DNA. This software includes two tools, Autodock and Auto grid. With this software, researchers can edit the target and ligand before docking, and visualize the output file after docking (Supporting Information Figure S1).

Next, we adjusted the grid box into the active site of the protein to show the software the exact docking location. Eventually, the program was run with the Lamarckian genetic algorithm at a population size of 100 to produce output conformer files (Figure 2). The overall energy profiles of modeling have been shown in

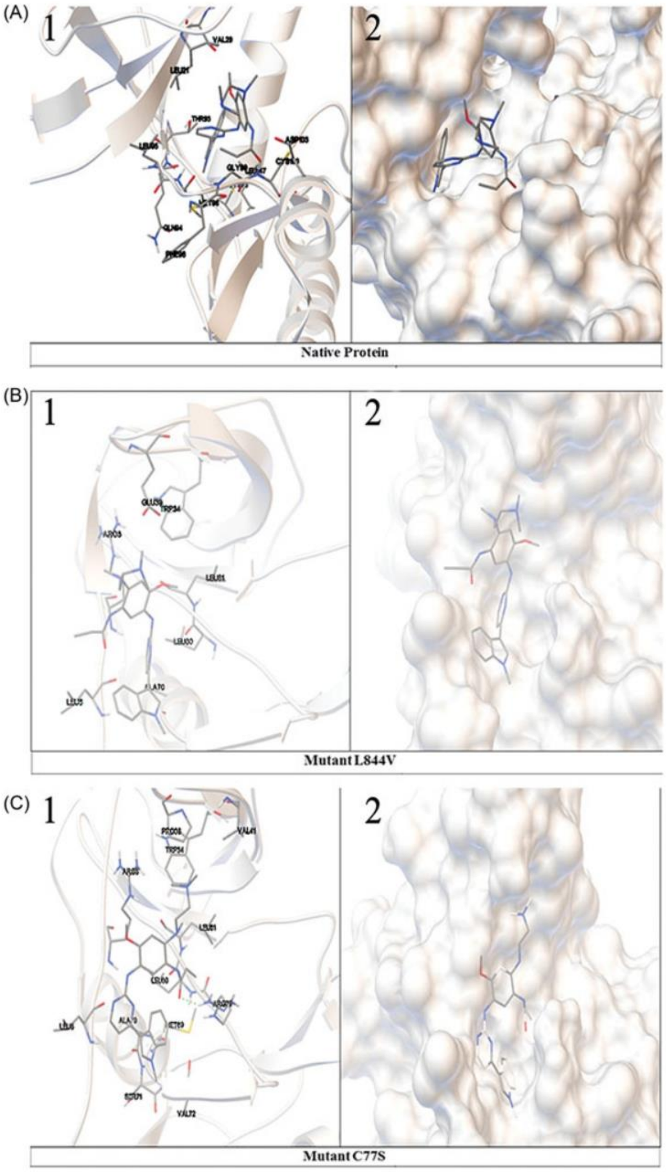
(A)
1
VAL29
THR30
2
Native Protein
(B)
1
TRP34
LEU81
LEU5
2
Mutant L844V
(C)
1
TRP34
VAL41
LEU81
VAL72
2
Mutant C77S

FIGURE 2 *EGFR* native and Mutants' interaction with AZD9291 drug. A, Native protein interaction parameters with AZD9291 in Figure 3A-1 (ribbon representation) and 3A-2 (surface representation). B, Mutant L844V interaction parameters with AZD9291 in Figure 3B-1 (ribbon representation) and 3B-2 (surface representation). C, Mutant C77S interaction parameters with AZD9291 in Figure 3C-1 (ribbon representation) and 3C-2 (surface representation). EGFR, epidermal growth factor receptor

Supporting Information Supplementary Table 1 which is indicative of calculation accuracy.

2.3 | Molecular dynamics (MD) simulation

Molecular dynamics (MD) simulation and molecular mechanics (MM) minimization were performed using Gromacs 4.5.6 under an AMBER ff99SB approach as previously described.[19] GAFF topologies for the drug were generated from the Antechamber software using partial charges calculated by the restrained electrostatic potential method. The GAFF topologies were converted into GROMACS format using the ACPYPE tool. We used Na^+/K^+ to neutralize the system charge. MD simulations were run with periodic boundary conditions. The Van der Waals forces were treated with a cut-off of 1.2 Å. The Particle-Mesh Ewald method was used with a 1.2 Å cut-off. The frequency to update the neighbor list was 10. We used the protonation state of the Gromacs package to calculate the total mutant charge. MD simulation was accomplished in four steps. Initially, the entire system was minimized using the steepest descent followed by conjugate gradient algorithms. In the second step (equilibration), heavy atoms were restrained using a force constant of 1000 kJ/mol nm, and the solvent and ions were allowed to evolve. This was undertaken by minimization and molecular dynamics in the NVT ensemble for 100 ps and in the NPT ensemble for 100 ps. Then, to obtain equilibrium geometry at 298 K and 1 atom, we increased the temperature of the system and reassigned the velocities at each step according to the Maxwell-Boltzmann distribution at that temperature and equilibrated it for 100 ps. Temperature coupling was set to 0.1 ps and pressure coupling to 2 ps. The Berendsen algorithm was used for the thermostat and barostat during the equilibration step. All bonds were constrained via the LINCS algorithm. In the last step (production phase), a 30 ns MD simulation was performed under an NPT ensemble. to maintain stable temperature and pressure in the production step, a Nosé-Hoover thermostat and Parrinello-Rahman barostat were applied by removing position restraints. The temperature was 298°K with a time-step of 2 fs. In this step, we used the LINCS algorithm to constrain the lengths of the hydrogen-containing bonds.

3 | RESULTS

3.1 | Protein and ligand interaction

As previously reported, Osimertinib binds on the outer edge of the ATP-binding pocket sandwiched between the P-loop and the protein backbone between Pro 794 and Cys797.[20] There are two hydrogen bonds that help anchor the ligand in place: Osimertinib N4 hydrogen bonds to the hinge atom N of Met 793 and the ligand carbonyl oxygen hydrogen bonds to the N of Cys 797. Supporting Information Figure S1 C, D as well as Figure 2 shows the side chain of the known covalent attachment site (Cys 797) as well as the reactive center on the Osimertinib molecule (C9). After docking, we sorted the conformations in terms of their binding energy and KI to find the top complex for simulation. The best hit was selected for the next stage. Then, MD was preceded. Figure 3A-C shows the docking and parameters of kI, binding, intermolecular, internal, and torsional energies for the native protein and both mutants.

The results of docking binding energies (without MD) of the mutants and native protein to the same ligand (Osimertinib) showed that replacement of the L residue by V at position 844 had a greater effect on receptor binding and inhibition compared with the C residue at position 77 in the other mutant.

3.2 | Root-mean-square deviation (RMSD)

The root-mean square deviation (RSMD) of the simulated structure over time is an appropriate, common technique to verify molecular dynamics simulation stability. Figure 3A shows that the onset of stability in all native and mutant proteins was observed around 15 ns and stability occurred at 20 ns. Therefore, during the simulation, all proteins had a validated structure.

3.3 | Root-mean square fluctuation (RMSF)

The root-mean-square fluctuation (RMSF) of the α-carbon is used to evaluate movement and structure flexibility. As depicted in Figure 3B, all the fluctuations were similar in most of the points, with the exception of the last pick.

3.4 | Radius of gyration

The radius of gyration is an important parameter in protein stability during simulation. If the protein was stable during the simulation, the radius of gyration would plateau on average. The evidence of protein stability can be found in (Figure 3C).

3.5 | Binding energy and hydrogen bonds

We used the MM/PBSA method to calculate binding energy. The MM/PBSA approach was originally

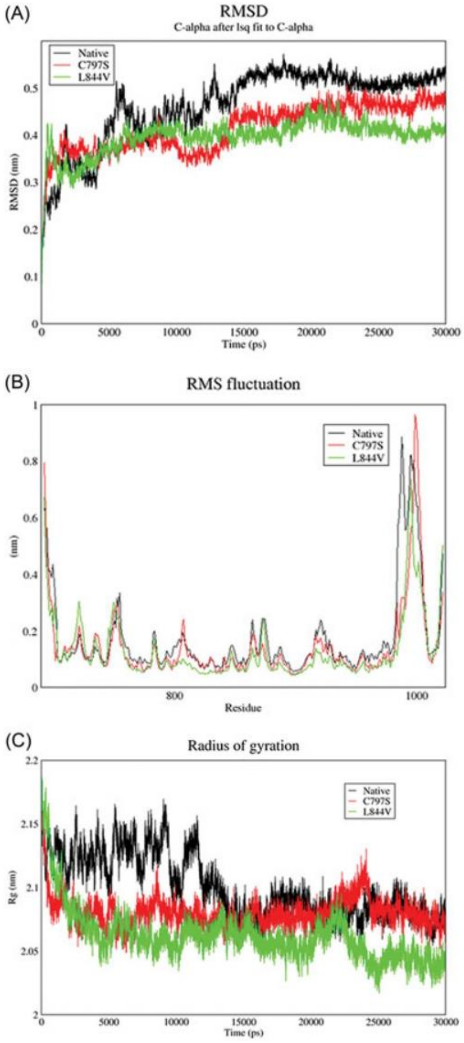

FIGURE 3 A, RMSD chart change during the simulation time suggests protein structure validation during simulation. B, RMS fluctuation shows approximately the same movements for all structures. C, Radius of gyration revealed the stability of structures. RMSD, root-mean square deviation

developed for the AMBER package and has several automated versions. The molecular mechanic energies combined with the Poisson-Boltzmann surface area continuum solvation method is a popular approach to estimate the free energy of small ligands that bind to biological macromolecules. It is typically based on molecular dynamics simulations of the receptor-ligand complex and is, thus, intermediate in both accuracy and computational effort between empirical scoring and strict alchemical perturbation methods. It has been applied to numerous systems with varying degrees of success[21] and it is calculated from simulations of the complex, the free ligand and the unbound receptor, as per this formula:

$$\Delta G_{\text{bind}} = G_{\text{complex}} - G_{\text{Free protein}} - G_{\text{Free ligand}}$$

The MM/PBSA equation can be summarized as follows:

In this equation, E_{gas} was obtained from the following formula:

We used APBS software for the Poisson-Boltzmann calculation. For the calculation based on this method, initially; we calculated the free energy of the protein and ligand separately. As it can be seen in Supporting Information Supplementary Table 1 these binding energies are not very different for the native proteins and the mutants. These calculations were repeated for the simulation and we established that the binding energies were then different (Table 1).

Experimental models showed that Osimertinib is effective for L844V mutants but not for C797S. Our computational study summarized on Table 1 exactly confirm this as the binding energy affinity for L844V complex-(356.354 ± 30.796 kJ/mol) is less than that of the others (−338.196 ± 28.014 kJ/mol and −276.519 ± 33.004 kJ/mol), and this means the greater binding affinity. This parameter is the greatest for C797S and this can be interpreted as weakest binding affinity. In conclusion, the significant changes of these parameters suggest the efficient function of the drug in binding to L844V and inefficiency in binding to C797S.

As summarized in Tables 1, L844V has more negative Van der Waals, electrostatic, SASA, and binding energies

TABLE 1 Summary of connector energies measured for native protein and its mutants C797S and L844V

	Calculated energy (kJ/mol)		
Energy type	**Native protein**	**C797S mutant**	**L844V mutant**
Van der Waal	−226.045 ± 15.958	−213.787 ± 16.561	−241.208 ± 25.991
Electrostatic	−337.136 ± 35.983	−276.191 ± 53.264	−380.346 ± 41.144
Polar solvation	247.255 ± 43.512	234.718 ± 49.531	288.303 ± 41.224
SASA	−22.270 ± 1.414	−21.259 ± 1.300	−23.103 ± 1.777
SAV	0.000 ± 0.000	0.000 ± 0.000	0.000 ± 0.000
WCA	0.000 ± 0.000	0.000 ± 0.000	0.000 ± 0.000
Binding	−338.196 ± 28.014	−276.519 ± 33.004	−356.354 ± 30.796

compared with the C797S mutant and native proteins, which indicates that of this mutant can be challenging for stability. However, the simulation has shown that it does not undergo major significant changes in conformation when interacting with the drug compared with the native protein. Overall, the data suggest the model is capable of achieving chemical accuracy in molecular simulations

Figure 4 shows the hydrogen bond simulation during 30 ns. The vertical axis indicates the number of hydrous bonds and the horizontal axis is the time scale.

We noted that, in a comparison, the native protein contained a larger average number of hydrogen bonds than the native protein, followed by L844V (Figure 4).

4 | DISCUSSION

Targeted therapy opens a new door for discovery of promising anticancer therapeutics. These therapeutics are routinely designed to recognize a target, usually, a protein such as EGFR, that plays a role in tumor growth and survival.[22] Mutations in these receptors or protein kinases can stimulate a complex cascade of cross-signaling pathways such as the RAS-RAF-MEK-ERK or MAPK, PI3K-AKT-mTOR, or JAK-STAT pathways.[1] Eventually, deregulation of cascades lead to uncontrolled growth, proliferation, survival, and, ultimately, cancer. Two different types of inhibitors suppress the protein's function: those which affect the external part of the protein (monoclonal antibody) and small-molecule inhibitors that inhibit TKIs.

EGFR is overexpressed in up to 40%-80% of NSCLC. Initially, it was a promising translational therapeutic target; however, researchers have subsequently discovered that activated mutations rather than overexpression of EGFR are the prime therapeutic targets. The two most frequent mutations are deletions in exon 19, with a 60% incidence, and missense substitutions in the L858R mutant at position

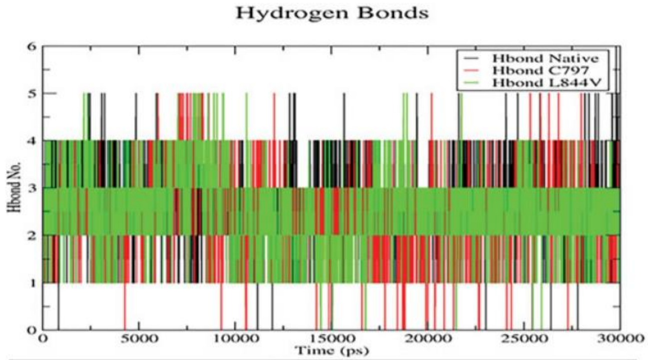

Hydrogen Bond	
Hbond Native	**2.6807730756**
Hbond L844V	**2.5234921693**
Hbond C797S	**2.46017994**

FIGURE 4 Analysis of hydrogen bond and it details are arranged in table below of figure

858 (35%) with a replacement of leucine by arginine, which would result in constitutive activation of the receptor without ligand binding.[23] Patients that have the EGFR L858R mutation initially respond to first generation TKIs (erlotinib or gefitinib); however, resistance usually develops after one year of treatment. The T790M mutation is responsible for half of the drug resistance. Research to develop medications that would overcome this resistance has led to the creation of a second generation TKI, afatinib. Despite the fact that afatinib could treat T790M, the need for a high dose to achieve clinical effectiveness is a considerable problem. This issue limited clinical application and paved the way for third generation drugs such as rociletinib (CO-1686), and WZ4002, which more efficiently fight both T790M mutations and all other sensitive mutations.[24] More importantly, these medications recognize and bind specifically to the mutations, providing decreased toxicity. Osimertinib has a 61% efficacy, whereas rociletinib has 59% efficacy against these mutations. A few studies have shown that new generation drugs are also threatened by mutation resistance. For example, the C797S mutation exists in 40% of Osimertinib-resistant T790M.[23] To date, this mutation has not been reported in rociletinib resistant tumors. Nevertheless, Osimertinib is an effective treatment for L844V, it has conditional efficiency for L718Q, and is not effective for C797S. Cells with T790M and C797 mutations show the most resistance against third generation drugs.

Previous models[8,25] have shown a covalent binding of the drug to EGFRT790M via Cys797. In the structural model, the drug through Cys-797 (acrylamide group) bind with a covalent bond to EGFR T790M. The pyrimidine core forms a couple of hydrogen bonds to Met 793 of the hinge region. In terms of orientation, the indole group is next to the gatekeeper residue and amine moiety positioned in the solvent channel.

In the present study, MD simulation suggested a more negative binding energy (−356.354 ± 30.796 kJ/mol) for L844V mutation compared with the other mutation, which indicated that Osimertinib had a better binding affinity and suitable inhibition of this protein. However, C797S had a more positive binding energy (−276.519 ± 33.004 kJ/mol) compared with the others which caused a binding deficiency of the mutation and its resistance to Osimertinib. L844V has a more negative van der Waals force and electrostatic interaction compared with the C797S mutation and native protein (Summarized in Table 1)

We validated the simulations with RMSD, RMSF, and ROG. The observed significant difference between these mutations implied a successful interaction of Osimertinib with L844V and its inability to efficiently bind C797S. Hence, newer anticancer drugs might be needed for these types of mutations.

The RMSD between structures created in the simulation in the time dimension was an appropriate criterion to ensure the stability of the dynamic molecular simulation. Therefore, changes in RMSD of the main chain atoms (carbon alpha) of the normal EGFR molecule and two mutations were calculated and extracted relative to the primary structure during a simulation time of 30 ns. Figure 3A shows the results of this calculation for all of the simulations. As seen in this chart, after approximately 15 ns, the structures of the mutation and native protein stabilize. In a comparison of the two mutants with normal EGFR, we observed the most fluctuation in the C797S mutation. The stimulations had acceptable stability where none of the structures produced in 30 ns had any apparent deviation from the primary structure.

An investigation of the changes in the RMSD ligand (Osimertinib) suggested that this ligand in the L844V mutant more rapidly stabilized and the RMSD amount during 30 ns of simulation remained constant. This showed high binding affinities of Osimertinib to C797S and L844V.

The dynamic behavior of the alpha carbon atoms in the structure contains sufficient information to determine important movements in proteins, and reflect the general movements of the structure. Thus, we have used the RMSF of the alpha carbon to evaluate structural movement and flexibility. A flexible structure comparison was performed to compare the normal EGFR with both mutants (Figure 3B).

In addition, the gyration radius is an important factor that indicates the amount of protein folding. If a protein is folded well, the gyration radius for that protein is fixed during simulation. This factor provides useful information about the distribution of proteins in the spherical form. Thus, changes in the structure of a protein can be examined by taking into consideration the gyration radius. Here, we have calculated the changes in the gyration radius of all three structures during 30 ns of dynamic molecular simulations (Figure 3C). As shown in Figure 3C, the gyration radius for all three structures during 30 ns showed that the radius of the gyration value of the protein and mutant complexes were virtually similar. Thus, it could be concluded that all three structures were folded adequately and had appropriate stability. This indicated that the protein did not undergo any major conformational changes and its solidity remained constant throughout the simulation period (10-30 ns). The C797S or L844V mutants resembled the normal EGFR structure from the point of view of gyration radius.

We also examined the changes in potential energy, pressure, temperature, and density for each of the structures through the equilibration phase to ensure the stability of the simulations. Each provided acceptable sustainability in all of the structures. The oscillatory patterns observed for all three structures were very similar. L844V had higher fluctuations in some residues (C- terminal residues) compared with the two other structures.

An investigation of hydrogen bonds between mutants and native protein showed that native protein has more hydrogen bonds (2.68) compared with L844V (2.52) and C797S (2.46). L844V (2.52) was located in the second position. The lowest number of hydrogen bonds belonged to C797S (2.46) as seen in Figure 4. Reductions in the number of hydrogen bonds would indicate instability of the mutants relative to native protein. Hydrogen bond formation is one of the signs of bond strength and sustainability of any chemical structure.

5 | CONCLUSION

Mutations not only affect genome stability but also can impact drug sensitivity and efficiency. Experimental studies have shown that Osimertinib is an effective drug for the L844V mutation but not for the C797S mutation, which we confirmed with computational simulation. These data showed the accuracy of the FDA approved drug efficiency; therefore, confirmed that the computational drug discovery can be a reliable option in the screening of the lead compounds.

ACKNOWLEDGMENT

We would like to appreciate the critical comments and contributions of Dr. Mohammad Mehdi Ranjbar and Dr. Ammar Mohseni to improve the quality of the manuscript.

FUNDING INFORMATION

BR was a recipient of the GUIPRS and GUPRS by Griffith University for the financial support.

CONFLICT OF INTERESTS

The authors disclose no potential conflict of interests.

ORCID

Behnam Rashidieh http://orcid.org/0000-0002-9831-0319

REFERENCES

1. Yarden Y. The EGFR family and its ligands in human cancer: Signalling mechanisms and therapeutic opportunities. *Eur J Cancer.* 2001;37:3-8.
2. Ferguson Kathryn M, Berger Mitchell B, Mendrola Jeannine M, Cho Hyun-Soo, Leahy Daniel J, Lemmon Mark A. EGF activates its receptor by removing interactions that autoinhibit ectodomain dimerization. *Mol Cell.* 2003;11(2):507-517.
3. Lynch Thomas J, Bell Daphne W, Sordella Raffaella, et al. Activating mutations in the epidermal growth factor receptor underlying responsiveness of non–small-cell lung cancer to gefitinib. *N Engl J Med.* 2004;350(21):2129-2139.
4. Savonarola A, Palmirotta R, Guadagni F, Silvestris F. Pharmacogenetics and pharmacogenomics: Role of mutational analysis in anti-cancer targeted therapy. *Pharmacogenomics J.* 2012;12(4):277-286.
5. Sharma Sreenath V, Bell Daphne W, Settleman Jeffrey, Haber Daniel A. Epidermal growth factor receptor mutations in lung cancer. *Nat Rev Cancer.* 2007;7(3):169-181.
6. Figueroa-Magalhães Maria Cristina, Jelovac Danijela, Connolly Roisin M, Wolff Antonio C. Treatment of HER2-positive breast cancer. *The Breast.* 2014;23(2):128-136.
7. Ward Richard A, Anderton Mark J, Ashton Susan, et al. Structure-and reactivity-based development of covalent inhibitors of the activating and gatekeeper mutant forms of the epidermal growth factor receptor (EGFR). *J Med Chem.* 2013;56(17):7025-7048.
8. Cross Darren AE, Ashton Susan E, Ghiorghiu Serban, et al. AZD9291, an irreversible EGFR TKI, overcomes T790M-mediated resistance to EGFR inhibitors in lung cancer. *Cancer Discov.* 2014;4(9):1046-1061.
9. Khozin S, Weinstock C, Blumenthal GM, et al. Osimertinib for the treatment of metastatic EGFR T790M mutation–positive non–small cell lung cancer. *Clin Cancer Res.* 2017;23(9):2131-2135.
10. Walter Annette O, Sjin Robert Tjin Tham, Haringsma Henry J, et al. Discovery of a mutant-selective covalent inhibitor of EGFR that overcomes T790M-mediated resistance in NSCLC. *Cancer Discov.* 2013;3(12):1404-1415.
11. Niederst Matthew J, Hu Haichuan, Mulvey Hillary E, et al. The allelic context of the C797S mutation acquired upon treatment with third-generation EGFR inhibitors impacts sensitivity to subsequent treatment strategies. *Clin Cancer Res.* 2015;21(17):3924-3933.
12. Song Haa-Na, Jung KiSun, Yoo Kwai Han, et al. Acquired C797S mutation upon treatment with a T790M-specific third-generation EGFR inhibitor (HM61713) in non–small cell lung cancer. *J Thorac Oncol.* 2016;11(4):e45-e47.
13. Thress Kenneth S, Paweletz Cloud P, Felip Enriqueta, et al. Acquired EGFR C797S mutation mediates resistance to AZD9291 in non-small cell lung cancer harboring EGFR T790M. *Nature Med.* 2015;21(6):560-562.
14. Ercan Dalia, Choi Hwan Geun, Yun Cai-Hong, et al. EGFR mutations and resistance to irreversible pyrimidine-based EGFR inhibitors. *Clin Cancer Res.* 2015;21(17):3913-3923.
15. Godin-Heymann Nadia, Ulkus Lindsey, Brannigan Brian W, et al. The T790M "gatekeeper" mutation in EGFR mediates resistance to low concentrations of an irreversible EGFR inhibitor. *Mol Cancer Ther.* 2008;7(4):874-879.
16. Yu Zhiwei, Boggon Titus J, Kobayashi Susumu, et al. Resistance to an irreversible epidermal growth factor receptor (EGFR) inhibitor in EGFR-mutant lung cancer reveals novel treatment strategies. *Cancer Res.* 2007;67(21):10417-10427.

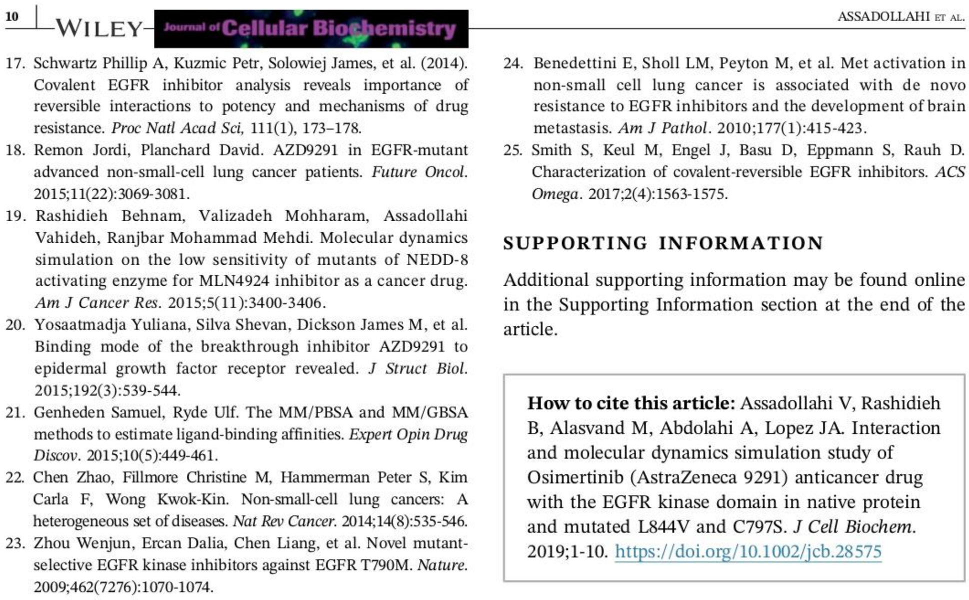

17. Schwartz Phillip A, Kuzmic Petr, Solowiej James, et al. (2014). Covalent EGFR inhibitor analysis reveals importance of reversible interactions to potency and mechanisms of drug resistance. *Proc Natl Acad Sci,* 111(1), 173–178.
18. Remon Jordi, Planchard David. AZD9291 in EGFR-mutant advanced non-small-cell lung cancer patients. *Future Oncol.* 2015;11(22):3069-3081.
19. Rashidieh Behnam, Valizadeh Mohharam, Assadollahi Vahideh, Ranjbar Mohammad Mehdi. Molecular dynamics simulation on the low sensitivity of mutants of NEDD-8 activating enzyme for MLN4924 inhibitor as a cancer drug. *Am J Cancer Res.* 2015;5(11):3400-3406.
20. Yosaatmadja Yuliana, Silva Shevan, Dickson James M, et al. Binding mode of the breakthrough inhibitor AZD9291 to epidermal growth factor receptor revealed. *J Struct Biol.* 2015;192(3):539-544.
21. Genheden Samuel, Ryde Ulf. The MM/PBSA and MM/GBSA methods to estimate ligand-binding affinities. *Expert Opin Drug Discov.* 2015;10(5):449-461.
22. Chen Zhao, Fillmore Christine M, Hammerman Peter S, Kim Carla F, Wong Kwok-Kin. Non-small-cell lung cancers: A heterogeneous set of diseases. *Nat Rev Cancer.* 2014;14(8):535-546.
23. Zhou Wenjun, Ercan Dalia, Chen Liang, et al. Novel mutant-selective EGFR kinase inhibitors against EGFR T790M. *Nature.* 2009;462(7276):1070-1074.
24. Benedettini E, Sholl LM, Peyton M, et al. Met activation in non-small cell lung cancer is associated with de novo resistance to EGFR inhibitors and the development of brain metastasis. *Am J Pathol.* 2010;177(1):415-423.
25. Smith S, Keul M, Engel J, Basu D, Eppmann S, Rauh D. Characterization of covalent-reversible EGFR inhibitors. *ACS Omega.* 2017;2(4):1563-1575.

SUPPORTING INFORMATION

Additional supporting information may be found online in the Supporting Information section at the end of the article.

How to cite this article: Assadollahi V, Rashidieh B, Alasvand M, Abdolahi A, Lopez JA. Interaction and molecular dynamics simulation study of Osimertinib (AstraZeneca 9291) anticancer drug with the EGFR kinase domain in native protein and mutated L844V and C797S. *J Cell Biochem.* 2019;1-10. https://doi.org/10.1002/jcb.28575

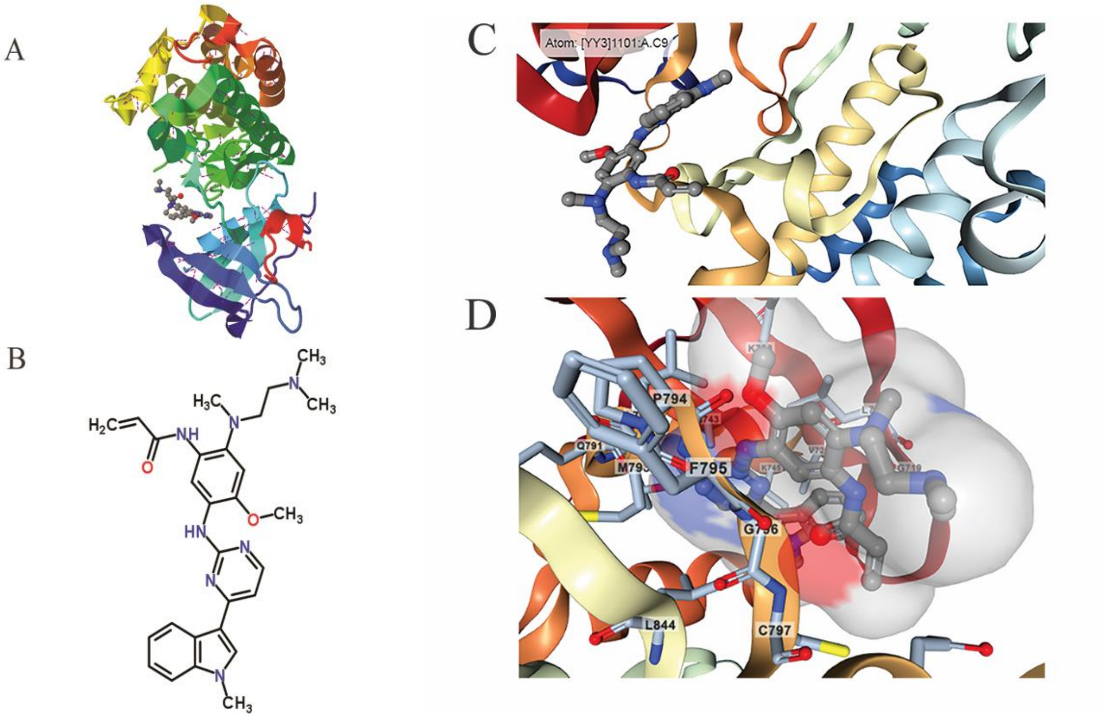

Supplementary Figure 1: EGFR and AZD9291 molecular schematics A: EGFR protein and the AZD9291 drug in the pocket of protein. H bonds have been shown with purple dash lines. PDB (http://www.rcsb.org) visualization based on Yosaatmadja *et al.*, 2015 publication. B: Chemical structure of AZD9291 retrieved from Chemspider database (http://www.chemspider.com). C: Interaction between AZD9291 with wild type EGFR in ribbon representation. Ligand can be seen in pocket of protein while AZD9291 C9 interacted with EGFR. Biological assembly generated by PISA. D: Residues C797, L844, P794 and M793 of EFGR are in contacts with AZD9291 visualized by NGL viewer software. NGL is a Web GL based 3D viewer powered by MMTF. (As described in Rose *et al.*, 2015).